PULSED POWER SYSTEM
脈衝功率系統

Po-Yu Chang

Institute of Space and Plasma Sciences, National Cheng Kung University

2023 Fall Semester

Tuesday 9:10-12:00

Lecture 14

http://capst.ncku.edu.tw/PGS/index.php/teaching/

Online courses:

https://nckucc.webex.com/nckucc/j.php?MTID=md577c3633c5970f80cbc9e821927e016

2023/12/25 updated

Final project and final presentation

- **Final project:**
  - **Due on 1/2.**
- **Final presentation:**
  - **12/26 10:00.**
  - **15 mins for each person**
  - **Applications of pulsed-power system**

Outlines

- Power and voltage adding
  - Marx generator
  - LC generator
  - Line pulse transformers
  - Induction voltage adder (IVA)
  - Linear induction accelerator (LIA)
  - Linear transformer driver (LTD)
- **Diagnostics**
  - **Voltage measurement**
  - **Current measurement**
- Applications of pulsed-power system

Diagnostics

- The basic electrical quantities are always the electromagnetic fields E and B from which pulse current and voltage must be derived.
- A suitable sensor does not perturb the fields to be measured is achieved with
  - capacitive sensors;
  - inductive sensors;
  - electro-optical methods;
  - resistive voltage dividers. It may create weak points in the high-voltage insulation.

Electromagnetic field sensors

- Rapidly changing electromagnetic fields, i.e., $\frac{d\vec{B}}{\mathrm{dt}}$ or $\frac{d\vec{E}}{\mathrm{dt}}$

  → induced currents / voltages in the conductors of a sensor.

  → only consider electrically short sensors:

  size < λ of the field where λ is the scale length or wavelength.

  or d << $c\tau_r$, the distance of the wave that propagates where τ_r is the pulse rise time

  → conduction current density: $\vec{j}_c = \sigma\vec{E}$

  displacement current density: $\vec{j}_d = \frac{\partial\vec{D}}{\partial t}$

  Maxwell's eq:

$$\nabla\times\vec{E} = -\frac{\partial\vec{B}}{\partial t}$$

$$\nabla\times\vec{H} = -\frac{\partial\vec{D}}{\partial t} + \vec{j}$$

Electromagnetic field sensors

- **Ideal conducting sensor of area *A*:**

$$\boldsymbol{i(t) = \left[j_c(t) + \dot{D}(t)\right]A = \left[\sigma E(t) + \epsilon\epsilon_o \dot{E}(t)\right]A}$$

The sensitivity depends on $\boldsymbol{\sigma}$, $\boldsymbol{\epsilon}$, *A*, $\boldsymbol{E(t)}$, $\boldsymbol{\dot{E}(t)}$, and $\boldsymbol{\omega}$.

- **Alternating magnetic fields => induce currents in conducting loops.**

$$\boldsymbol{u(t) = -\oint \dot{\vec{B}}(t) d\vec{A} \approx -\dot{\vec{B}}(t)\vec{A}}$$ **<= if field is homogeneous.**

The sensitivity depends on *A*, $\boldsymbol{\dot{B}(t)}$, and $\boldsymbol{\omega}$.

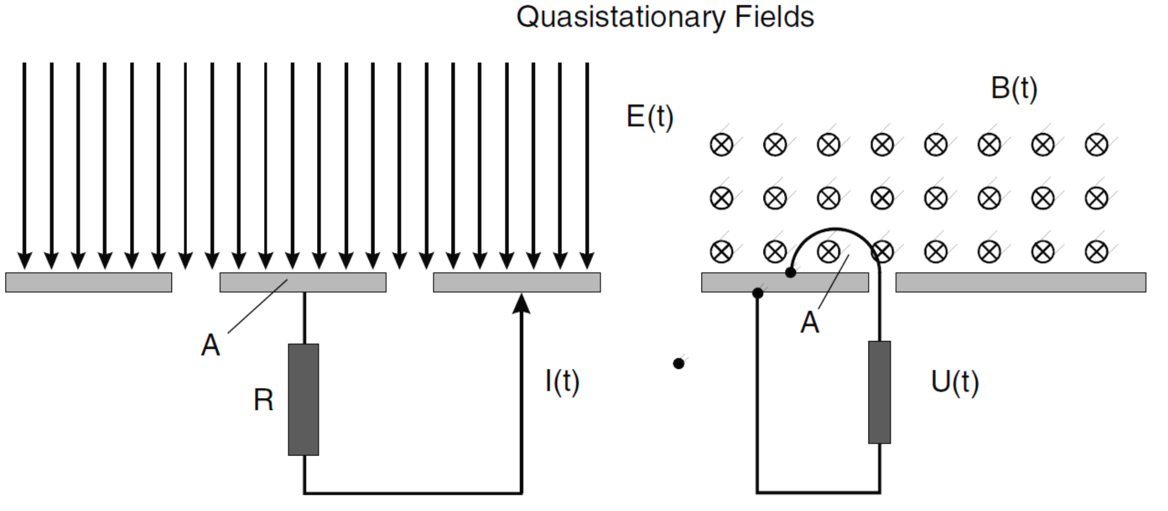

- **The coupling may also couple the undesired noise.**

Capacitive/Inductive sensors

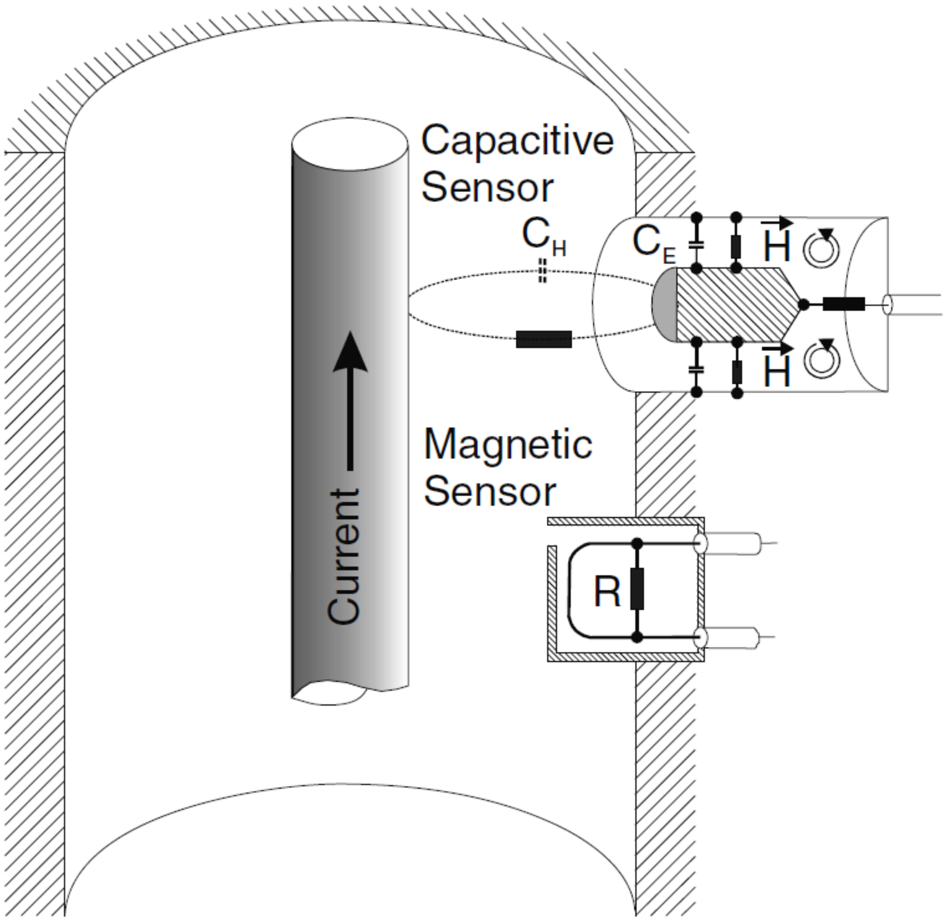

$$u(t) = \frac{C_H}{C_H + C_E} U(t)$$

$$u(t) = -\oint \dot{\vec{B}}(t) d\vec{A} = -\frac{\mathrm{d}\phi}{\mathrm{dt}}$$

Capacitive sensor for voltage measurement

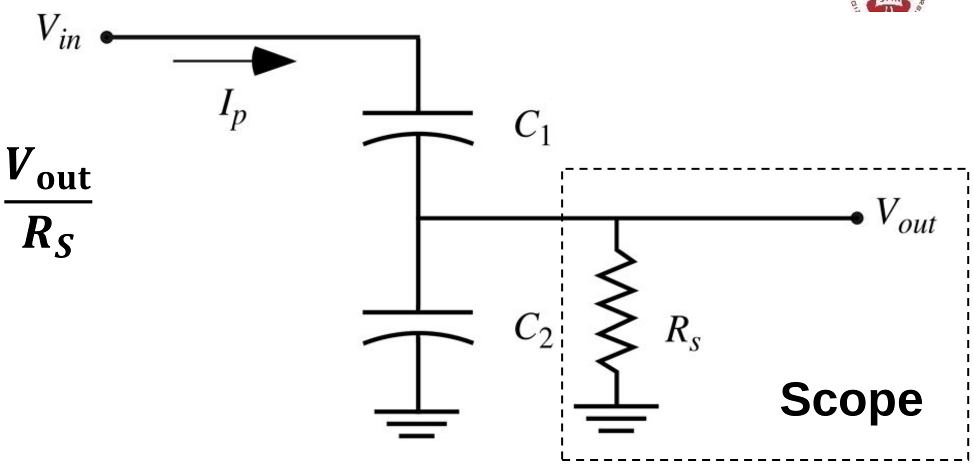

$$V_{\text{in}} = V_{C_1} + V_{\text{out}} \qquad I_p = I_{C_2} + I_{R_s}$$

$$I_p = C_1 \frac{\mathrm{d}V_{C_1}}{\mathrm{dt}} \qquad I_{C_2} = C_2 \frac{\mathrm{dV_{out}}}{\mathrm{dt}} \qquad I_{R_S} = \frac{V_{\text{out}}}{R_S}$$

$$C_1 \frac{\mathrm{d}V_{C_1}}{\mathrm{dt}} = C_2 \frac{\mathrm{dV_{out}}}{\mathrm{dt}} + \frac{V_{\text{out}}}{R_S}$$

$$\frac{dV_{C_1}}{\mathrm{dt}} = \frac{C_2}{C_1} \frac{\mathrm{dV_{out}}}{\mathrm{dt}} + \frac{V_{\text{out}}}{R_S C_1}$$

$$\frac{dV_{\text{in}}}{\mathrm{dt}} = \frac{\mathrm{d}V_{C_1}}{\mathrm{dt}} + \frac{\mathrm{dV_{out}}}{\mathrm{dt}}$$

$$\frac{dV_{\text{in}}}{\mathrm{dt}} = \left(\frac{C_1 + C_2}{C_1}\right) \frac{\mathrm{dV_{out}}}{\mathrm{dt}} + \frac{V_{\text{out}}}{R_S C_1}$$

$$\frac{V_{\text{in}}}{V_{\text{out}}} = \left(\frac{C_1 + C_2}{C_1}\right) + \frac{1}{\mathrm{sR}_S C_1}$$

$$= \left(\frac{C_1 + C_2}{C_1}\right)\left[1 + \frac{1}{\mathrm{sR}_S (C_1 + C_2)}\right]$$

$$\omega_{3\text{dB}} = \frac{1}{R_S (C_1 + C_2)}$$

- **Low frequency:**

$$V_{\text{out}} = \frac{C_1}{C_1 + C_2} V_{\text{in}}$$

- **High frequency:**

$$V_{\text{out}} = R_S C_1 \frac{\mathrm{dV_{in}}}{\mathrm{dt}}$$

Inductive sensor with RC integrator for current measurement

$$|u(t)| = \frac{\mathrm{d\phi}}{\mathrm{dt}} = L\frac{\mathrm{di}}{\mathrm{dt}} + \mathrm{Ri} + \frac{1}{C}\int_0^t i dt'$$

$$|u(t)| = \frac{\mathrm{d\phi}}{\mathrm{dt}} = k\frac{\mathrm{di}}{\mathrm{dt}}$$

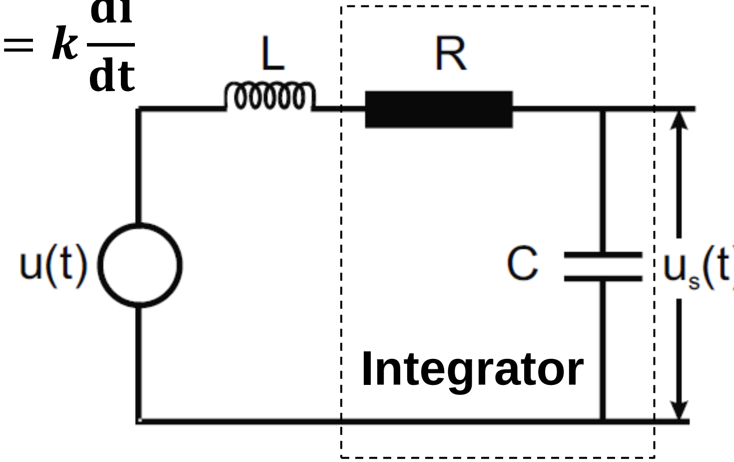

$$|u(t)| = \frac{\mathrm{d\phi}}{\mathrm{dt}} \approx \mathrm{Ri} + \frac{1}{C}\int_0^t i dt'$$

$$u_s = \frac{1}{C}\int_0^t i dt' => C\dot{u}_S = i$$

$$u = \mathrm{RC}\dot{u}_S + u_s$$

$$\dot{u}_S + \frac{1}{\mathrm{RC}}u_s = \frac{1}{\mathrm{RC}}u$$

$$\dot{u}_S e^{\frac{1}{\mathrm{RC}}t} + \frac{1}{\mathrm{RC}}u_s e^{\frac{1}{\mathrm{RC}}t} = \frac{1}{\mathrm{RC}}u e^{\frac{1}{\mathrm{RC}}t}$$

$$\frac{d}{\mathrm{dt}}\left(u_S e^{\frac{1}{\mathrm{RC}}t}\right) = \frac{1}{\mathrm{RC}}u e^{\frac{1}{\mathrm{RC}}t}$$

$$\int d\left(u_S e^{\frac{1}{\mathrm{RC}}t'}\right) = \frac{1}{\mathrm{RC}}\int_0^t u e^{\frac{1}{\mathrm{RC}}t'} dt'$$

$$u_S e^{\frac{1}{\mathrm{RC}}t} - u_S(0) = \frac{1}{\mathrm{RC}}\int_0^t u e^{\frac{1}{\mathrm{RC}}t'} dt'$$

$$u_s = \frac{e^{-\frac{1}{\mathrm{RC}}t}}{\mathrm{RC}}\int_0^t u e^{\frac{1}{\mathrm{RC}}t'} dt' \approx \frac{1}{\mathrm{RC}}\int_0^t u dt'$$

$$= \frac{k}{RC} i(t)$$

- **Working regime:**

$$RC >> t \approx \frac{1}{\omega} \qquad \omega >> \frac{1}{\mathrm{RC}}$$

Rogowski coil

- **In situ calibration is needed to obtain *k*.**

$$|u(t)| = \frac{\mathrm{d}\phi}{\mathrm{dt}} = k\frac{\mathrm{di}}{\mathrm{dt}}$$

- **If in situ calibration is not possible, Rogowski coil instead of a simple current loop is used.**
- **Rogowski coil is a coil consisting of many windings lined up in a toroidal configuration encircling the current path.**

$$\oint \vec{B} \cdot d\,\vec{l} = \mu_o I \qquad B = \frac{\mu_o}{2\pi r} I$$

$$\phi_1 = BA = \frac{\mu_o A}{2\pi r} I$$

$$|u| = \frac{\mathrm{d}\phi}{\mathrm{dt}} = N\frac{\mathrm{d}\phi_1}{\mathrm{dt}} = \frac{\mu_o AN}{2\pi r}\frac{\mathrm{dI}}{\mathrm{dt}}$$

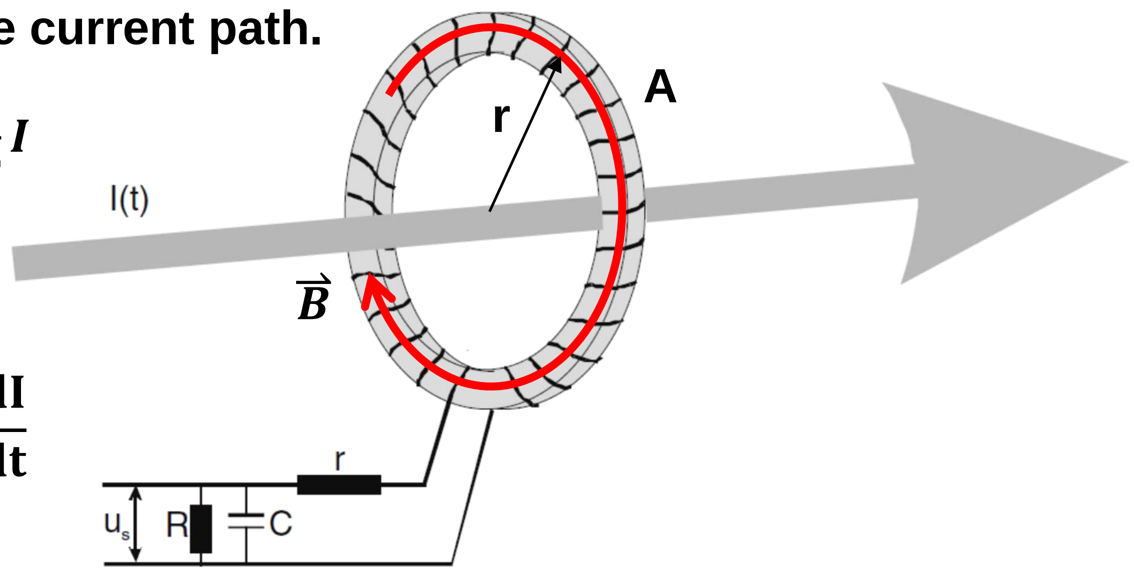

$$u_S(t) = \frac{1}{RC}\int \mathrm{udt} = \frac{1}{RC}\frac{\mu_o AN}{2\pi r}\int \frac{\mathrm{dI}}{\mathrm{dt}}\mathrm{dt} = \frac{1}{RC}\frac{\mu_o AN}{2\pi r} I$$

Assumption for Rogowski coil

- Neglect the spatial dependence of the magnetic induction over the area A
- Cross section A are all the same.
- Number of turns per unit length is const.
- When #/ of turns increase,

  L may be large

  => Lω << R may not be met.

  => use the opposite regime

  where Lω >> R.

  It becomes "self-integrated."

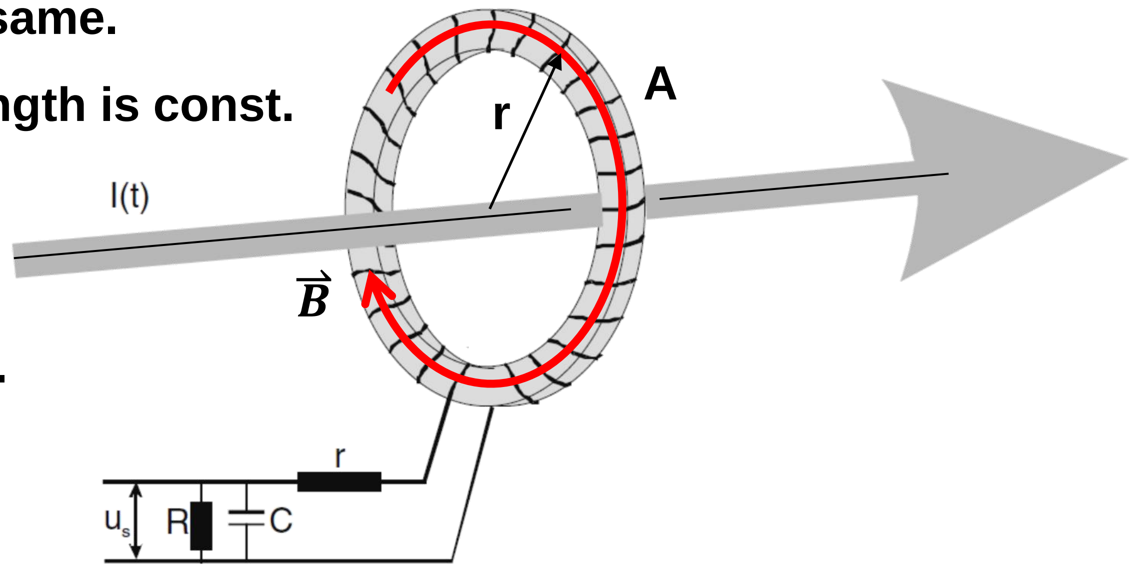

Self-integrated current monitor where Lω >> R

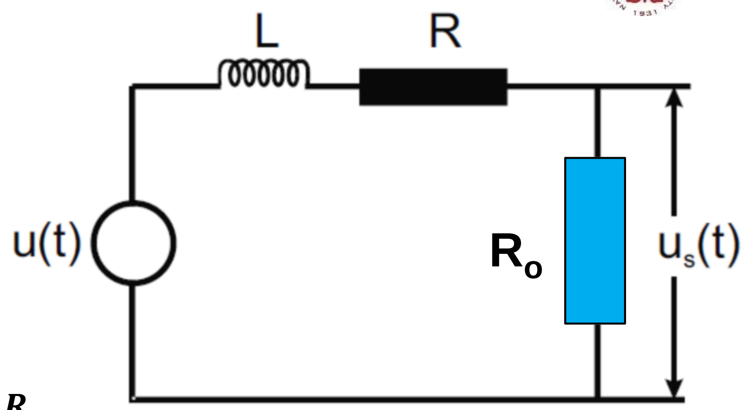

$R_o >> R \qquad L\omega >> R_o + R$

$u - L\frac{\mathrm{dI}}{\mathrm{dt}} = u_S \qquad u_S = \mathrm{IR}_o$

$u - \frac{L}{R_o}\frac{\mathrm{du}_s}{\mathrm{dt}} = u_S \qquad \frac{du_S}{\mathrm{dt}} + \frac{R_o}{L}u_S = \frac{R_o}{L}u$

$e^{-\frac{R_o}{L}t}\frac{d}{\mathrm{dt}}\left(u_s e^{\frac{R_o}{L}t}\right) = \frac{R_o}{L}u \qquad \frac{d}{\mathrm{dt}}\left(u_s e^{\frac{R_o}{L}t}\right) = \frac{R_o}{L}\mathrm{ue}^{\frac{R_o}{L}t}$

$u_S e^{\frac{R_o}{L}t} - u_S(0) = \frac{R_o}{L}\int \mathrm{ue}^{\frac{R_o}{L}t'}\mathrm{dt}'$

$u_s = \frac{R_o}{L}e^{-\frac{R_o}{L}t}\int \mathrm{ue}^{\frac{R_o}{L}t'}\mathrm{dt}' \qquad \mathrm{L}\omega >> R_o \qquad t\frac{R_o}{L} \ll 1 \quad |u| = \frac{\mathrm{d\phi}}{\mathrm{dt}} = N\frac{\mathrm{d\phi_1}}{\mathrm{dt}} = \frac{\mu_o\mathrm{AN}}{2\pi\mathrm{r}}\frac{\mathrm{dI}}{\mathrm{dt}}$

$u_s = \frac{R_o}{L}\int \mathrm{udt}' = \frac{R_o}{L}\int \frac{\mu_o\mathrm{AN}}{2\pi\mathrm{r}}\frac{\mathrm{dI}}{\mathrm{dt}}\mathrm{dt}' = \frac{R_o}{L}\frac{\mu_o\mathrm{AN}}{2\pi\mathrm{r}}I$ **<= self integrated!**

$\boxed{u_S \propto R_o}$

- **Ferromagnetic material in the torus may be used to increase inductance.**

Additional note for Rogowski coil

- To reduce the capacitive coupling, wrap the Rogowski coil with a slotted metallic case. However, it need to let the flux goes into the winding. NO closed loop is allowed.
- A large flux penetrating the main opening of the torus may induce additional voltage. To compensate for this signal, feed one end of the wire back through the windings

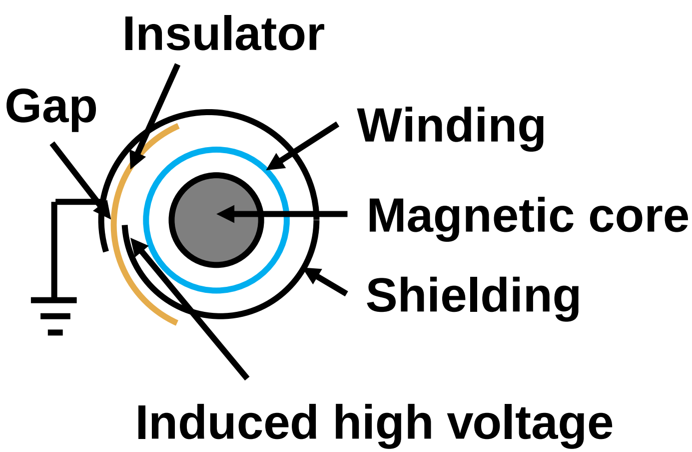

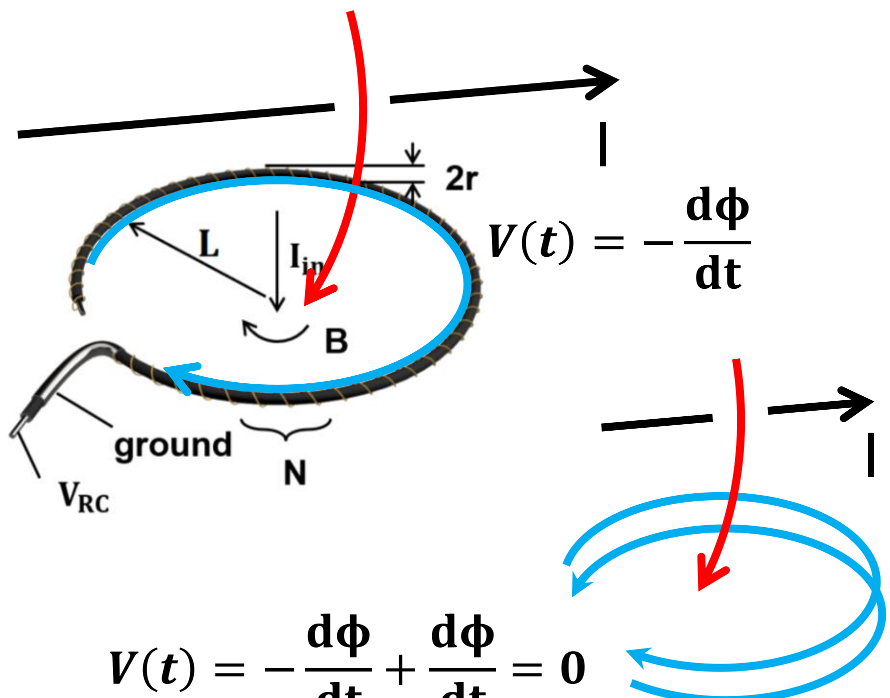

$$V(t) = -\frac{\mathrm{d}\phi}{\mathrm{d}t}$$

$$V(t) = -\frac{\mathrm{d}\phi}{\mathrm{d}t} + \frac{\mathrm{d}\phi}{\mathrm{d}t} = 0$$

Chih-Rui Hsieh, Master thesis (2020)

Fabrication of the Rogowski coil using a coaxial cable

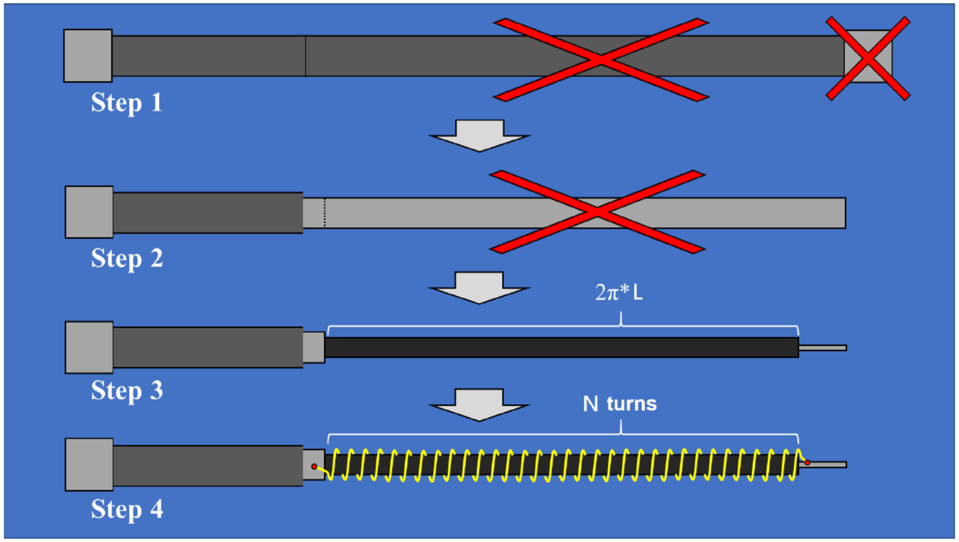

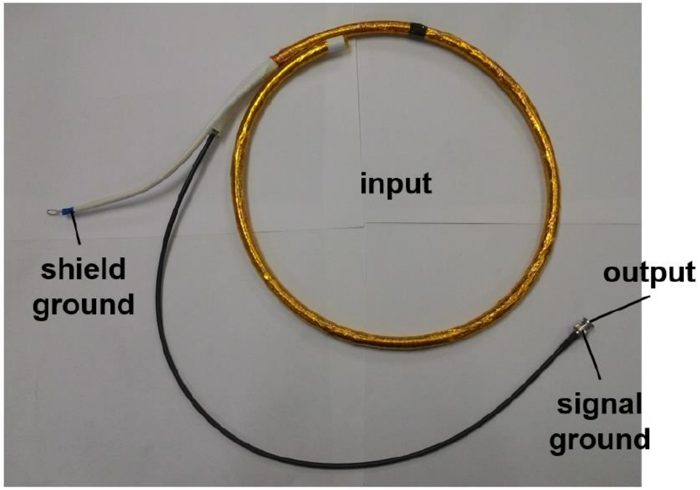

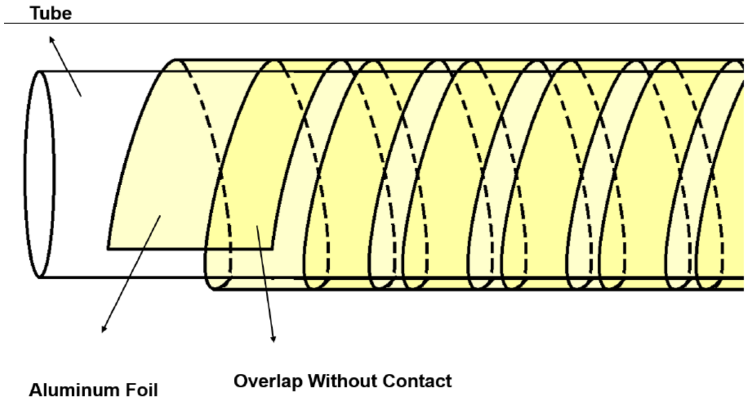

Chih-Rui Hsieh, Master thesis (2020)

Other ways of making compensated Rogowski coil

- **Bifiliar**
- **Inner compensating coil**
- **Outer compensating coil**

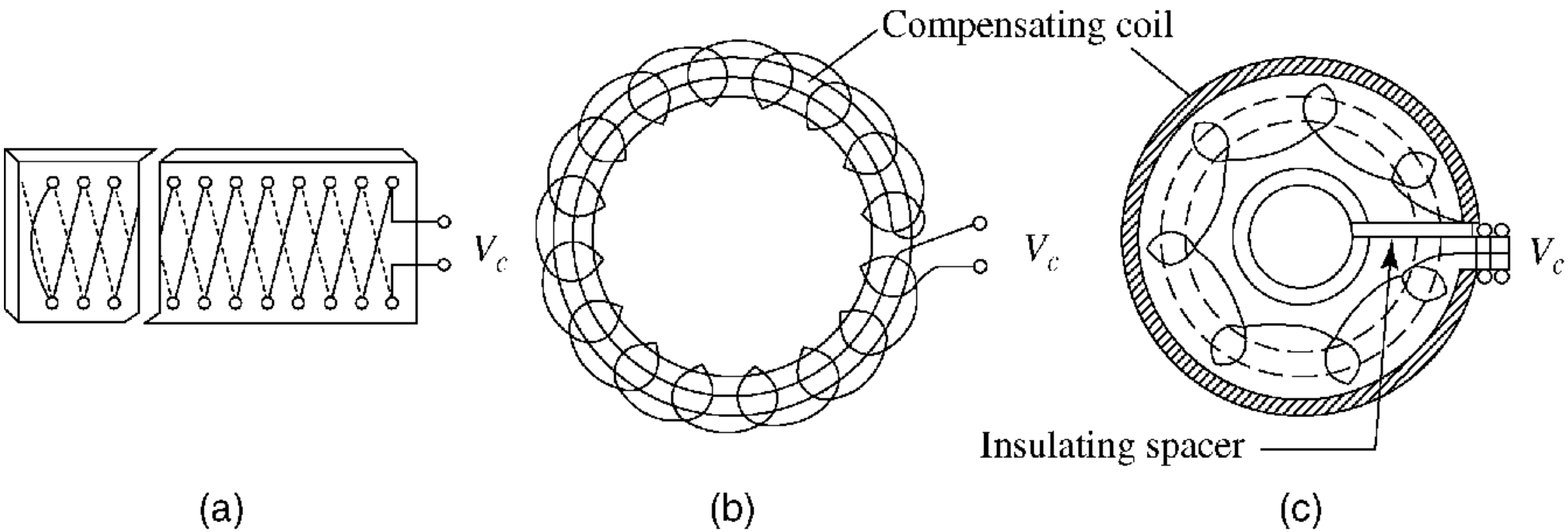

Current-viewing resistors (CVRs)

- **It is also called "shunts."**
- **Measurement of the voltage drop across a resistor of known value, incorporated into the circuit.**

$$I = \frac{V}{R}$$

- **The current path and the measuring circuit are coupled not only through the Ohmic resistor but also magnetically.**

=> preferable to place the metering contact in a field-free space or reduce the coupling efficiency.

- **Cylindrically symmetric shunt geometry provides an zero magnetic coupling.**

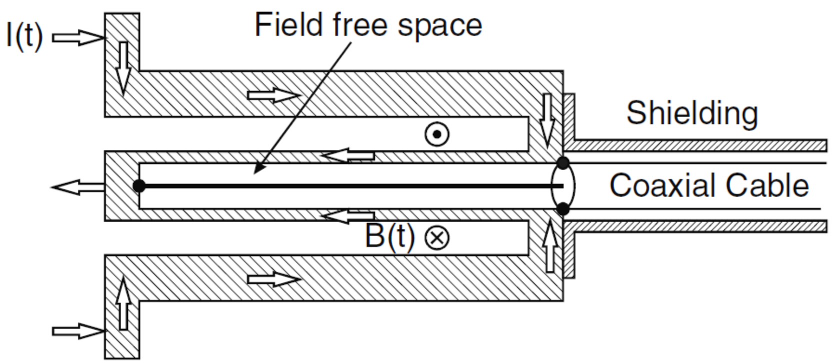

Shunts

- **Folded strip shunt**

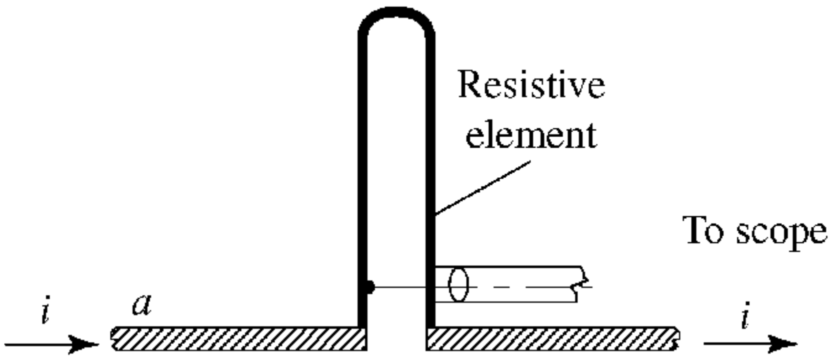

(a)

- **Parallel twisted shunt**

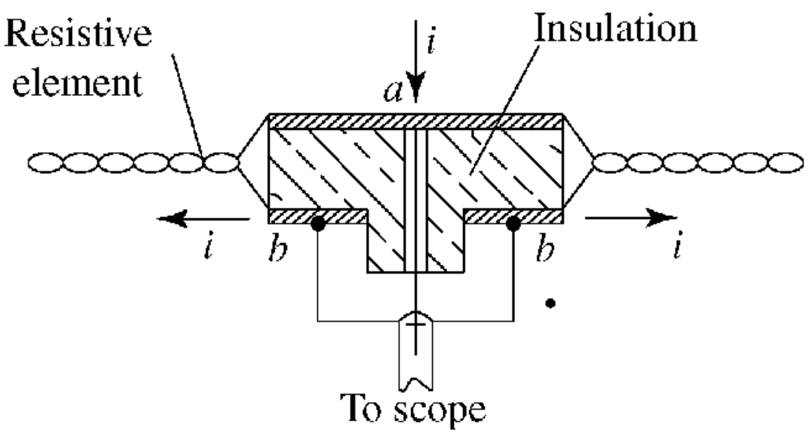

(b)

CVR integrated into the outer conductor of a coaxial transmission line

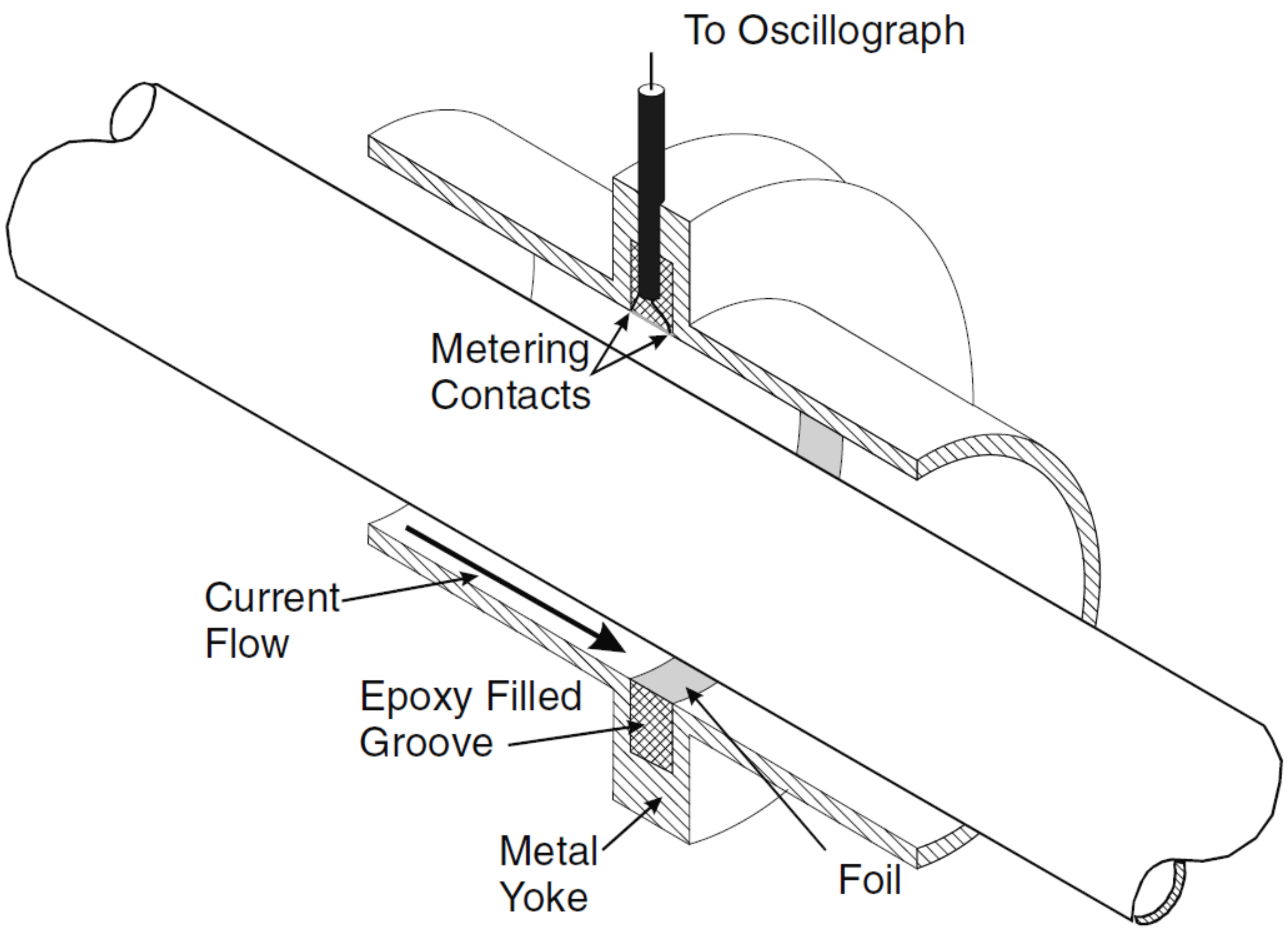

Example of current and voltage monitor using B-dot and D-dot monitors

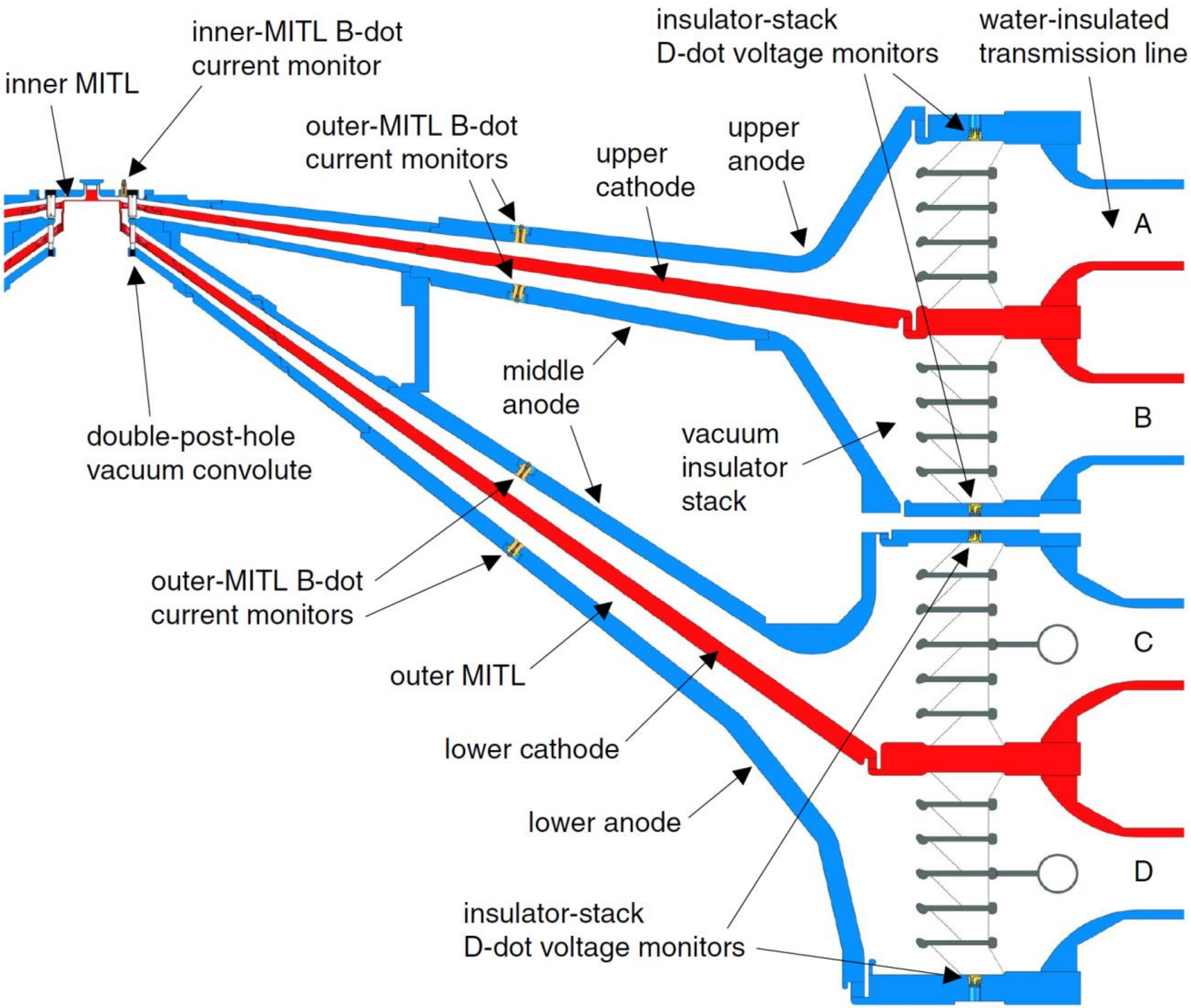

T. C. Wagoner, etc., Phys. Rev. ST Accel. Beams 11, 100401 (2008)

Differential current monitors

- **Outer MITL B-dot current monitors:**

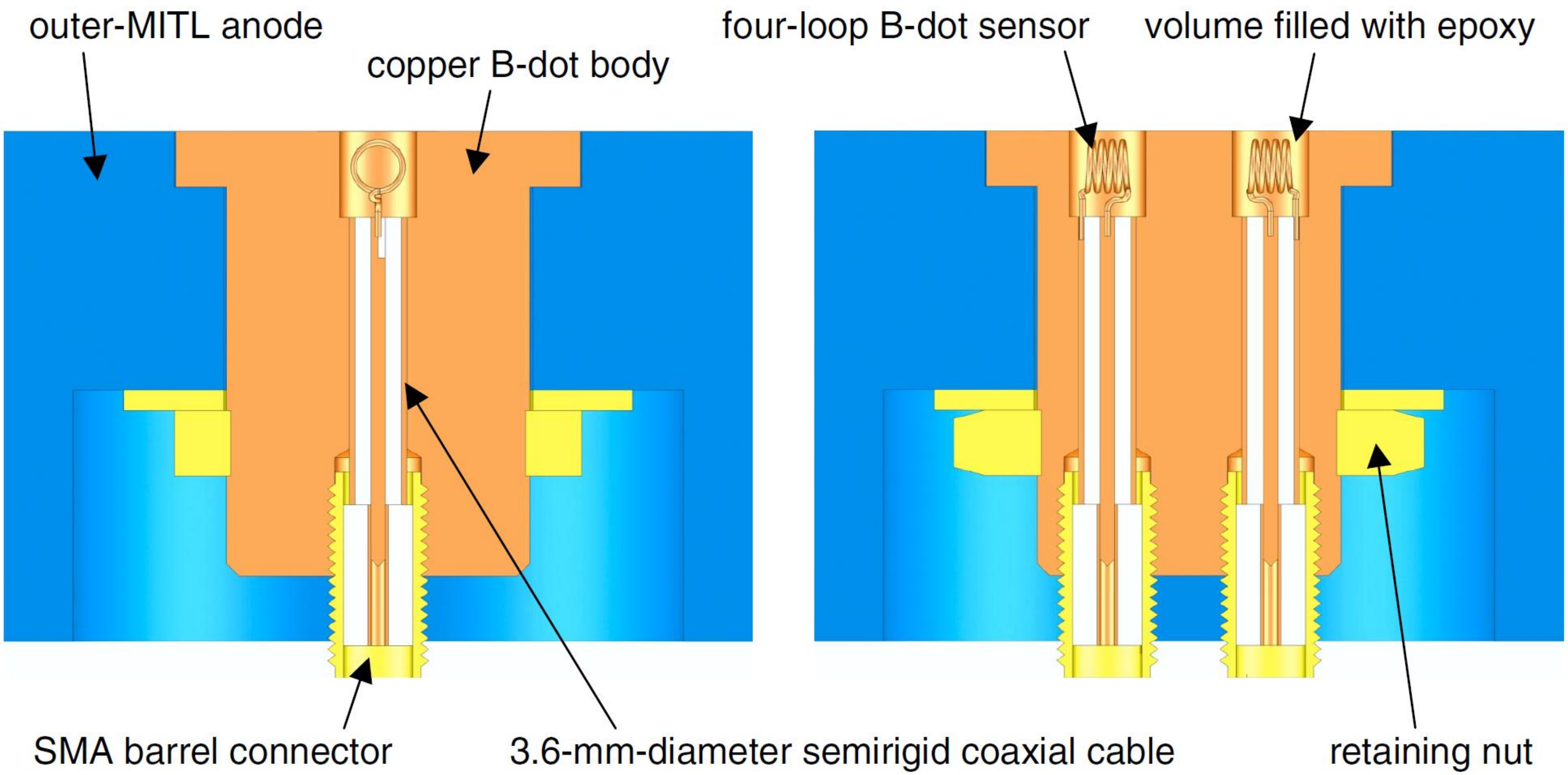

Differential current monitors

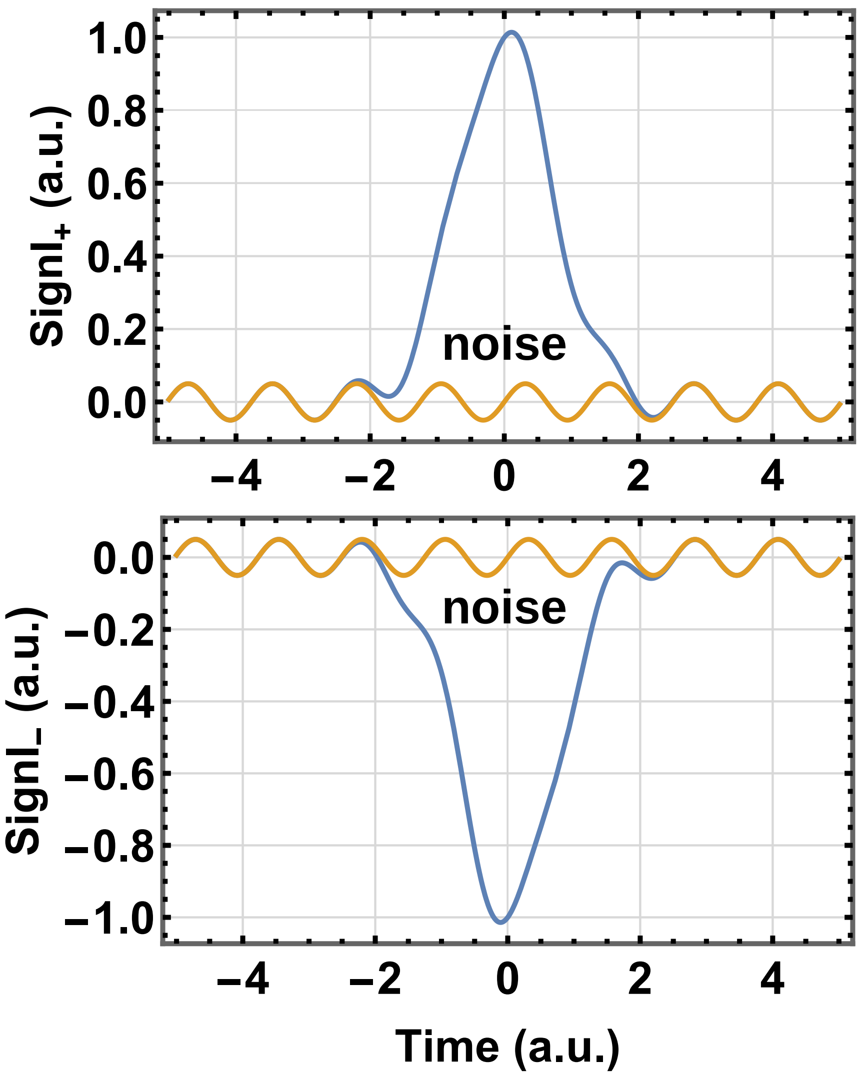

- The two B-dot sensors of each B-dot current monitor are designed to produce "opposite-polarity" signals for "common-mode-noise" rejection.

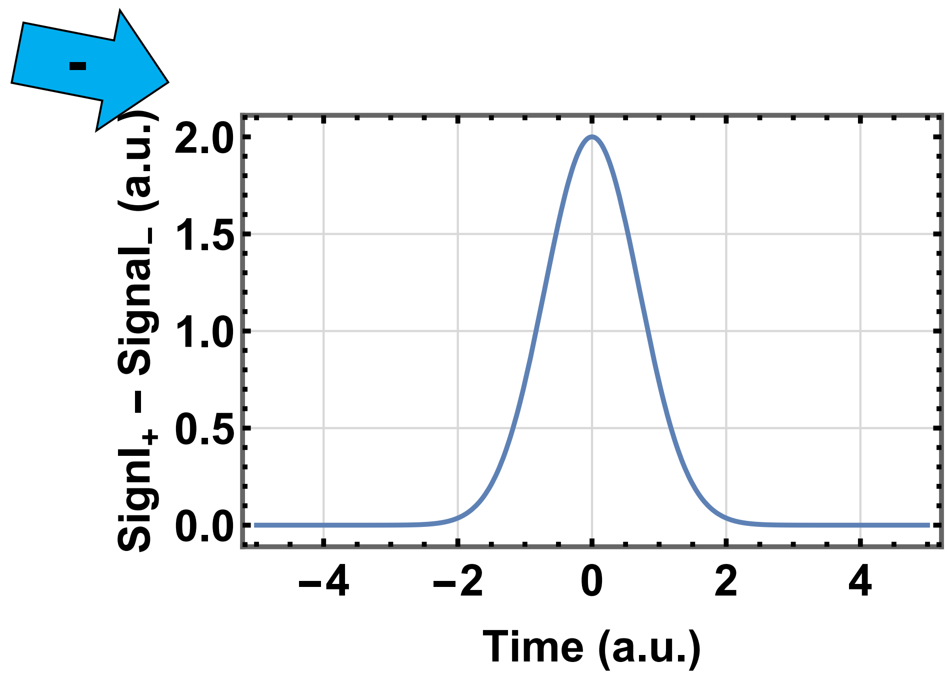

Differential voltage monitor

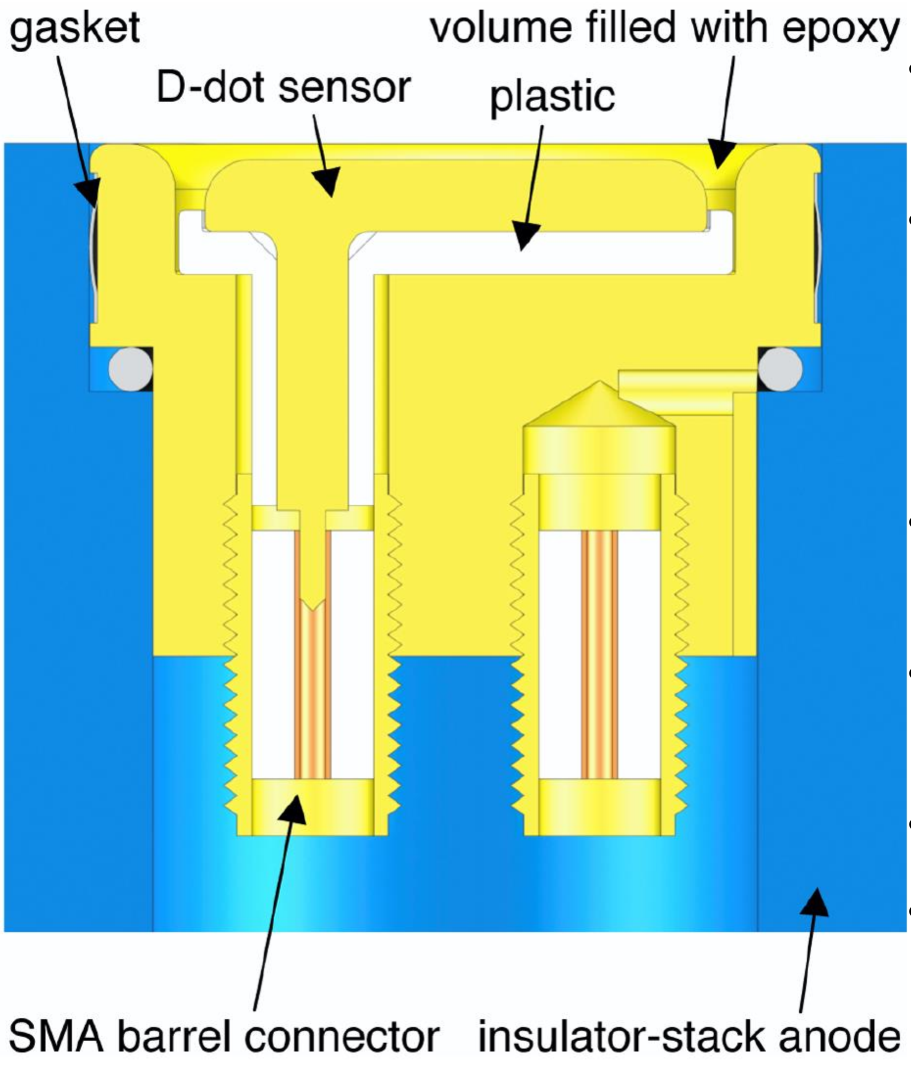

- **D-dot voltage monitor: the displacement-current monitor**
- **Opening-circuit termination for null measurements, i.e., common-mode noise reduction.**

- **Vacuum potted using stycast epoxy.**
- **Common-mode noise reduction is applied.**
- **Numerically cable compensated.**
- **Numerically integrated the signal.**

Voltage divider using resistors

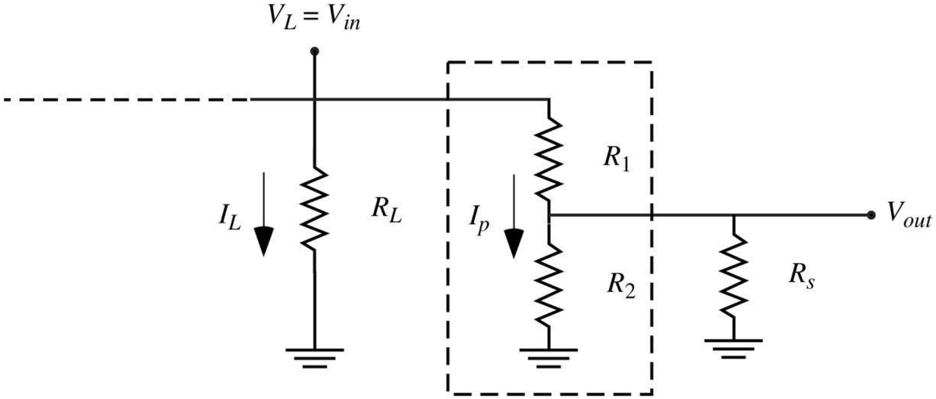

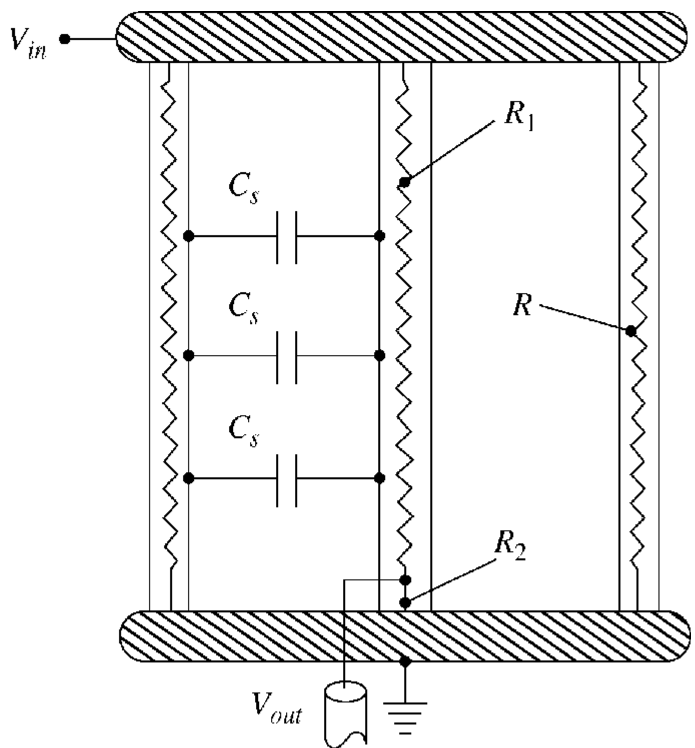

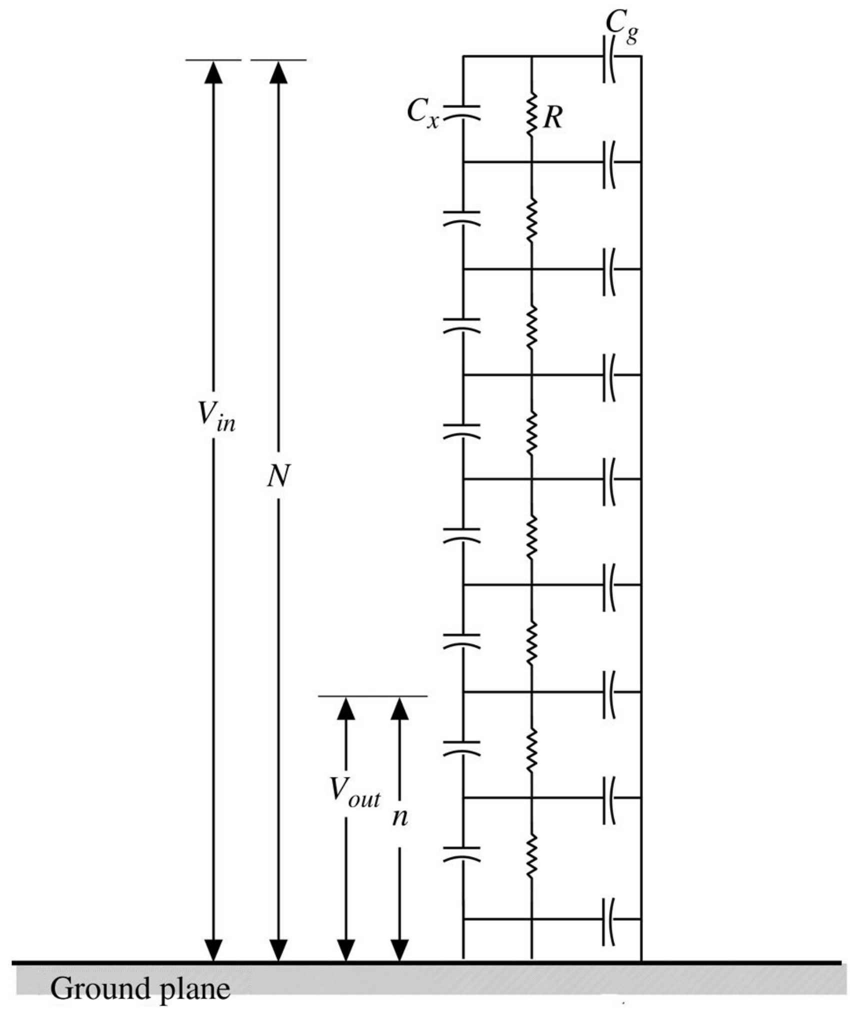

Voltage divider liquid resistors and grading electrodes

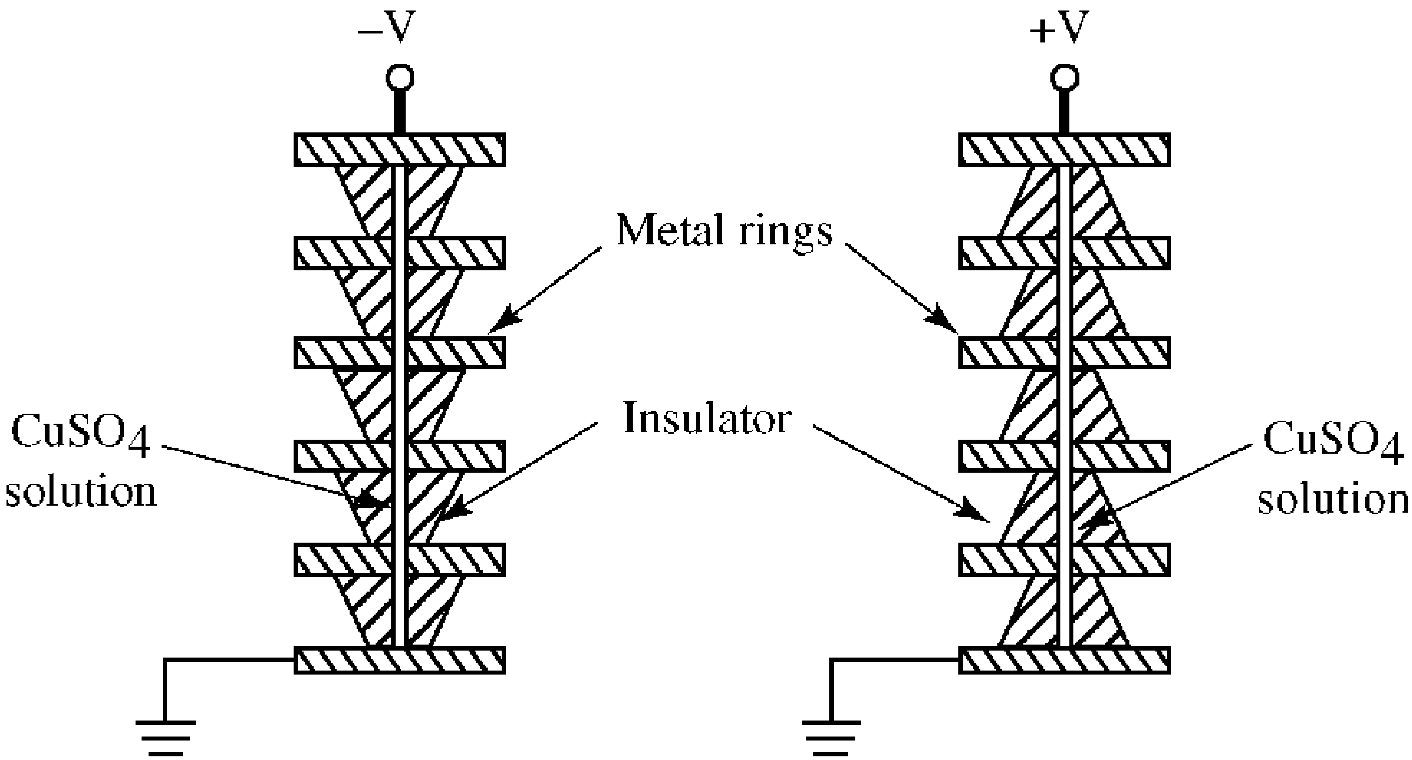

Voltage divider on Mega Ampere Generator for Plasma Implosion Experiments (MAGPIE) facility

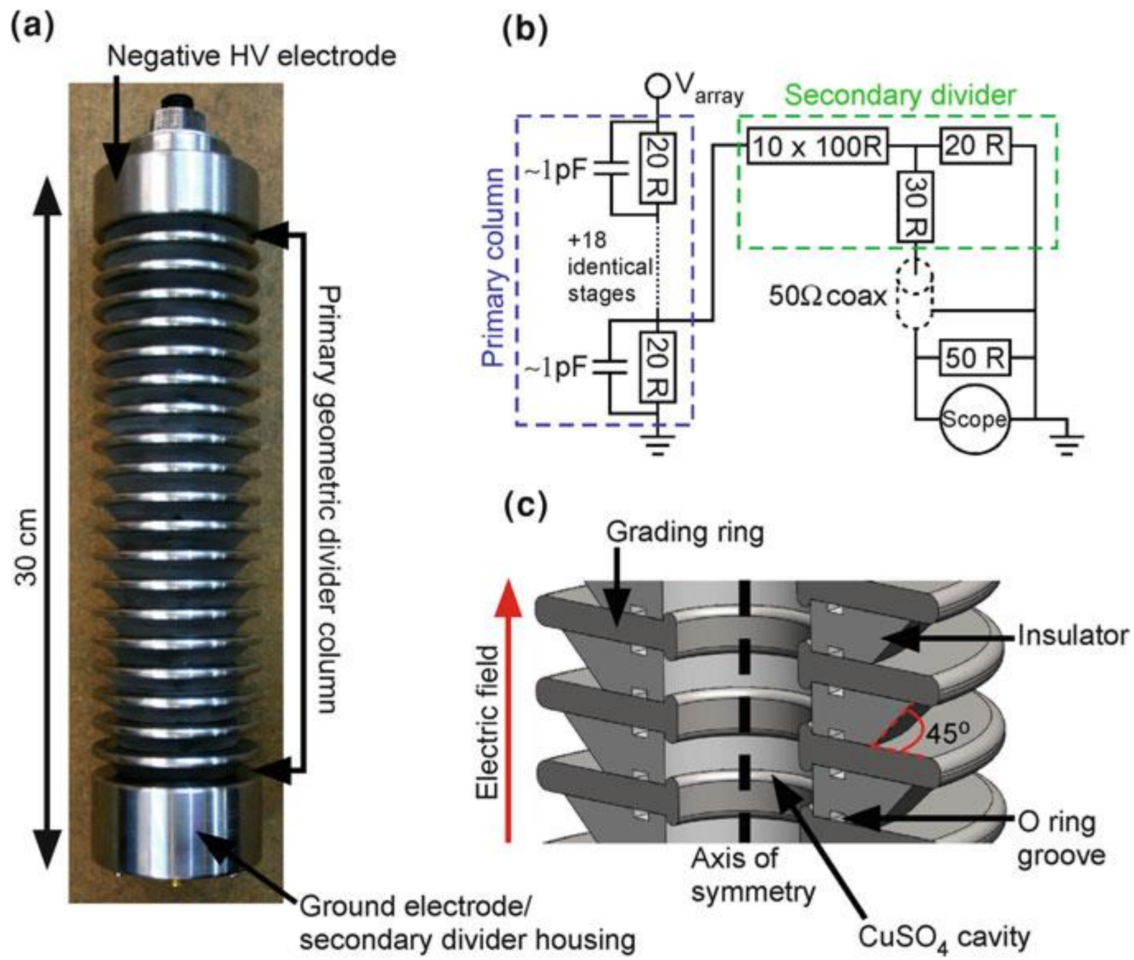

Guy C. Burdiak, Cylindrical Liner Z-pinches as Drivers for Converging Strong Shock Experiments

Voltage divider on Mega Ampere Generator for Plasma Implosion Experiments (MAGPIE) facility

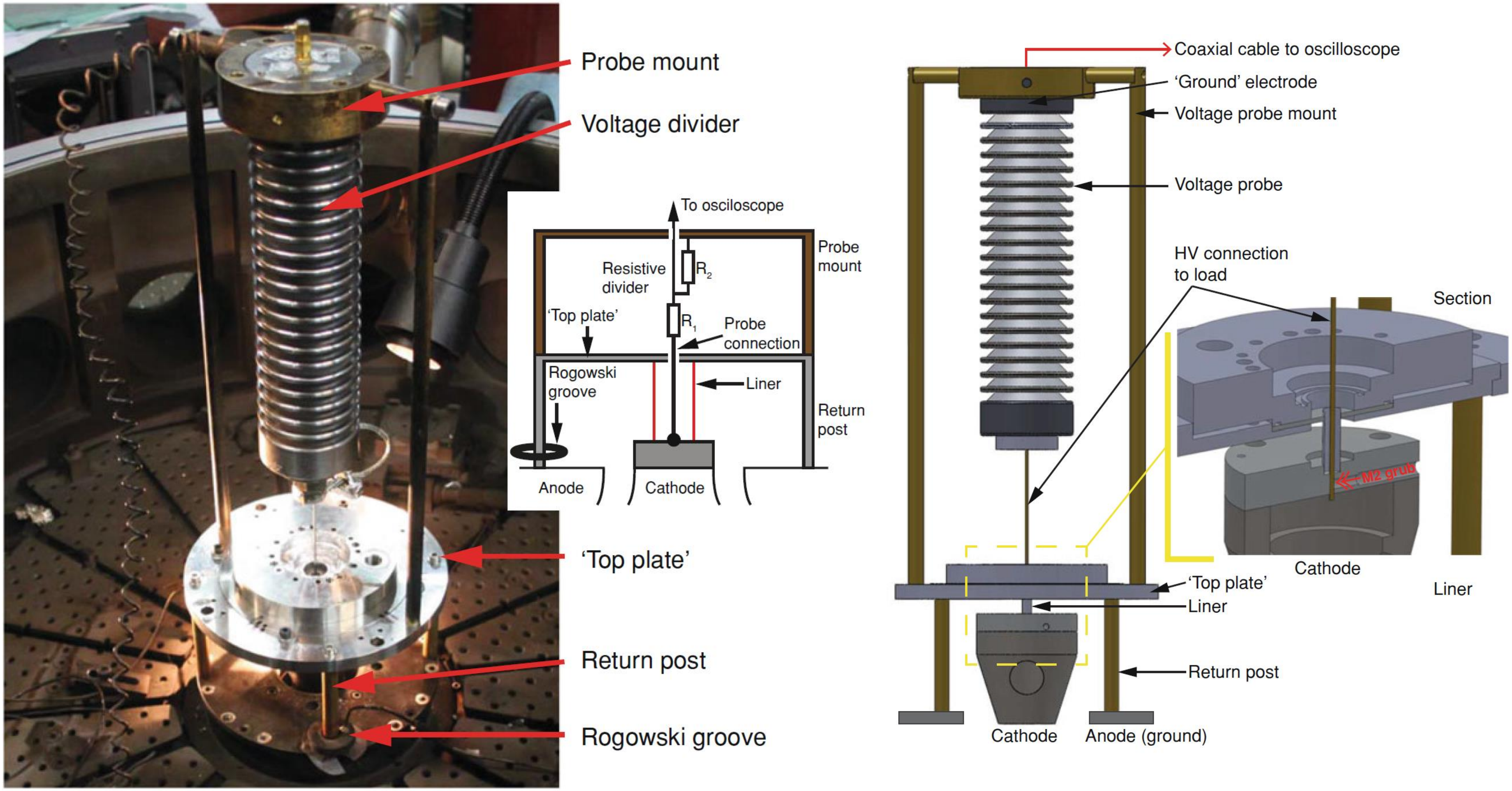

Guy C. Burdiak, Cylindrical Liner Z-pinches as Drivers for Converging Strong Shock Experiments

Voltage divider on Mega Ampere Generator for Plasma Implosion Experiments (MAGPIE) facility

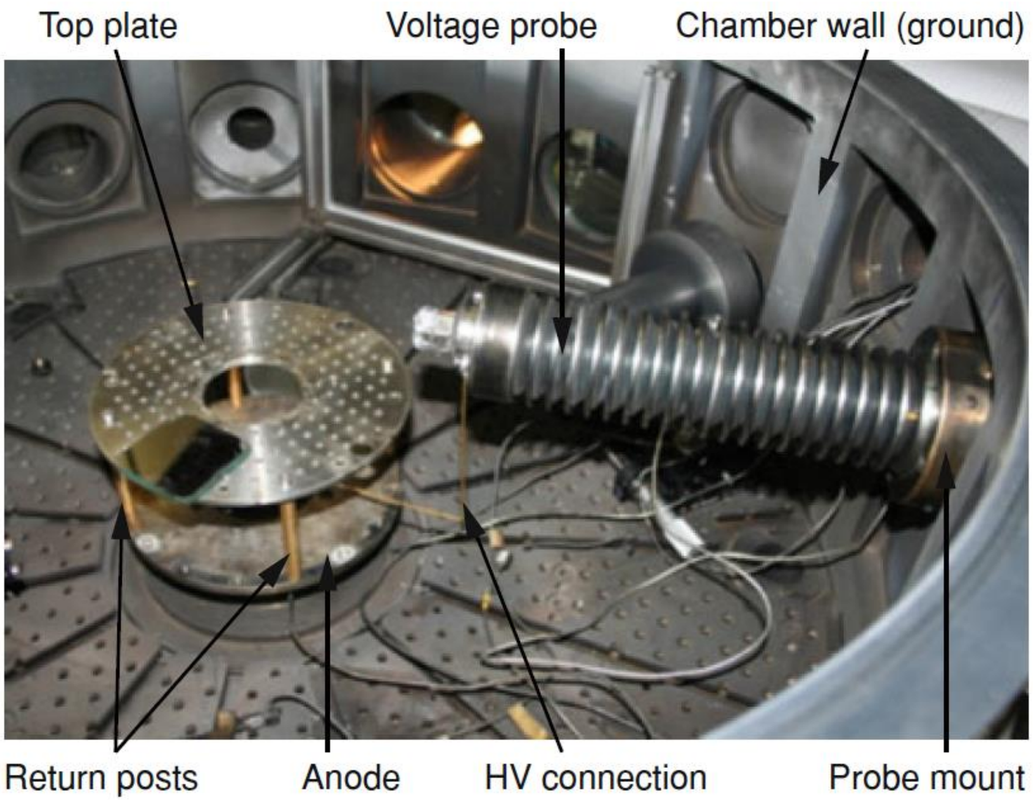

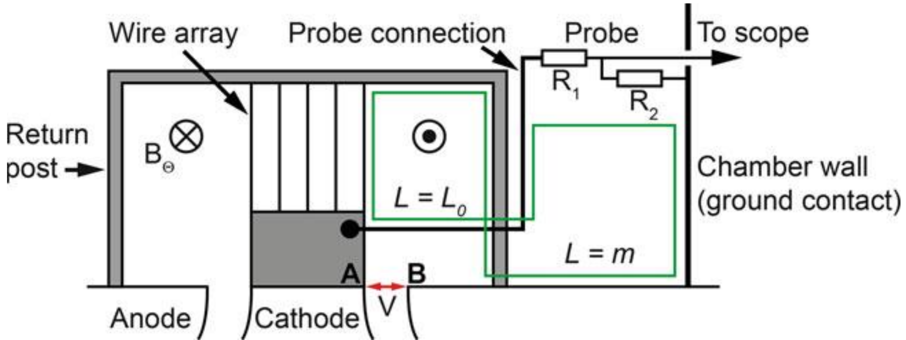

Guy C. Burdiak, Cylindrical Liner Z-pinches as Drivers for Converging Strong Shock Experiments

Voltage divider using both resistors and capacitors

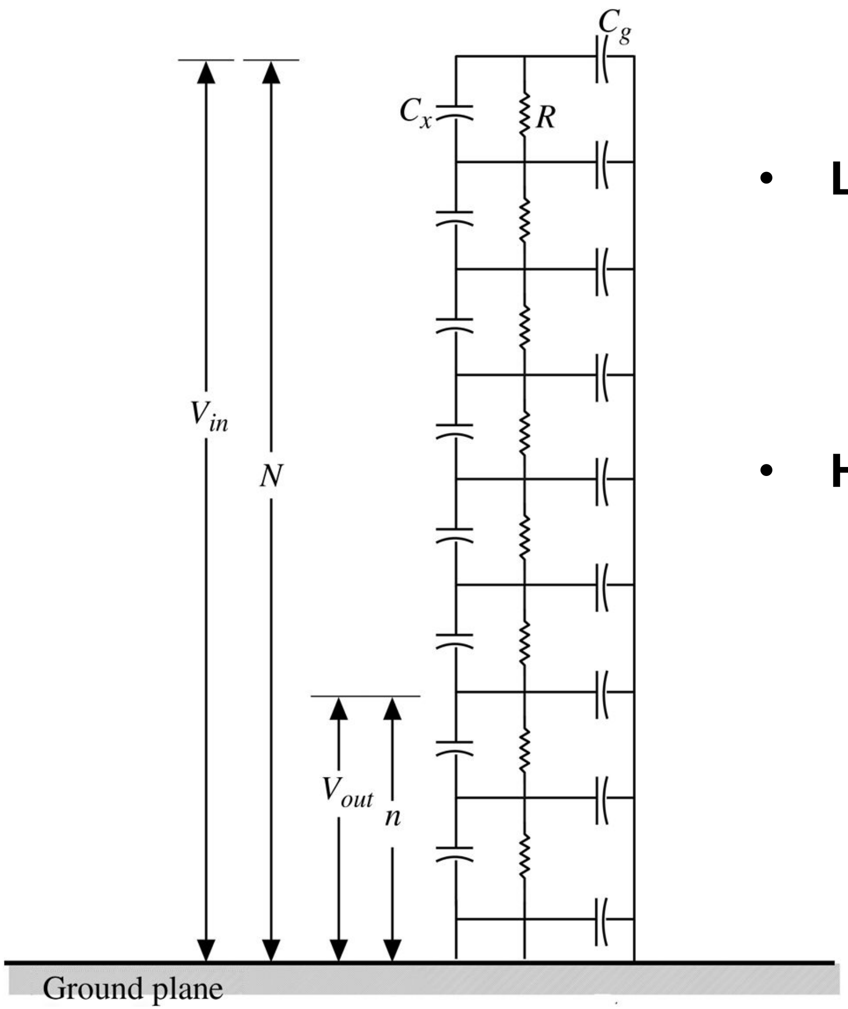

- **Low frequency:**

$$V_{\text{out}} = \frac{R_o}{\Sigma R_o} V_{\text{in}} = \frac{R_o}{N R_o} V_{\text{in}} = \frac{1}{N} V_{\text{in}}$$

- **High frequency:**

$$V_{\text{out}} = \frac{\dfrac{C_o}{N-1}}{\dfrac{C_o}{N-1} + C_o} V_{\text{in}} = \frac{\dfrac{1}{N-1}}{\dfrac{1}{N-1} + 1} V_{\text{in}}$$

$$= \frac{1}{1 + (N-1)} V_{\text{in}} = \frac{1}{N} V_{\text{in}}$$

or $$V_{\text{out}} = \frac{\dfrac{1}{j\omega C_o}}{\sum \dfrac{1}{j\omega C_o}} V_{\text{in}} = \frac{1}{N} V_{\text{in}}$$

Voltage divider on Mega Ampere Generator for Plasma Implosion Experiments (MAGPIE) facility

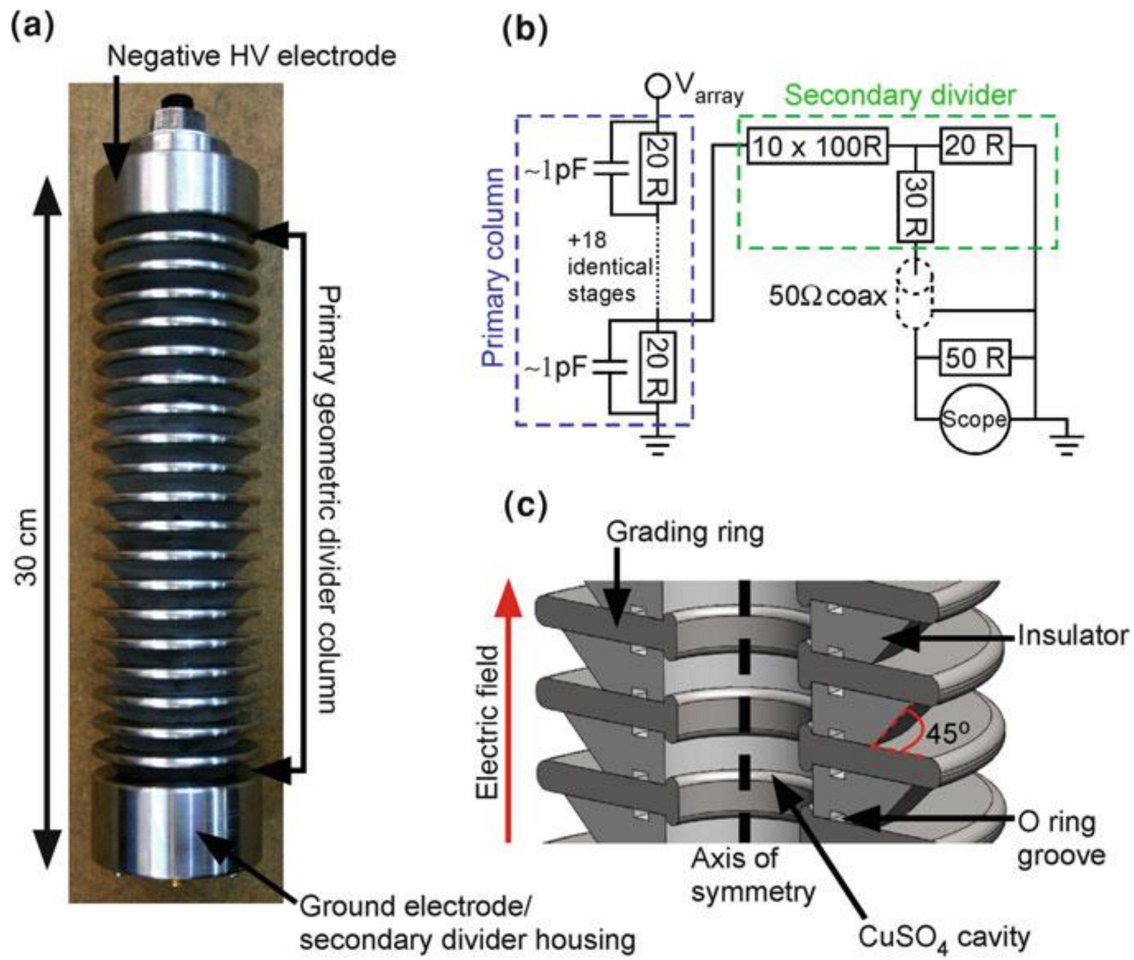

Guy C. Burdiak, Cylindrical Liner Z-pinches as Drivers for Converging Strong Shock Experiments

Voltage divider on Mega Ampere Generator for Plasma Implosion Experiments (MAGPIE) facility

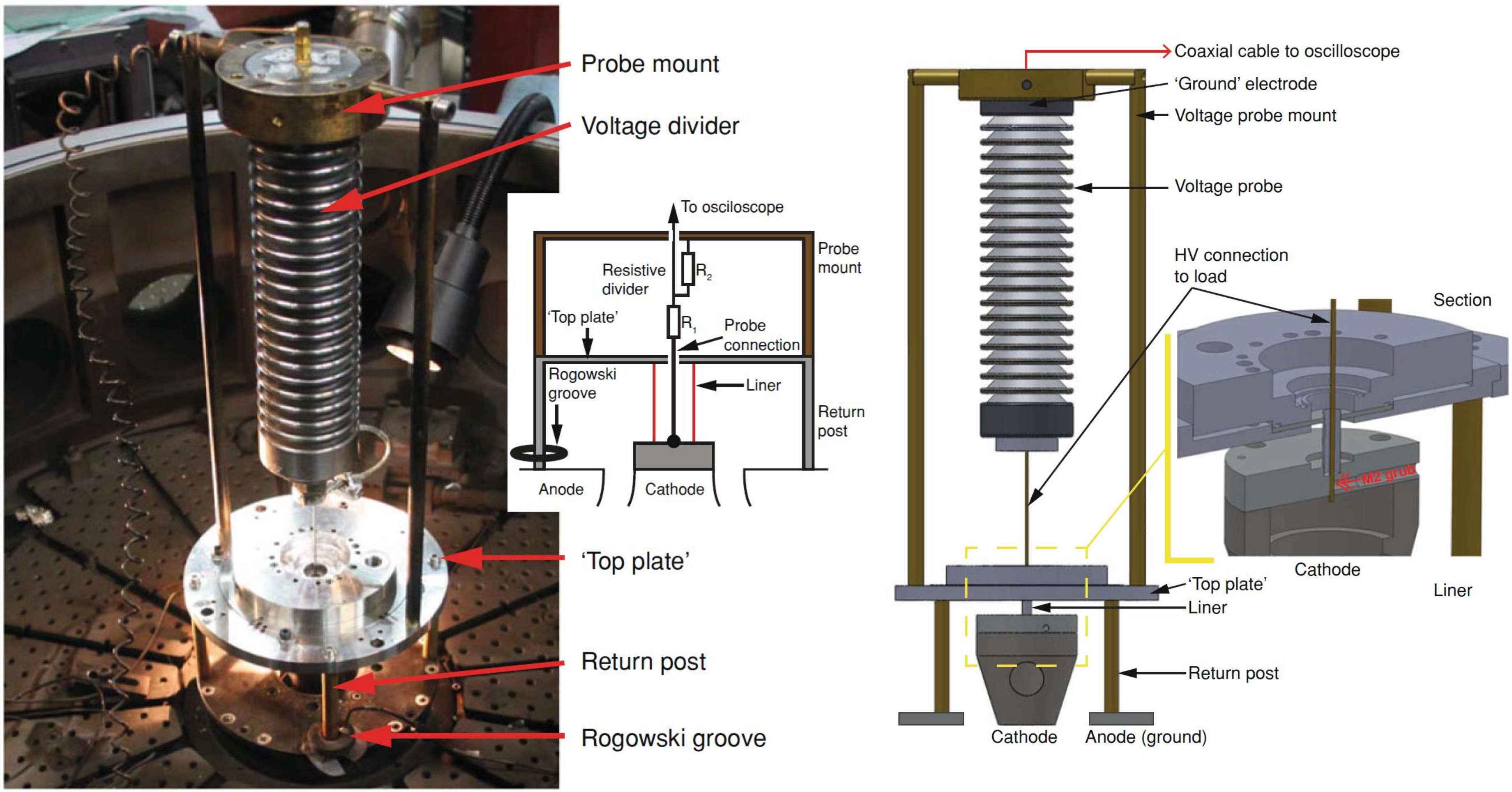

Guy C. Burdiak, Cylindrical Liner Z-pinches as Drivers for Converging Strong Shock Experiments

Voltage divider on Mega Ampere Generator for Plasma Implosion Experiments (MAGPIE) facility

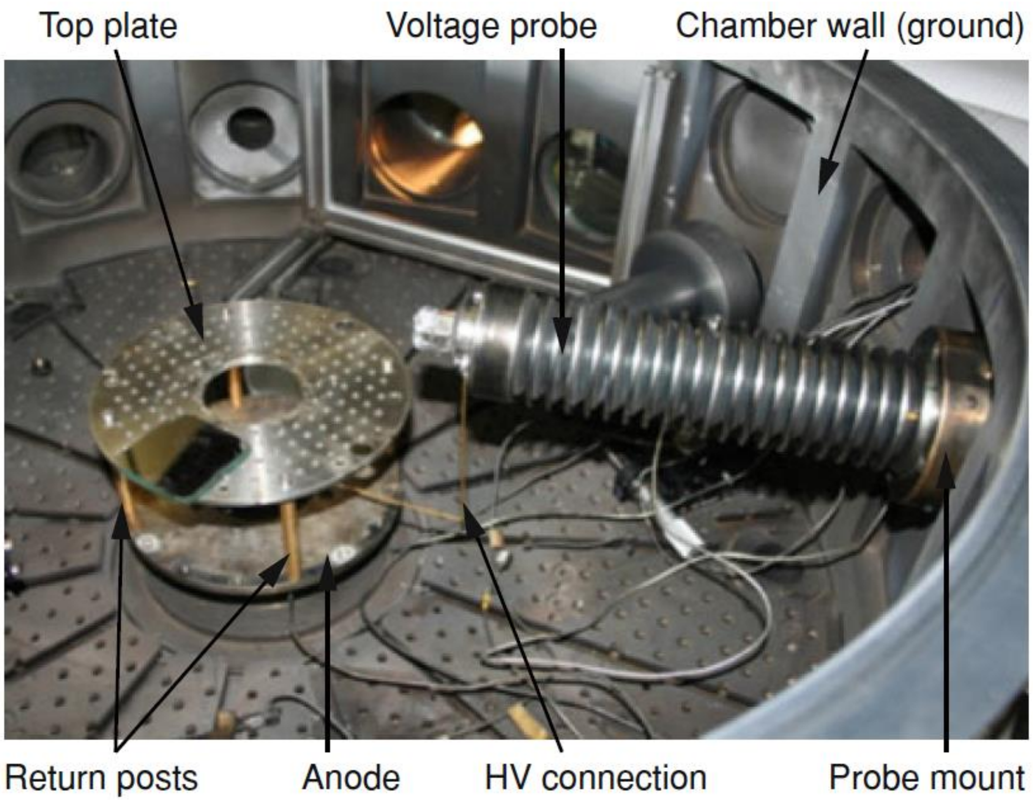

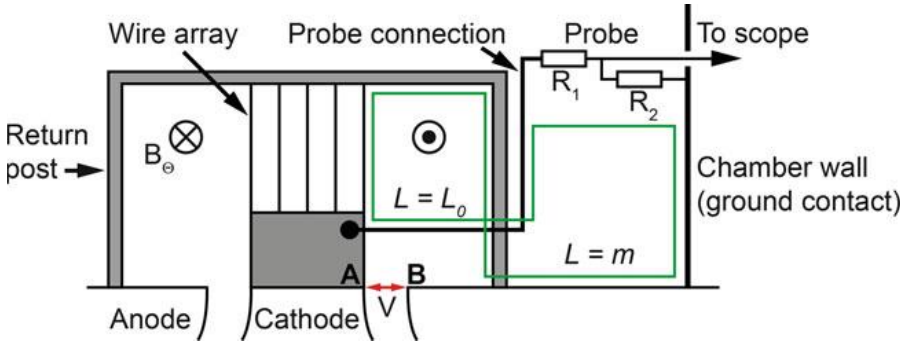

Guy C. Burdiak, Cylindrical Liner Z-pinches as Drivers for Converging Strong Shock Experiments

Voltage divider using both resistors and capacitors

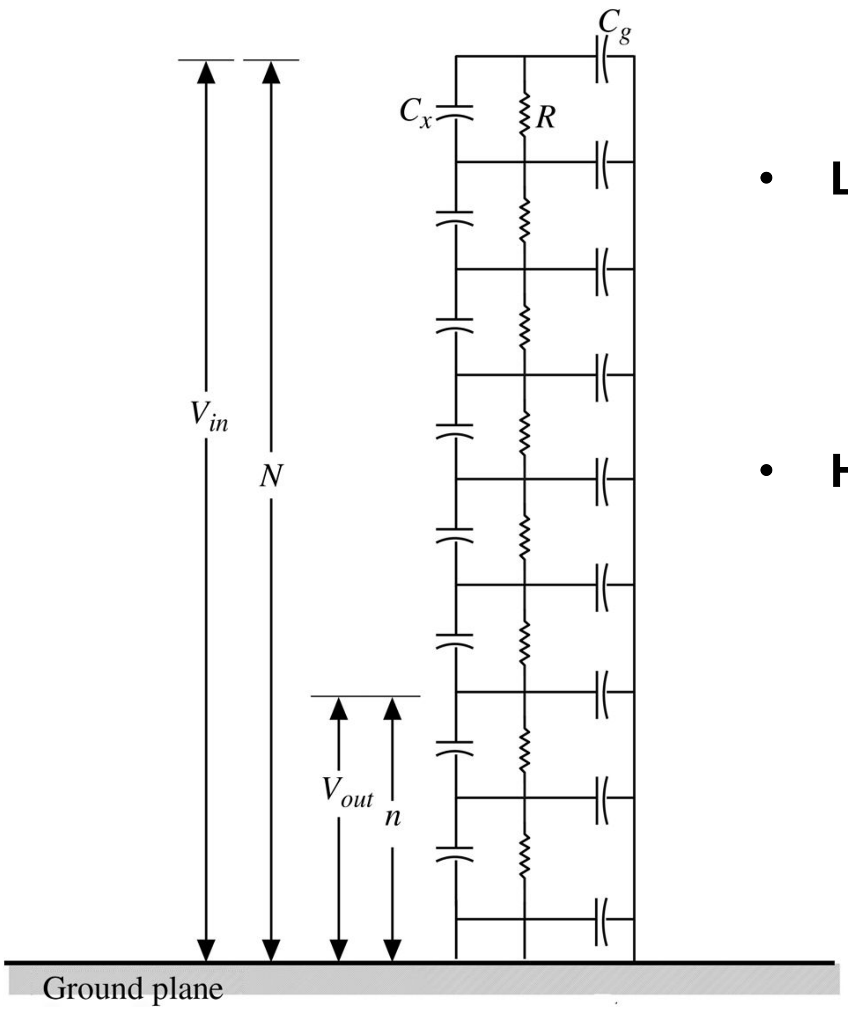

- **Low frequency:**

$$V_{\text{out}} = \frac{R_o}{\Sigma \mathrm{R}_o} V_{\text{in}} = \frac{R_o}{\mathrm{NR}_o} V_{\text{in}} = \frac{1}{N} V_{\text{in}}$$

- **High frequency:**

$$V_{\text{out}} = \frac{\frac{C_o}{N-1}}{\frac{C_o}{N-1} + C_o} V_{\text{in}} = \frac{\frac{1}{N-1}}{\frac{1}{N-1} + 1} V_{\text{in}}$$

$$= \frac{1}{1 + (N-1)} V_{\text{in}} = \frac{1}{N} V_{\text{in}}$$

or $$V_{\text{out}} = \frac{\frac{1}{j\omega C_o}}{\sum \frac{1}{j\omega C_o}} V_{\text{in}} = \frac{1}{N} V_{\text{in}}$$

Outlines

- Power and voltage adding
  - Marx generator
  - LC generator
  - Line pulse transformers
  - Induction voltage adder (IVA)
  - Linear induction accelerator (LIA)
  - Linear transformer driver (LTD)
- Diagnostics
  - Voltage measurement
  - Current measurement
- **Applications of pulsed-power system**

Karlsruche Light Ion Facility (KALIF)

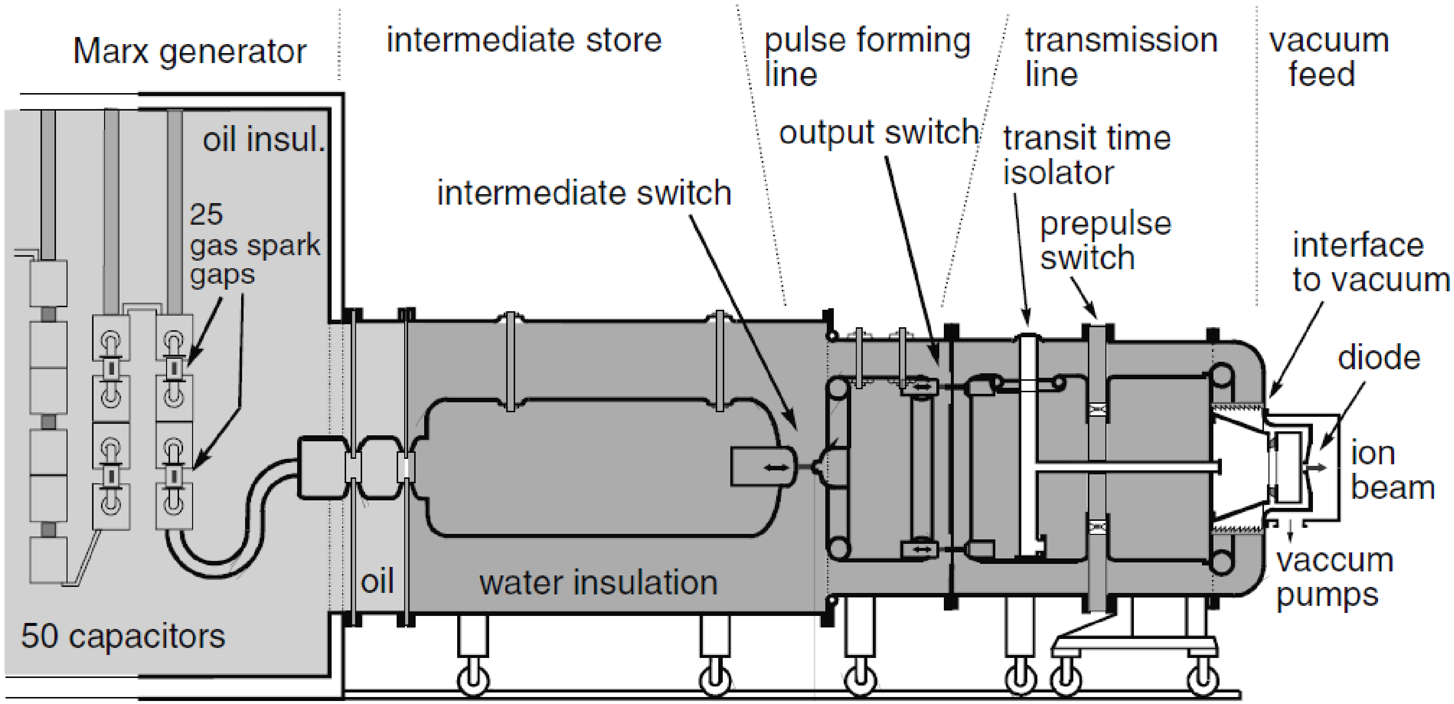

Fig. 8.1. Schematic illustration of the 1.5 TW pulse generator KALIF. The data for the pulse at the vacuum interface are: power = 1.5 TW, voltage = 1.7 MV, pulse duration = 50 ns, pulse energy = 75 kJ, electrical efficiency = 30%

Magpie at Imperial college

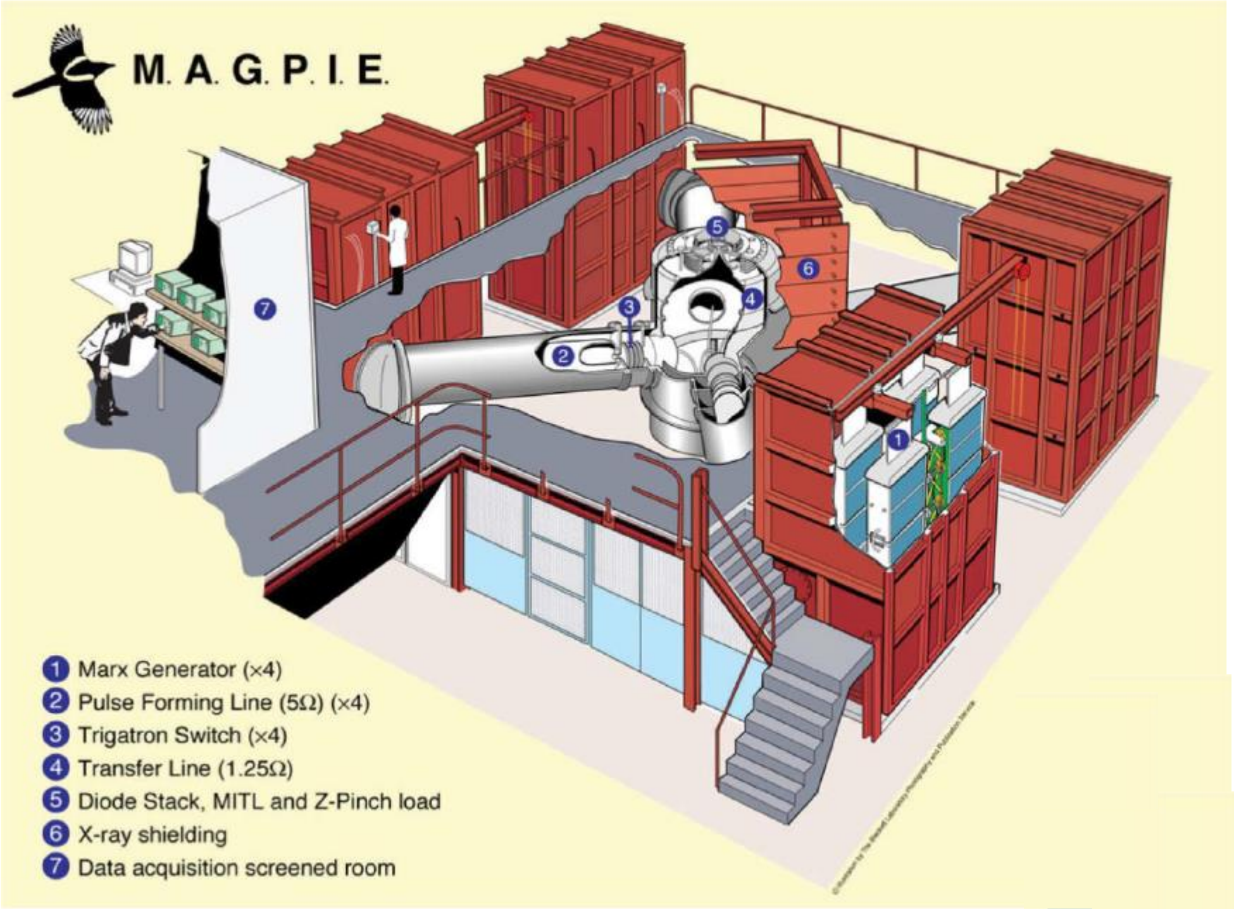

E = 86 kJ
I = 1 MA
T_{rise} = 250 ns

R. D. McBride, *et. cl.*, IEEE TRANS. PLAS. SCIE., 46, 3928 (2018)

Cobra at Cornell University

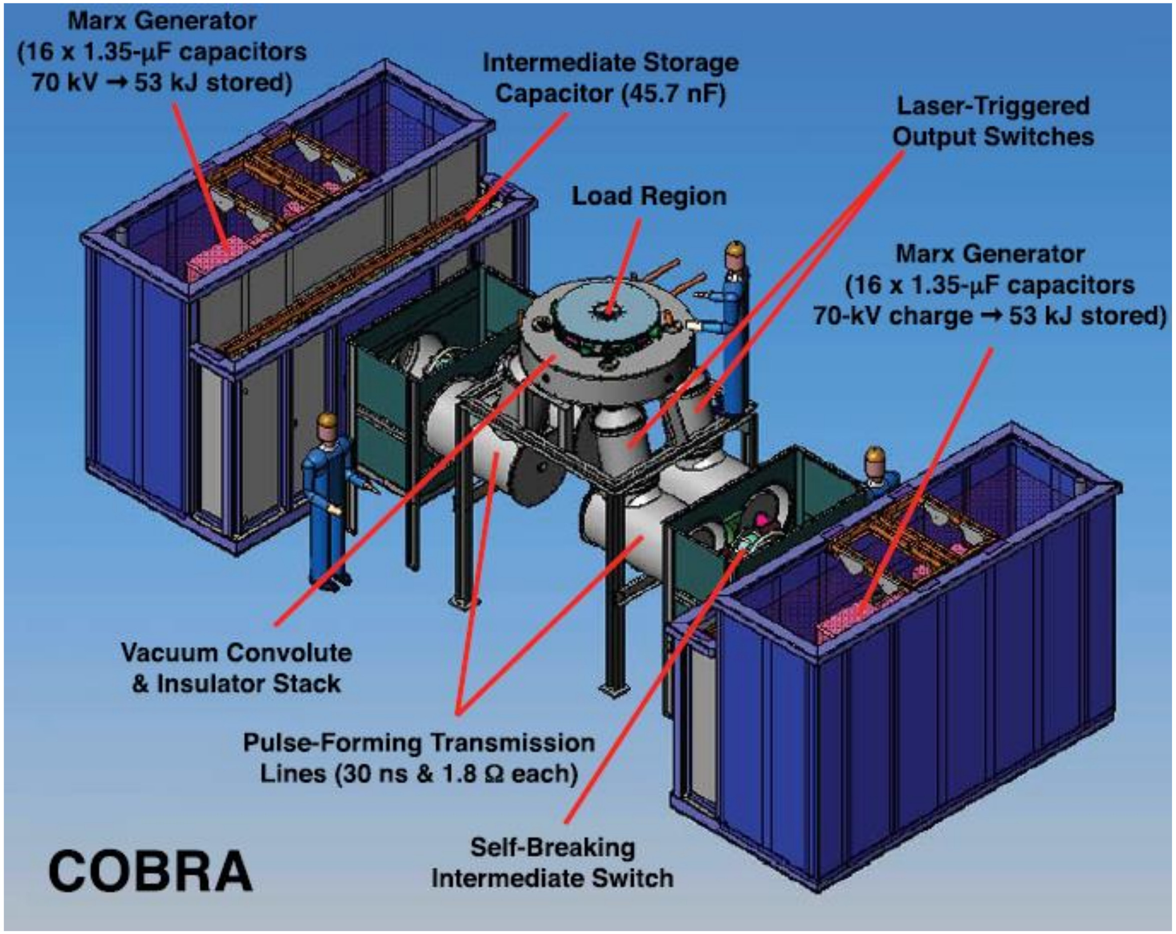

E = 105 kJ
I = 1 MA
T_{rise} = 100 ns

R. D. McBride, *et. cl.*, IEEE TRANS. PLAS. SCIE., 46, 3928 (2018)

Zebra at University of Nevada, Reno

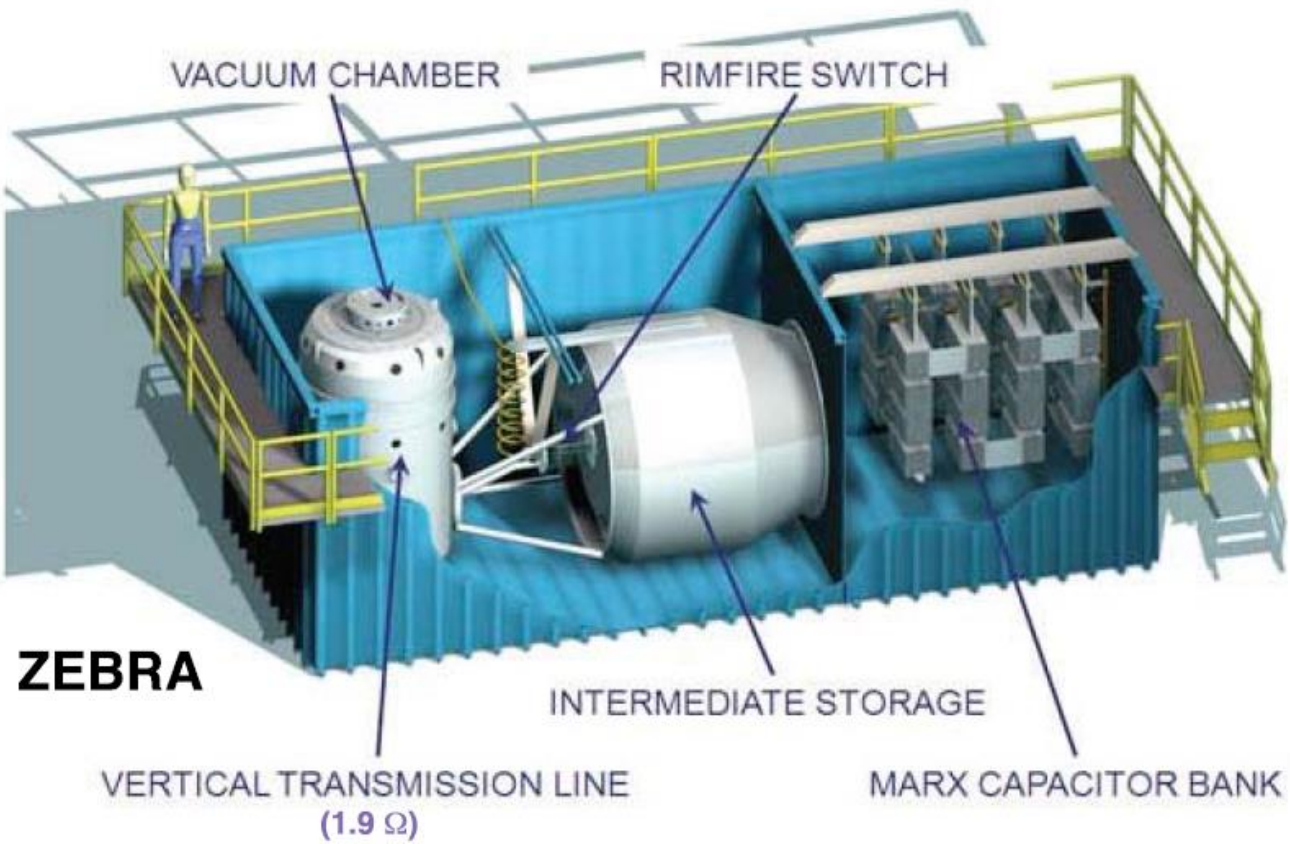

E = 200 kJ
I = 1 MA
T_{rise} = 100 ns

R. D. McBride, *et. cl.*, IEEE TRANS. PLAS. SCIE., 46, 3928 (2018)

Maize LTD at University of Michigan

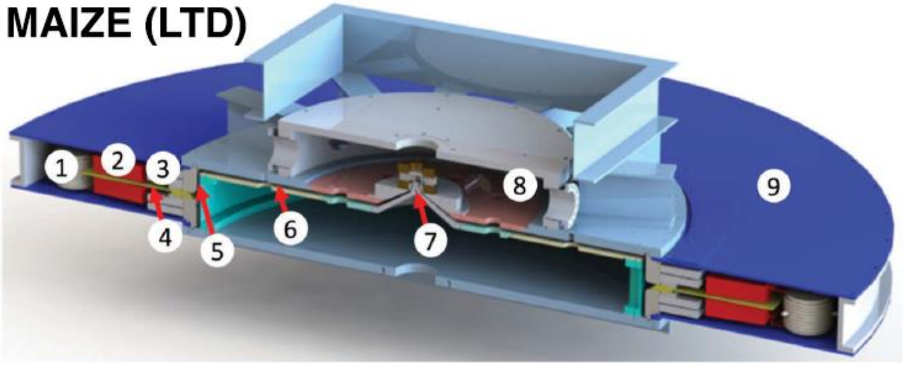

E = 16 kJ
I = 1 MA
T_{rise} = 100 ns

R. D. McBride, *et. cl.*, IEEE TRANS. PLAS. SCIE., 46, 3928 (2018)

Hades at University of Rochester

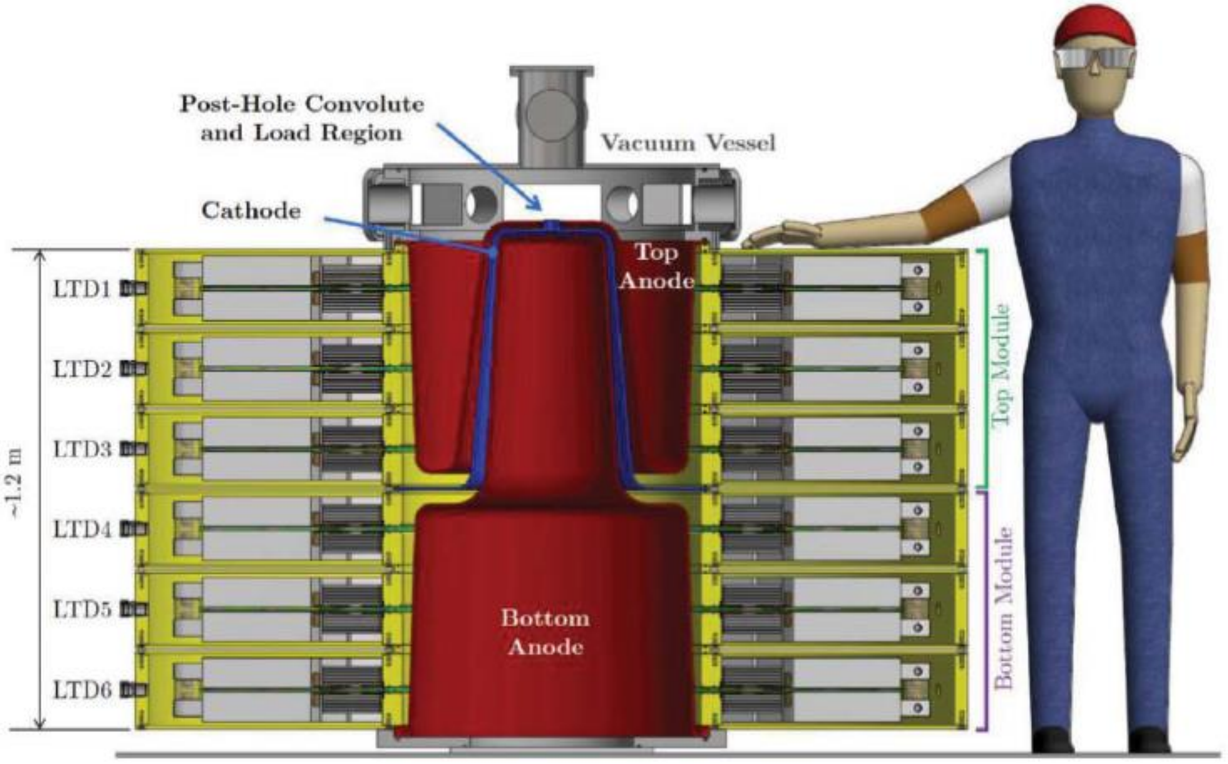

E = 75 kJ
I = 1 MA
T_{rise} = 125 ns

R. D. McBride, *et. cl.*, IEEE TRANS. PLAS. SCIE., 46, 3928 (2018)

Particle Beam Fusion Accelerator (PBFA 2) and the Z-Machine

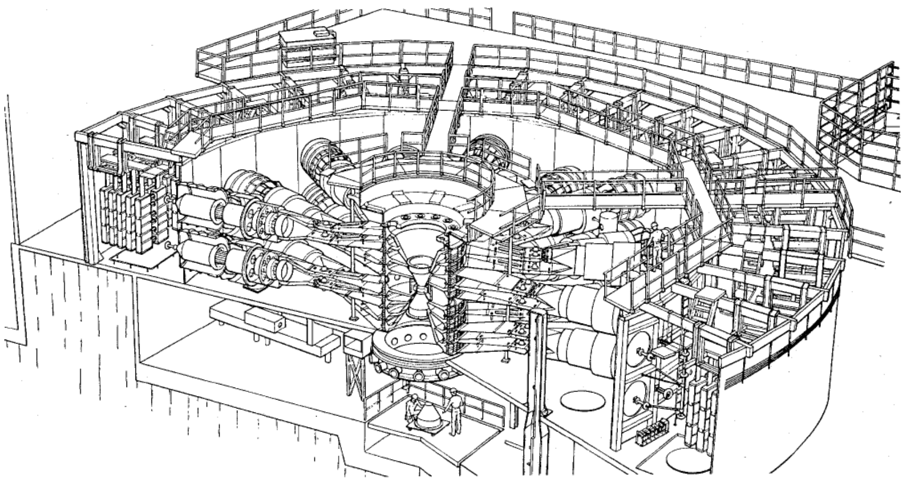

Fig. 8.2. Perspective drawing of the multimodular generator PBFA 2

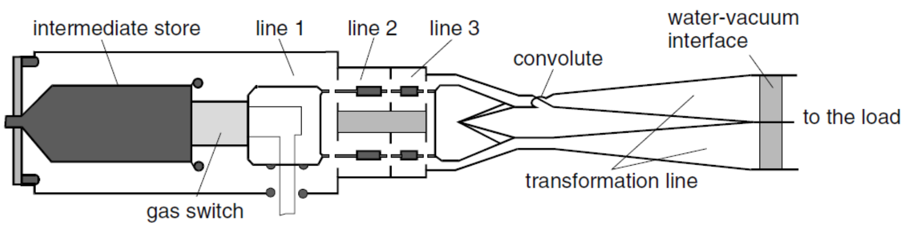

Fig. 8.3. Pulse-forming network of a single module of the PBFA 2 device

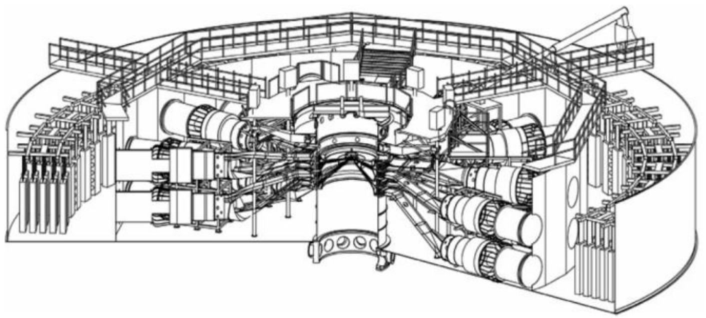

Fig. 8.4. Schematic illustration of the Z-Machine for driving Z-pinches, located at Sandia National Laboratory

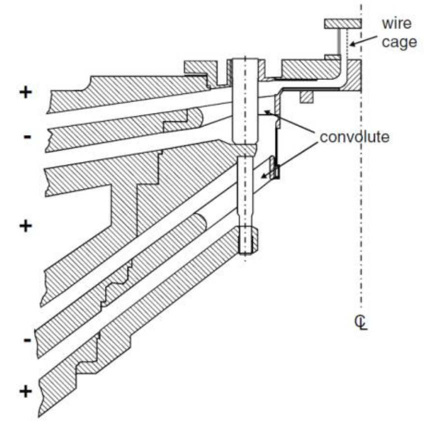

Fig. 8.5. Post-hole convolute in the Z-Machine

Sandia’s Z machine is the world's most powerful and efficient laboratory radiation source

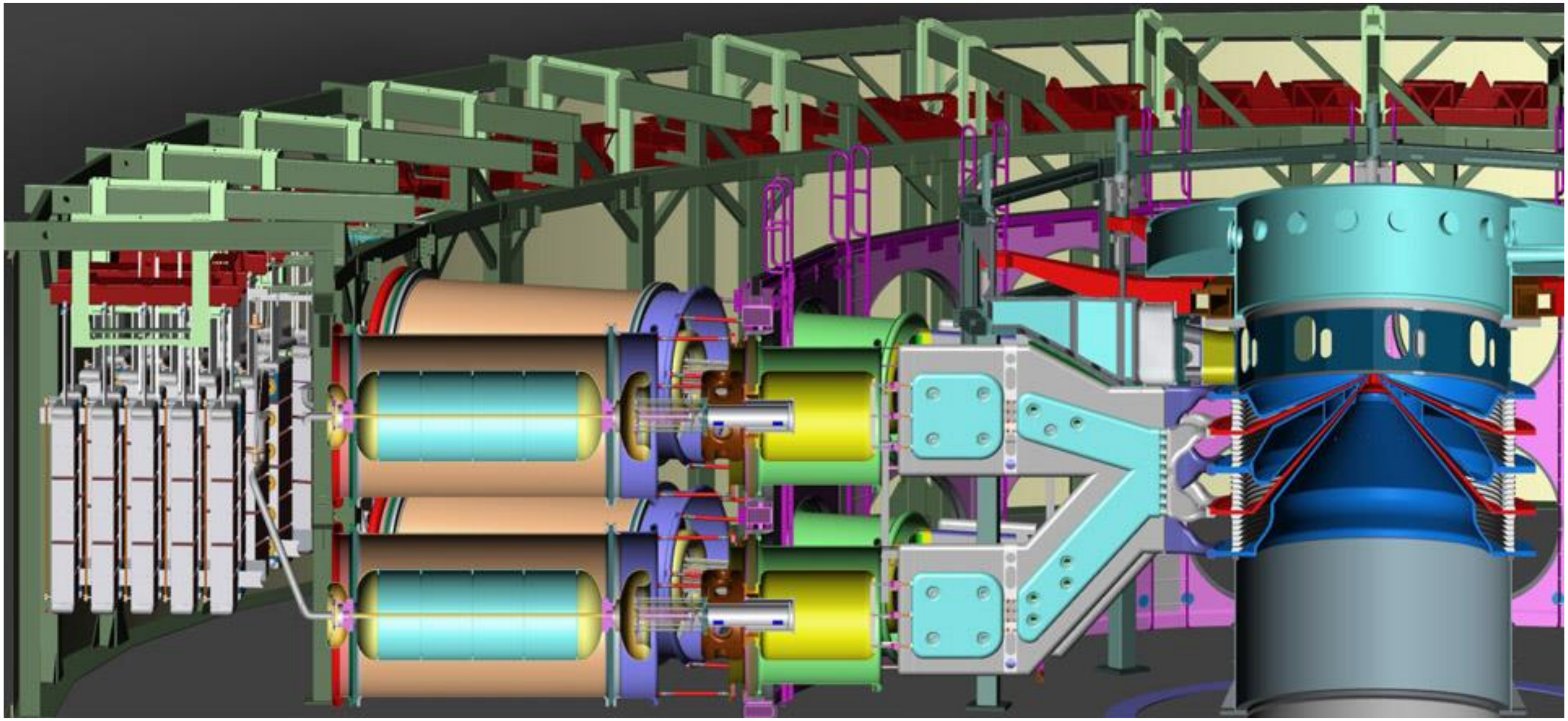

- **Stored energy: 20 MJ**
- **Marx charge voltage: 85 kV**
- **Peak electrical power: 85 TW**
- **Peak current: 26 MA**
- **Rise time: 100 ns**
- **Peak X-ray emissions: 350 TW**
- **Peak X-ray output: 2.7 MJ**

Z pulsed-power accelerator: 20 MA, 3MV, 55TW

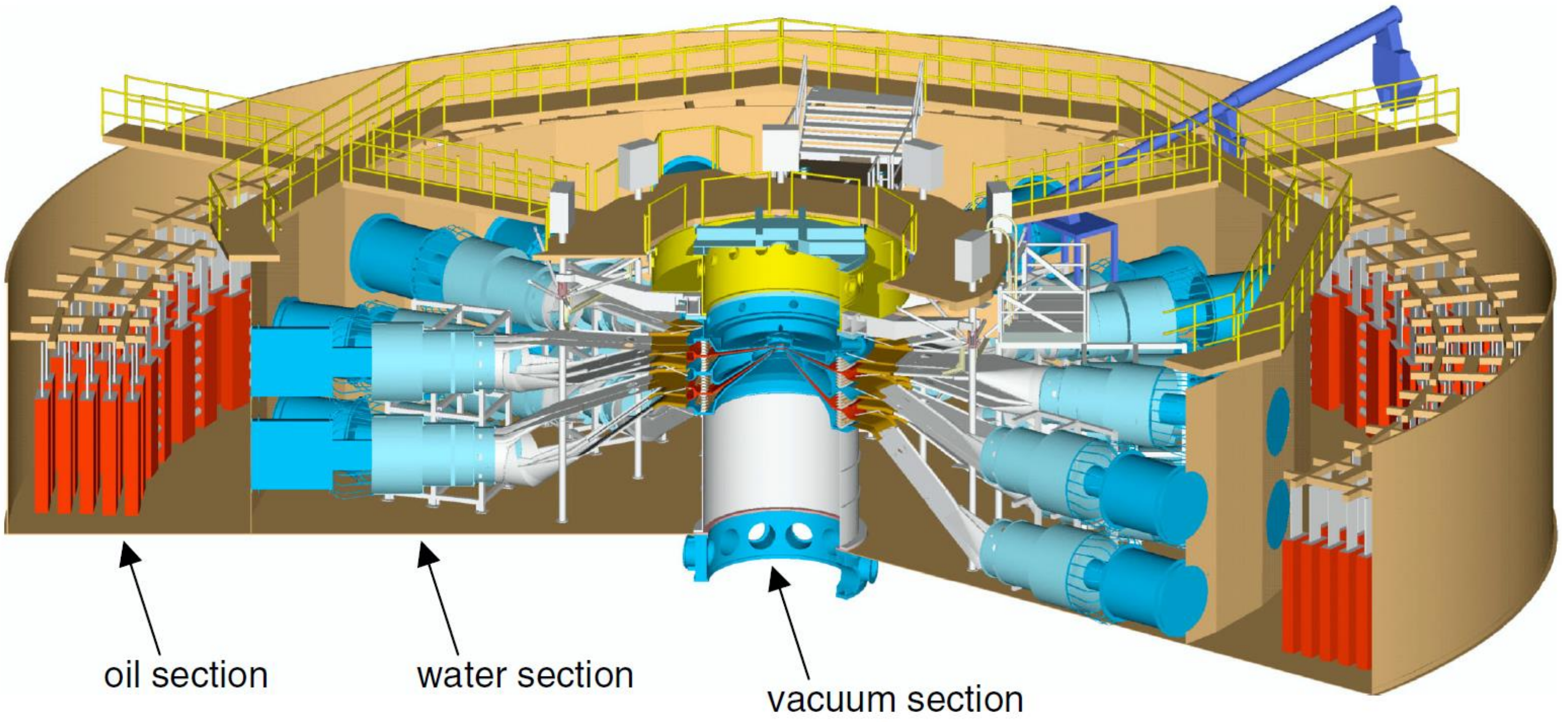

Self-magnetically insulated vacuum transmission lines (MITLs)

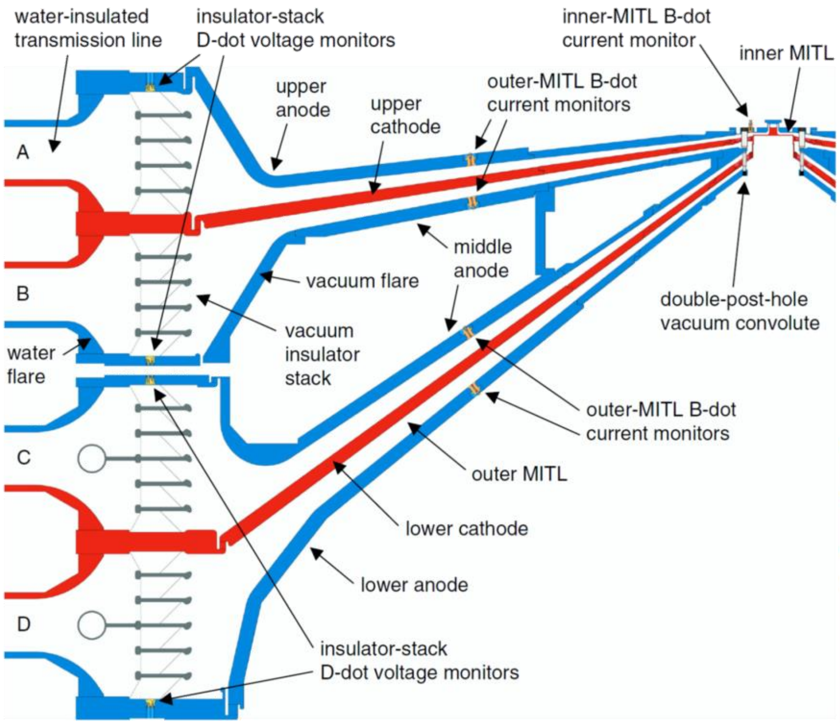

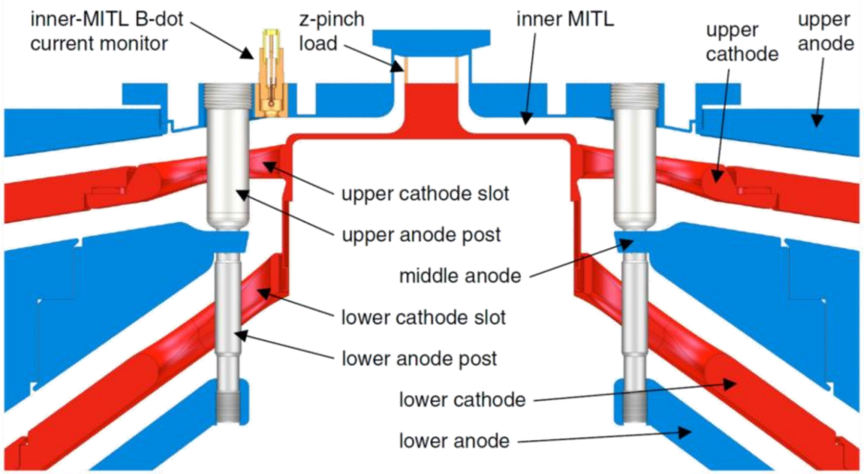

Z machine

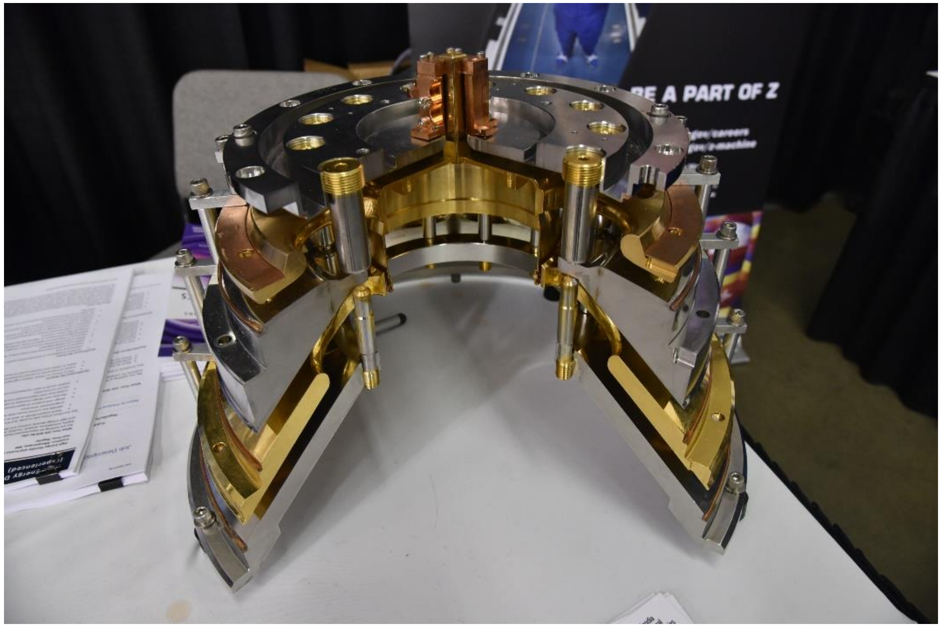

Z machine

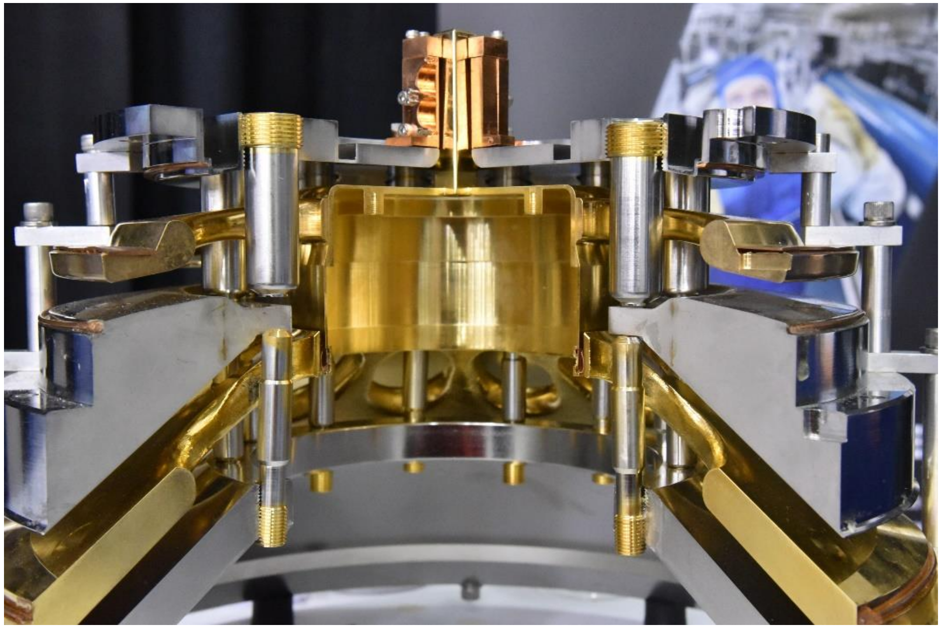

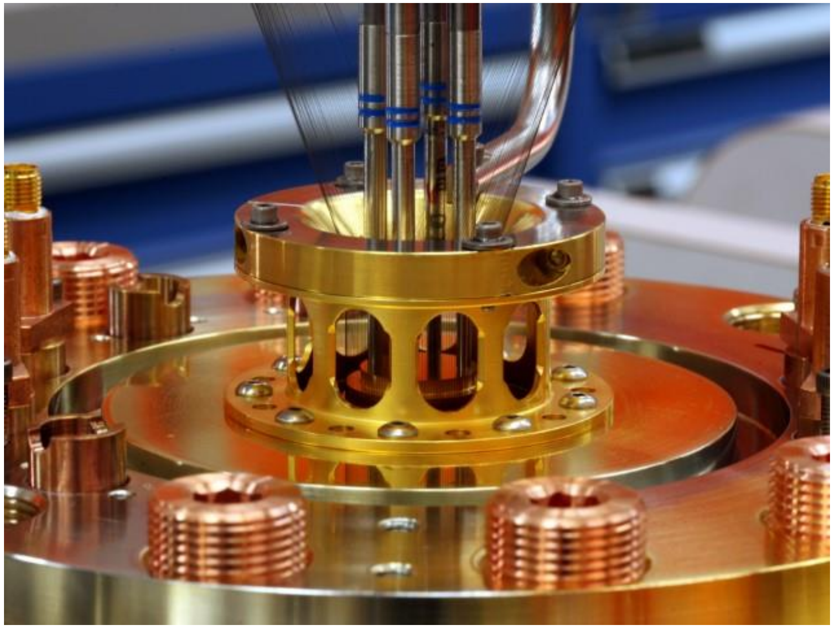

Z machine discharge

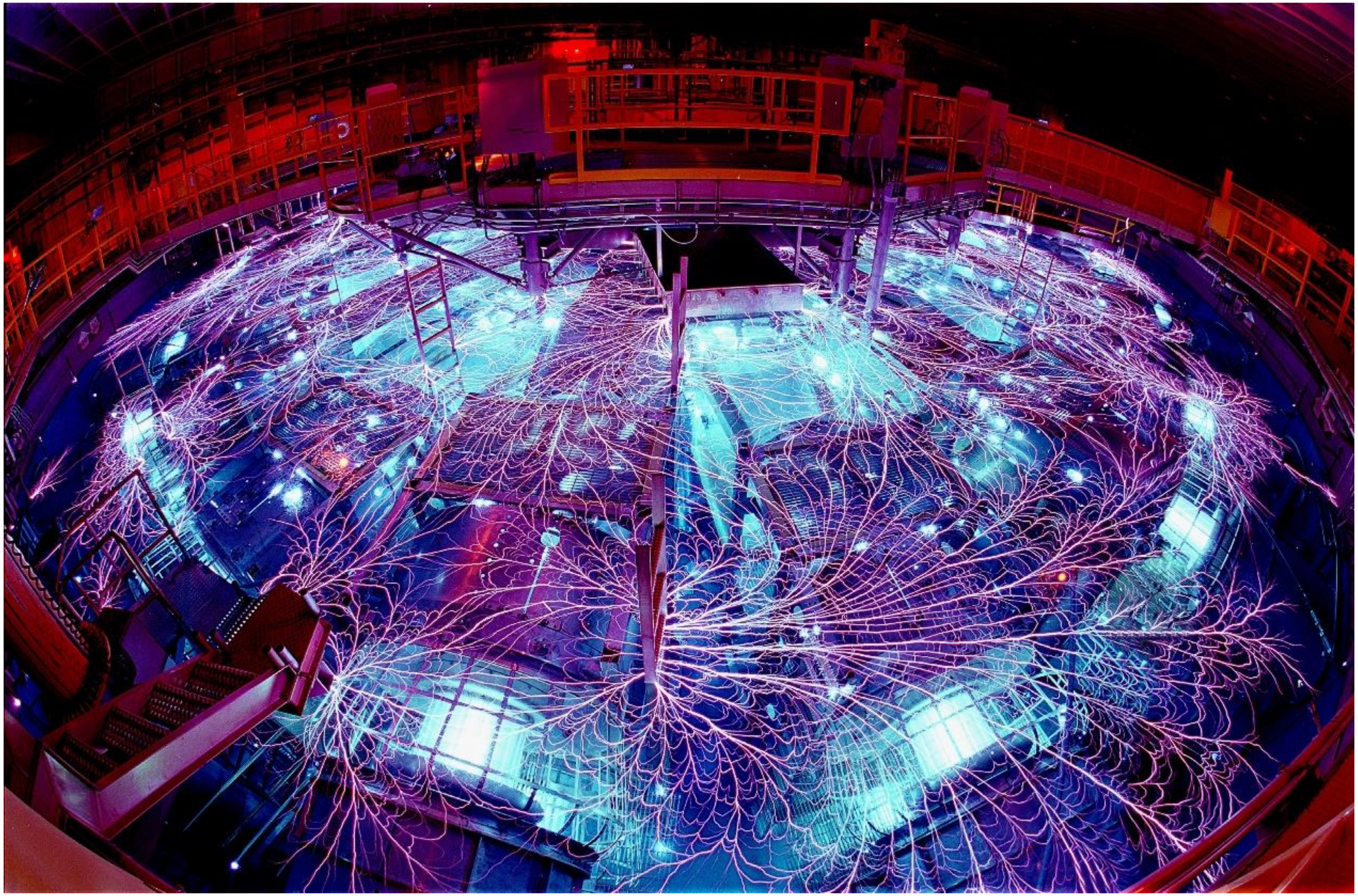

Before and after shots

- **Before shots**

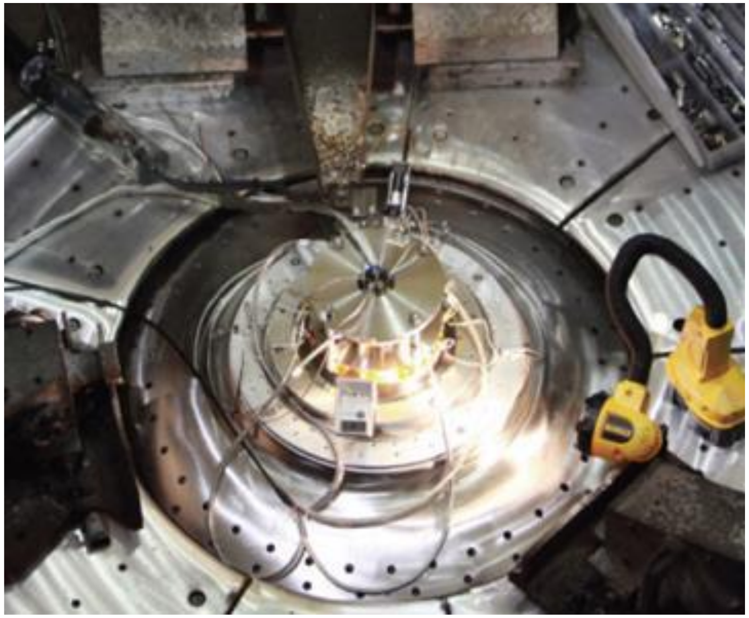

- **After shots**

SAND2017-0900PE_The sandia z machine - an overview of the world's most powerful pulsed power facility.pdf

The “iron group” of isotopes are the most tightly bound

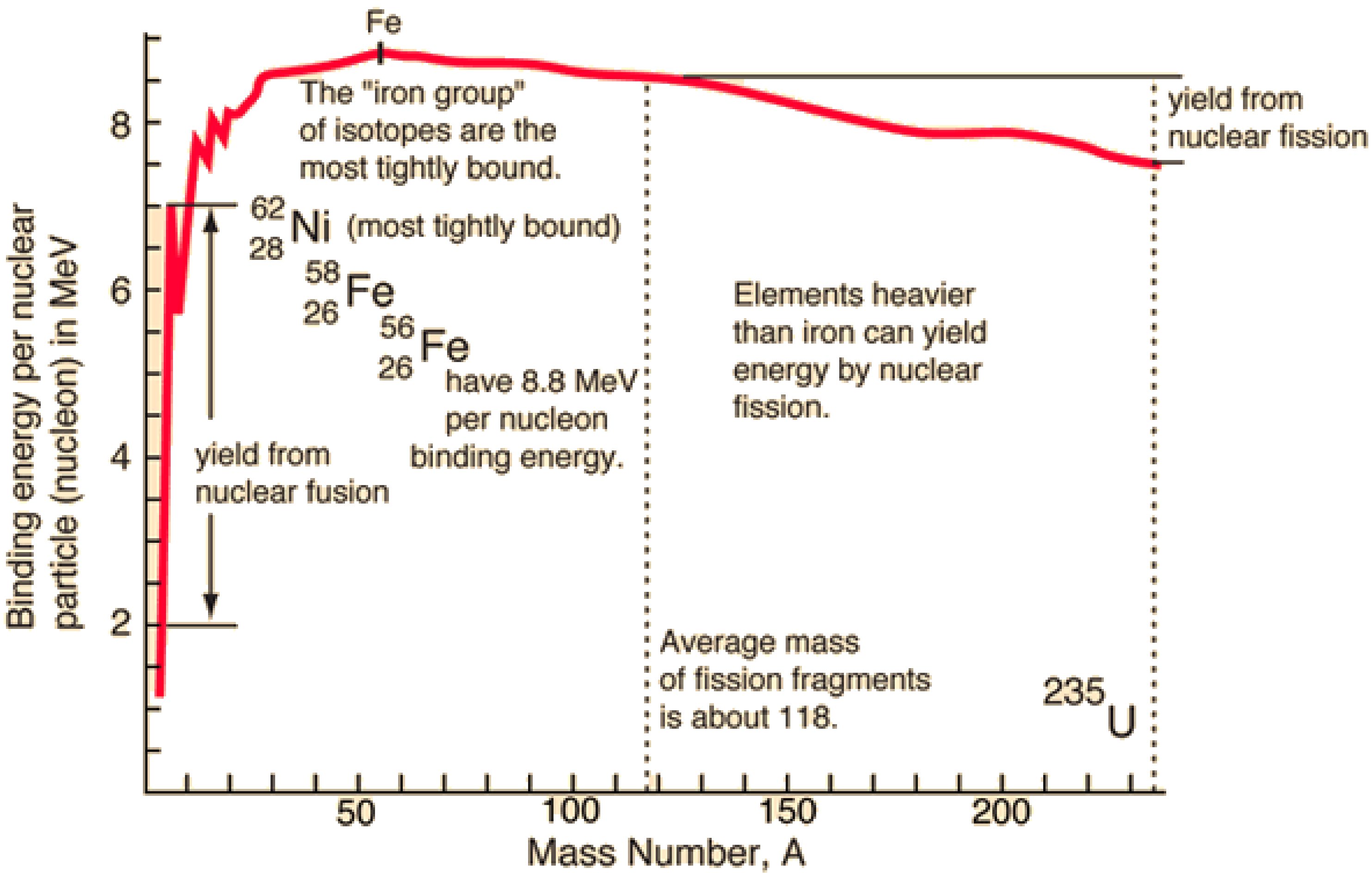

Fusion is much harder than fission

- **Fission:** $n +^{235}_{92} U \rightarrow^{236}_{92} U \rightarrow^{144}_{56} Ba +^{89}_{36} Kr + 3n + 177 \text{ MeV}$

- **Fusion:** $D + T \rightarrow He^4\,(3.5 \text{ MeV}) + n\,(14.1 \text{ MeV})$

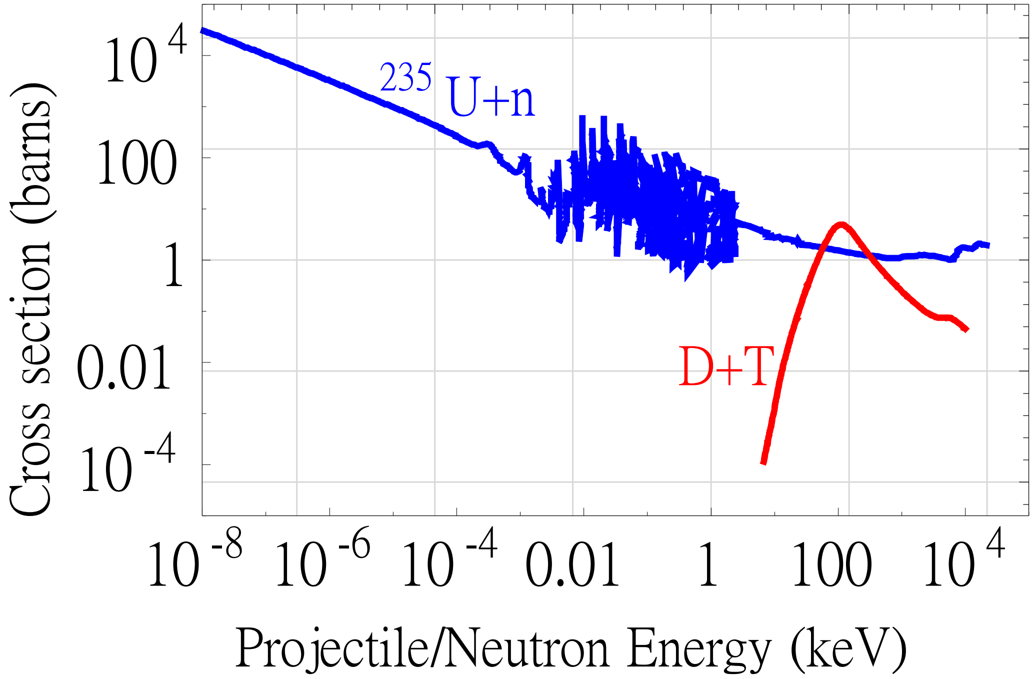

The fusion process

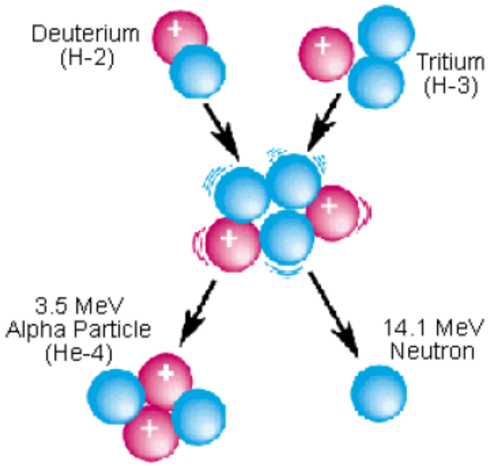

Deuterium-Tritium Fusion Reaction

$^2H+^3H \Rightarrow {}^4He+n+Q \equiv 17.6$ MeV

Energy release Q=17.6 MeV

In comparison

$^2H+^2H \Rightarrow {}^1H+^3H + Q \equiv 4.0$ MeV
$^2H+^2H \Rightarrow {}^3He+n + Q \equiv 3.2$ MeV
$^3H+^3H \Rightarrow {}^4He+2n+Q \equiv 11.3$ MeV
$^{235}U+n \Rightarrow X_A+X_B+3n + Q \approx 200$ MeV

Fusionable Material, deuterium ^2H (D) and tritium ^3H (t):

Deuterium: natural occurrence (heavy water) (0.015%).

Tritium: natural occurrence in atmosphere through cosmic ray bombardment; radioactive with $T_{1/2}$=12.3 y.

Enormous fusion fuel can be produced from sea water

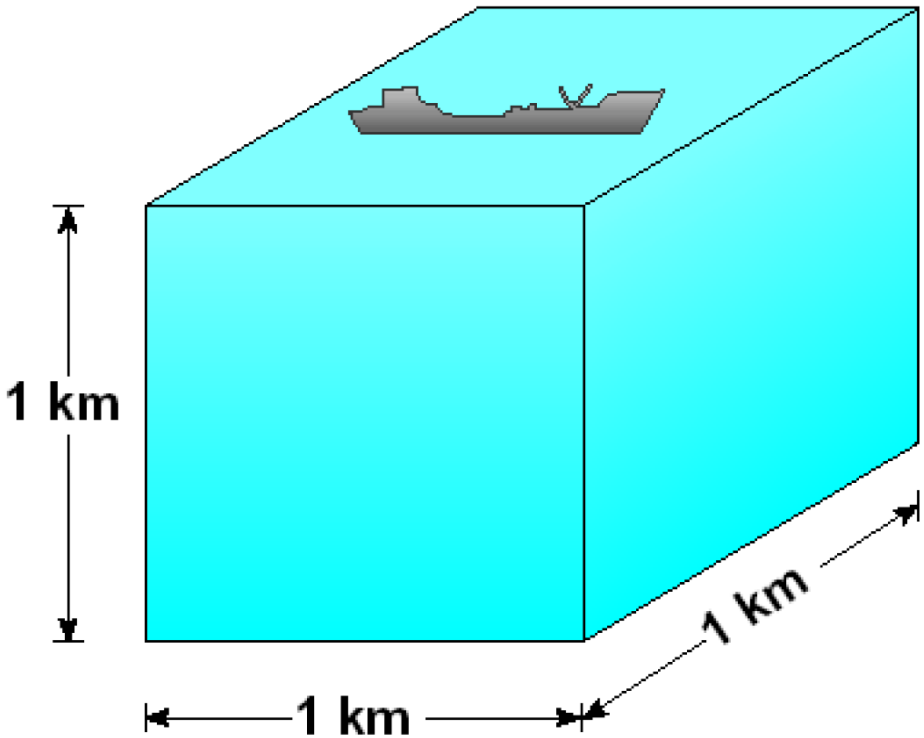

= Total energy of world oil reserve

“Advantages” of hydrogen bomb

Fusion of $^2H+^3H$: $$\frac{Q}{A}=\frac{17.6\ MeV}{(3+2)\ amu}=3.5\ \frac{MeV}{amu}$$

Fission of ^{235}U: $$\frac{Q}{A}=\frac{200\ MeV}{236\ amu}=0.85\ \frac{MeV}{amu}$$

Fusion is 4 times more powerful than fission
and generates 24 times more neutrons!

https://isnap.nd.edu/Lectures/phys20061/pdf/10.pdf

Fusion doesn’t come easily

$$\text{averaged reaction rate}: \quad \langle \sigma v \rangle = \int\int d\vec{v}_1 d\vec{v}_2 \sigma_{1,2}(v)\, v f_1(v_1)$$

$$f_j(v_j) = \left(\frac{m_j}{2\pi k_{\mathrm{B}} T}\right)^{3/2} \exp\left(-\frac{m_j v_j^2}{2 k_{\mathrm{B}} T}\right)$$

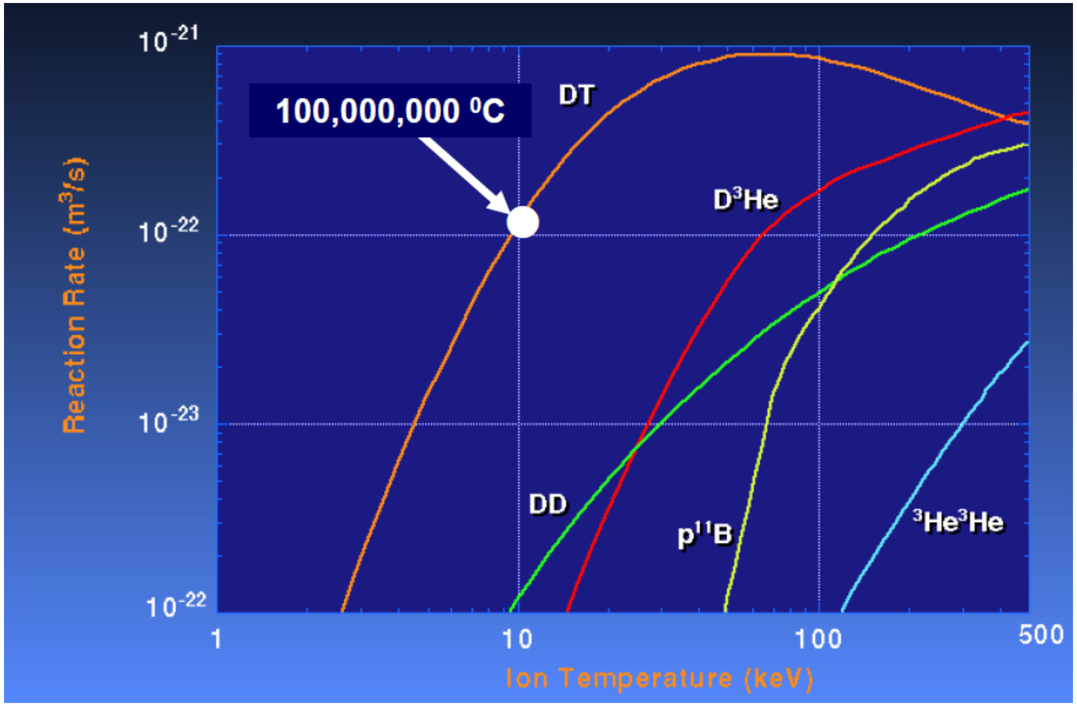

- **Use α particles to heat the plasma** $D + T \rightarrow He^4\,(3.5\ \mathrm{MeV}) + n\,(14.1\ \mathrm{MeV})$

Magnetic confinement fusion (MCF) vs Inertial confinement fusion (ICF)

Tokamak

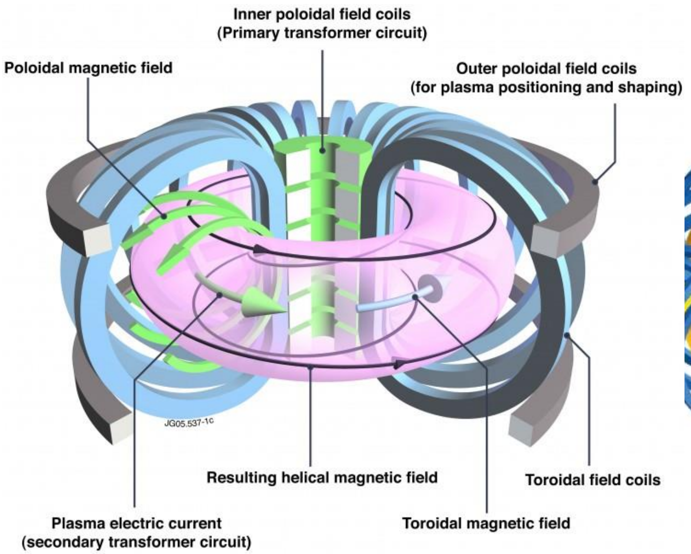

P~atm, τ~sec, T~10 keV

Stellarator

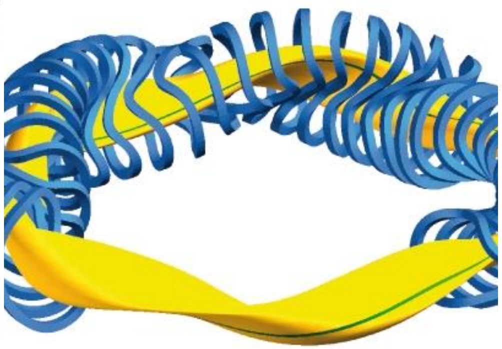

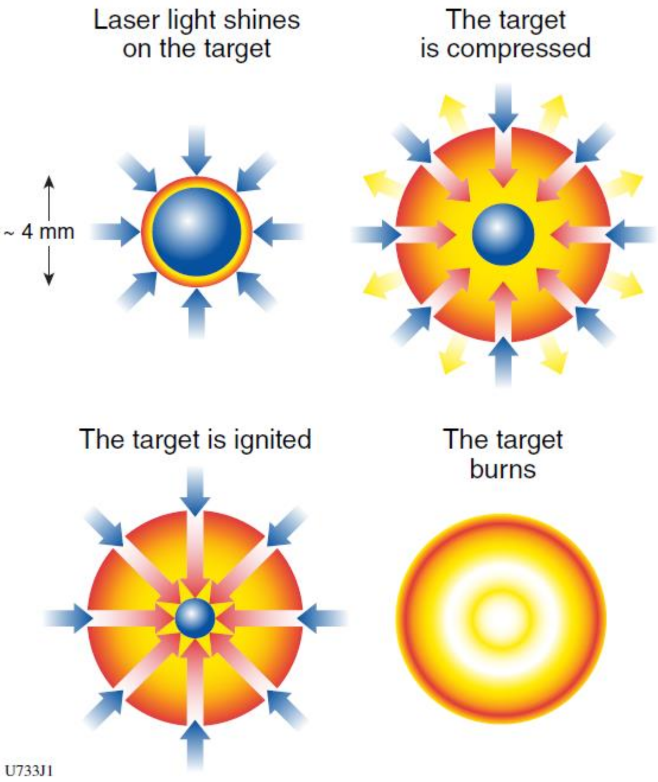

P~Gigabar, τ~nsec, T~10 keV

https://www.euro-fusion.org/2011/09/tokamak-principle-2/
https://en.wikipedia.org/wiki/Stellarator

Inertial confinement fusion

Direct-drive target

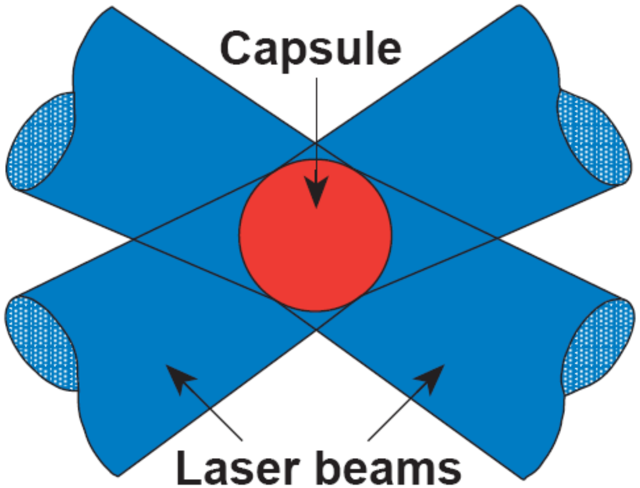

Indirect-drive target

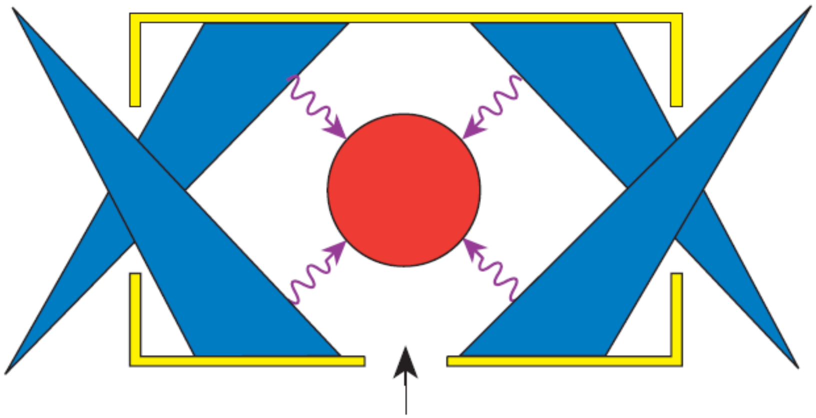

Hohlraum **using**
a cylindrical high-Z case

Reference:
Riccardo Betti,
University of Rochester,
HEDSA HEDP summer school,
San Diego, CA, August 16-21, 2015

Hohlraum at National Ignition Facility (NIF)

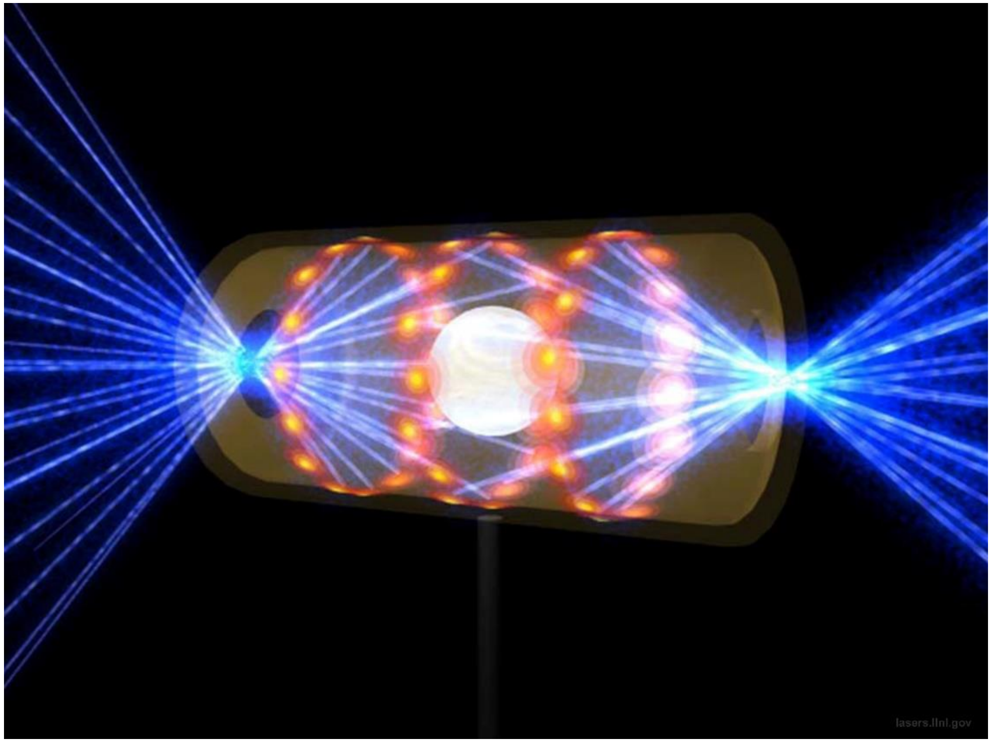

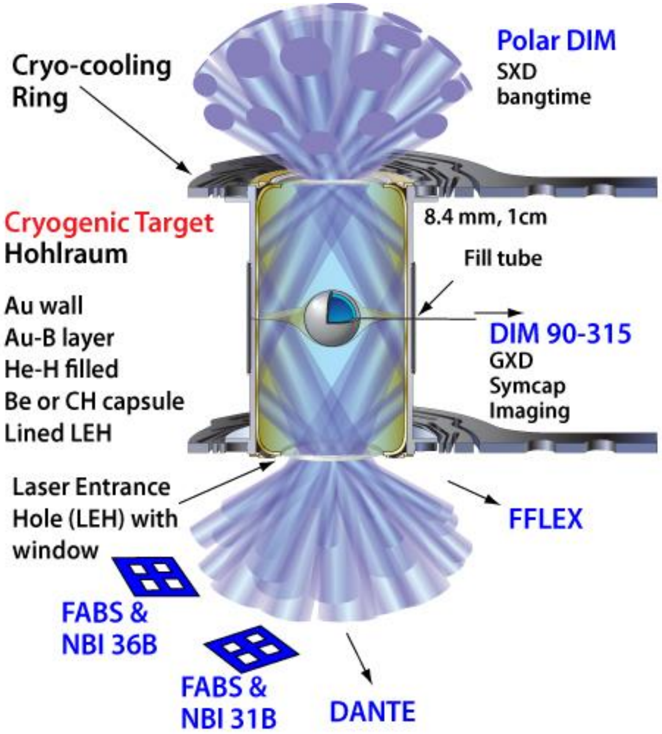

NIF target

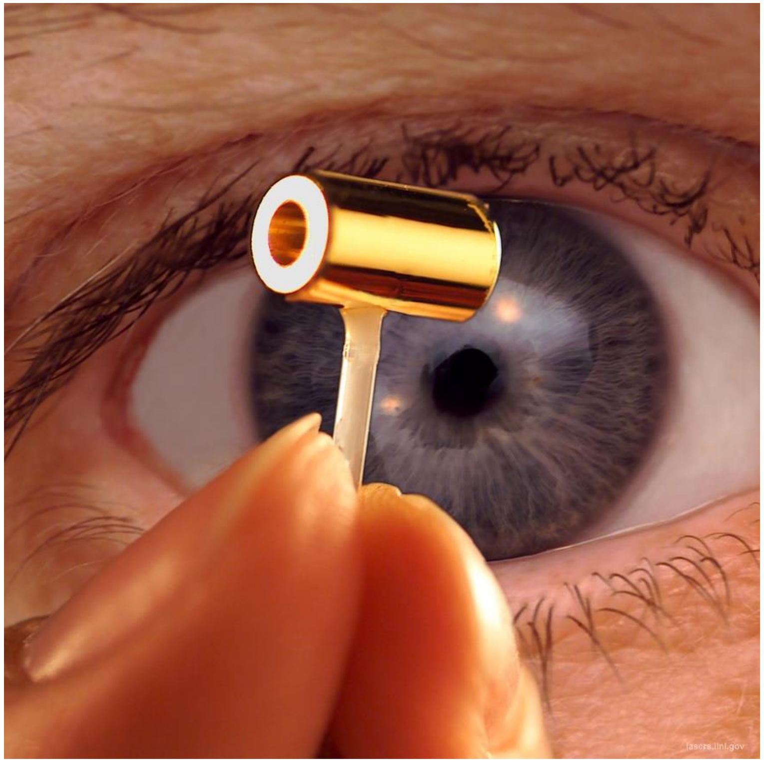

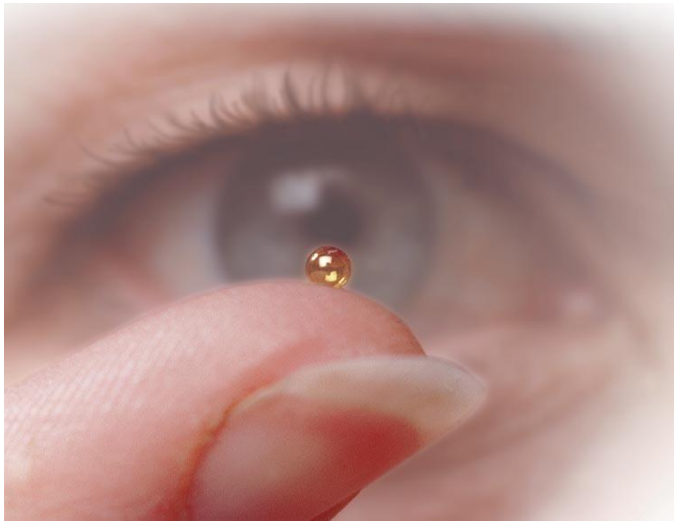

Targets used in ICF

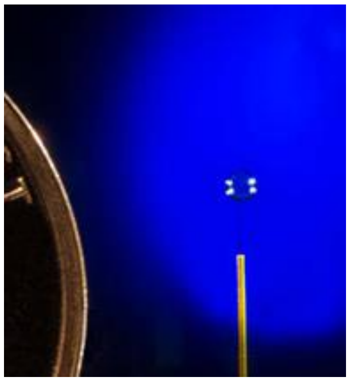

a

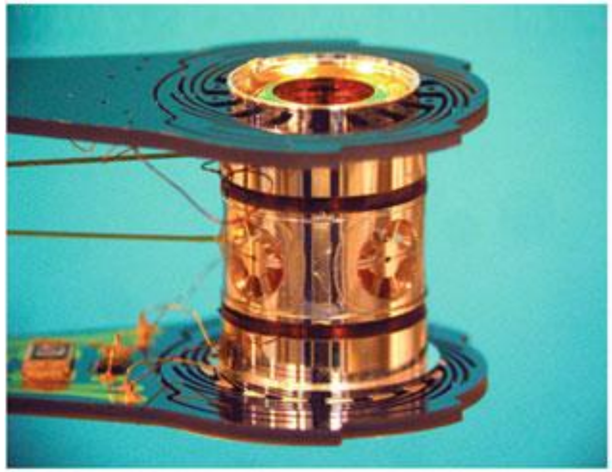

b

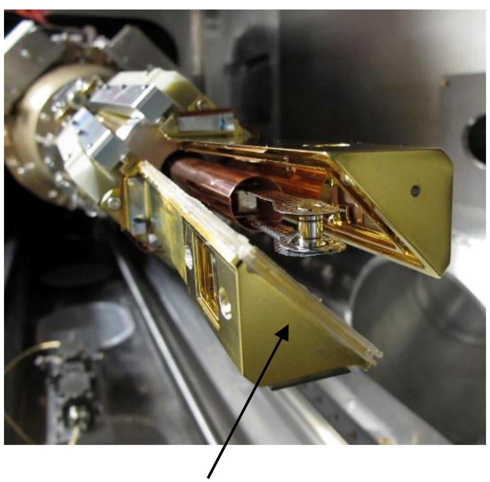

Cryogenic shroud

c **Rugby hohlraum**

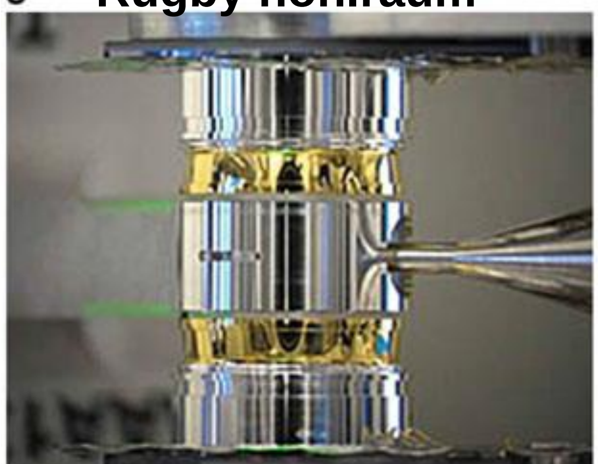

d **Tent holder**

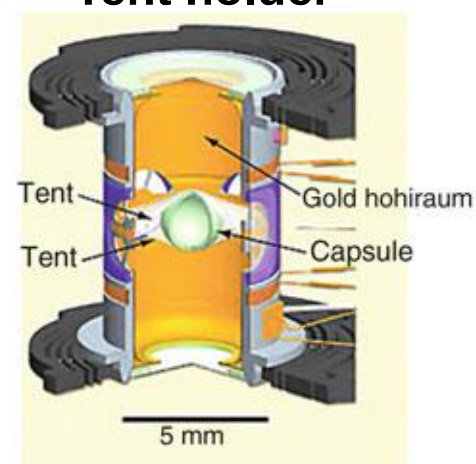

https://www.lle.rochester.edu
https://upload.wikimedia.org/wikipedia/commons/7/7b/Nif-shot_target-arm-before_big.jpg
https://www.lle.rochester.edu/index.php/2014/11/10/next-generation-cryo-target/

NIF achieved ignition (Q=1.5) on Dec. 5, 2022

- **Input Laser energy: 2.05 MJ**
- **Output energy: 3.15 MJ**

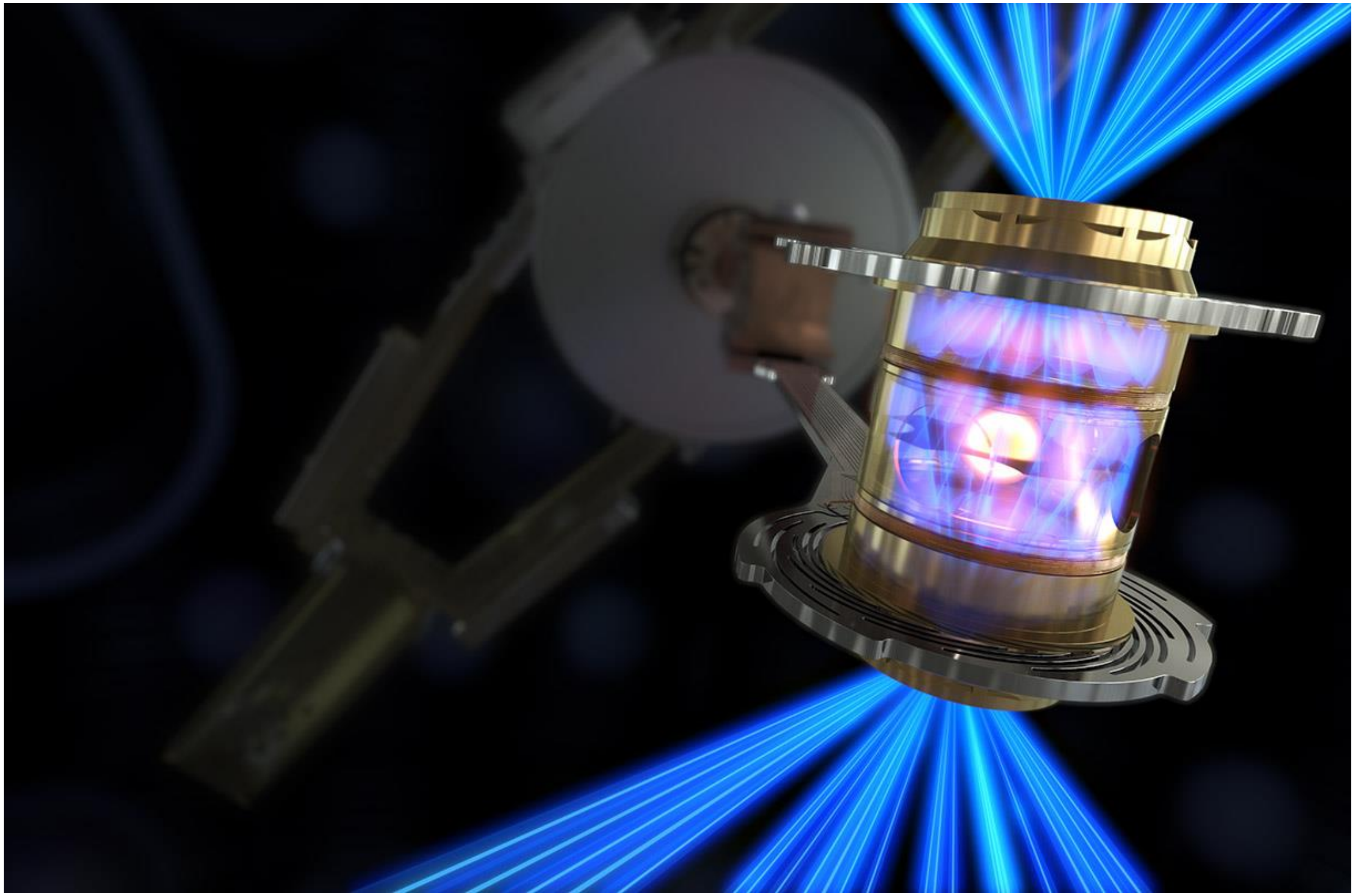

https://www.science.org/content/article/historic-explosion-long-sought-fusion-breakthrough

National Ignition Facility (NIF) achieved a yield of more than 1.3 MJ from ~1.9 MJ of laser energy in 2021 (Q~0.7)

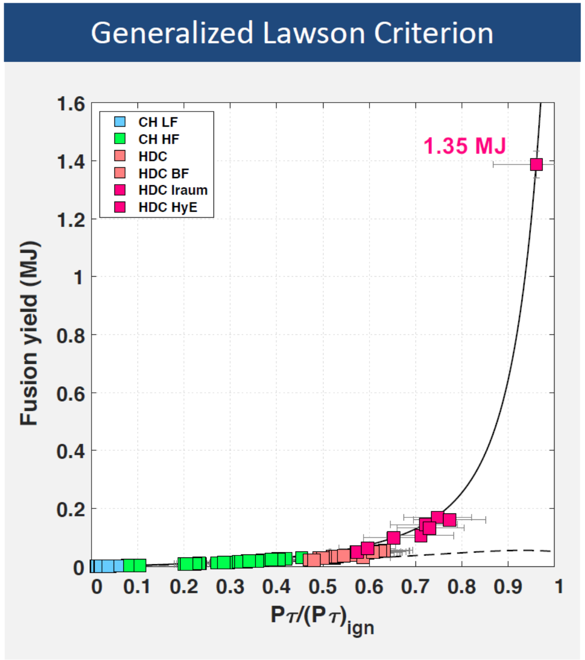

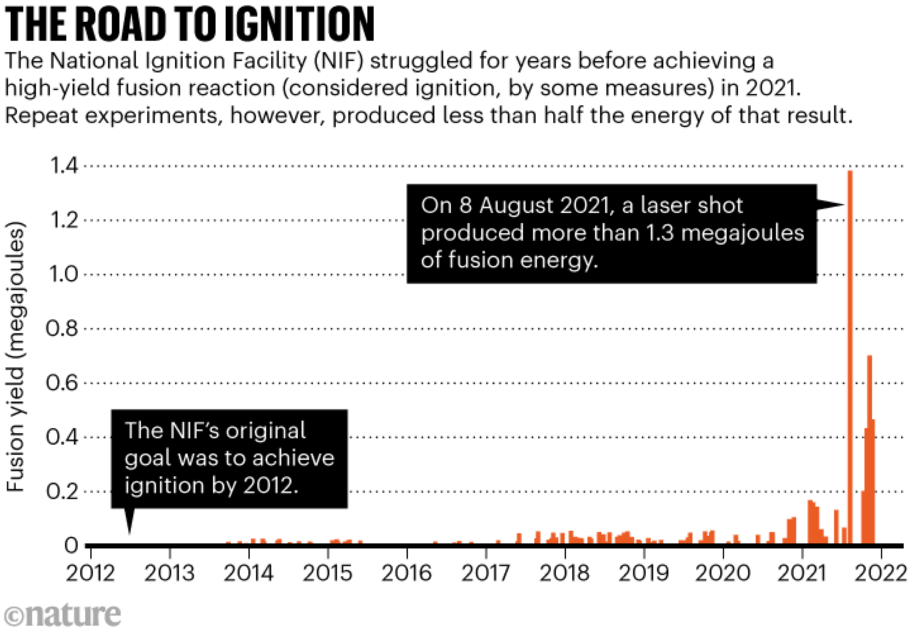

- National Ignition Facility (NIF) achieved a yield of more than 1.3 MJ (Q~0.7). This advancement puts researchers at the threshold of fusion ignition.

- Laser-fusion facility heads back to the drawing board.

T. Ma, ARPA-E workshop, April 26, 2022
J. Tollefson, Nature (News) 608, 20 (2022)

“Ignition” (target yield larger than one) was achieved in NIF on 2022/12/5

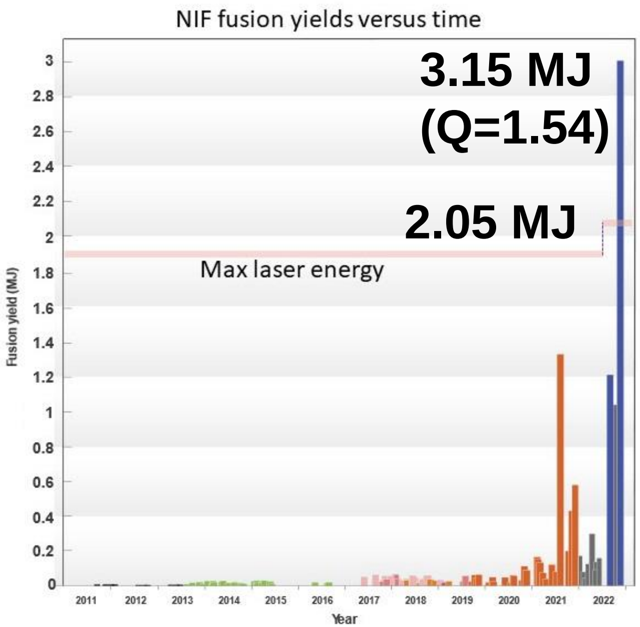

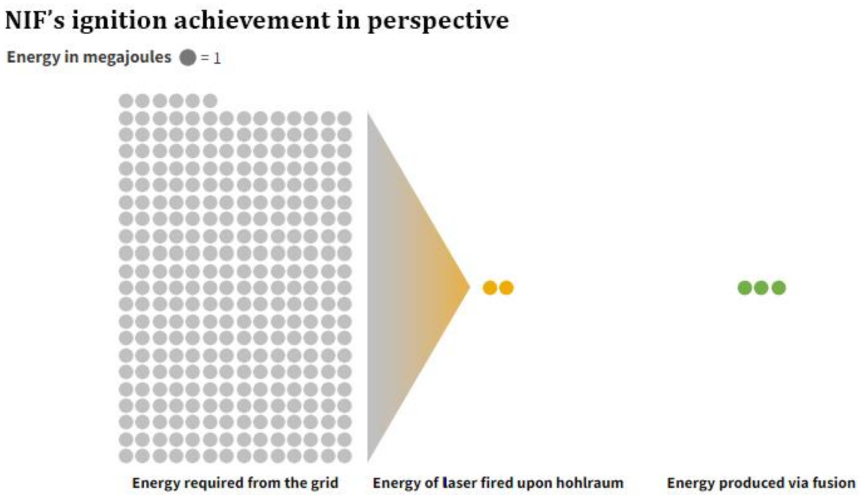

300 MJ 2.05 MJ 3.15 MJ

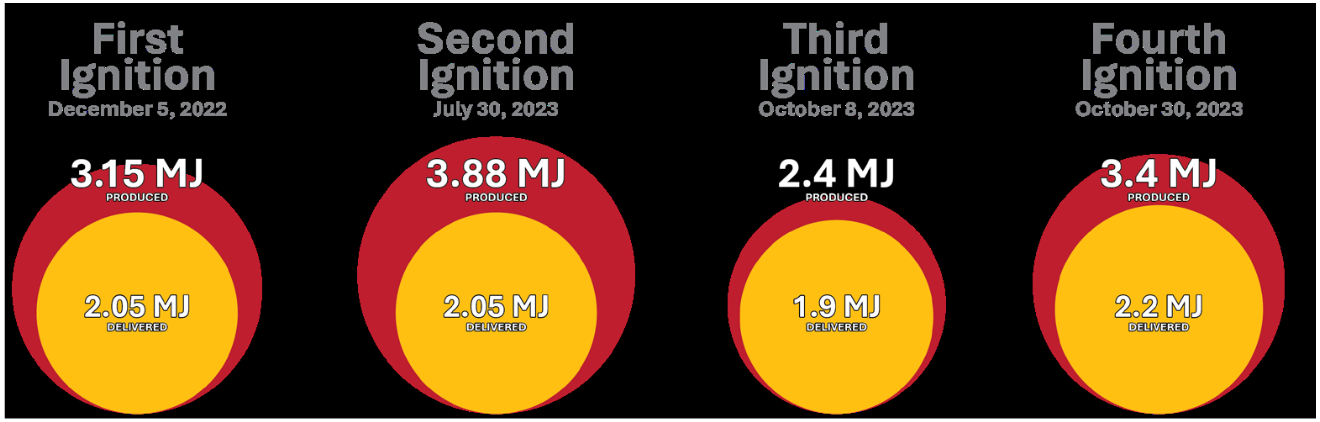

https://physicstoday.scitation.org/do/10.1063/PT.6.2.20221213a/full/
The age of ignition: anniversary edition, LLNL-BR-857901

ICF via z pinch or z-pinch driven dynamic-hohlraums

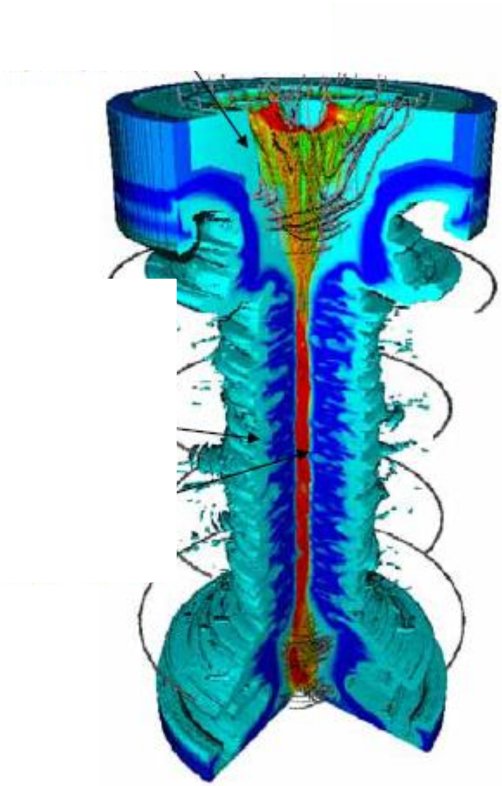

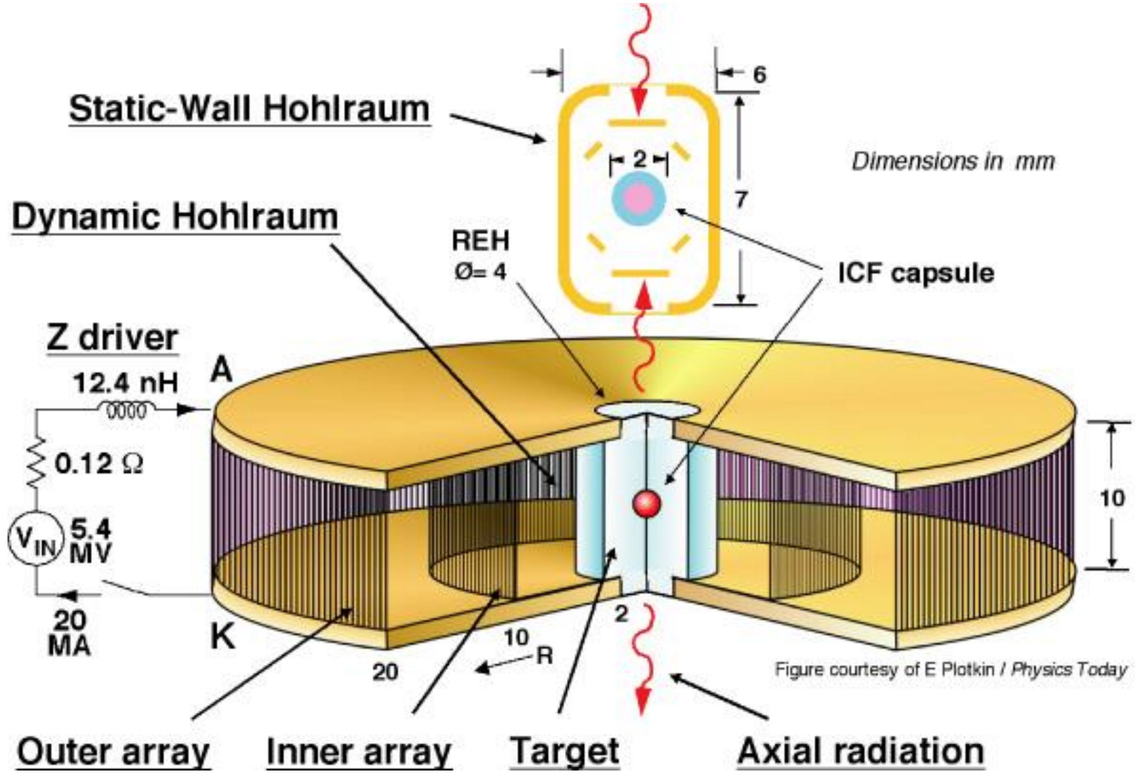

magnetized liner inertial fusion (MagLIF)

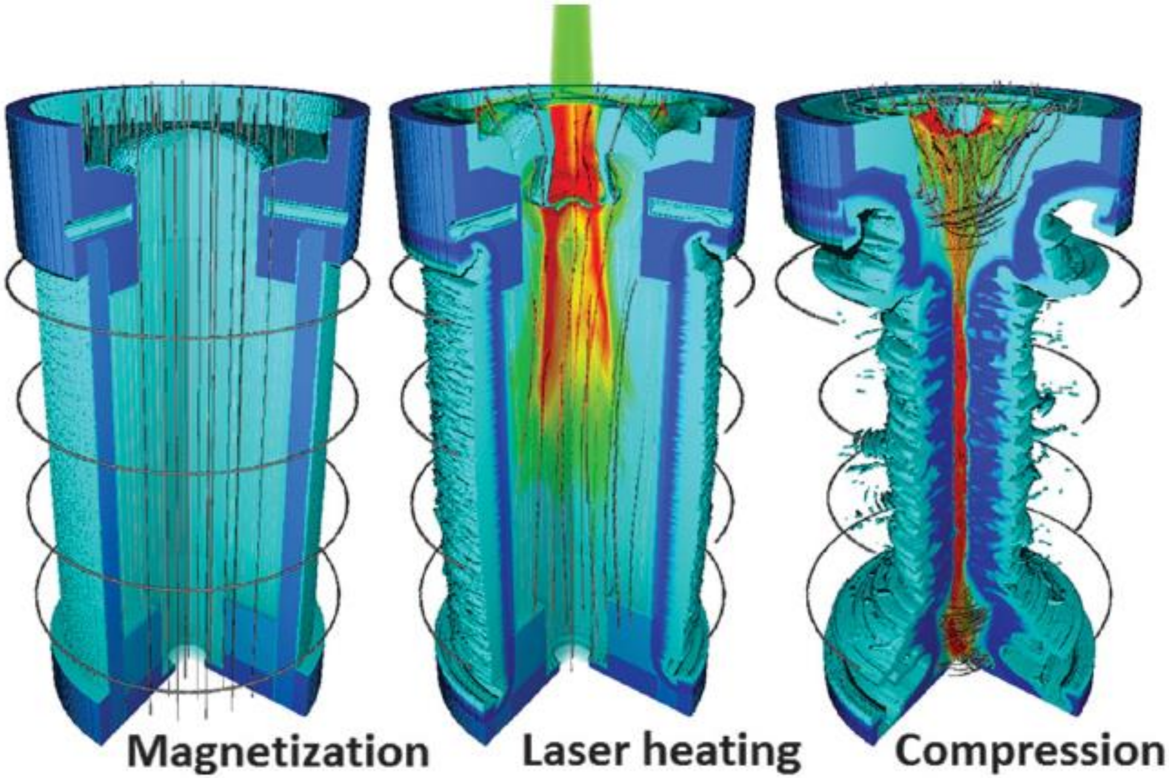

M. R. Gomez, *et. cl.*, Phys. Rev. Let., 113, 155003 (2014)

MagLIF target

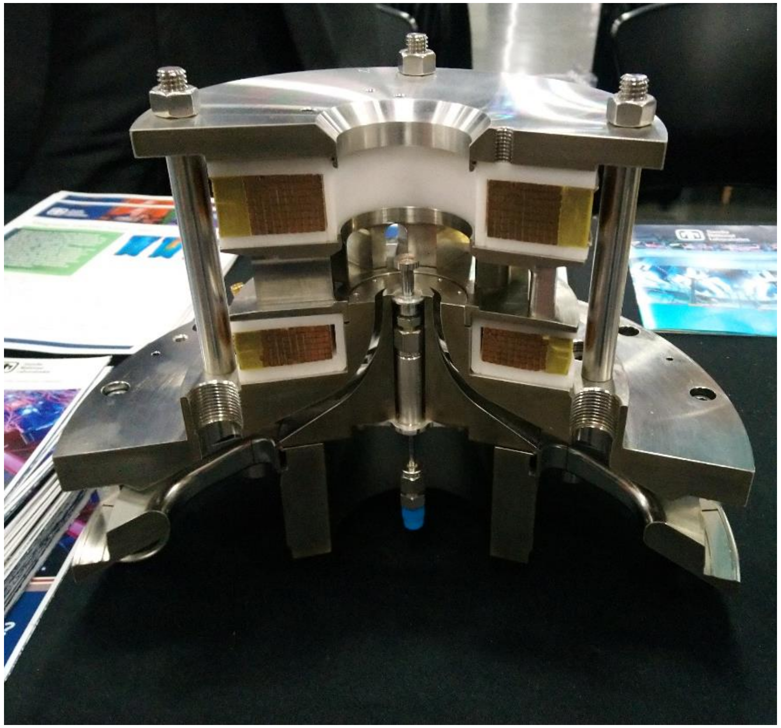

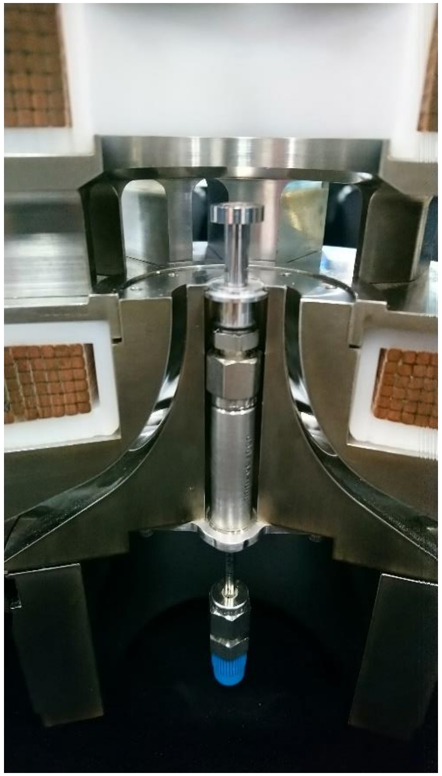

Neutron yield increased by 100x with preheat and external magnetic field.

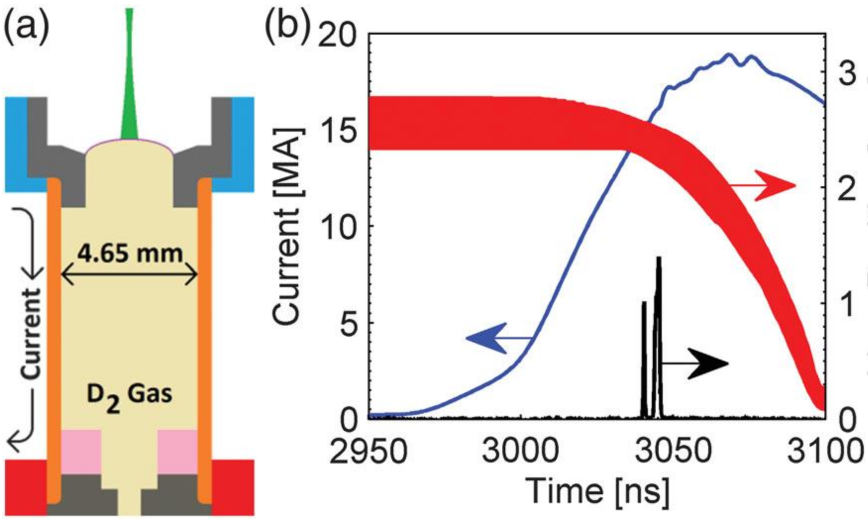

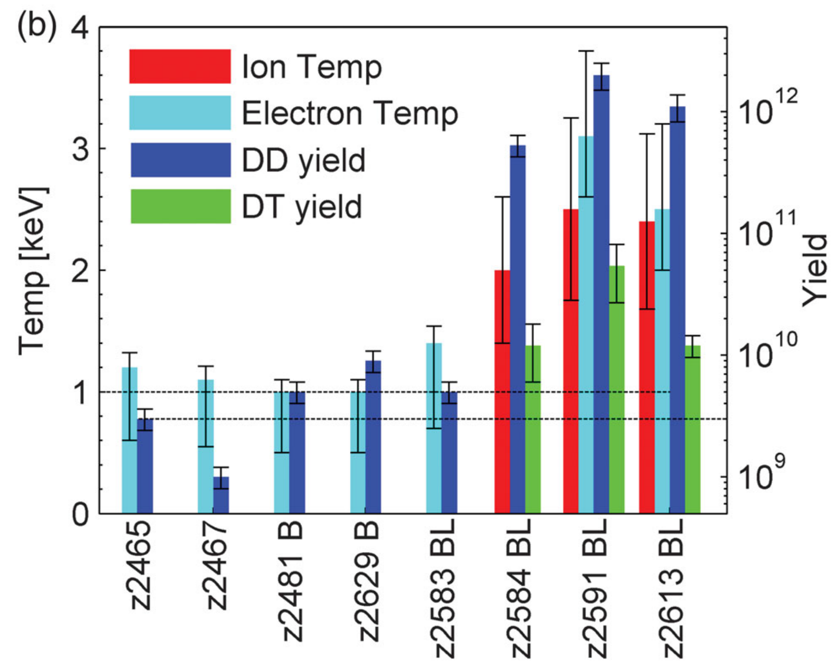

M. R. Gomez *et al* Phys. Rev. Lett. 113 155003 (2014)

Sheared flow stabilizes MHD instabilities

m = 0 (sausage)

Perturbation $\propto e^{(im\theta + ikz + \gamma t)}$

m = 1 (kink)

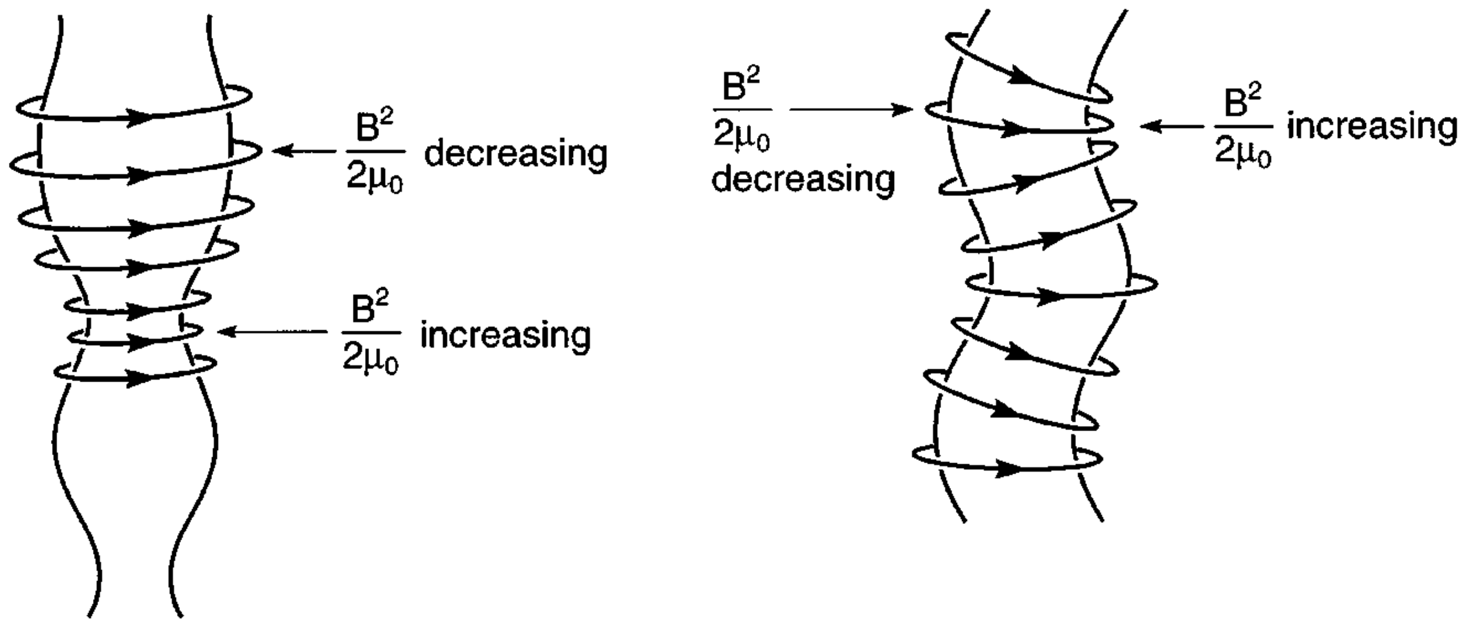

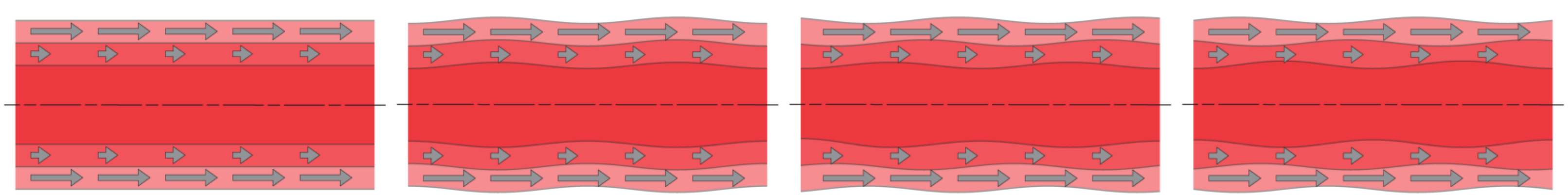

$$\frac{dV_Z}{dr} \neq 0$$

M. G. Haines, etc., Phys. Plasmas 7, 1672 (2000)
U. Shumlak, etc., Physical Rev. Lett. 75, 3285 (1995)
U. Shumlak, etc., ALPHA Annual Review Meeting 2017

A z-pinch plasma can be stabilized by sheared flows

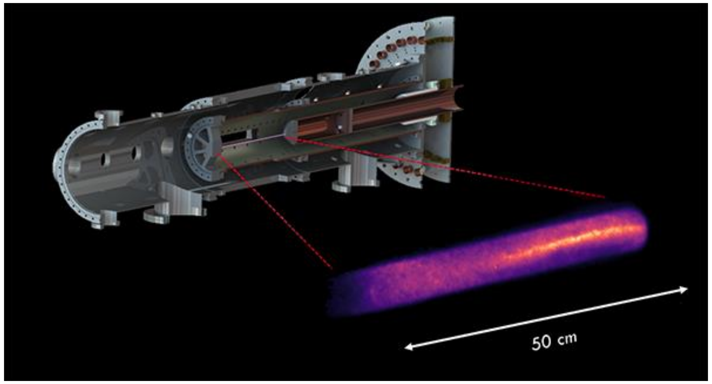

ZAP ENERGY™

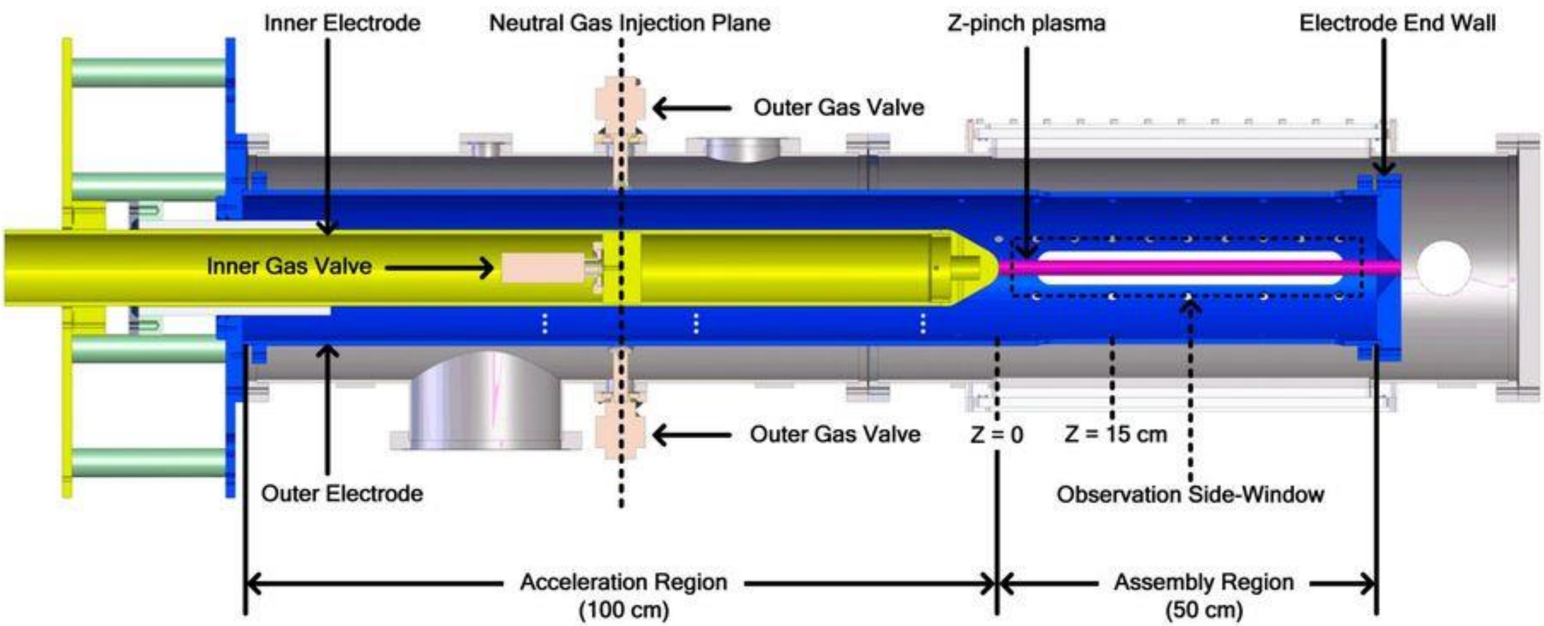

https://www.zapenergyinc.com/about
A. D. Stepanov, etc., Phys. Plasmas 27, 112503 (2020)

Fusion reactor concept by ZAP energy

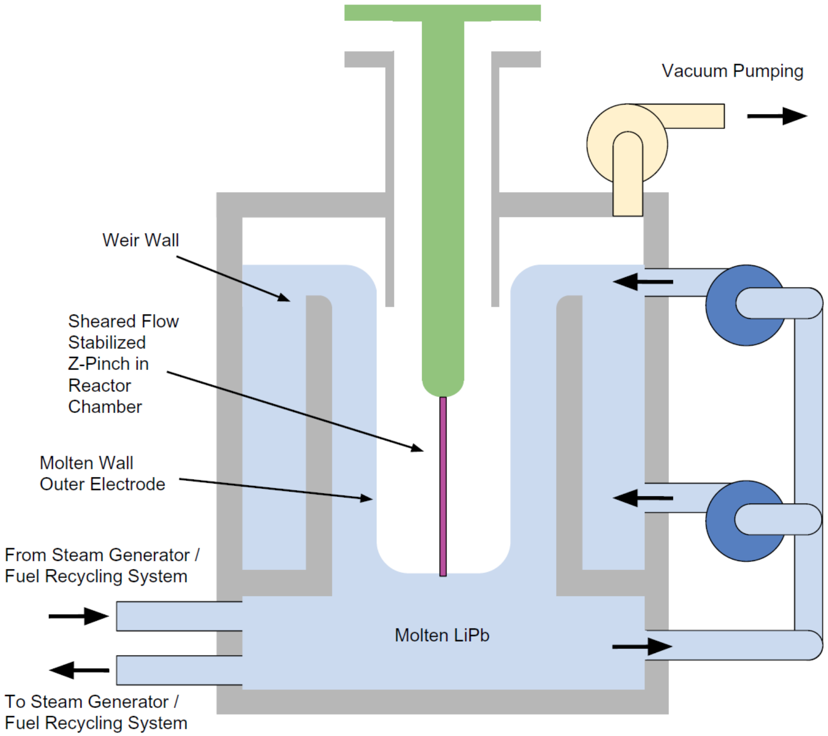

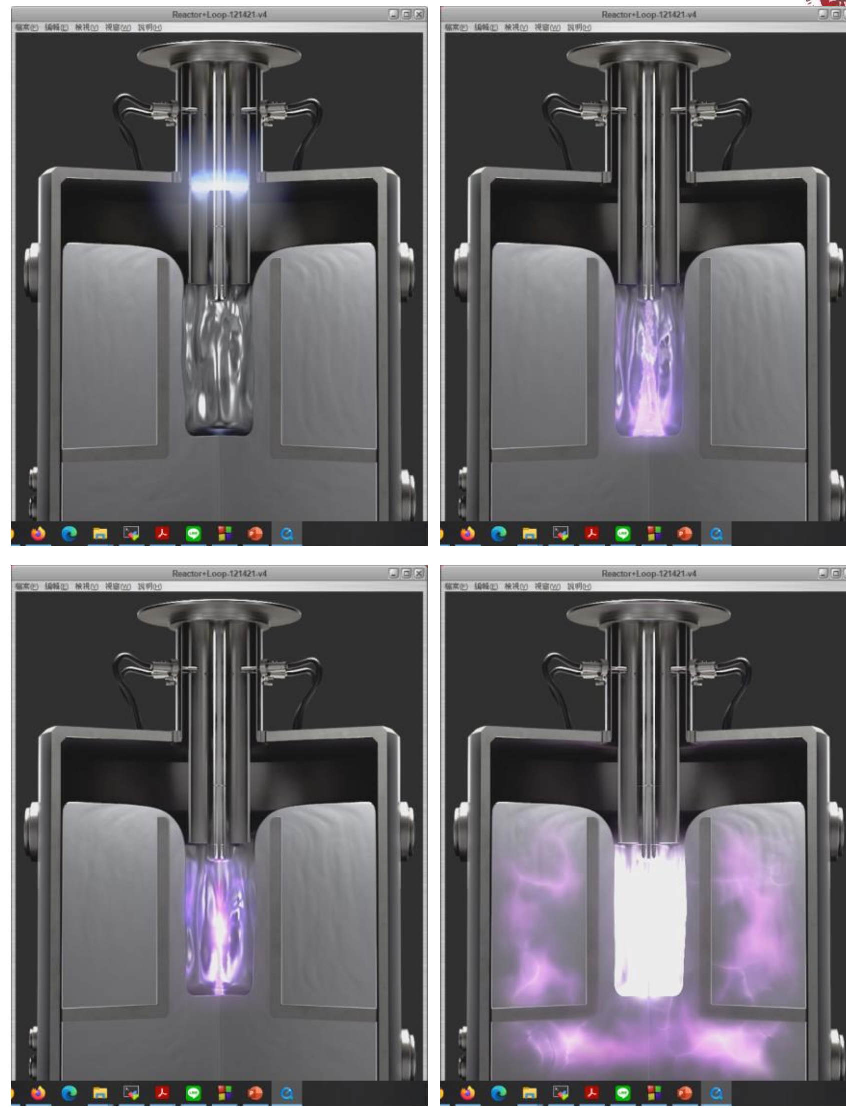

https://www.zapenergyinc.com/about
E. G. Forbes, etc., Fusion Sci. Tech. 75, 599 (2019)

First light fusion, UK

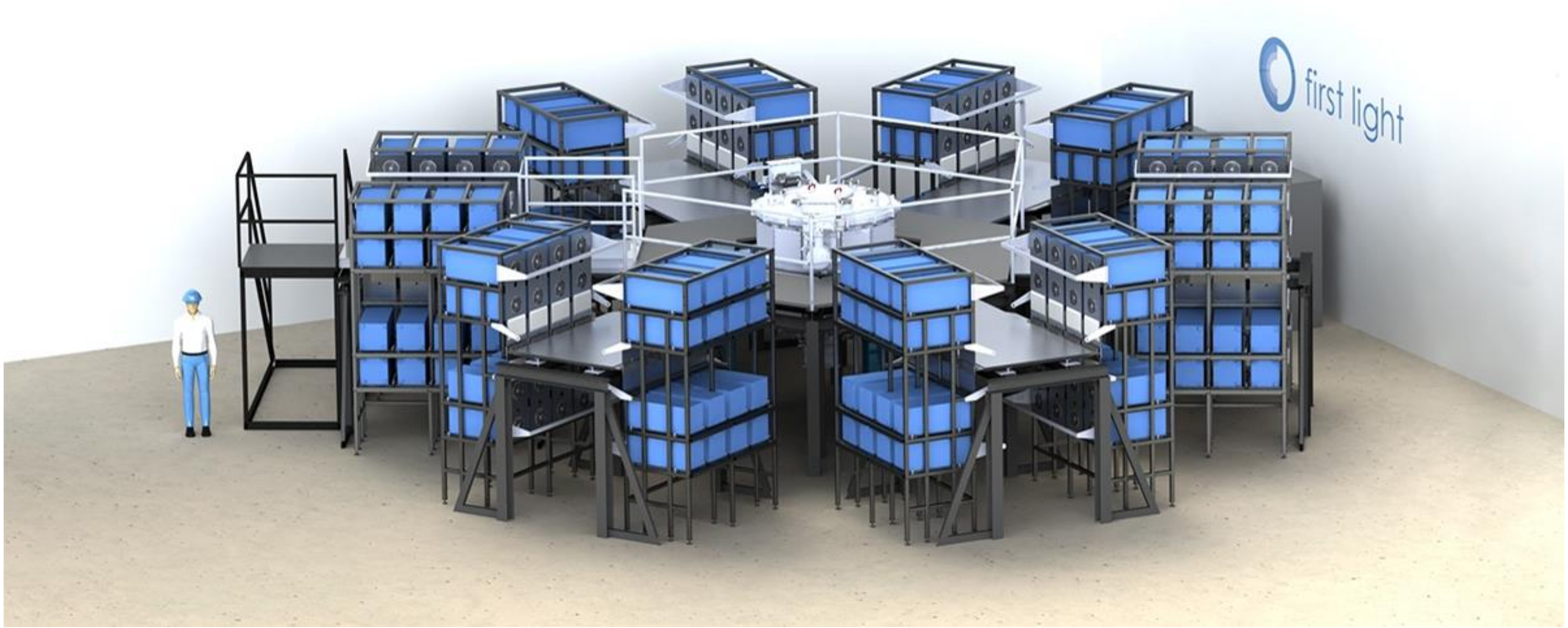

- **2.5 MJ @ 200 kV**
- **14 MA with t_{rise}~2 us**

https://images.app.goo.gl/vcsJTuwVrbY29QELA

First light fusion, UK

https://www.all-electronics.de/wp-content/uploads/2019/08/1_Pic_192-capacitors-around-vaccum-chamber_lowres-1024x768.jpg

Projectile Fusion is being established at First Light Fusion Ltd, UK

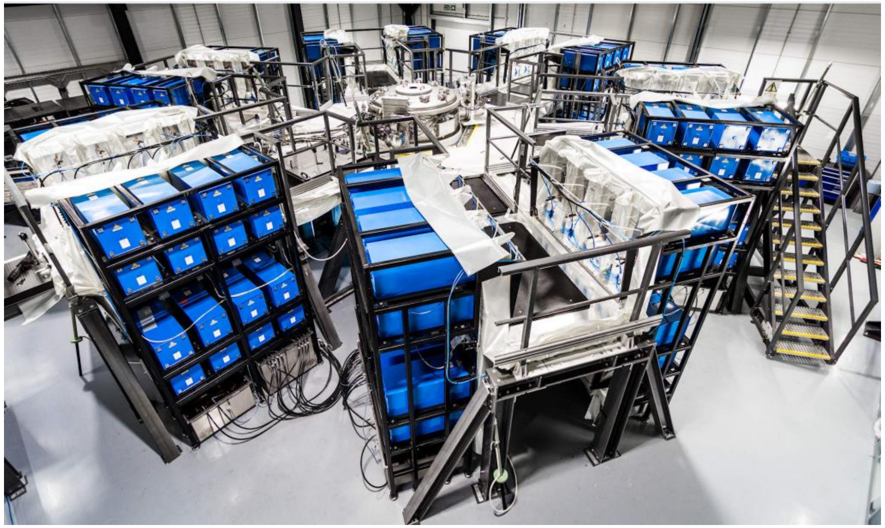

- **Stored energy: 2.5 MJ @ 200 kV (C_{tot}=125 uF)**
- **I_{peak}=14 MA w/ T_{rise}~2us.**

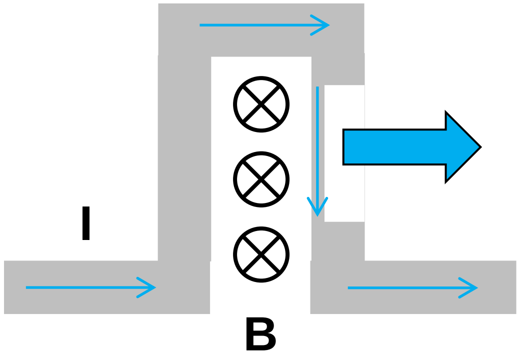

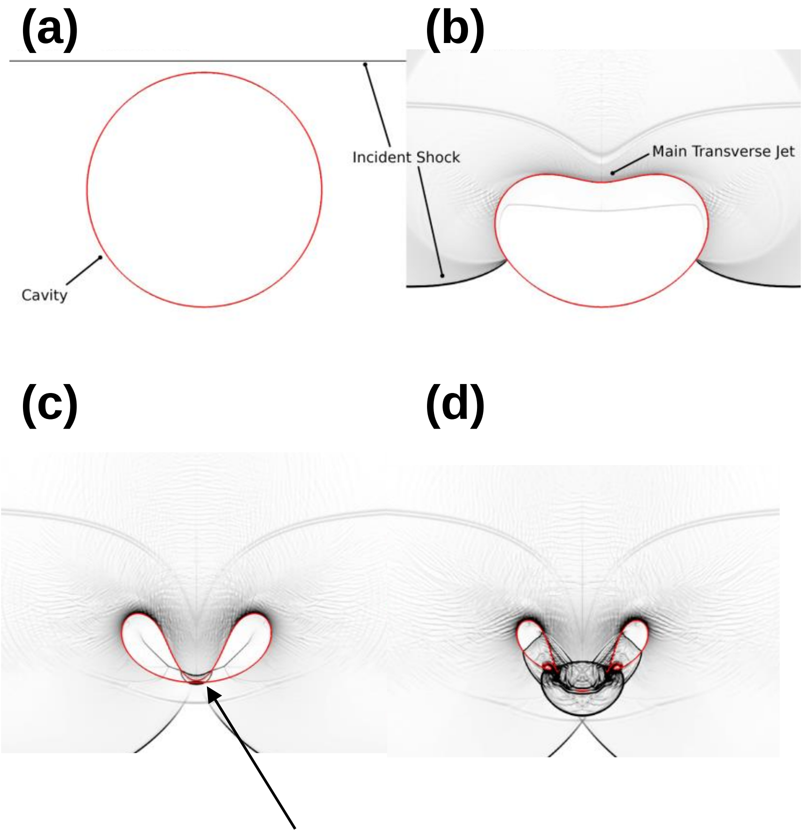

- **High pressure is generated by the colliding shock.**

https://firstlightfusion.com/
B. Tully and N. Hawker, Phys. Rev. **E93**, 053105 (2016)

First light fusion, UK – achieving ignition using shock wave

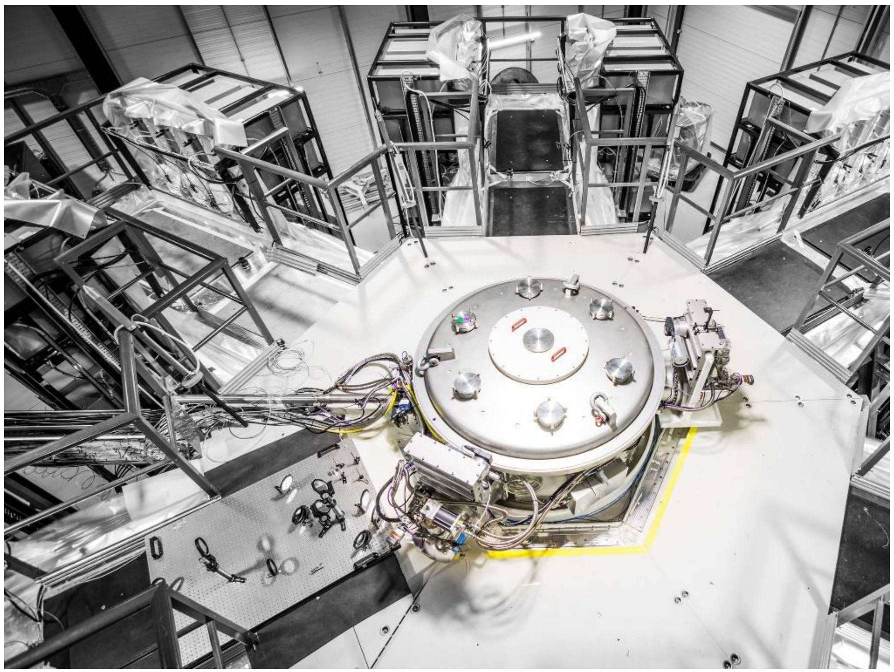

First Light Fusion

First Light Fusion is a spin-off from Oxford University department of mechanical engineering and claims to be able to harness instabilities by using asymmetrical implosion.

See http://firstlightfusion.com/

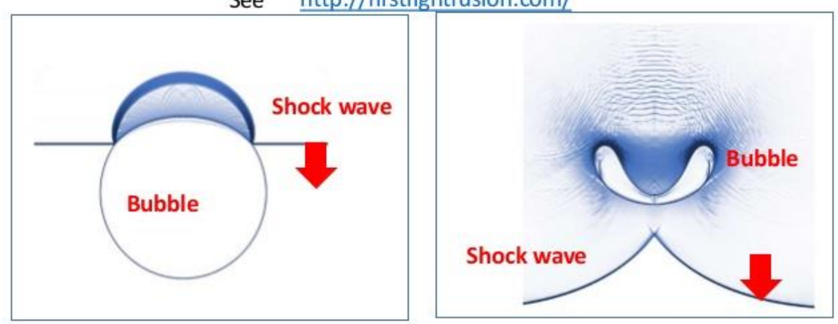

https://fsmedia.imgix.net/27/26/b2/01/8b3f/4aee/810c/8da397223c59/machine-3-23jpg.jpeg?crop=edges&fit=crop&auto=format%2Ccompress&dpr=2&h=900&w=1200
http://laurencehunt.blogspot.com/2019/

A gas gun is used to eject the projectile

https://www.youtube.com/watch?v=JN7lyxC11n0
https://www.youtube.com/watch?v=aW4eufacf-8

The pulsed-power system was built by only students

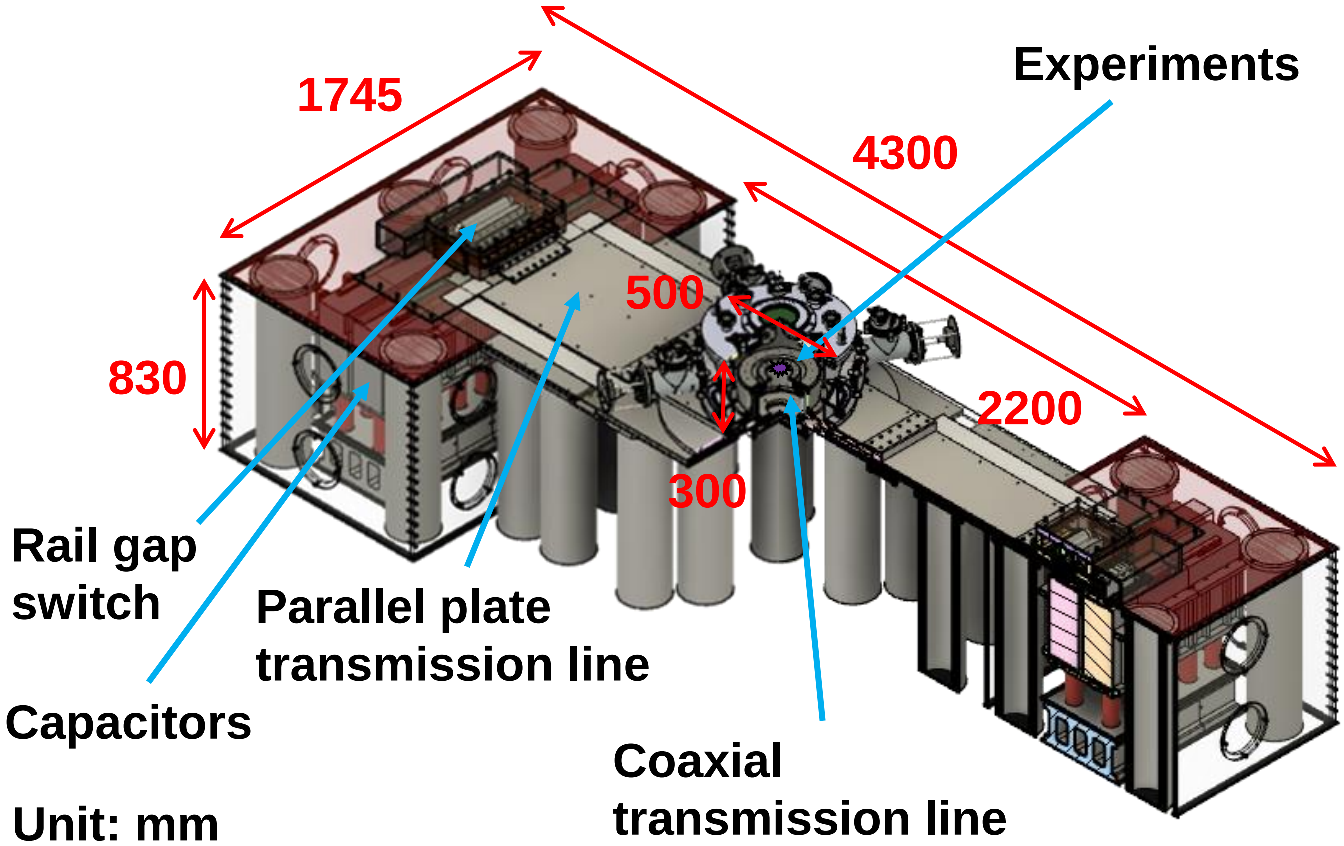

- **A 1 kJ pulsed-power system at ISAPS, NCKU started being operated since September, 2019.**

The 1-kJ pulsed-power system

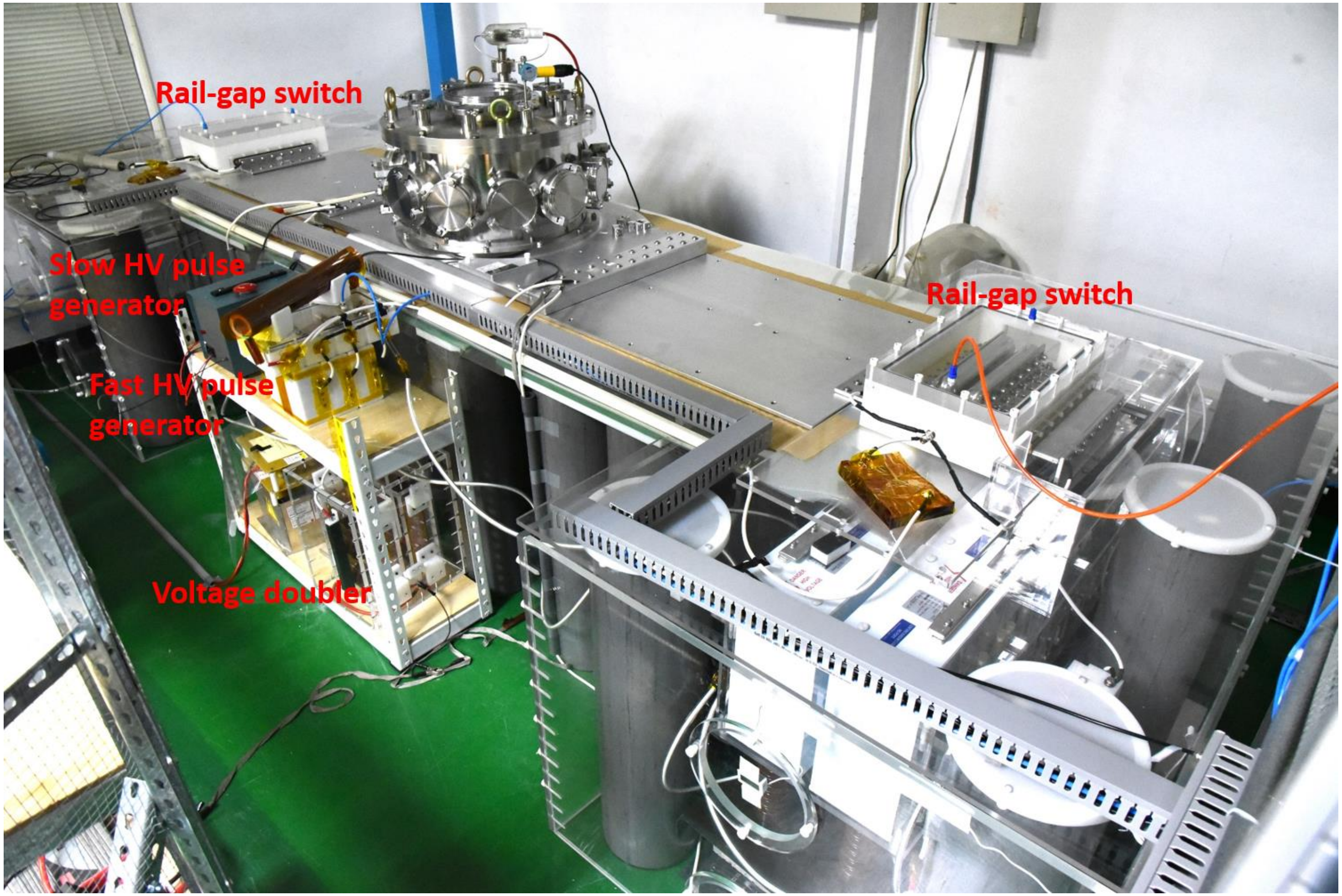

A peak current of ~135 kA with a rise time of ~1.6 us is provided by the pulsed-power system

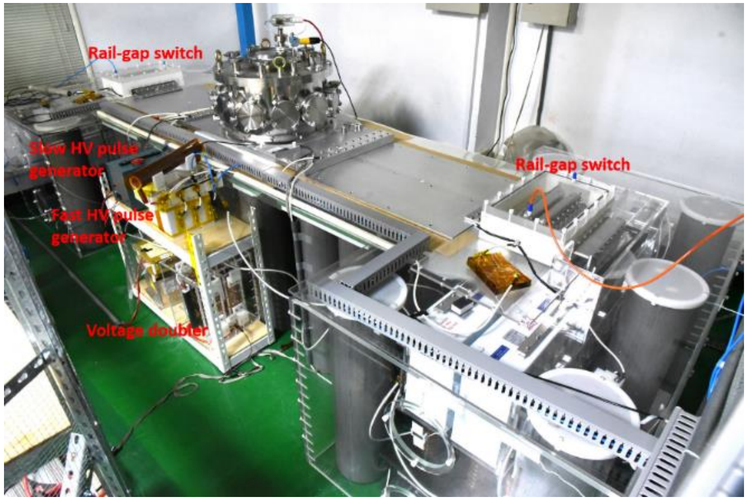

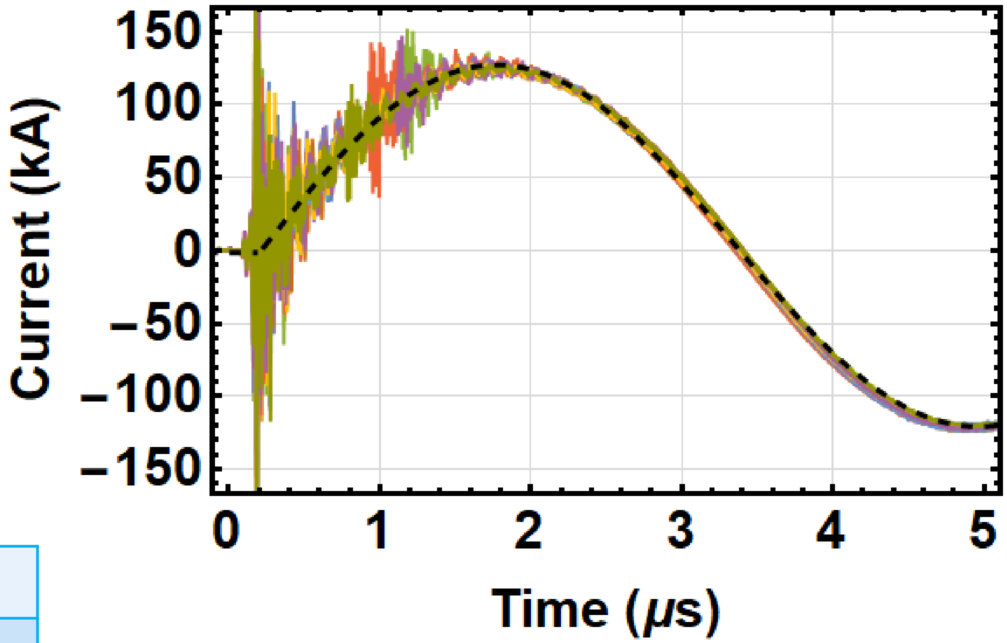

Capacitance (μF)	5
V_{charge} (kV)	20
Energy (kJ)	1
Inductance (nH)	204 ± 4
Rise time (quarter period, ns)	1592 ± 3
I_{peak} (kA)	135 ± 1

First shot with two synchronized rail-gap switches

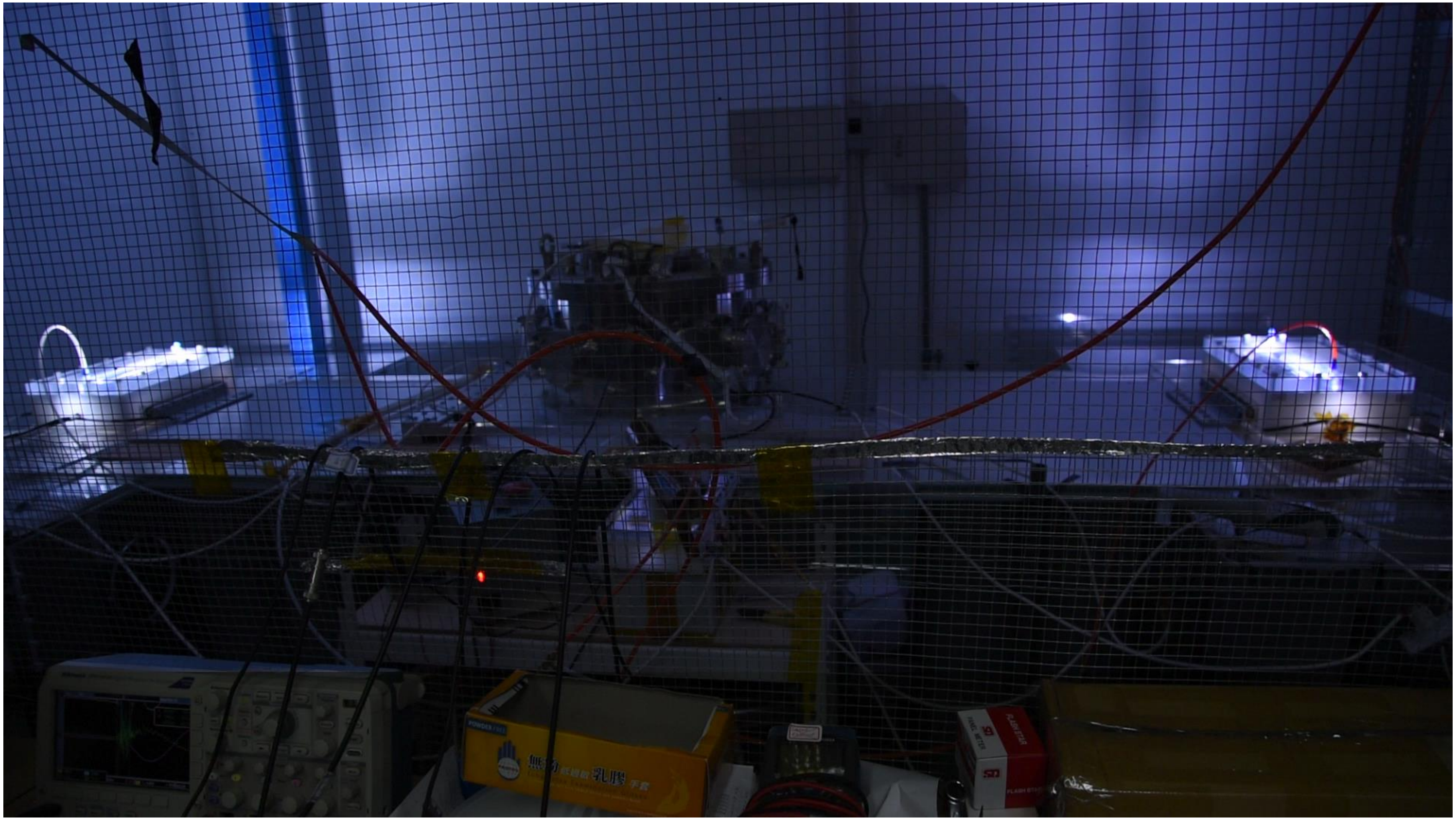

Time-resolved imaging system with temporal resolution in the order of nanoseconds was implemented

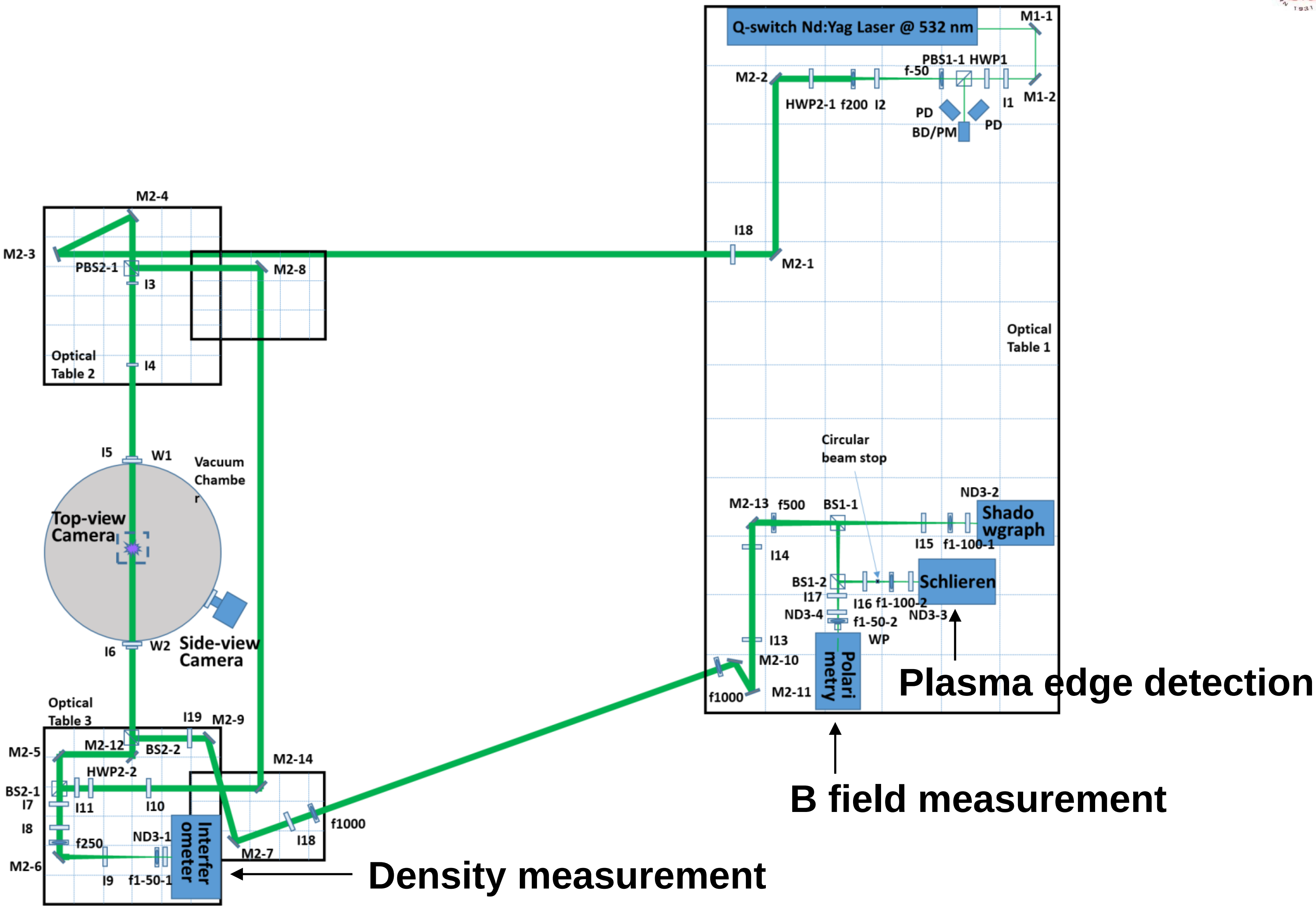

Varies diagnostics were integrated to the system

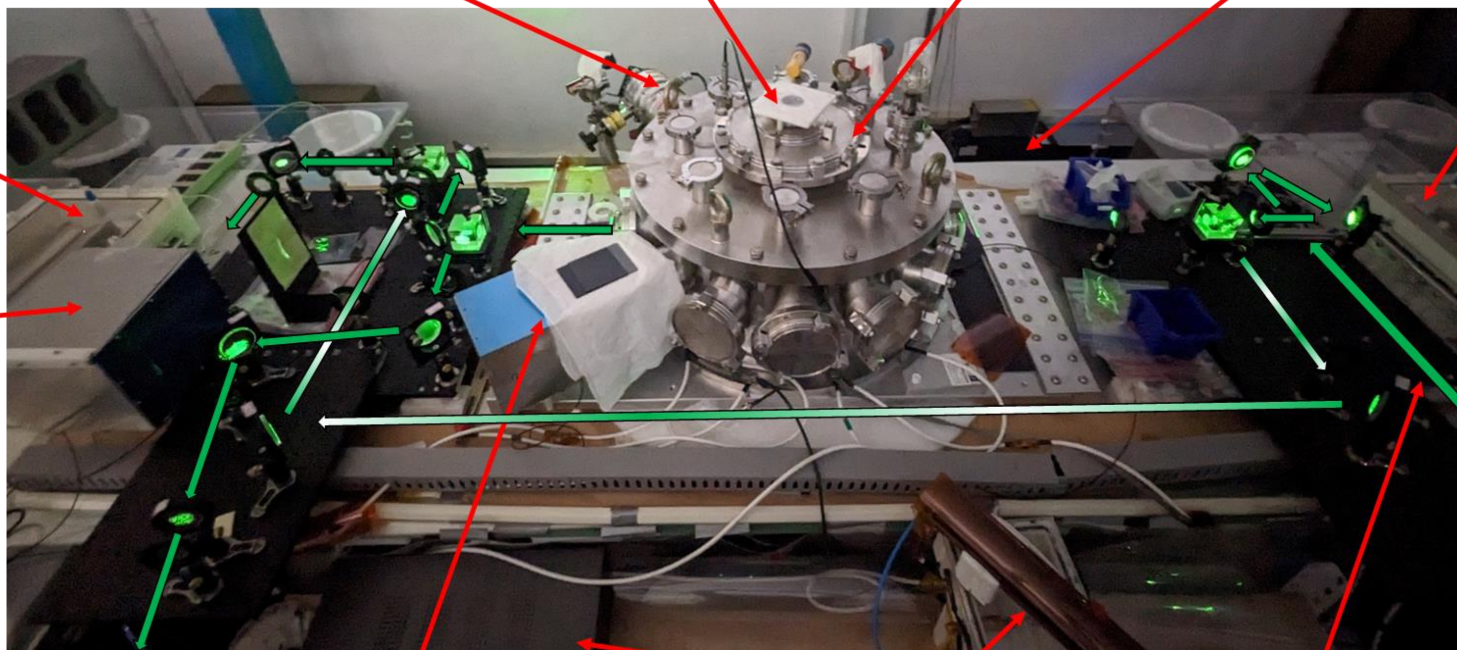

Beam path

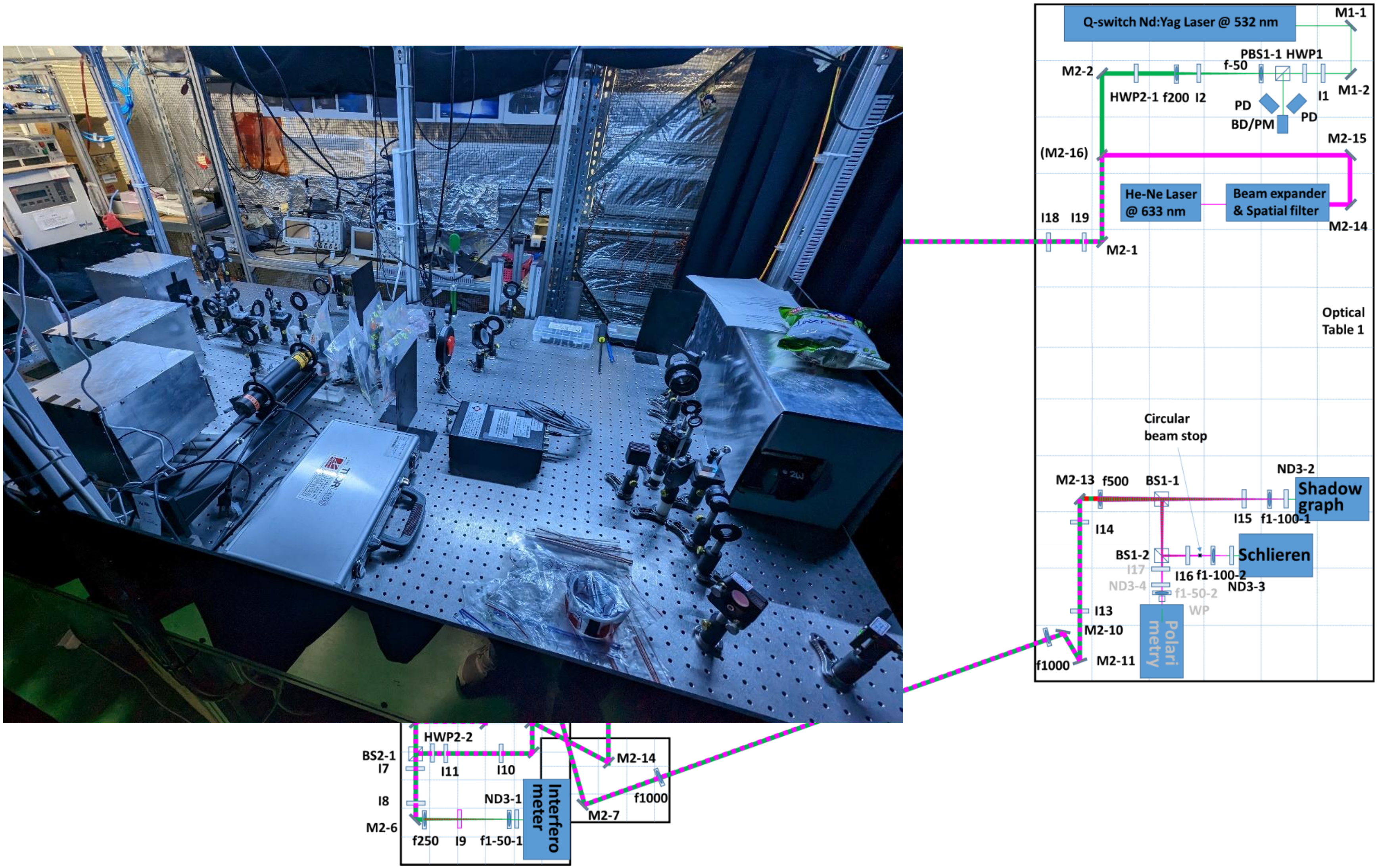
Q-switch Nd:Yag Laser @ 532 nm
M1-1
PBS1-1 HWP1
f-50
M2-2
HWP2-1 f200 I2
I1
M1-2
PD
PD
BD/PM
M2-15
(M2-16)
He-Ne Laser @ 633 nm
Beam expander & Spatial filter
I18 I19
M2-14
M2-1
Optical Table 1
Circular beam stop
ND3-2
M2-13 f500
BS1-1
Shadow graph
I15 f1-100-1
I14
BS1-2
Schlieren
I17
I16 f1-100-2
ND3-4
f1-50-2
ND3-3
WP
I13
M2-10
Polari metry
f1000
M2-11
HWP2-2
BS2-1
I7
I11
I10
M2-14
I8
ND3-1
Interfero meter
f1000
M2-7
M2-6
f250
I9
f1-50-1

Beam path

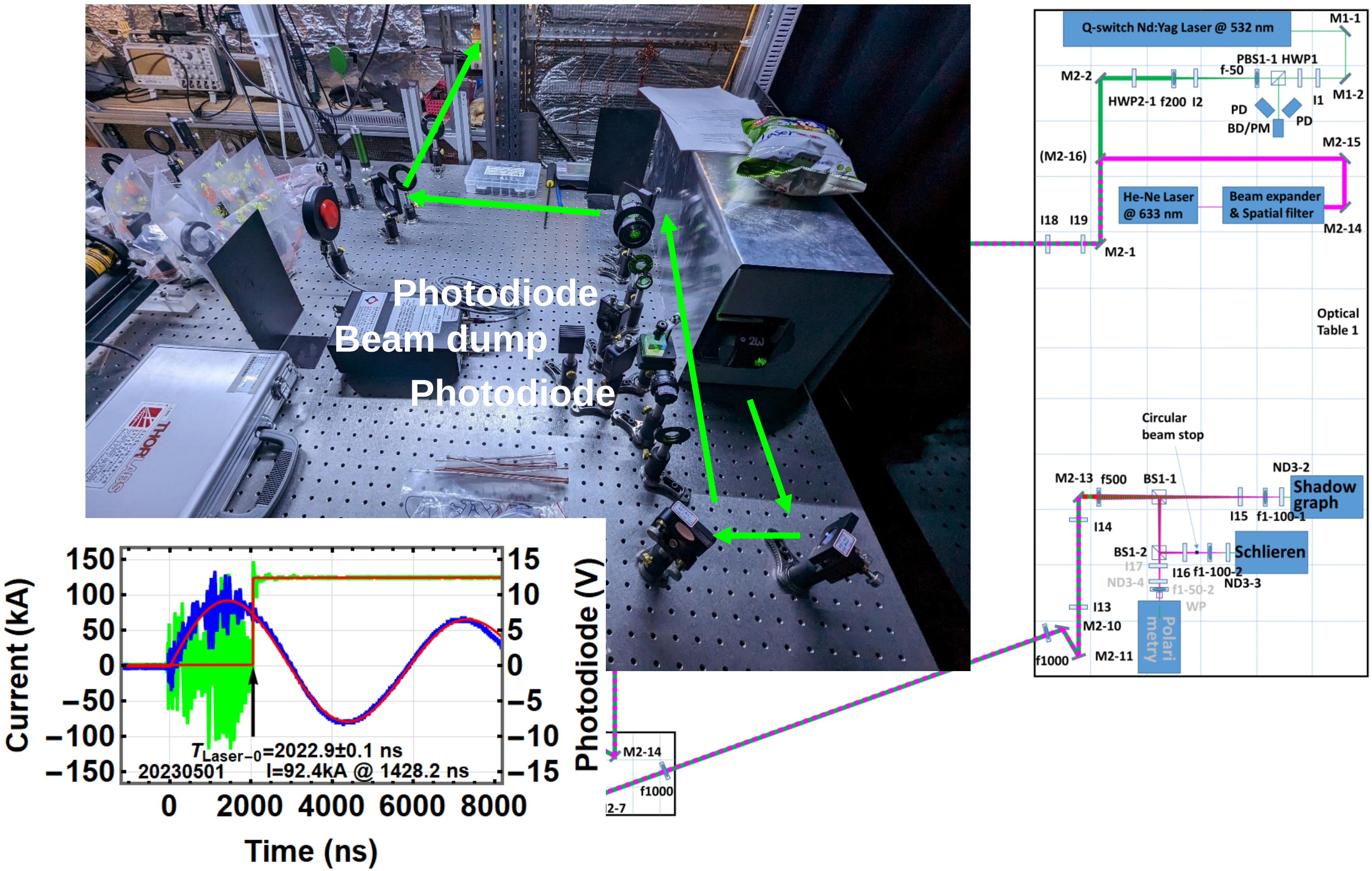
Photodiode
Beam dump
Photodiode
Current (kA)
Photodiode (V)
Time (ns)
150
100
50
0
−50
−100
−150
15
10
5
0
−5
−10
−15
0
2000
4000
6000
8000
$T_{Laser-0}$=2022.9±0.1 ns
20230501
I=92.4kA @ 1428.2 ns
Q-switch Nd:Yag Laser @ 532 nm
M1-1
M1-2
PBS1-1 HWP1
f-50
M2-2
HWP2-1 f200 I2
I1
PD
PD
BD/PM
M2-15
(M2-16)
He-Ne Laser @ 633 nm
Beam expander & Spatial filter
M2-14
I18
I19
M2-1
Optical Table 1
Circular beam stop
ND3-2
M2-13
f500
BS1-1
Shadow graph
I14
I15
f1-100-1
BS1-2
Schlieren
I17
I16 f1-100-2
ND3-4
f1-50-2
ND3-3
WP
I13
M2-10
Polari metry
f1000
M2-11
M2-14
f1000
2-7

Beam path

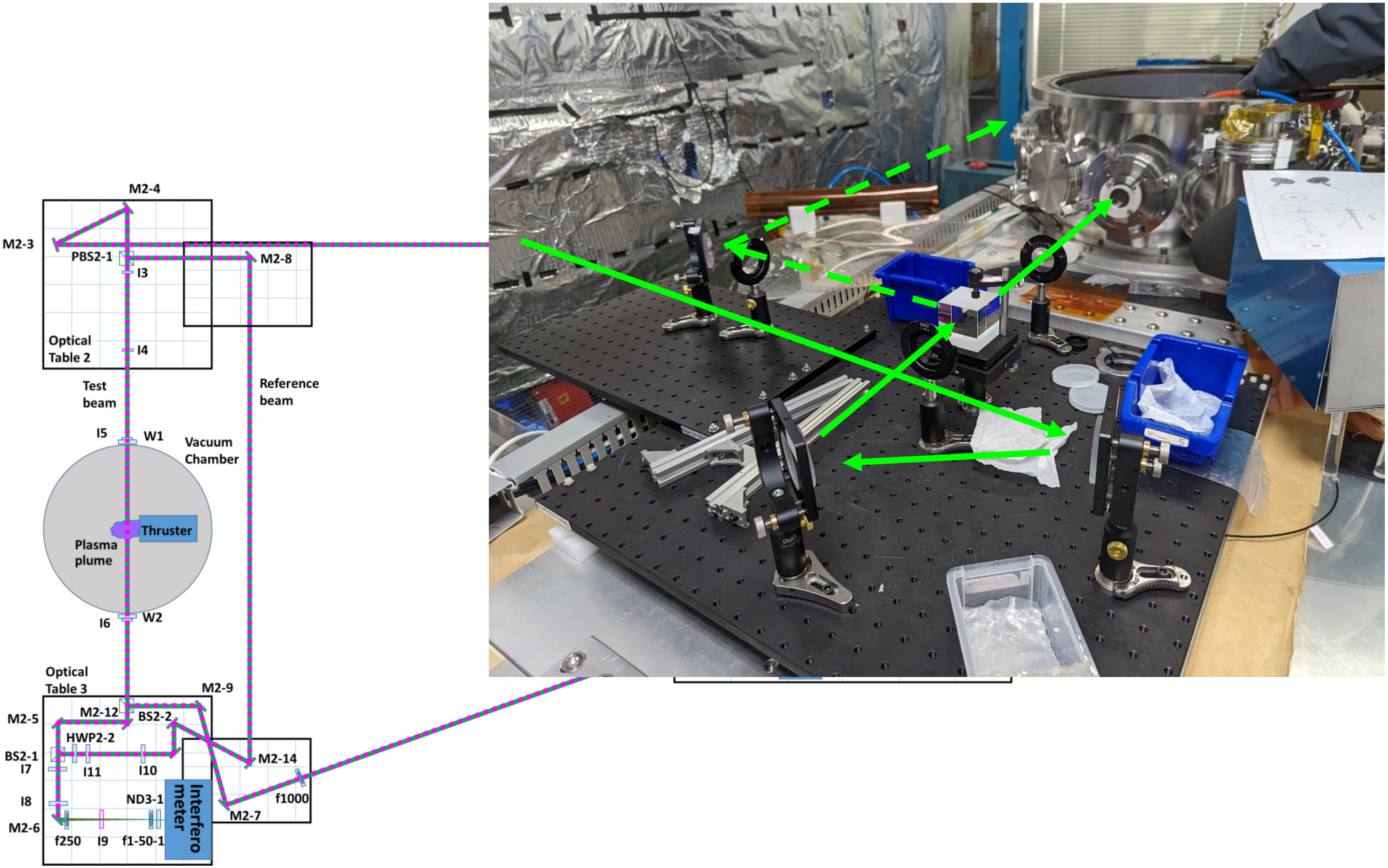
M2-4
M2-3
PBS2-1
I3
M2-8
Optical Table 2
I4
Test beam
Reference beam
I5
W1
Vacuum Chamber
Thruster
Plasma plume
I6
W2
Optical Table 3
M2-9
M2-5
M2-12
BS2-2
HWP2-2
BS2-1
I7
I11
I10
M2-14
I8
ND3-1
Interfero meter
f1000
M2-6
f250
I9
f1-50-1
M2-7

Beam path

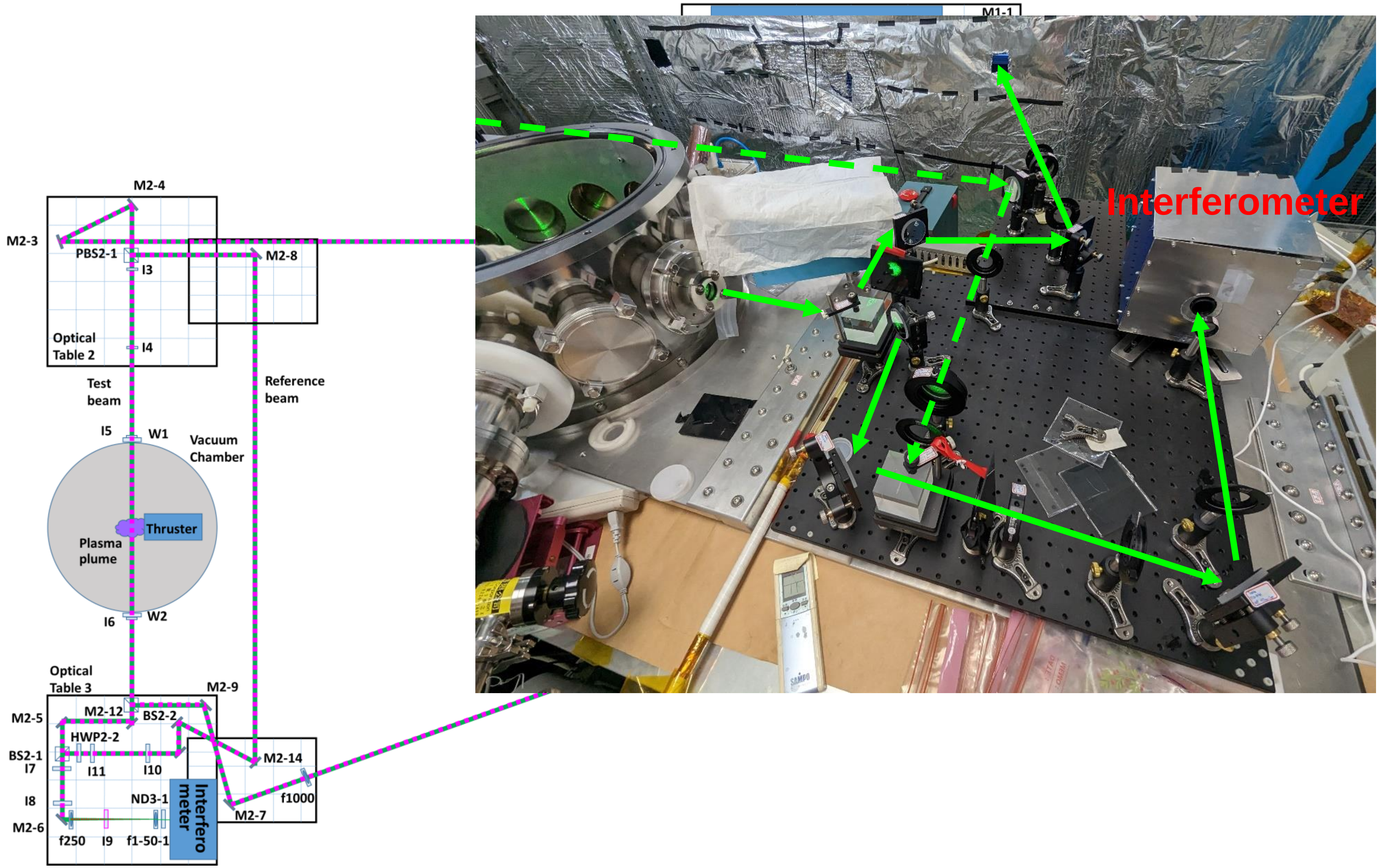
M1-1
Interferometer
M2-4
M2-3
PBS2-1
I3
M2-8
Optical
Table 2
I4
Test
beam
Reference
beam
I5
W1
Vacuum
Chamber
Thruster
Plasma
plume
W2
I6
Optical
Table 3
M2-9
M2-5
M2-12
BS2-2
HWP2-2
BS2-1
I7
I11
I10
M2-14
I8
ND3-1
Interfero
meter
f1000
M2-7
M2-6
f250
I9
f1-50-1

Beam path

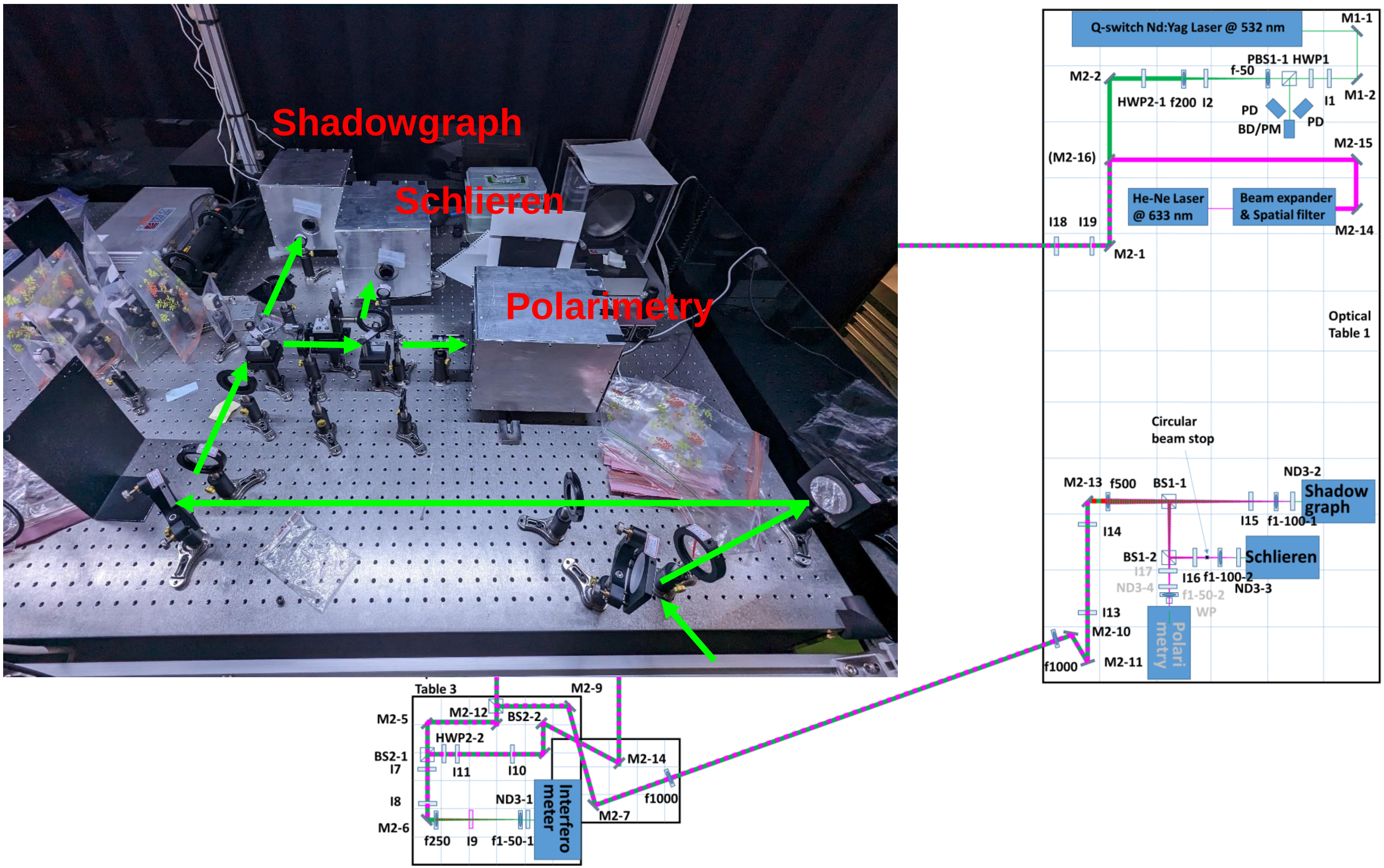

Shadowgraph
Schlieren
Polarimetry
Q-switch Nd:Yag Laser @ 532 nm
M1-1
PBS1-1 HWP1
f-50
M2-2
HWP2-1 f200 I2
I1
M1-2
PD
PD
BD/PM
M2-15
(M2-16)
He-Ne Laser @ 633 nm
Beam expander & Spatial filter
I18 I19
M2-14
M2-1
Optical Table 1
Circular beam stop
ND3-2
M2-13 f500
BS1-1
Shadow graph
I14
I15 f1-100-1
BS1-2
Schlieren
I17
I16 f1-100-2
ND3-4
f1-50-2
ND3-3
WP
I13
M2-10
Polari metry
f1000
M2-11
Table 3
M2-9
M2-5
M2-12
BS2-2
HWP2-2
BS2-1
I7
I11
I10
M2-14
I8
ND3-1
Interfero meter
f1000
M2-6
M2-7
f250 I9 f1-50-1

Laboratory astrophysics: plasma jet can be generated by a conical-wire array driven by the PGS machine

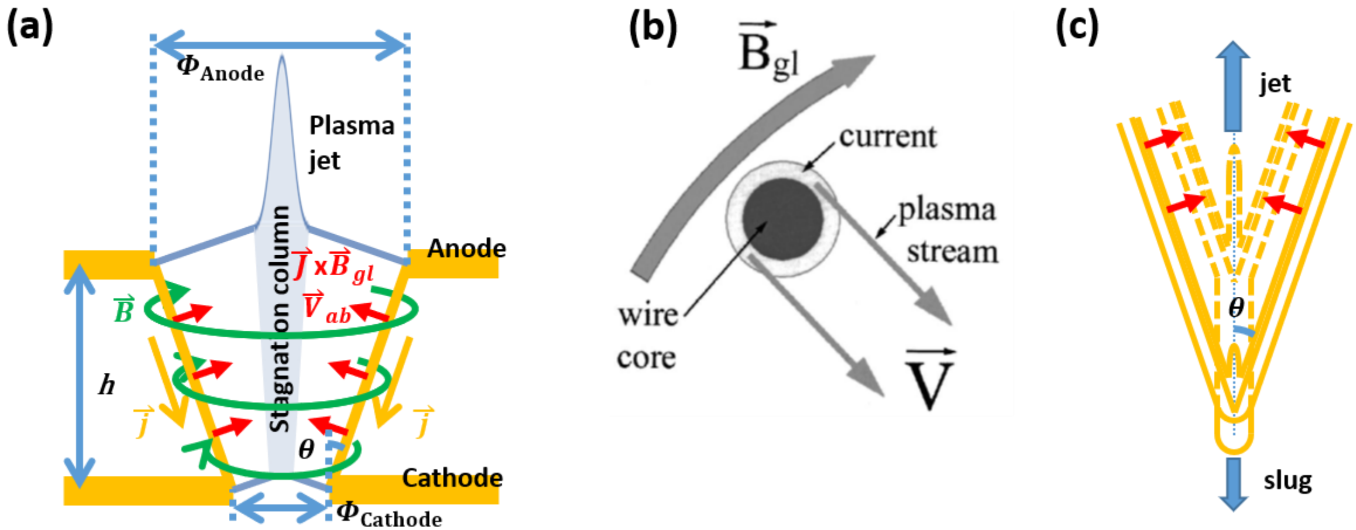

- **Herbig-Haro (HH) 111 is a plasma jet driven by a compact molecular core in the L1617 cloud complex where a young star locates*. The plasma jet in HH 111 is well collimated with the velocity of 220−330 km/s**.**

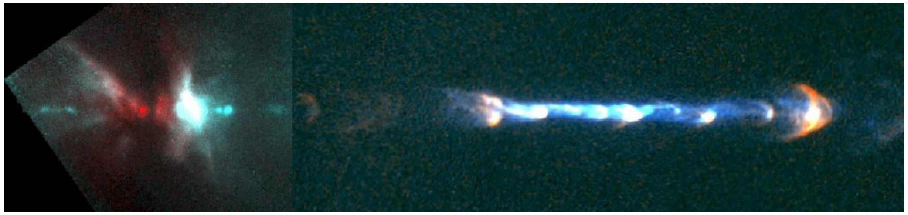

*Bo Reipurth and Steve Heathcote. 50 Years of Herbig-Haro Research, pages 3–18. Springer Netherlands, Dordrecht, 1997.
**Patrick Hartigan, Jon A. Morse, Bo Reipurth, Steve Heathcote, and John Bally. The Astrophysical Journal, 559(2):L157–L161, oct 2001.
*** Bo Reipurth and John Bally. Annual Review of Astronomy and Astrophysics, 39(1):403–455, sep 2001.

Our conical-wire array consists of 4 tungsten wires with an inclination angle of 30° with respect to the axis

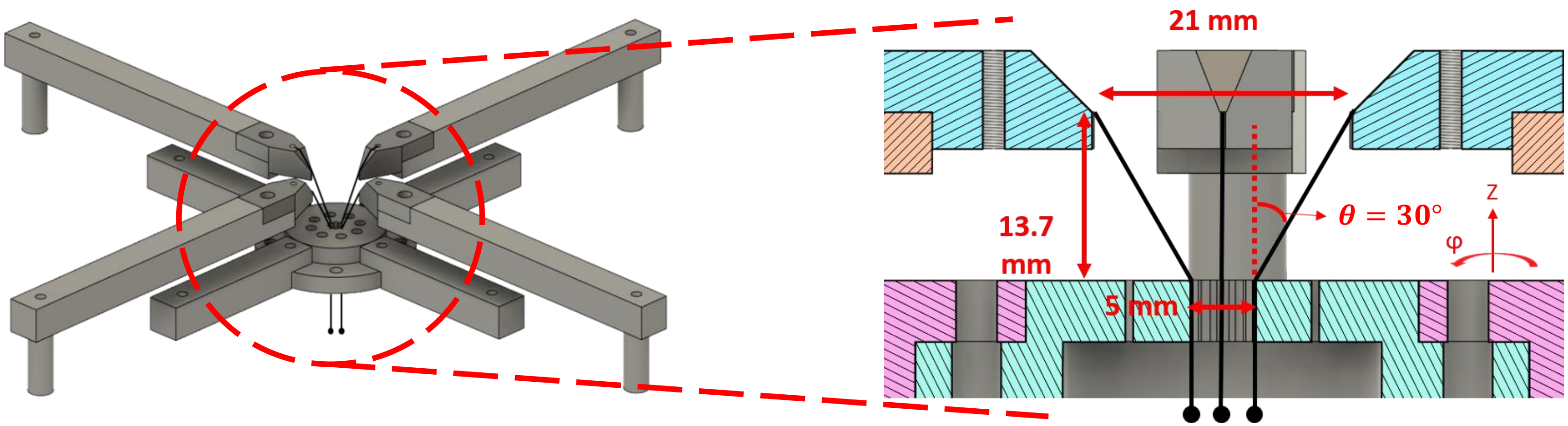

- **Conical-wire array**

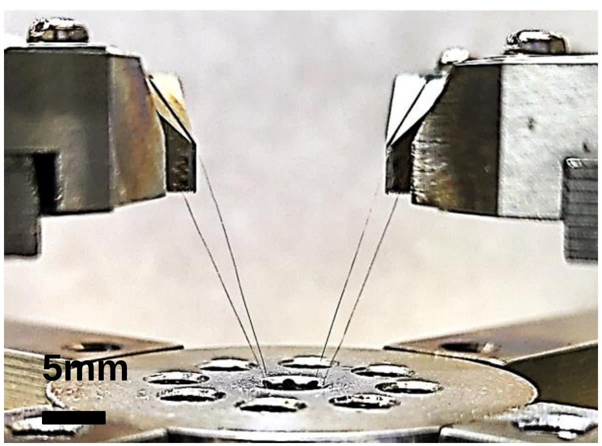

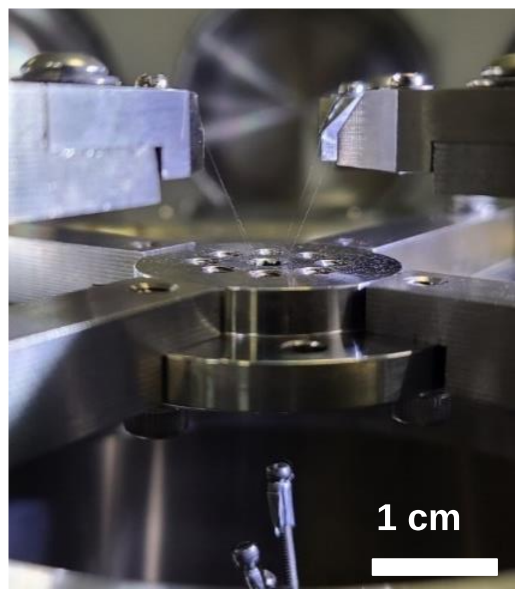

- **Material : Tungsten.**
- **Number of wires : 4.**
- **Diameter : 20 μm.**

Y.-C. Lin, NCKU Master Thesis 2021

Self-emission of the plasma jet in the UV to soft x-ray regions was captured by the pinhole camera

- Image in UV/soft x ray

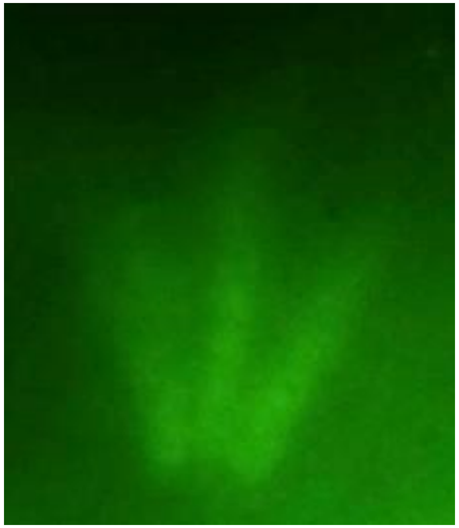

(Brightness is increased by 40 %.)

- Pinhole diameter: 0.5 mm, i.e., spatial resolution: 1 mm.

- Image in visible light

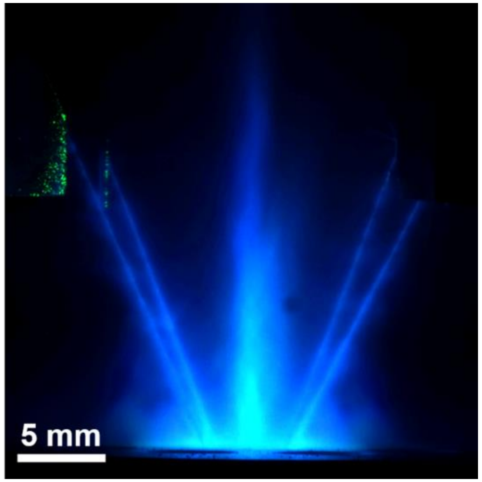

(Enhanced by scaling the intensity range linearly from 0 − 64 to 0 − 255.)

Y.-C. Lin, NCKU Master Thesis 2021
P.-Y. Chang, etc, Rev. Sci. Instrum., 93, 043505 (2022)

The MCP was burned due to the higher DC voltage supply

- Image in UV/soft x ray

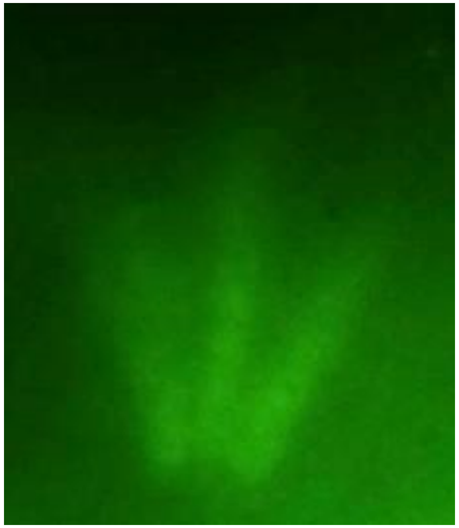

(Brightness is increased by 40 %.)

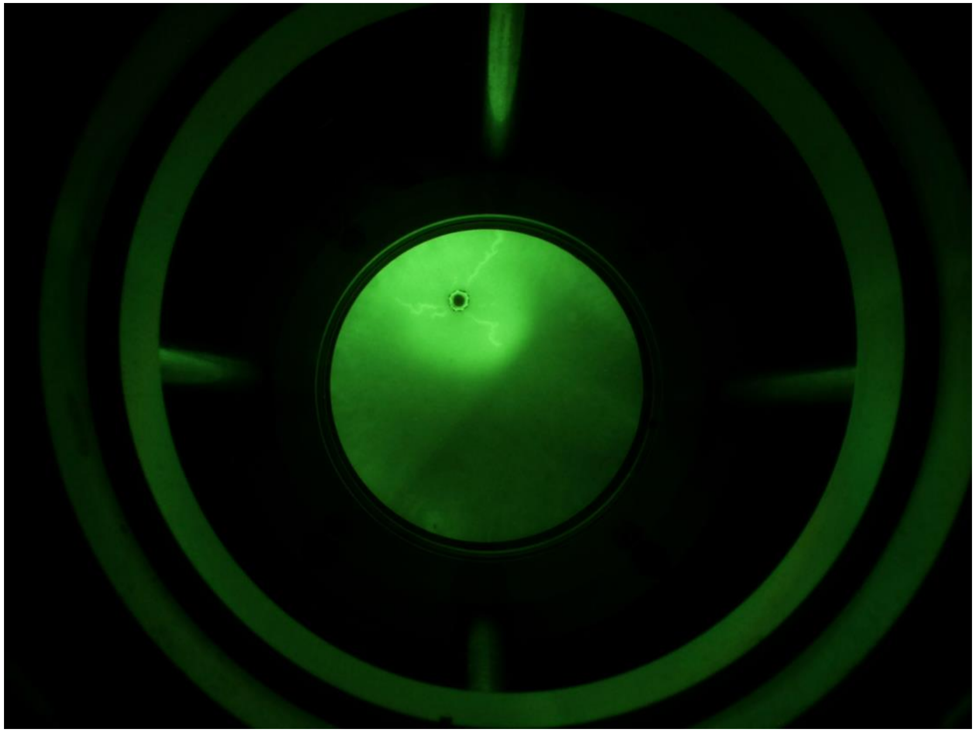

- Pinhole diameter: 0.5 mm, i.e., spatial resolution: 1 mm.

Y.-C. Lin, 2021/8/31 Final report
P.-Y. Chang, etc, Rev. Sci. Instrum., 93, 043505 (2022)

Plasma jet propagation was observed using laser diagnostics

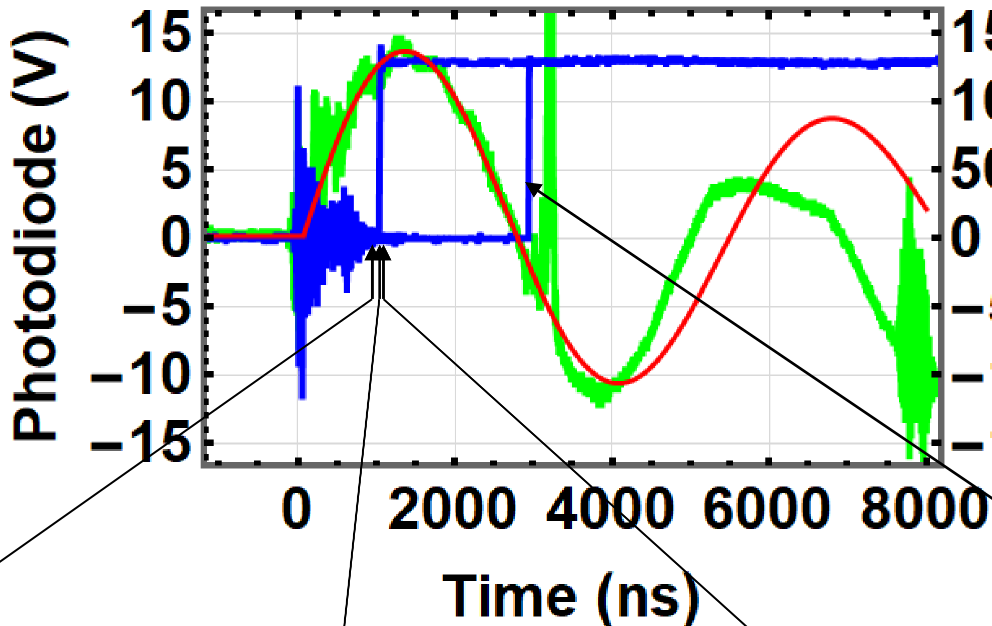

- **Shadowgraph images:**

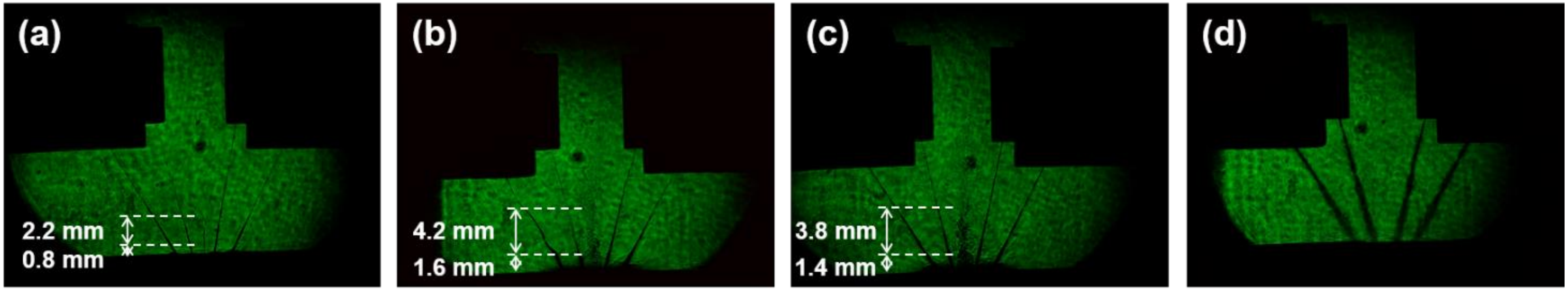

930 $\pm$ **20 ns** | **975** $\pm$ **2 ns** | **985** $\pm$ **3 ns** | **2945** $\pm$ **2 ns**

P.-Y. Chang, etc, Rev. Sci. Instrum., 93, 043505 (2022)

Length of the plasma jet at different time was obtained by the Schlieren images at different times

- **Shadowgraph images:**

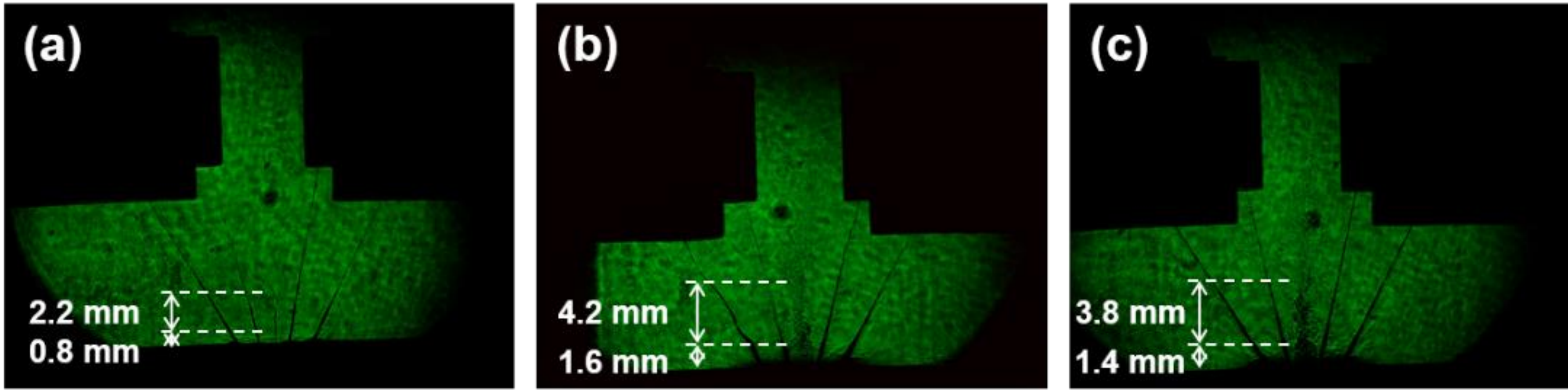

- **Schlieren images:**

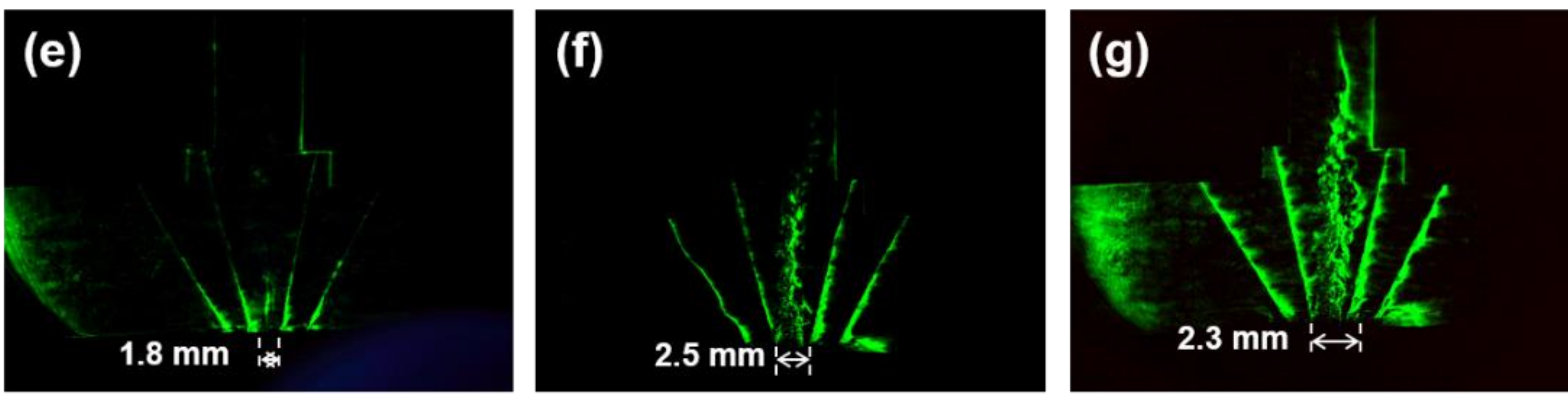

930 ± 20 ns **975 ± 2 ns** **985 ± 3 ns**

P.-Y. Chang, etc, Rev. Sci. Instrum., 93, 043505 (2022)

The measured plasma jet speed is 170 ± 70 km/s with the corresponding Mach number greater than 5

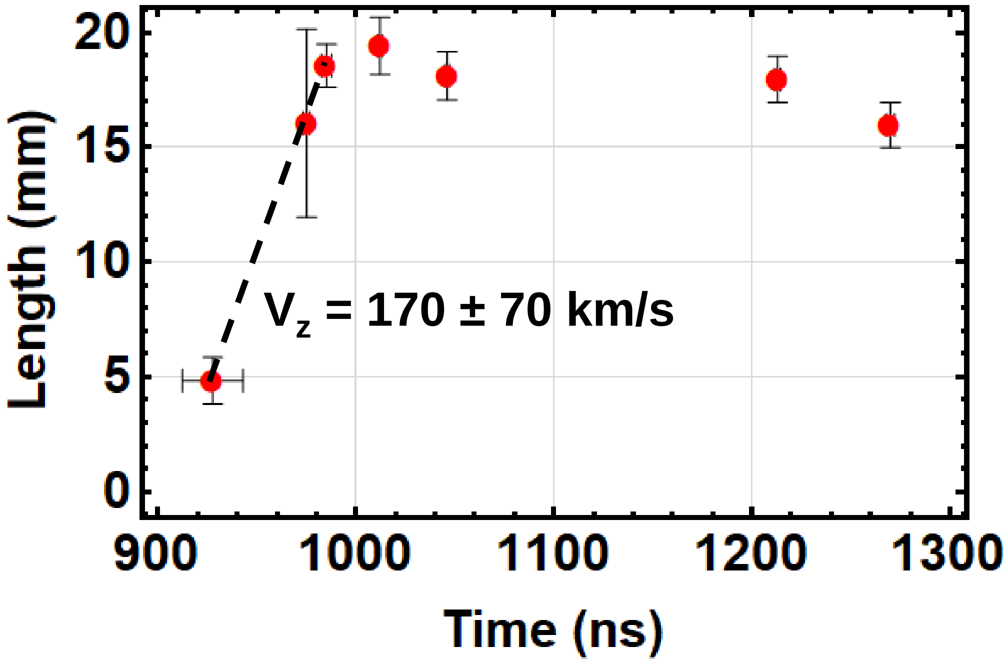

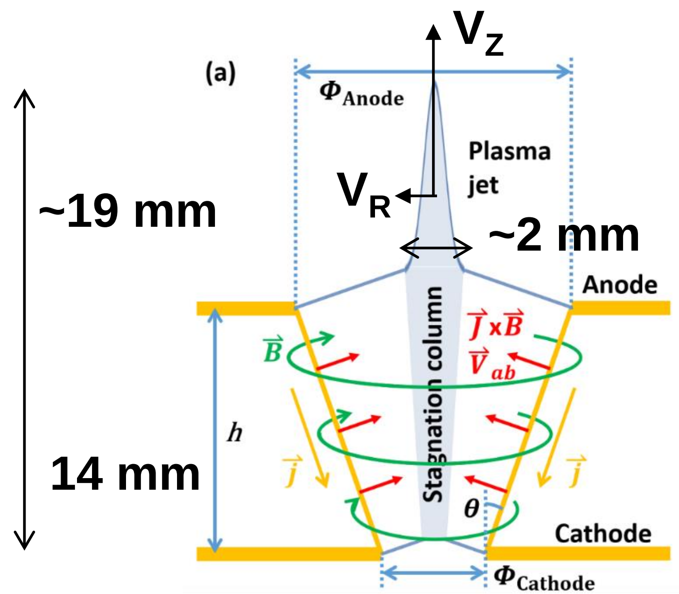

$$M = \frac{V_Z}{V_R} \geq \frac{Z}{r} \approx \frac{(19-14)\ \mathrm{mm}}{\frac{2\ \mathrm{mm}}{2}} = 5$$

$$V_{\mathrm{ab}} = V_{\mathrm{j}} \frac{\sin\theta}{1+\cos\theta} = 50\ \pm 20\ \mathrm{km/s}$$

P.-Y. Chang, etc, Rev. Sci. Instrum., 93, 043505 (2022)

Can a rotating plasma disk be formed?
To be continue…

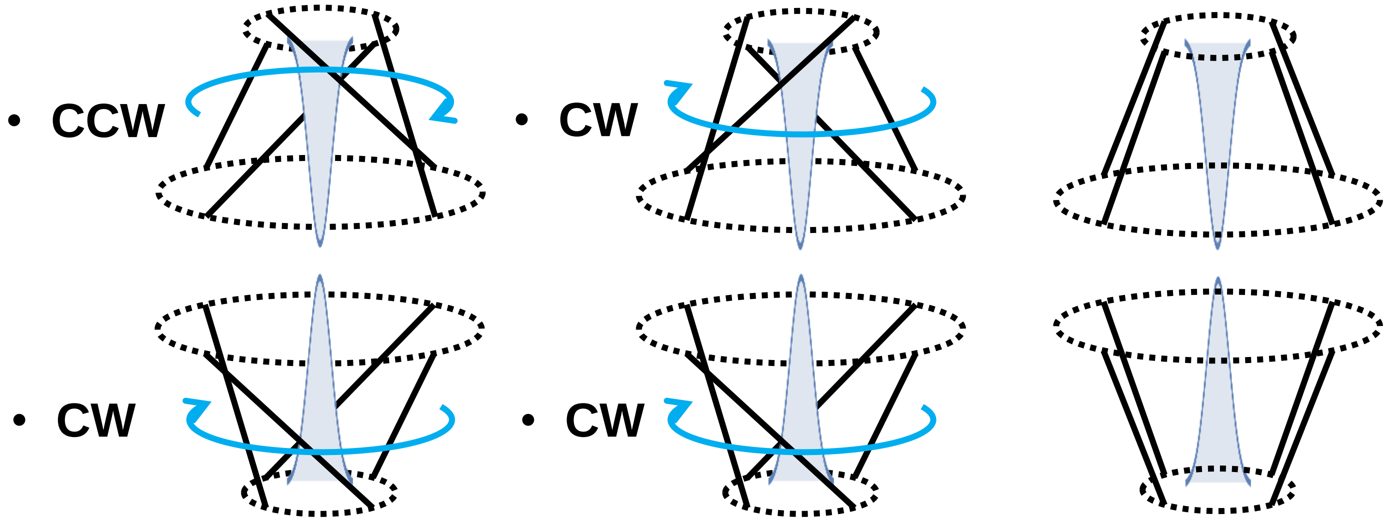

• **No rotation**

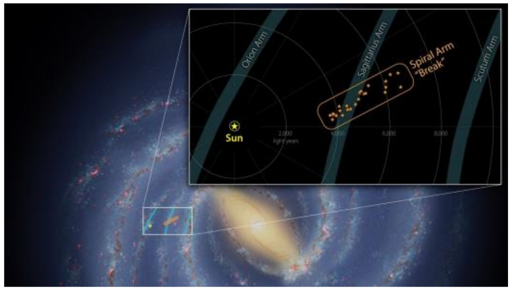

- **Astronomers Find a 'Break' in One of the Milky Way's Spiral Arms.**

https://www.nasa.gov/feature/jpl/astronomers-find-a-break-in-one-of-the-milky-way-s-spiral-arms

Plasma disk can be formed when two head-on plasma jets collide with each other

- **Astronomers Find a ‘Break’ in One of the Milky Way’s Spiral Arms.**

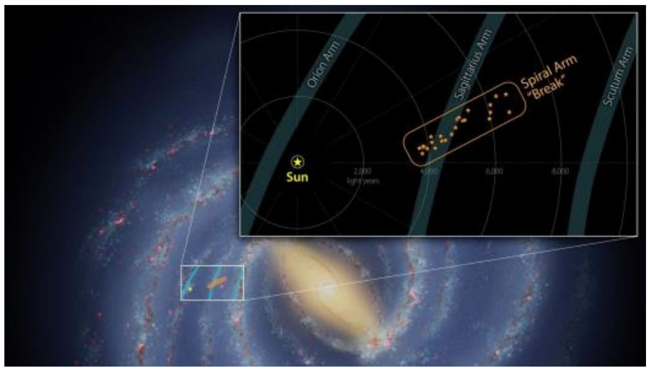

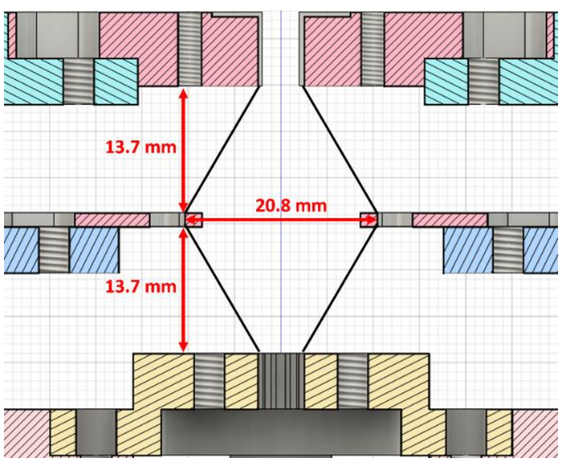

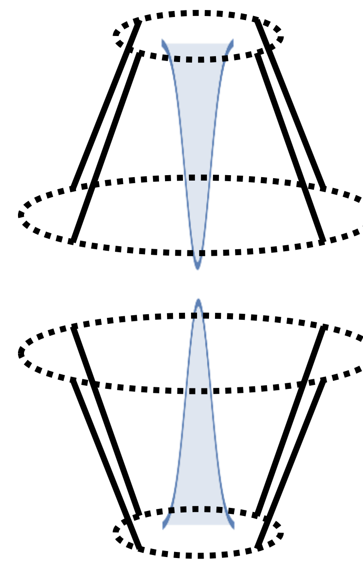

Jet Propulsion Laboratory [NASA/JPL] Astronomers Find a ‘Break’ in One of the Milky Way’s Spiral Arms (Aug 17, 2021)

A plasma disk with a height of ~0.68 mm and a width of ~7.51 mm was generated ~0.15 mm above the middle plane

- **Schlieren image:**

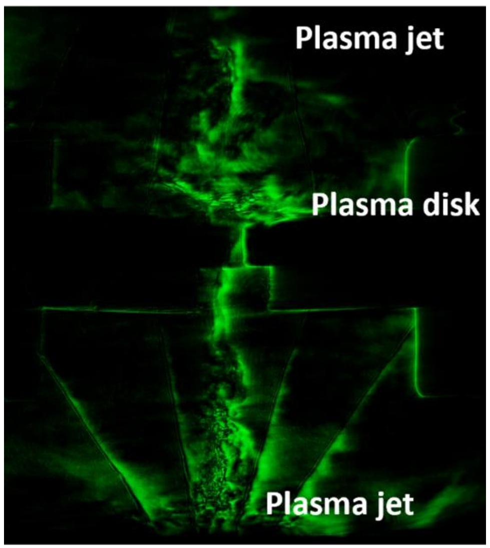

- **Time-integrated image:**

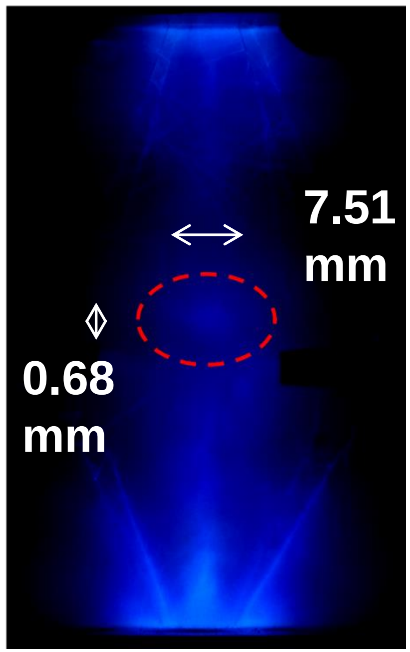

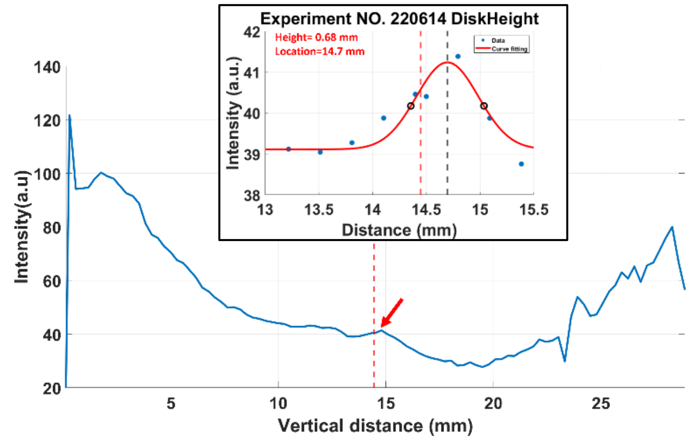

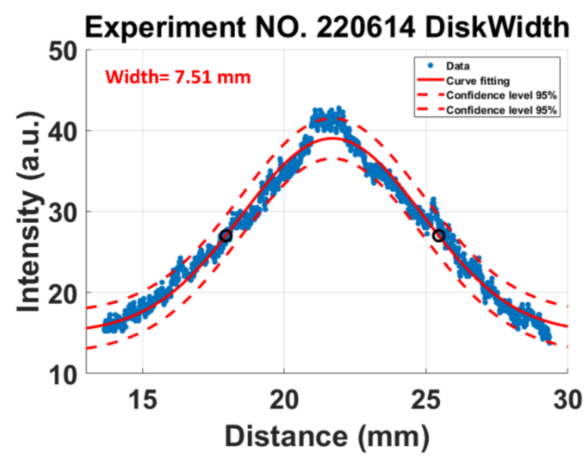

M.-S. Kuo, NCKU Master Thesis 2022

Plasma disk can be formed when two head-on plasma jets collide with each other

Schlieren

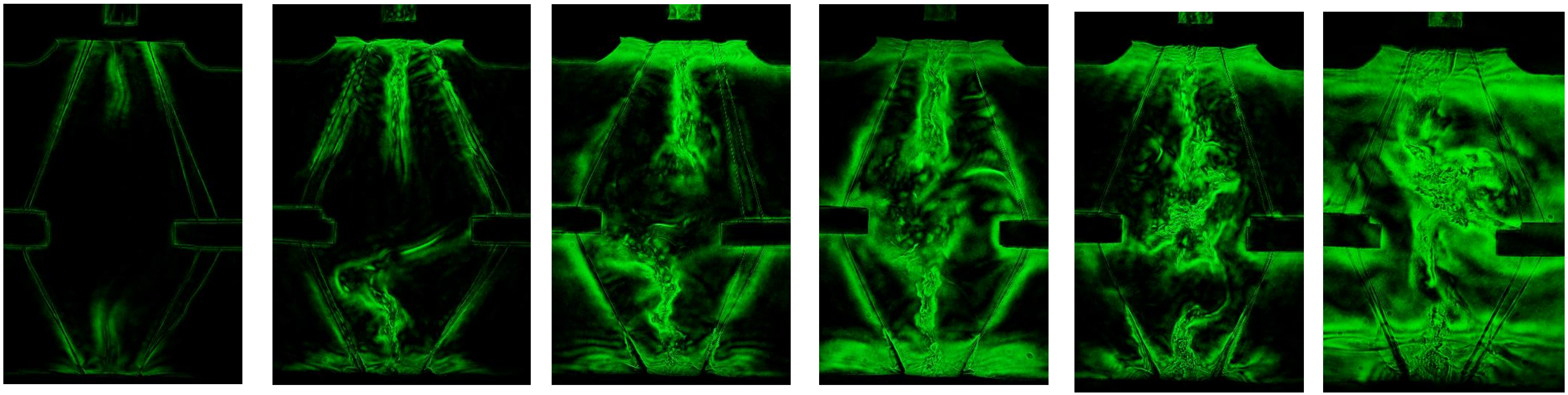

Interferometer

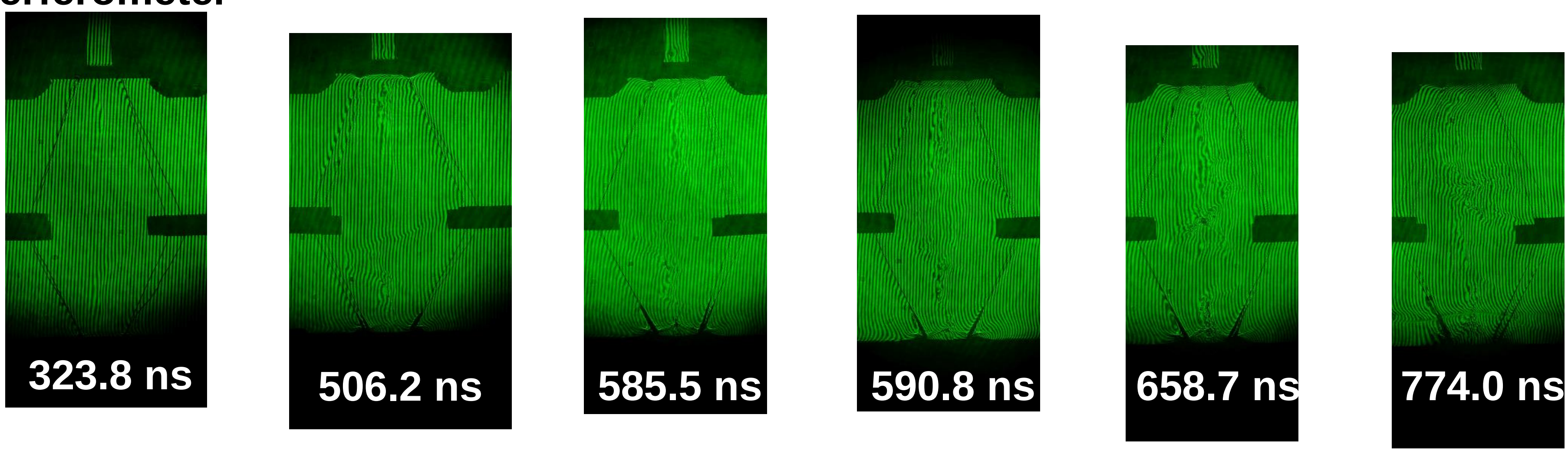

The plasma disk with a number density of ~ 10^{18} cm^{-3} was generated

Schlieren

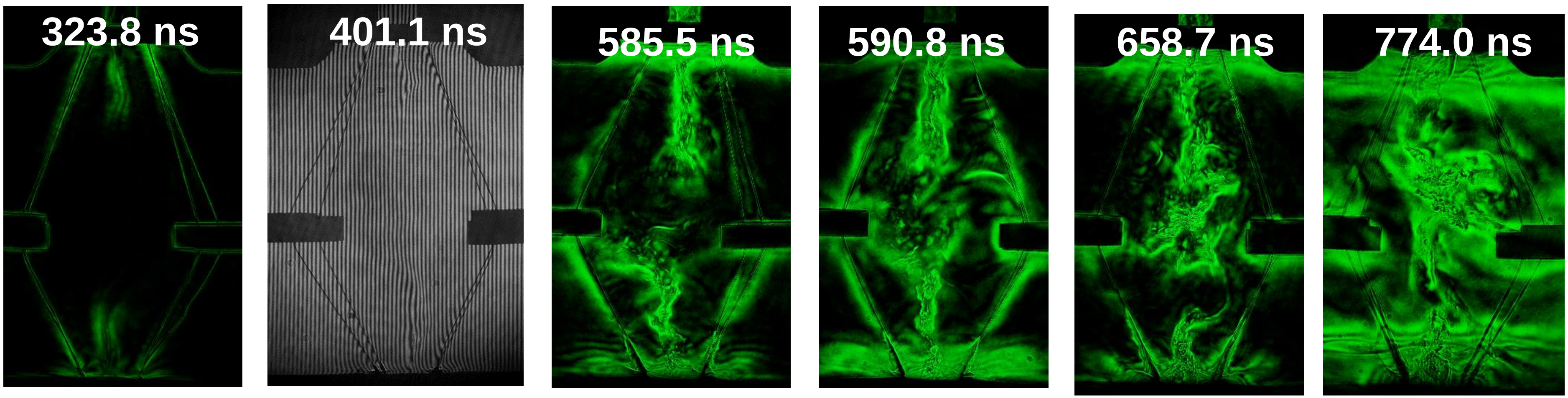

Interferometer

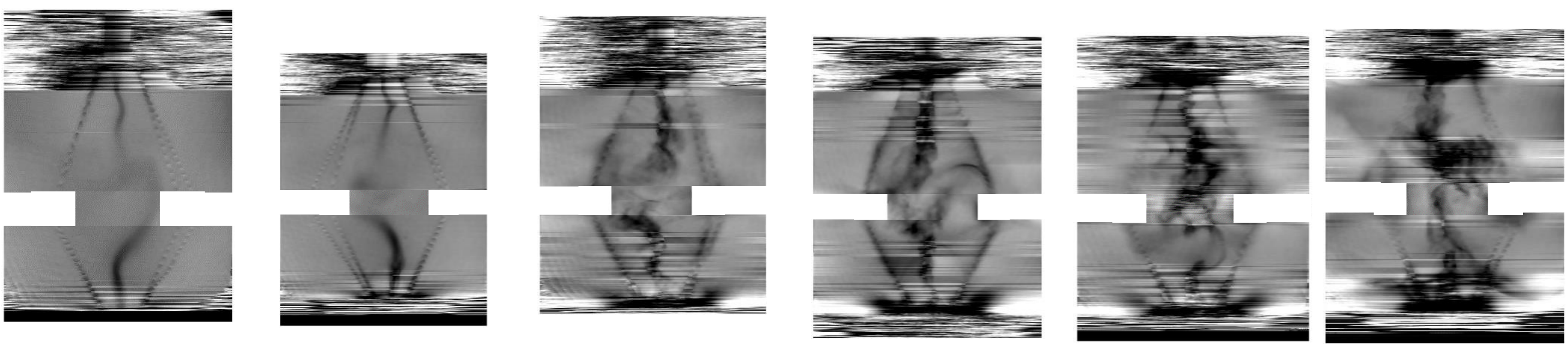

$-2\pi \sim 2\pi \Rightarrow 0 \sim 4.2 \times 10^{17}$ cm^{-2}

$\Rightarrow 8.4 \times 10^{17}$ cm^{-3} for L= 5mm

Φ(rad)

What if we twist the conical-wire array?

- **Non-rotation**

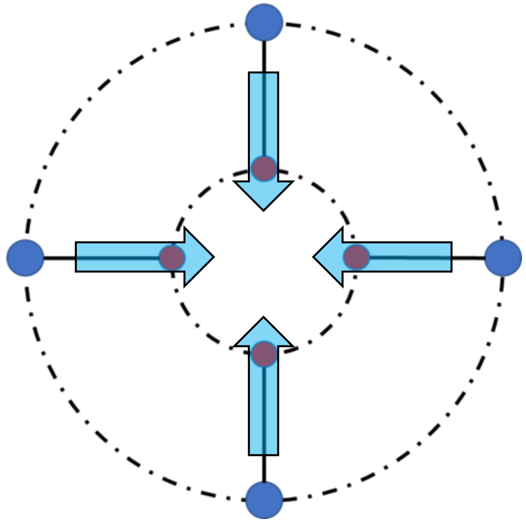

- **Clockwise 45°**

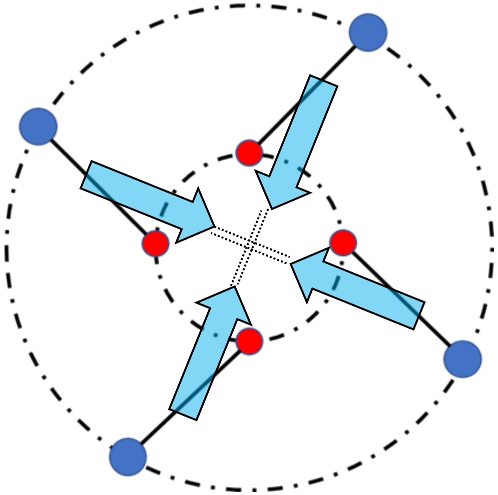

- **CCW 45°**

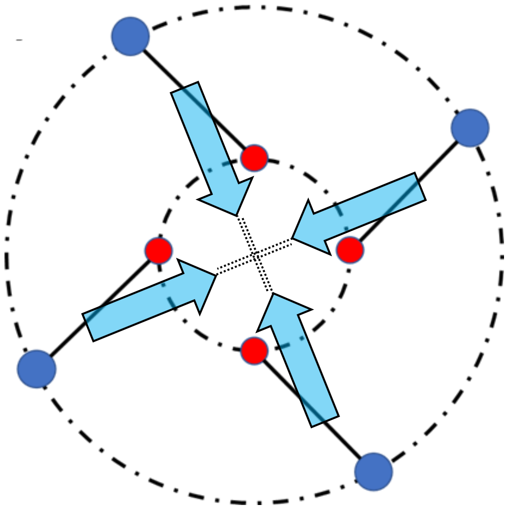

Y.-C. Lin, NCKU Master Thesis 2021

The plasma jet is a bright spot from the top view

- **Non-rotation**

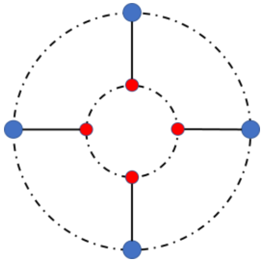

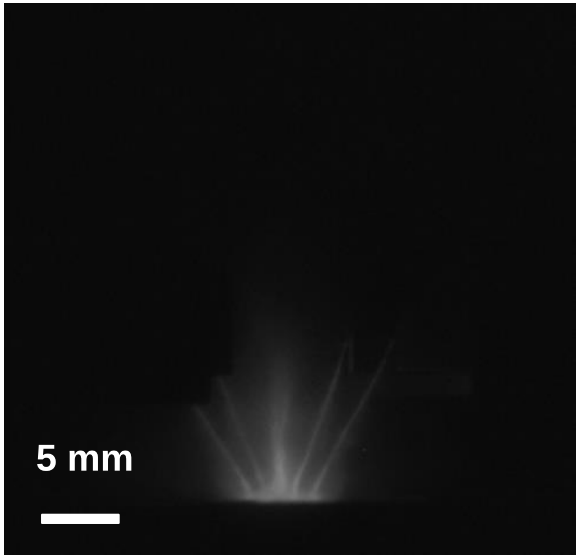

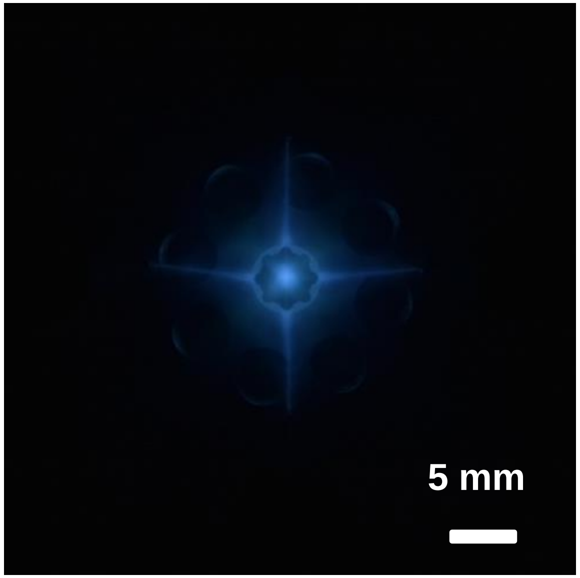

Hollow plasma jets were generated when the conical-wire arrays were twisted

- **Clockwise 30 °**

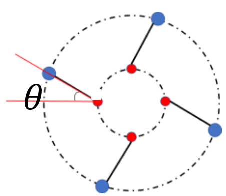

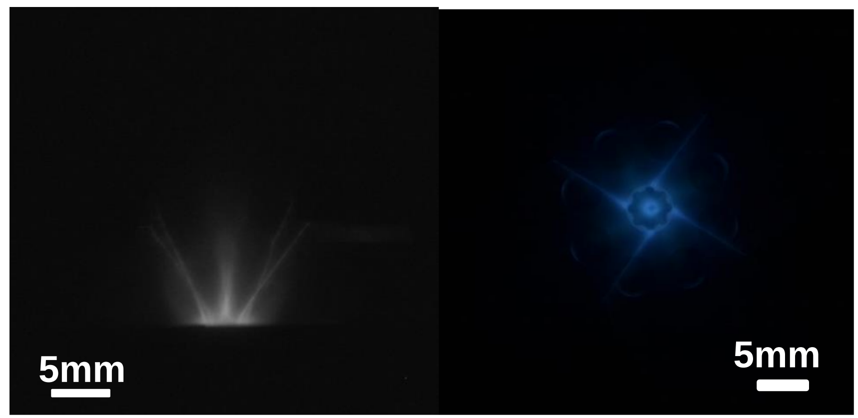

- **Counter clockwise 30 °**

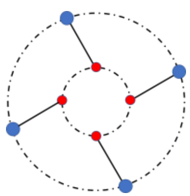

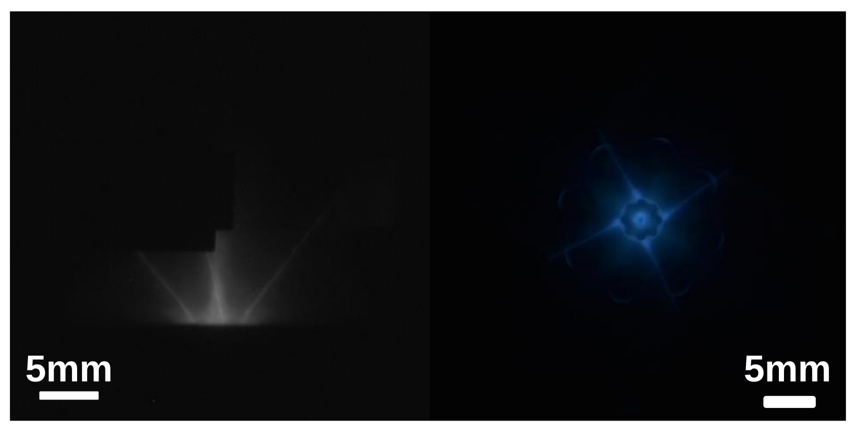

Y.-C. Lin, NCKU Master Thesis 2021

The hollow region at the center was due to angular momentum conservation of the in-coming plasma flow

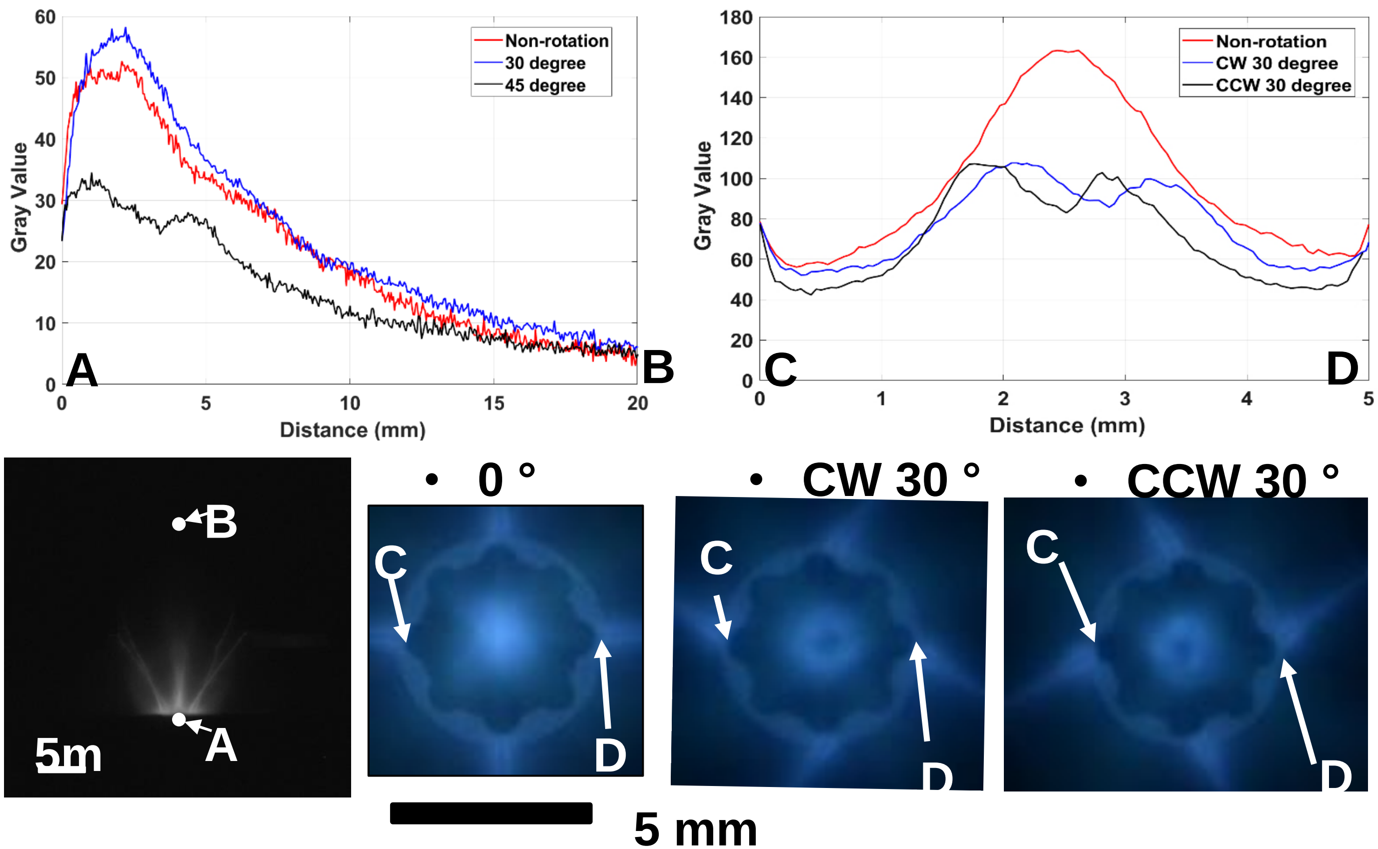

D. J. Ampleforda, et al., PRL 100, 035001 (2008)
Y.-C. Lin, NCKU Master Thesis 2021

A “tornado” is generated by the twisted conical-wire array

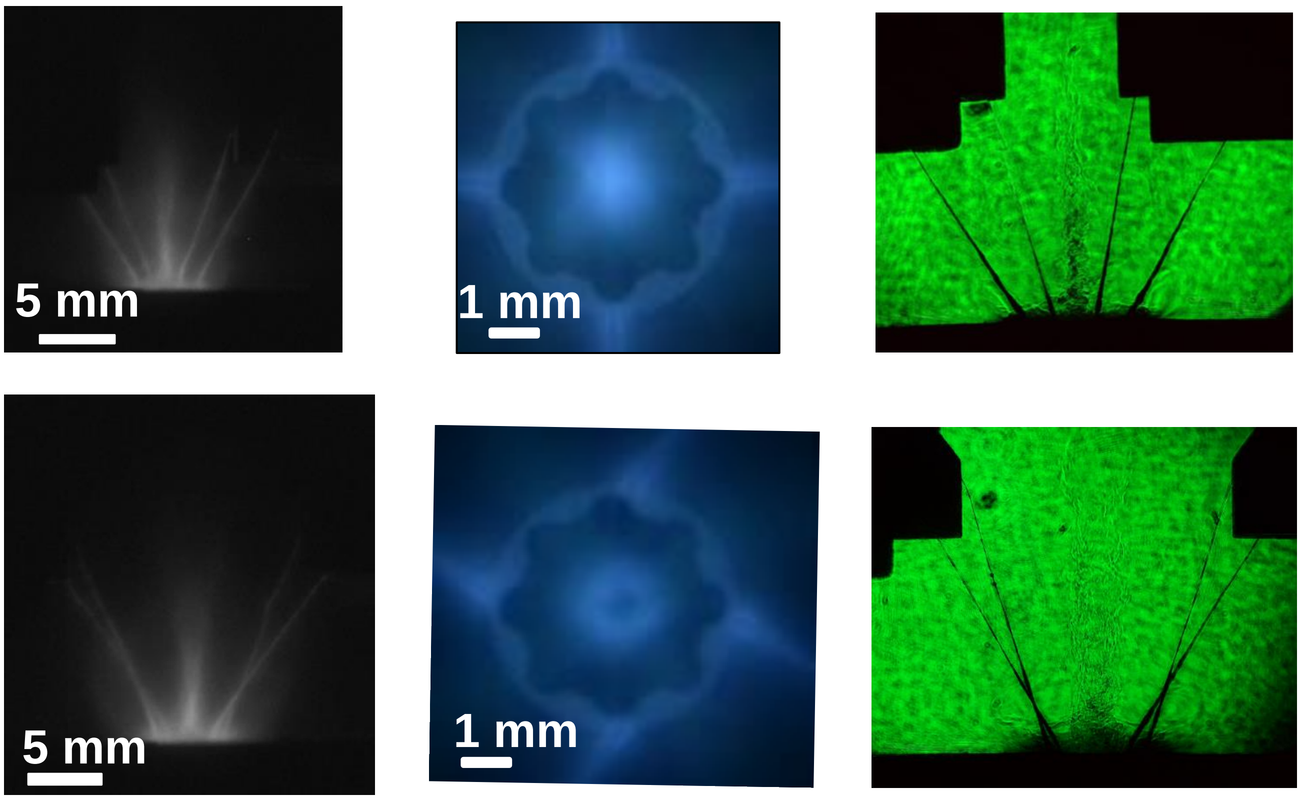

A “tornado” is generated by the twisted conical-wire array

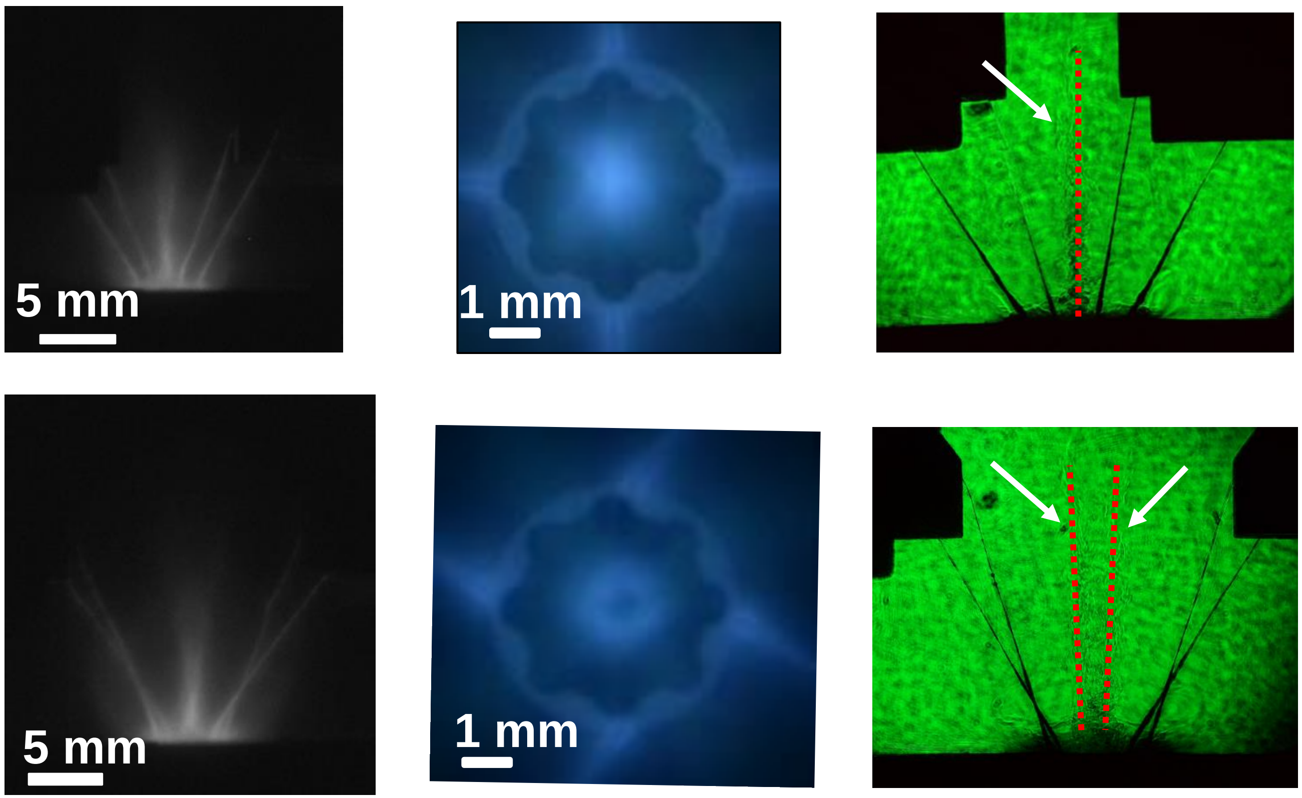

High energy density plasma (HEDP) is the regime where the pressure is greater than 0.1 T Pa (1 Mbar)

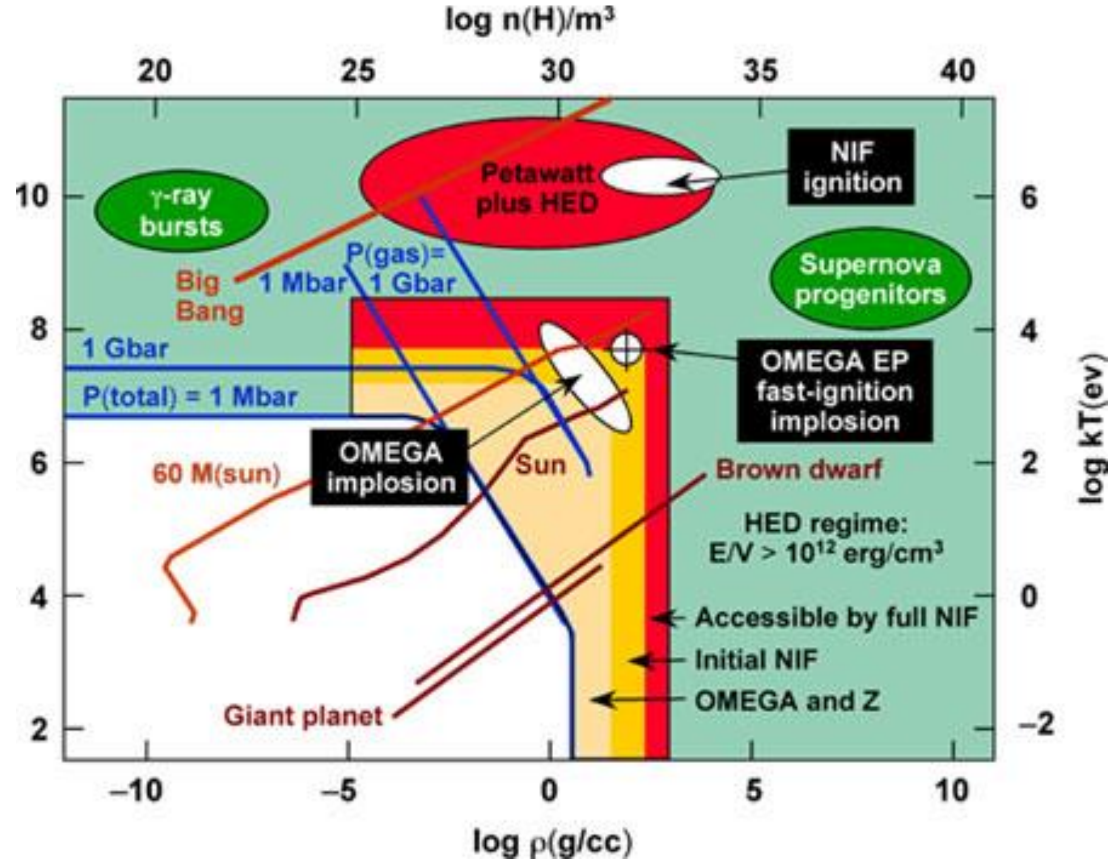

- **The energy density of HEDP regime is higher than 1 kJ of energy per 10 mm^3.**

Frontiers in High Energy Density Physics: The X-Games of Contemporary Science © (2003) by the National Academy of Sciences, courtesy of the National Academies Press, Washington, D.C.

Softer material can be compressed to higher density

- **Compression of a baseball**

- **Compression of a tennis ball**

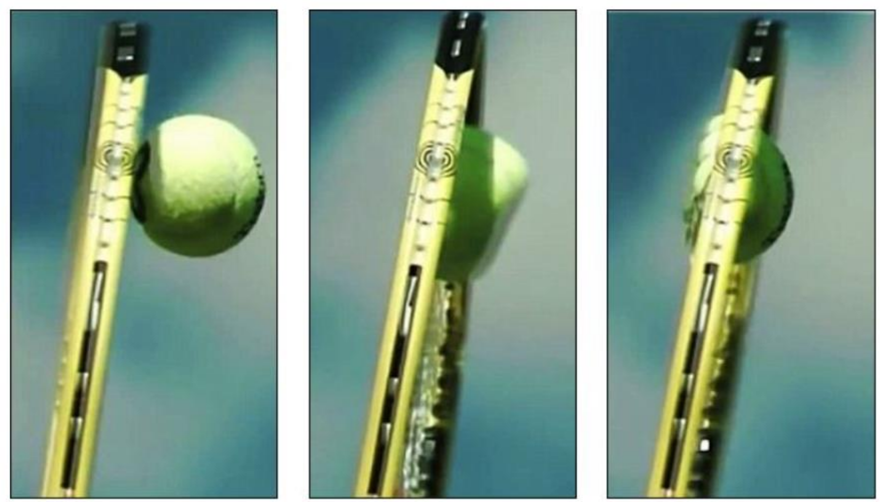

https://www.youtube.com/watch?v=uxlIdMoAwbY
https://newsghana.com.gh/wimbledon-slow-motion-video-of-how-a-tennis-ball-turns-to-goo-after-serve/

A shock is formed due to the increasing sound speed of a compressed gas/plasma

- **Wave in the ocean:**

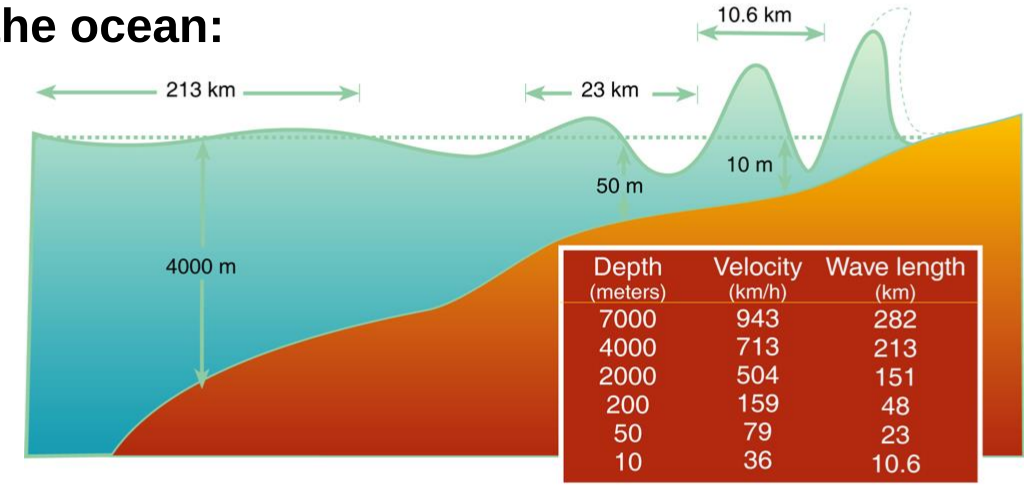

Depth (meters)	Velocity (km/h)	Wave length (km)
7000	943	282
4000	713	213
2000	504	151
200	159	48
50	79	23
10	36	10.6

- **Acoustic/compression wave driven by a piston:**

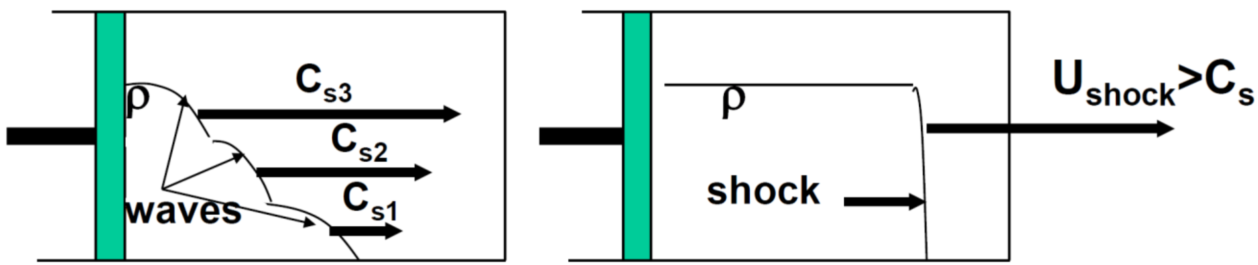

$$c_S \sim \sqrt{\gamma \frac{p}{\rho}} \sim \sqrt{\frac{\alpha\rho^{5/3}}{\rho}} \sim \sqrt{\alpha}\,\rho^{1/3}$$

http://neamtic.ioc-unesco.org/tsunami-info/the-cause-of-tsunamis
*R. Betti, HEDSA HEDP Summer School, 2015

A wave with small amplitude (perturbation) travels with the sound speed

$$\frac{\partial \rho}{\partial t} + \nabla \cdot (\rho \vec{u}) = 0$$

$$\rho \left(\frac{\partial \vec{u}}{\partial t} + \vec{u} \cdot \nabla \vec{u} \right) = -\nabla p + \rho \vec{f}$$

$$\frac{\partial}{\partial t} \left(\frac{\rho u^2}{2} + \rho \varepsilon \right) + \nabla \cdot \vec{u} \left[\left(\frac{\rho u^2}{2} + \rho \varepsilon \right) + p \right] = \rho \vec{f} \cdot \vec{u} - \nabla \cdot \vec{q}$$

$$\rho = \rho_o + \Delta \rho \qquad p = p_o + \Delta p \qquad \vec{u} = \vec{u}_o + \Delta \vec{u} \equiv (u_o + \Delta u)\hat{x} \equiv \Delta u \, \hat{x}$$

$$\frac{\partial \Delta \rho}{\partial t} = -\rho_o \frac{\partial \Delta u}{\partial x} \qquad \rho_o \frac{\partial \Delta u}{\partial t} = -\frac{\partial p}{\partial x} = -\left(\frac{\partial p}{\partial \rho} \right)_S \frac{\partial \Delta \rho}{\partial x} \equiv -{c_s}^2 \frac{\partial \Delta \rho}{\partial x}$$

$$\frac{\partial^2 \Delta \rho}{\partial t^2} = {c_s}^2 \frac{\partial^2 \Delta \rho}{\partial x^2}$$

$$\Delta \rho = \Delta \rho (x \pm c_S t)$$

$$\Delta p = \Delta p (x \pm c_S t)$$

$$\Delta u = \Delta u (x \pm c_S t)$$

$$c_S \sim \sqrt{\gamma \frac{p}{\rho}} \sim \sqrt{\frac{\alpha \rho^{5/3}}{\rho}} \sim \sqrt{\alpha} \rho^{1/3}$$

Y. B. Zel'dovich & Y. P. Raizer, Physics of shock waves and high-temperature hydrodynamic phenomena
Maria Alejandra Barrios Garcia, PhD Thesis, U of Rochester, 2010

A wave is distorted when the sound speed is not a constant

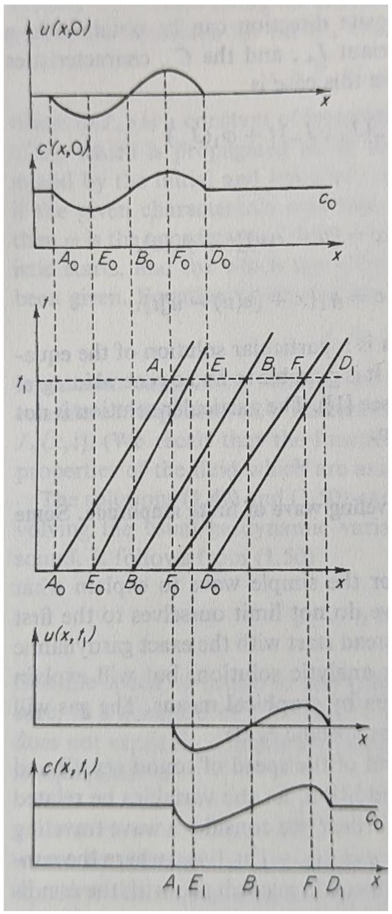

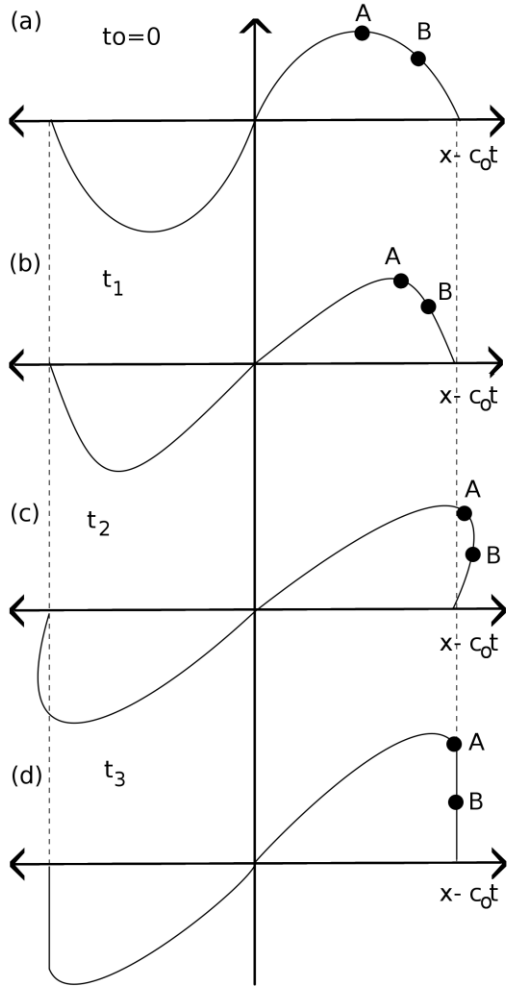

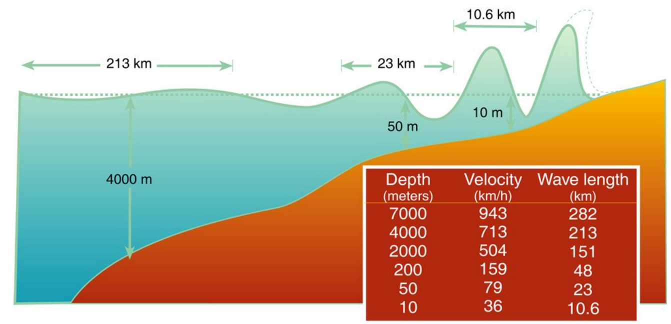

Depth (meters)	Velocity (km/h)	Wave length (km)
7000	943	282
4000	713	213
2000	504	151
200	159	48
50	79	23
10	36	10.6

- **A shock wave is formed when a discontinuity is formed.**

$$c_S \sim \sqrt{\alpha}\rho^{1/3}$$

Y. B. Zel'dovich & Y. P. Raizer, Physics of shock waves and high-temperature hydrodynamic phenomena
Maria Alejandra Barrios Garcia, PhD Thesis, U of Rochester, 2010
http://neamtic.ioc-unesco.org/tsunami-info/the-cause-of-tsunamis

A shock is formed when characteristics merge while a rarefaction wave is formed when characteristics spread out

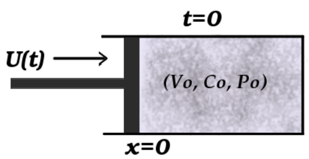

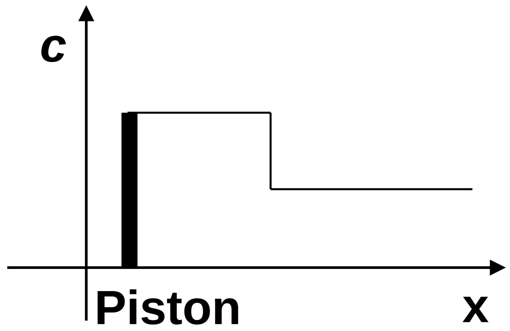

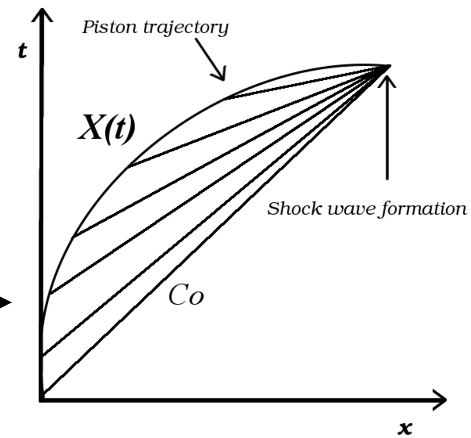

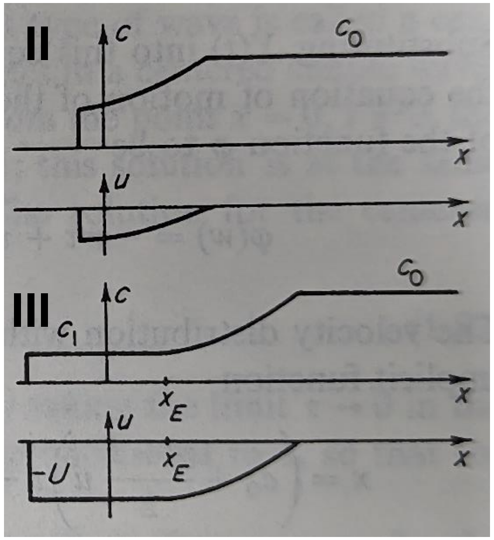

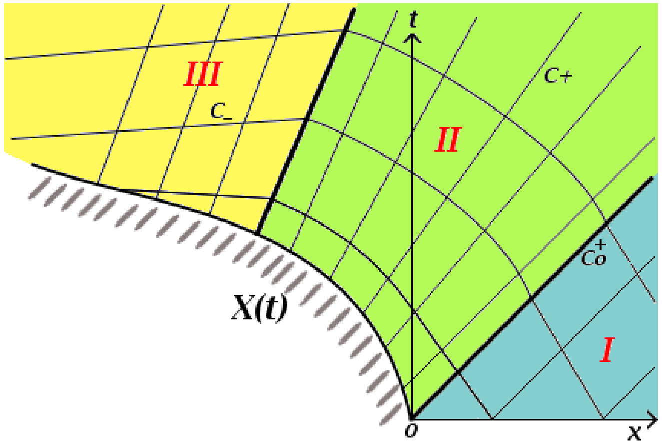

Y. B. Zel’dovich & Y. P. Raizer, Physics of shock waves and high-temperature hydrodynamic phenomena
Maria Alejandra Barrios Garcia, PhD Thesis, U of Rochester, 2010

A shock or a rarefaction wave may be formed depending on the driving force from the piston

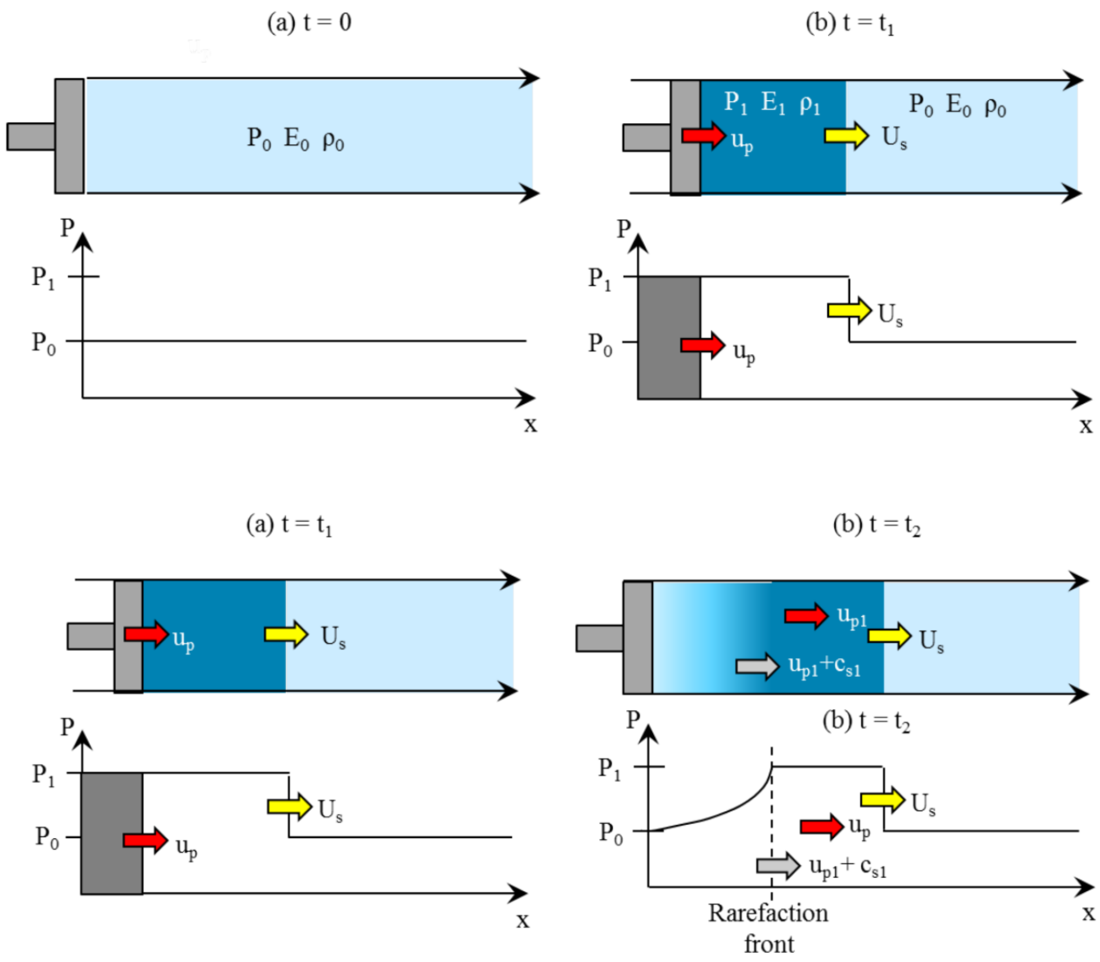

- **Show simulations.**

Michelle Colleen Gregor, PhD Thesis, U of Rochester, 2017

Mass, momentum, and energy is conserved across the shock front

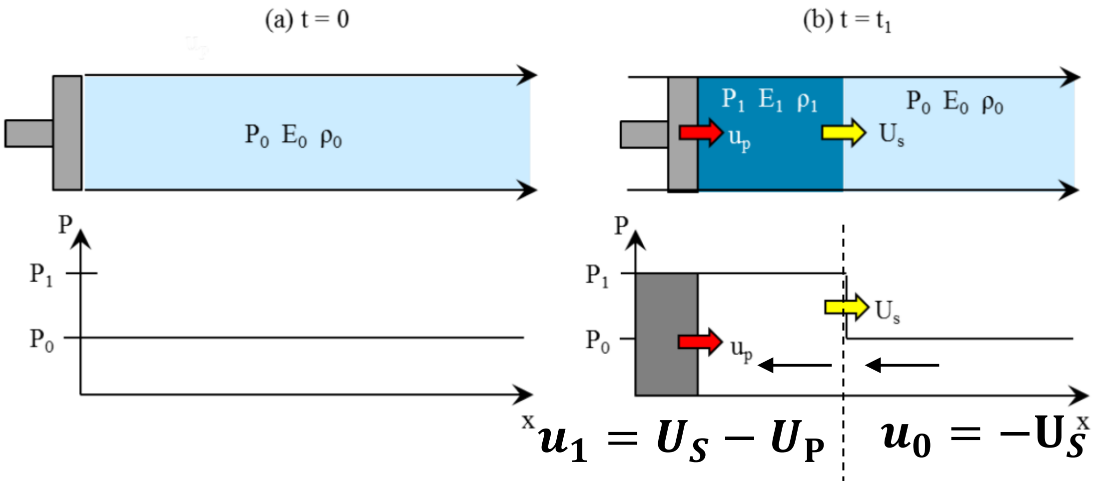

$$\frac{\partial \rho}{\partial t} + \nabla \cdot (\rho\, \vec{u}) = 0$$

$$\rho\left(\frac{\partial\, \vec{u}}{\partial t} + \vec{u} \cdot \nabla\, \vec{u}\right) = -\nabla p + \rho\, \vec{f}$$

$$\frac{\partial}{\partial t}\left(\frac{\rho u^2}{2} + \rho\varepsilon\right) + \nabla \cdot \vec{u}\left[\left(\frac{\rho u^2}{2} + \rho\varepsilon\right) + p\right] = \rho\, \vec{f} \cdot \vec{u} - \nabla \cdot \vec{q}$$

$$\rho_1 u_1 = \rho_0 u_0$$

$$p_1 + \rho_1 {u_1}^2 = p_0 + \rho_0 {u_0}^2$$

$$\epsilon_1 + \frac{p_1}{\rho_1} + \frac{{u_1}^2}{2} = \epsilon_0 + \frac{p_0}{\rho_0} + \frac{{u_0}^2}{2}$$

Michelle Colleen Gregor, PhD Thesis, U of Rochester, 2017

The Hugoniot equations relate the pre- and post-shock conditions via the particle velocity(U_p) and shock velocity (U_s)

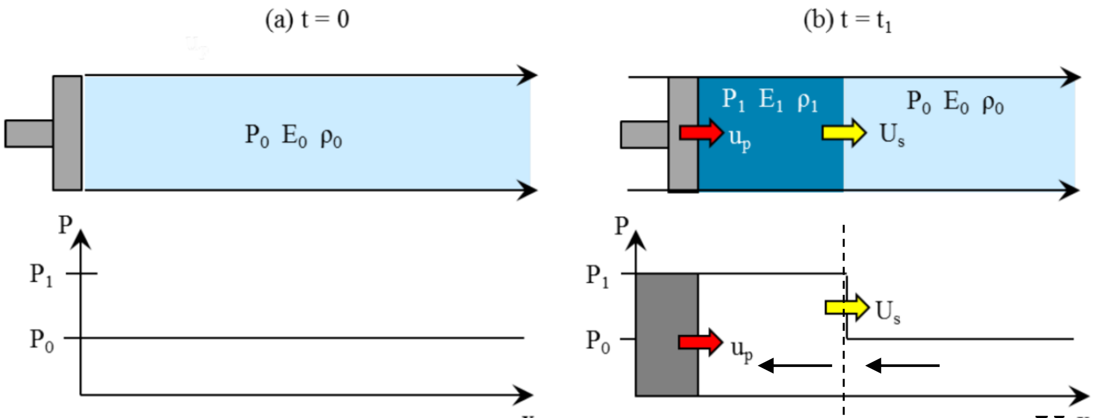

$$u_1 = U_S - U_P \qquad u_0 = -U_S$$

$$\rho_1 u_1 = \rho_0 u_0$$

$$p_1 + \rho_1 {u_1}^2 = p_0 + \rho_0 {u_0}^2$$

$$\epsilon_1 + \frac{p_1}{\rho_1} + \frac{{u_1}^2}{2} = \epsilon_0 + \frac{p_0}{\rho_0} + \frac{{u_0}^2}{2}$$

$$\rho_0 U_S = \rho_1 \left(U_S - U_p\right)$$

$$p_1 - p_0 = \rho_o U_S U_p$$

$$u_0 \left[\frac{\rho_0 {u_0}^2}{2} + \rho_0 \epsilon_0 + p_0\right] = u_1 \left[\frac{\rho_1 {u_1}^2}{2} + \rho_1 \epsilon_1 + p_1\right]$$

$$p_0 u_0 - p_1 u_1 = \rho_1 u_1 \left(\epsilon_1 + \frac{{u_1}^2}{2}\right) - \rho_0 u_0 \left(\epsilon_0 + \frac{{u_0}^2}{2}\right) = \rho_0 u_0 \left[\left(\epsilon_1 + \frac{{u_1}^2}{2}\right) - \left(\epsilon_0 + \frac{{u_0}^2}{2}\right)\right]$$

Michelle Colleen Gregor, PhD Thesis, U of Rochester, 2017

The Hugoniot equations relate the pre- and post-shock conditions via the particle velocity(U_p) and shock velocity (U_s) – cont.

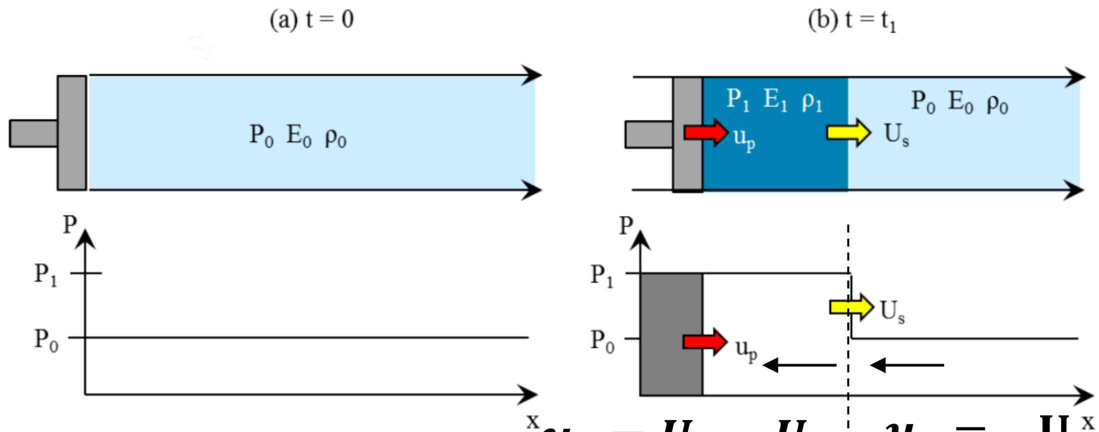

$$u_1 = U_S - U_P \qquad u_0 = -U_S$$

$$\rho_0 U_S = \rho_1 (U_S - U_p) \qquad u_0\left[\frac{\rho_0 u_0^2}{2} + \rho_0\epsilon_0 + p_0\right] = u_1\left[\frac{\rho_1 u_1^2}{2} + \rho_1\epsilon_1 + p_1\right]$$

$$p_1 - p_0 = \rho_o U_S U_p$$

$$p_0 u_0 - p_1 u_1 = \rho_1 u_1\left(\epsilon_1 + \frac{u_1^2}{2}\right) - \rho_0 u_0\left(\epsilon_0 + \frac{u_0^2}{2}\right) = \rho_0 u_0\left[\left(\epsilon_1 + \frac{u_1^2}{2}\right) - \left(\epsilon_0 + \frac{u_0^2}{2}\right)\right]$$

$$\text{Let } V_{1,2} \equiv \frac{1}{\rho_{1,2}} \qquad u_0^2 = V_0^2\frac{p_1 - p_0}{V_0 - V_1} \qquad u_1^2 = V_1^2\frac{p_1 - p_0}{V_0 - V_1}$$

$$\epsilon_1 - \epsilon_0 = \frac{1}{2}(p_0 + p_1)(V_0 - V_1)$$

Michelle Colleen Gregor, PhD Thesis, U of Rochester, 2017

The density is only compressed by a limited amount even in a strong shock

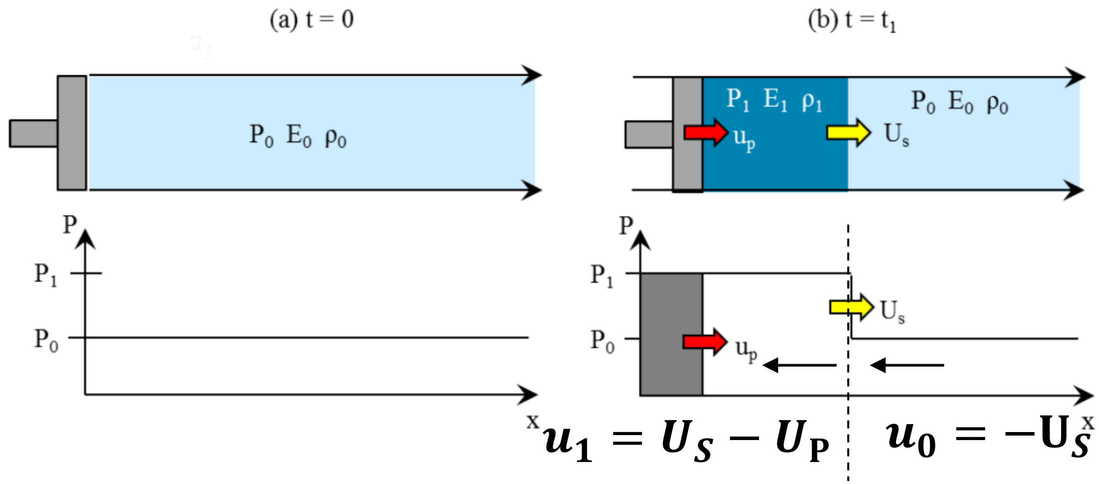

$$u_1 = U_S - U_P \qquad u_0 = -U_S$$

$$V_{0,1} \equiv \frac{1}{\rho_{0,1}} \quad u_0{}^2 = V_0{}^2 \frac{p_1 - p_0}{V_0 - V_1} \quad u_1{}^2 = V_1{}^2 \frac{p_1 - p_0}{V_0 - V_1} \quad \epsilon_1 - \epsilon_0 = \frac{1}{2}(p_0 + p_1)(V_0 - V_1)$$

$$\frac{\rho_1}{\rho_0} = \frac{V_0}{V_1} = \frac{p_1(\gamma+1) + p_0(\gamma-1)}{p_1(\gamma-1) + p_0(\gamma+1)} \sim \frac{\gamma+1}{\gamma-1}\left(\text{for } \frac{p_1}{p_0} \gg 1\right) \sim 4\left(\text{for } \gamma = \frac{5}{3}\right)$$

$$u_0{}^2 = \frac{V_0}{2}[(\gamma-1)p_0 + (\gamma+1)p_1] = \frac{p_0}{\rho_0}\frac{(\gamma+1)\,p_1/p_0 + (\gamma-1)}{2}$$

$$u_1{}^2 = \frac{V_0}{2}\frac{[(\gamma+1)p_0 + (\gamma-1)p_1]^2}{(\gamma-1)p_0 + (\gamma+1)p_1}$$

Michelle Colleen Gregor, PhD Thesis, U of Rochester, 2017

The Hugoniot curve is a curve on the *p*, *V* diagram passing through the initial state p_0, V_0

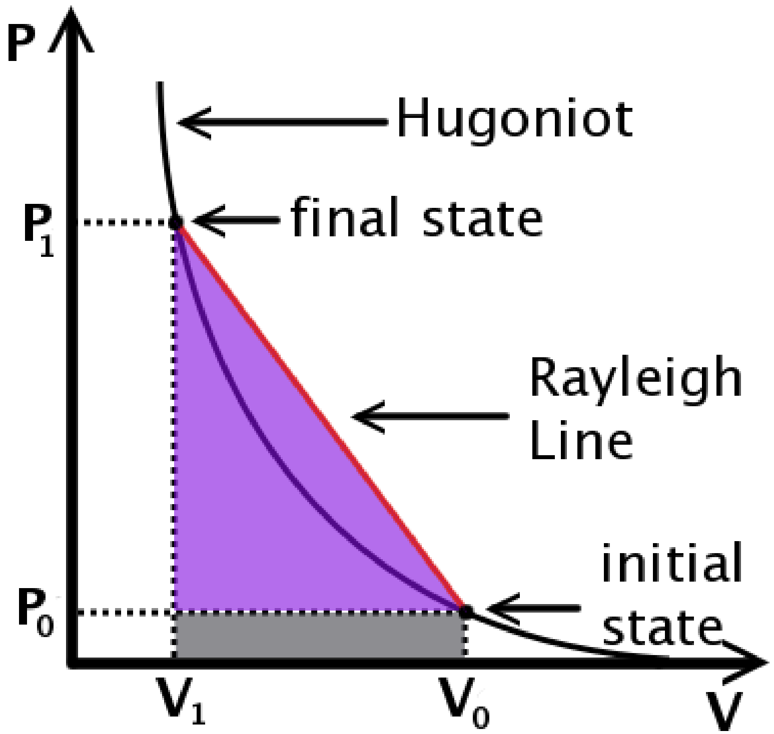

$$\frac{V_0}{V_1} = \frac{p_1(\gamma+1) + p_0(\gamma-1)}{p_1(\gamma-1) + p_0(\gamma+1)}$$

$$V_{0,1} \equiv \frac{1}{\rho_{0,1}}$$

Maria Alejandra Barrios Garcia, PhD Thesis, U of Rochester, 2010

Pressure can be referred by measuring the shock speed with a sample with known Hugoniot curve

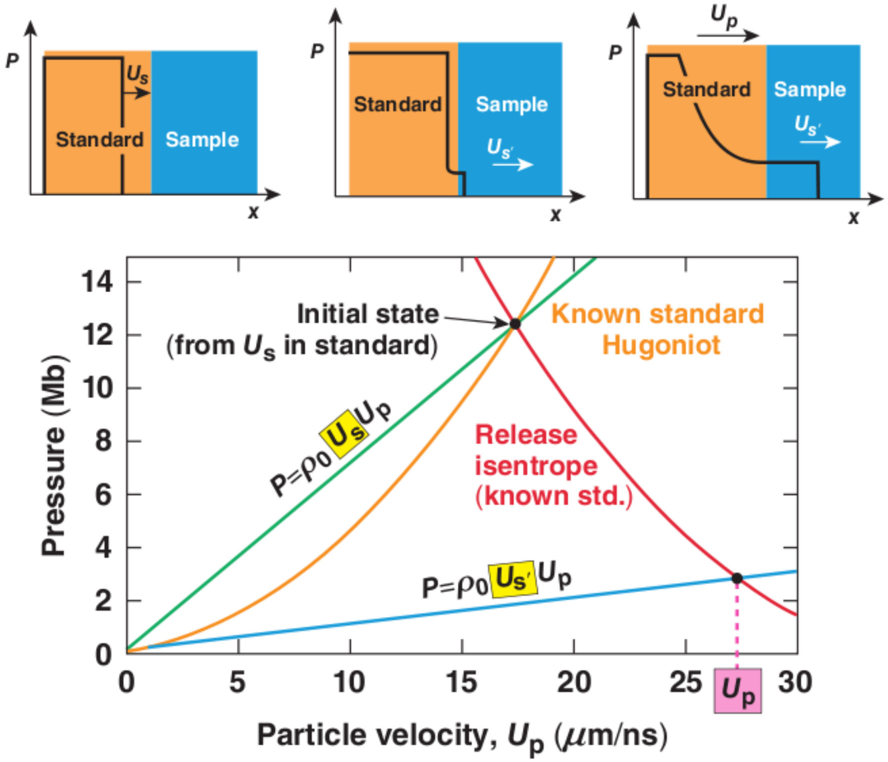

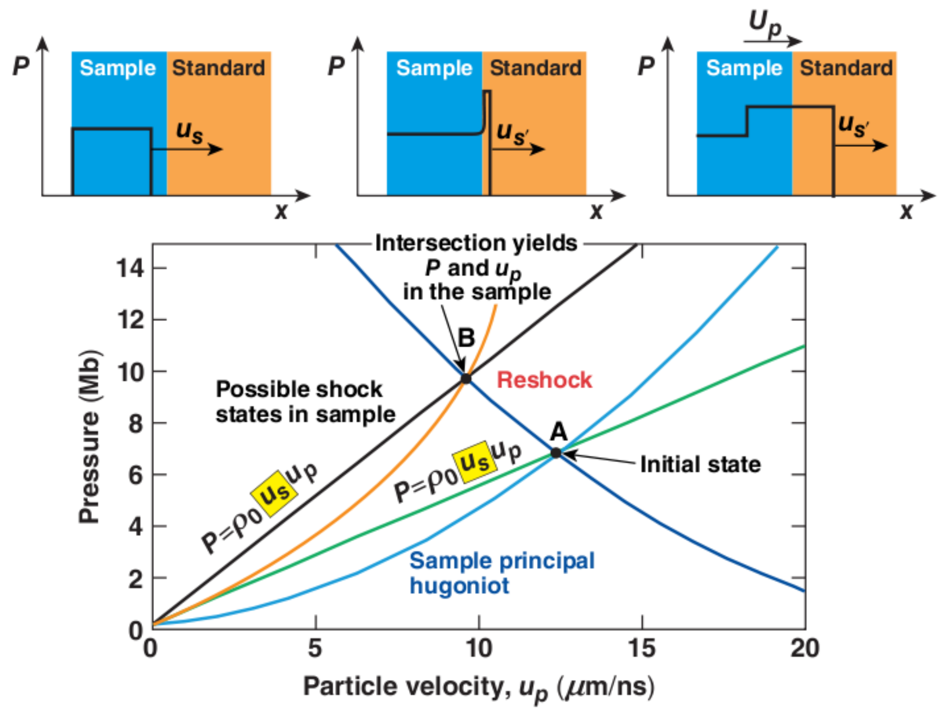

$$p_1 - p_0 = \rho_o U_S U_p$$

Isentrope: adiabatic flow with no change in entropy

Maria Alejandra Barrios Garcia, PhD Thesis, U of Rochester, 2010

Shock velocities are measured using time-resolved Velocity Interferometer System for Any Reflector (VISAR)

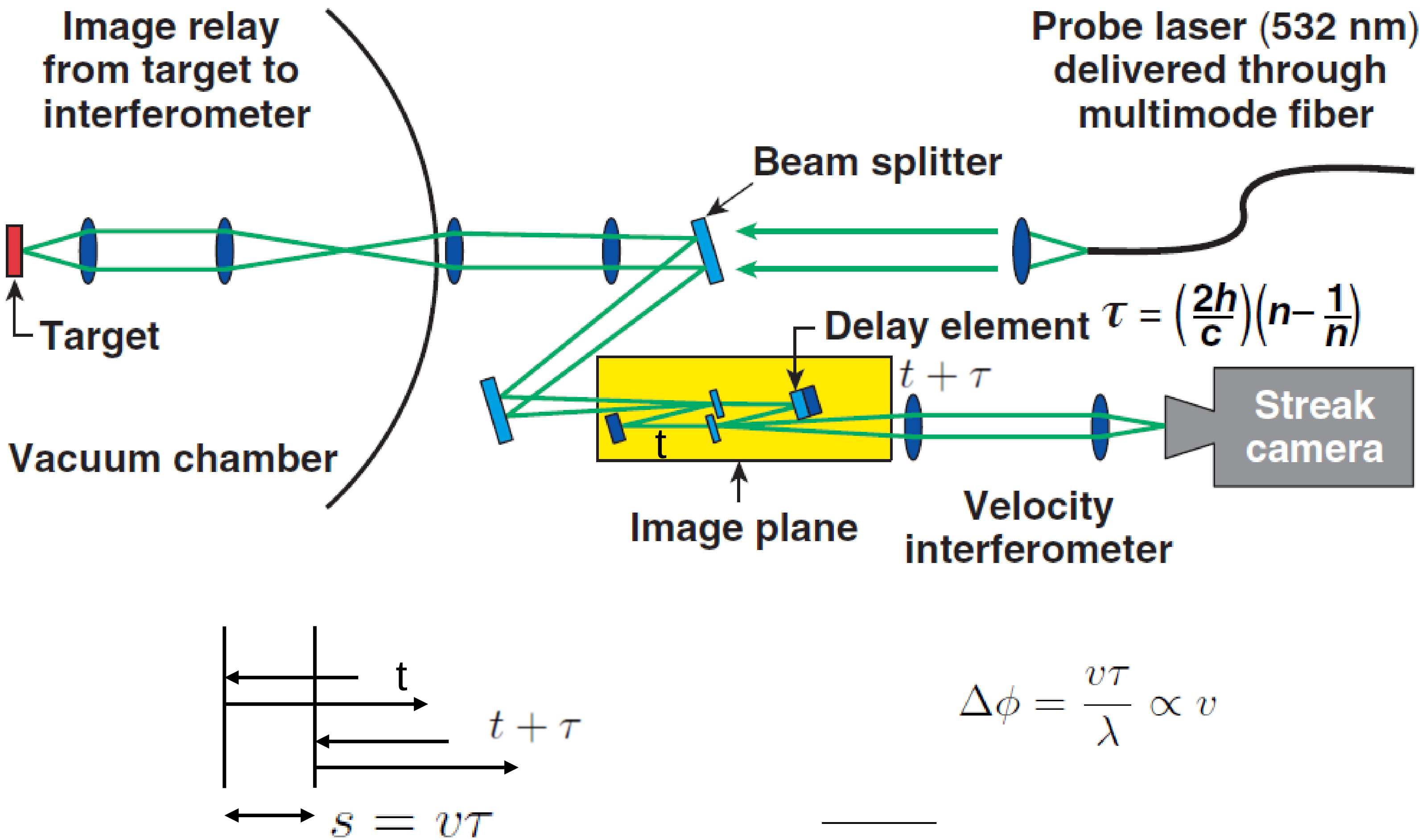

$$\Delta\phi = \frac{v\tau}{\lambda} \propto v$$

http://hedpschool.lle.rochester.edu/1000_proc2013.php

Shock velocities are measured using time-resolved Velocity Interferometer System for Any Reflector (VISAR)

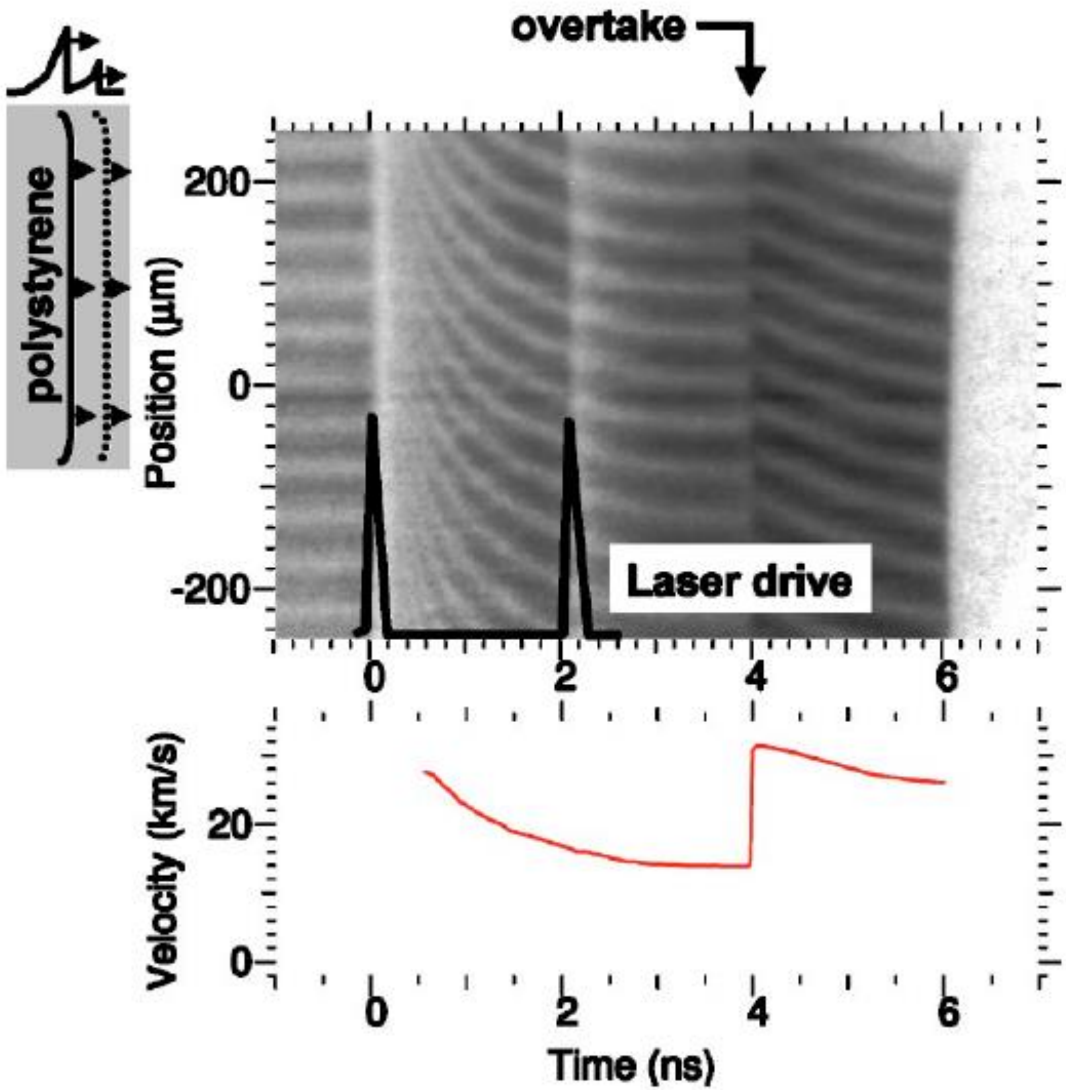

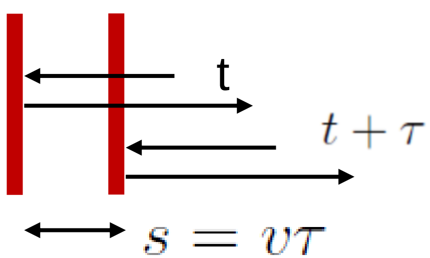

P. M. Celliers *et al.*, Rev. Sci. Insytum. **75**, 4916 (2004)

A piston can be driven by a gas gun

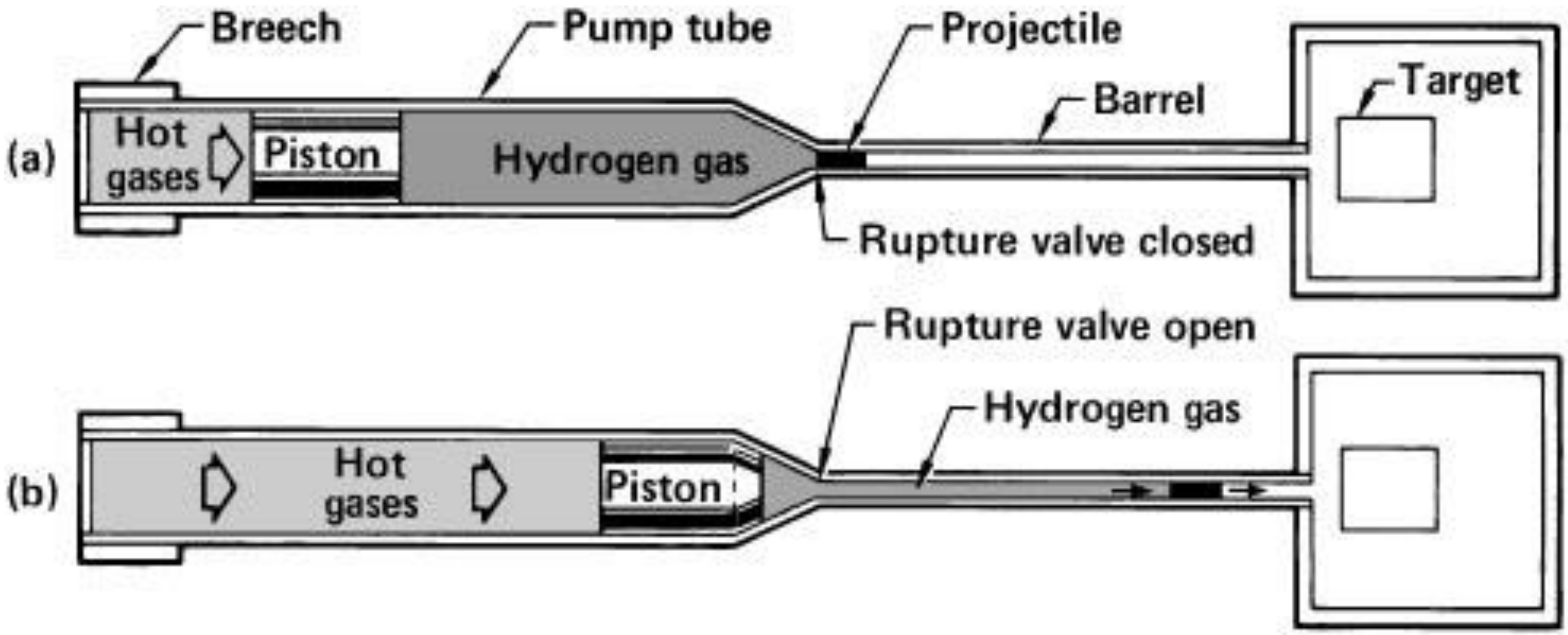

J. Freim, etc., J. Materials Research 11, 112 (1996)

Rochester is known as “The World's Image Center”

There are many famous optical companies at Rochester

Kodak

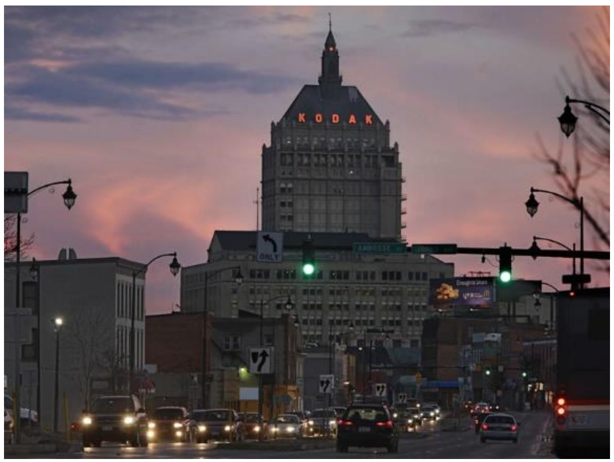

xerox ®

Eastman school of music

BAUSCH + LOMB

Laboratory for Laser Energetics, University of Rochester is a pioneer in laser fusion

- OMEGA Laser System
  - 60 beams
  - >30 kJ UV on target
  - 1%~2% irradiation nonuniformity
  - Flexible pulse shaping

- OMEGA EP Laser System
  - 4 beams; 6.5 kJ UV (10ns)
  - Two beams can be high-energy petawatt
    - 2.6 kJ IR in 10 ps
    - Can propagate to the OMEGA or OMEGA EP target chamber

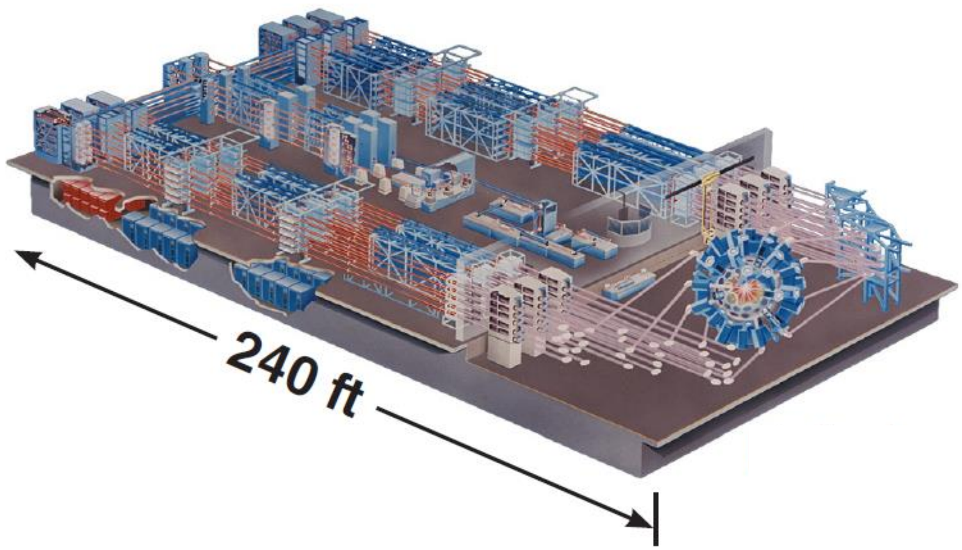

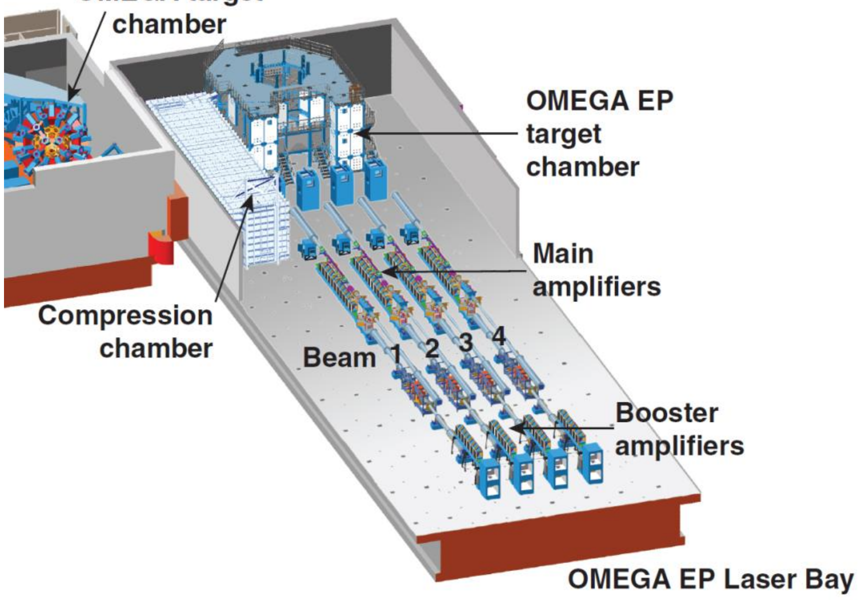

The OMEGA Facility is carrying out ICF experiments using a full suite of target diagnostics

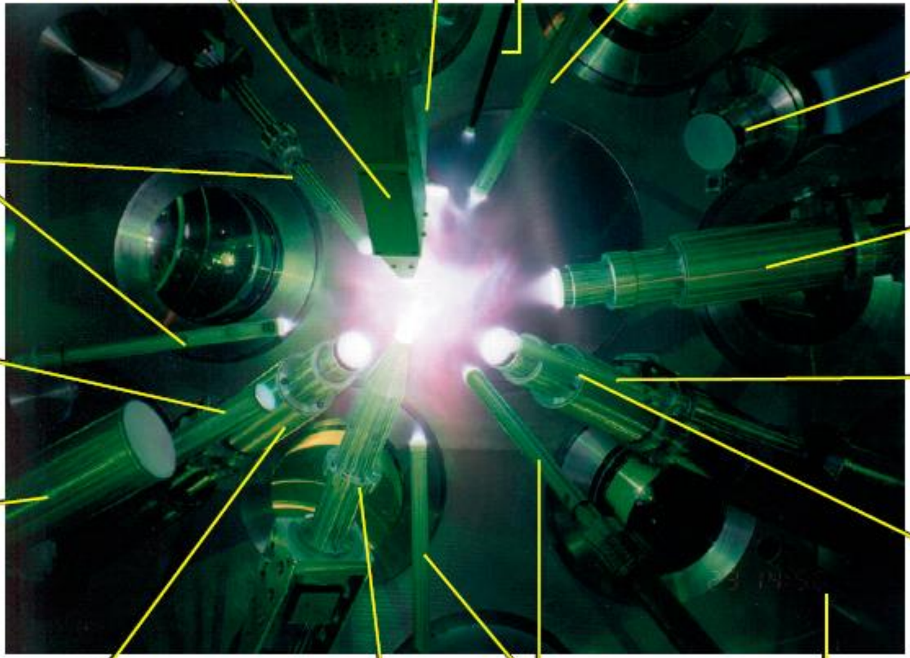

E8012b

Photo taken from port H11B

The 1.8-MJ National Ignition Facility (NIF) will demonstrate ICF ignition and modest energy gain

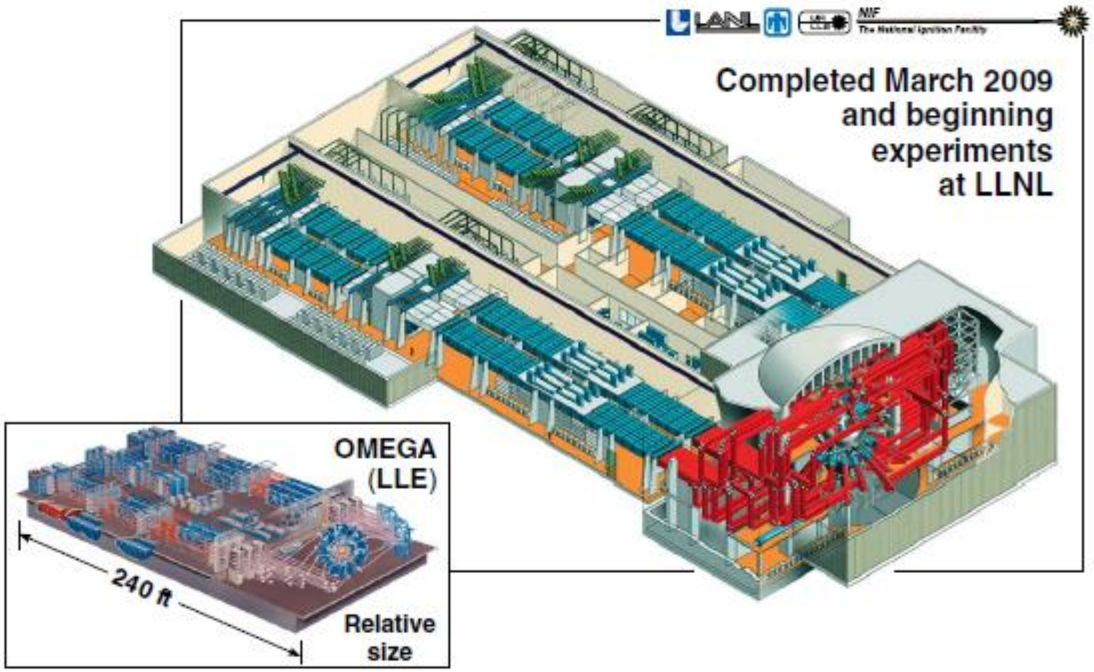

OMEGA experiments are integral to an ignition demonstration on the NIF.

A strong shock can be generated using a high power laser

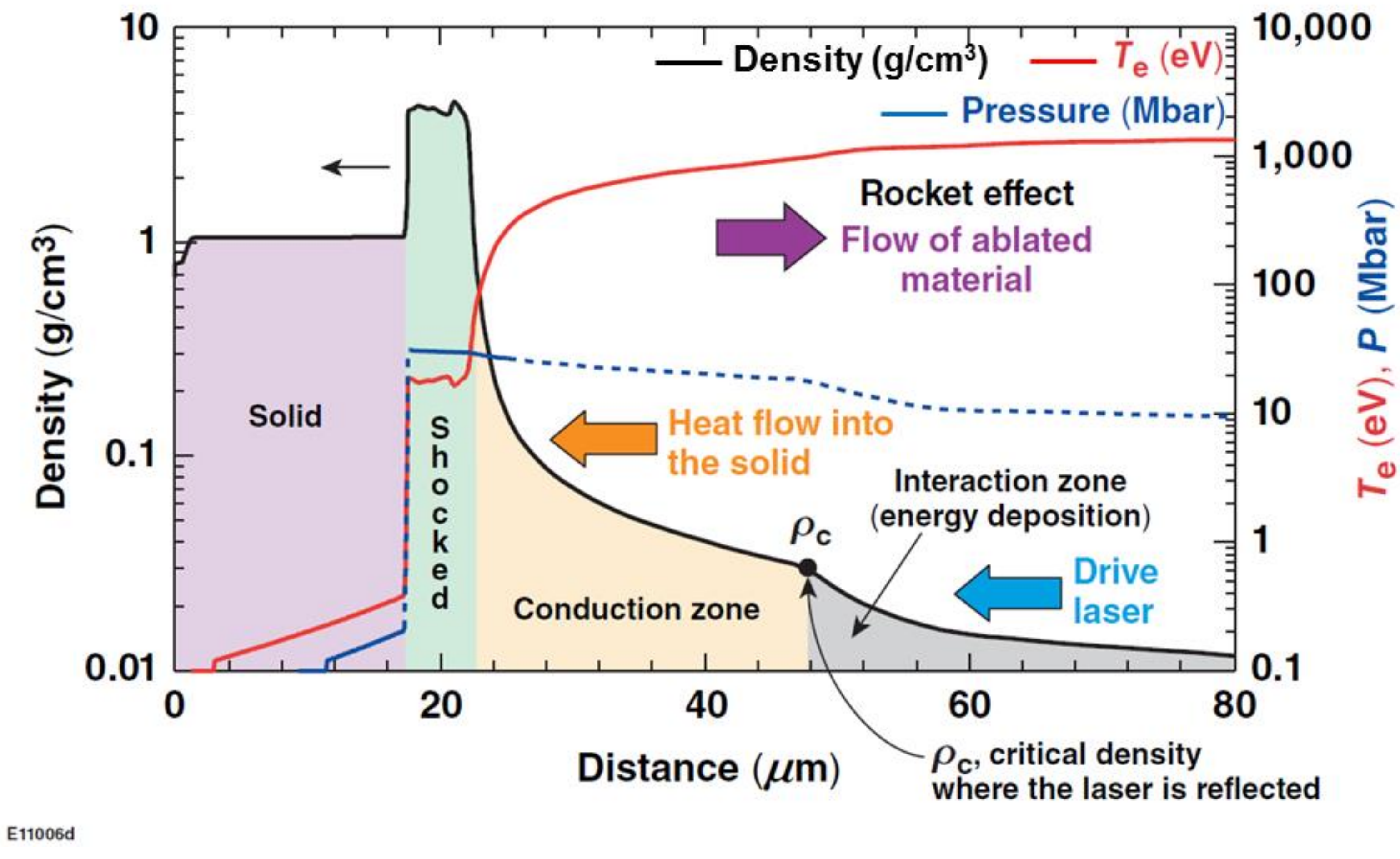

LLE viewgraph database

Danae Nicole Polsin, PhD Thesis, U of Rochester, 2018

The powder x-ray diffraction image plate (PXRDIP) package for studying the shock phenomena

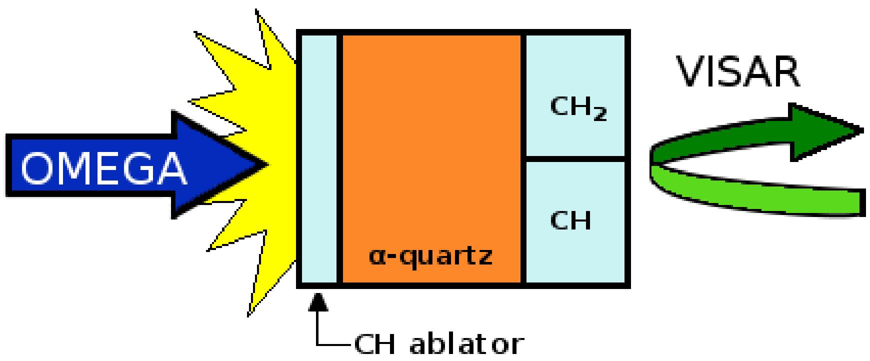

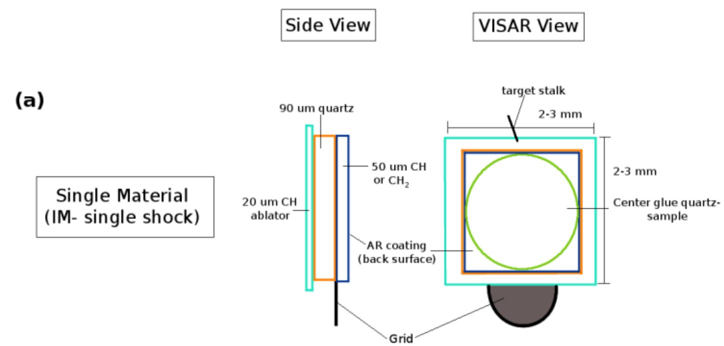

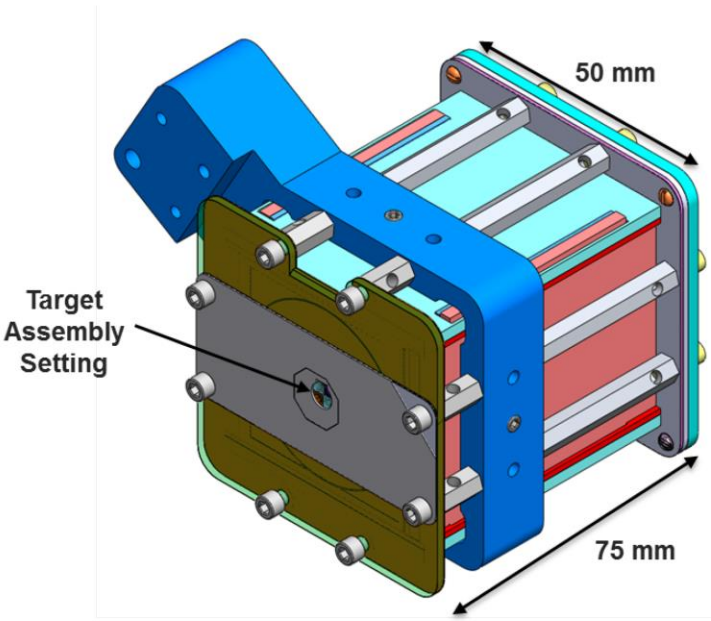

16 Omega beams

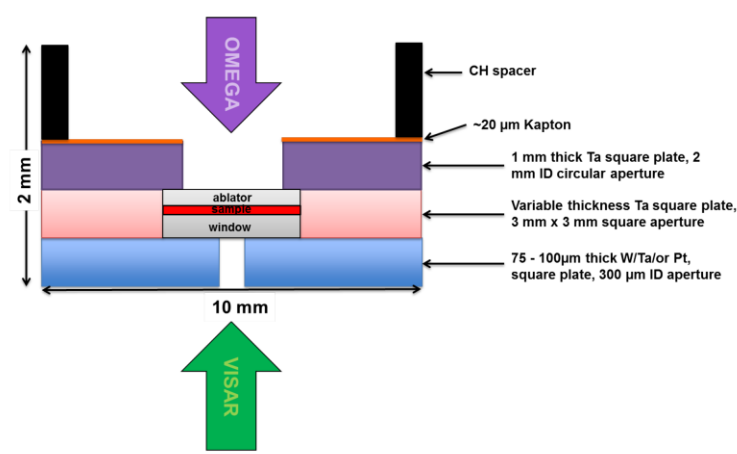

Maria Alejandra Barrios Garcia, PhD Thesis, U of Rochester, 2010
Danae Nicole Polsin, PhD Thesis, U of Rochester, 2018
J. R. Rygg, etc., Rev. Sci. Instrum. 83, 113904 (2012)

The PXRDIP box in the chamber

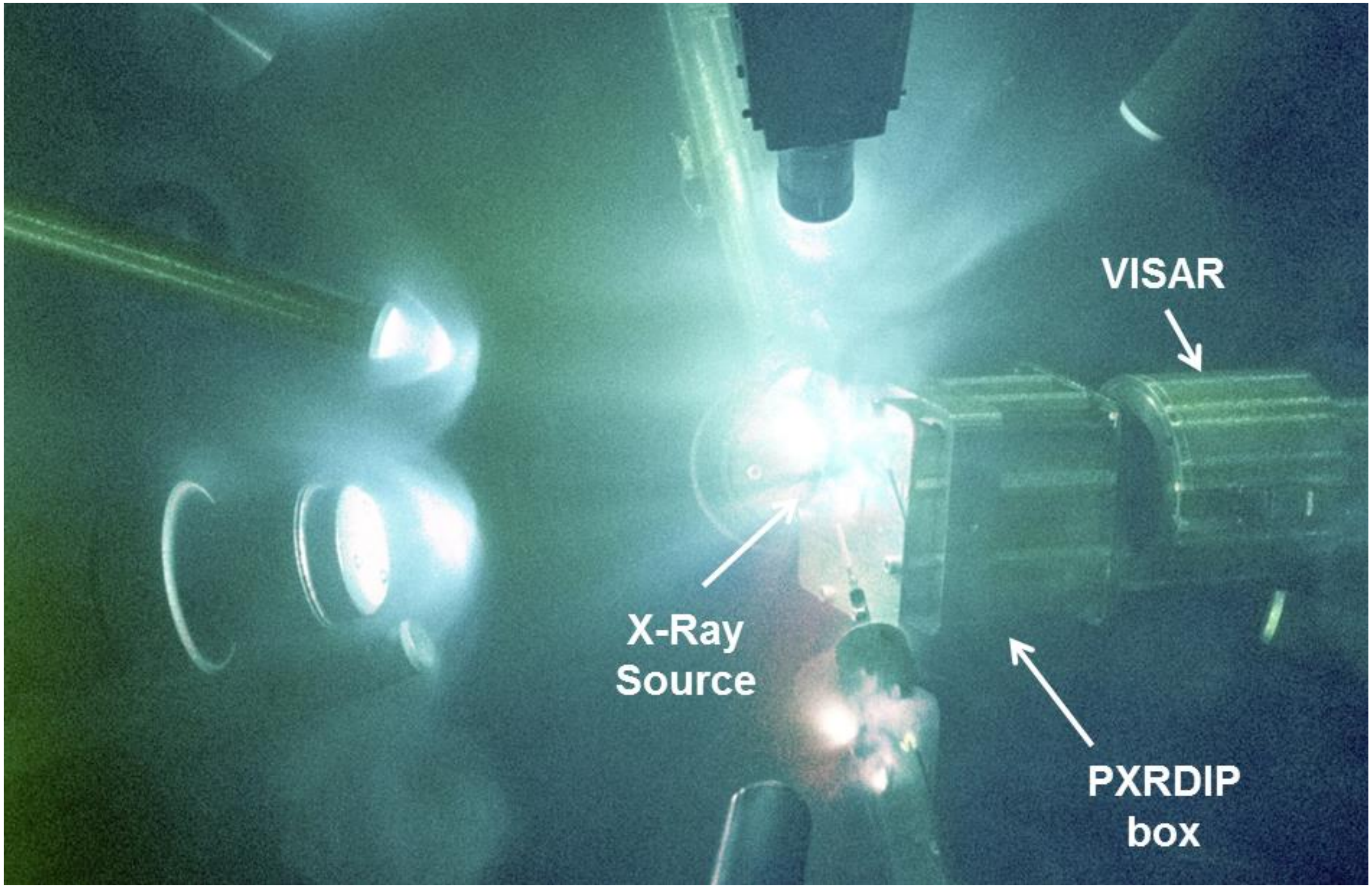

Danae Nicole Polsin, PhD Thesis, U of Rochester, 2018

Interference pattern shifts when a shock breakouts

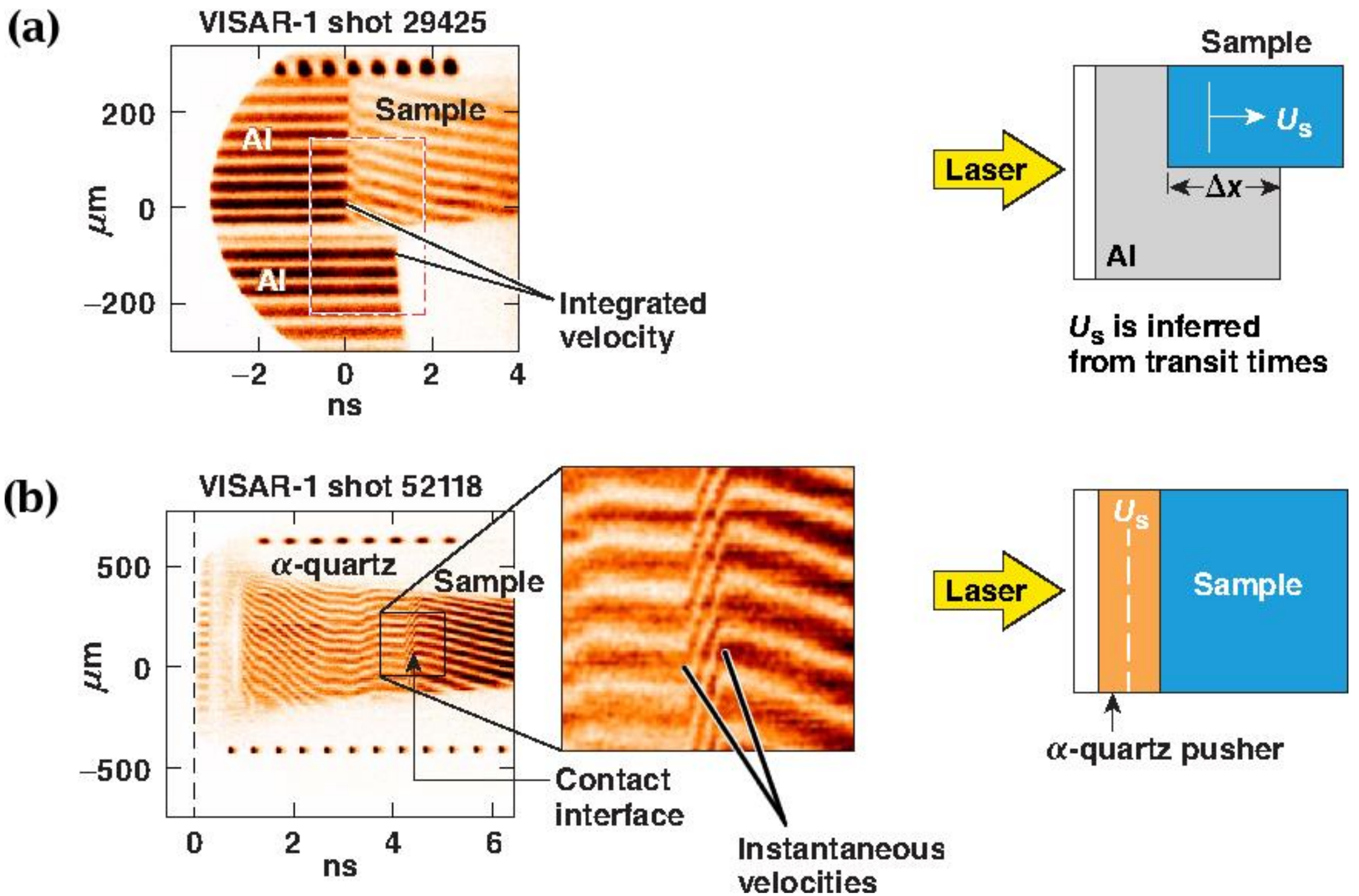

Maria Alejandra Barrios Garcia, PhD Thesis, U of Rochester, 2010

The pressure studied using high-power laser is in the range of 1 TPa (10 Mbar)

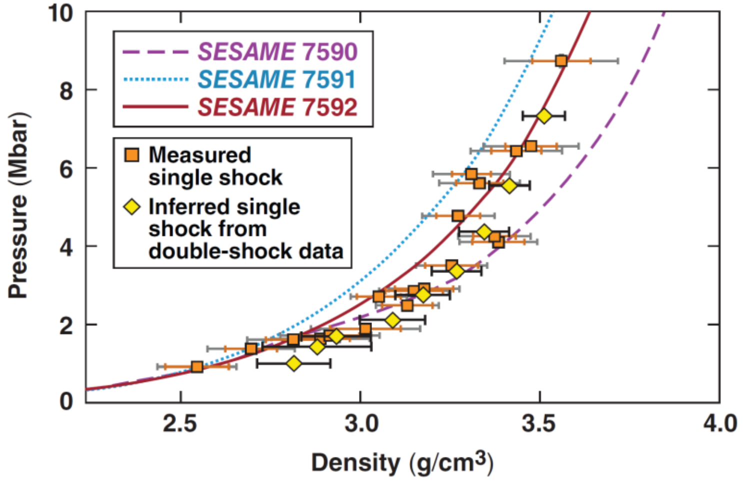

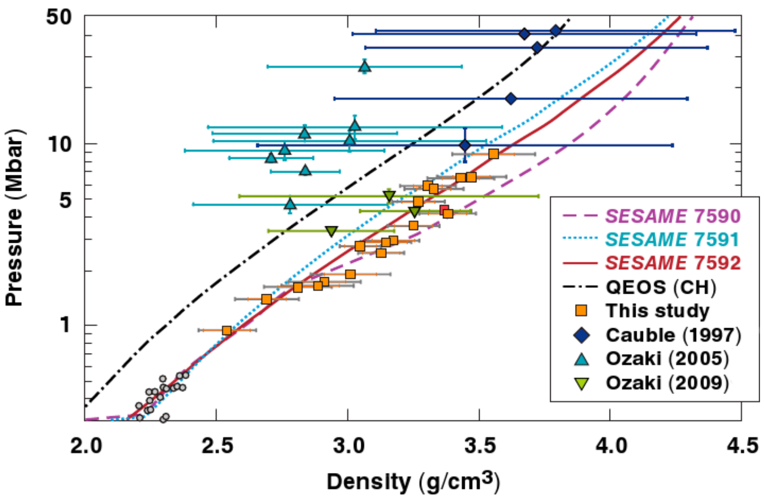

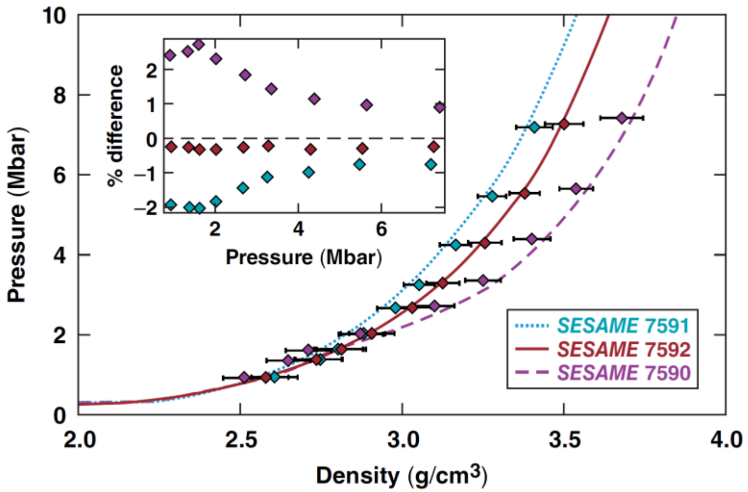

Maria Alejandra Barrios Garcia, PhD Thesis, U of Rochester, 2010

A flyer plate can be used to as the "piston" to generate the shock in a sample

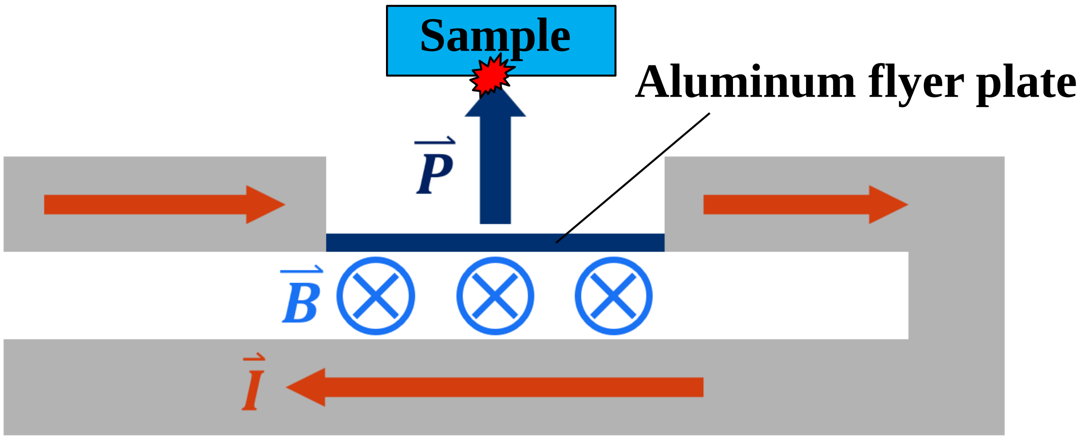

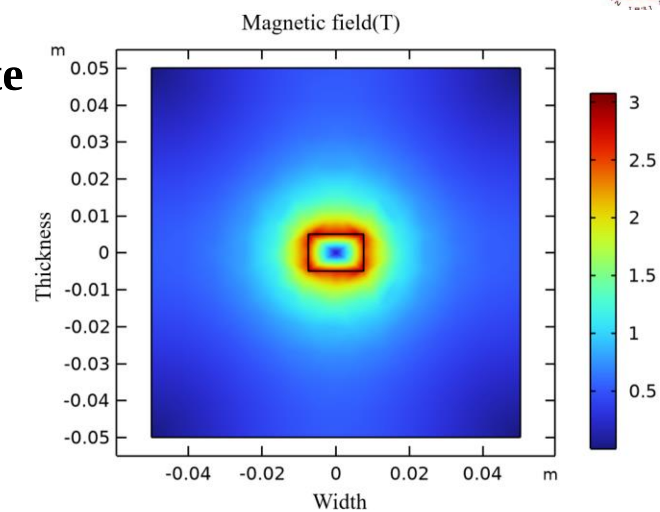

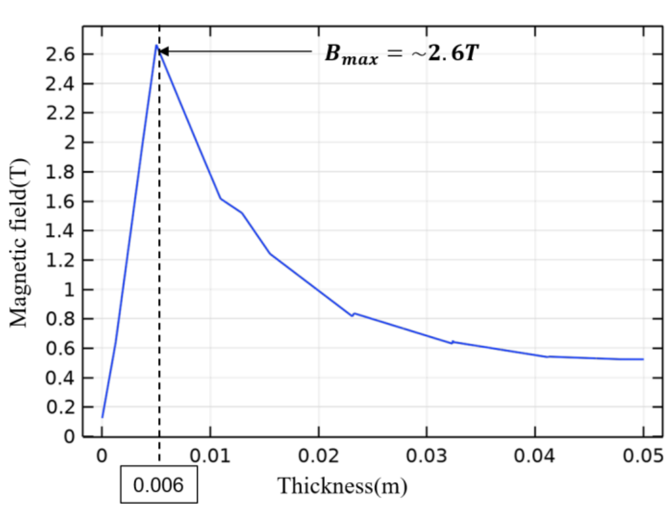

$$B = \frac{\mu_0 I}{w}$$

$$P = \frac{B^2}{2\mu_0} = \frac{\mu_0 I^2}{2w^2}$$

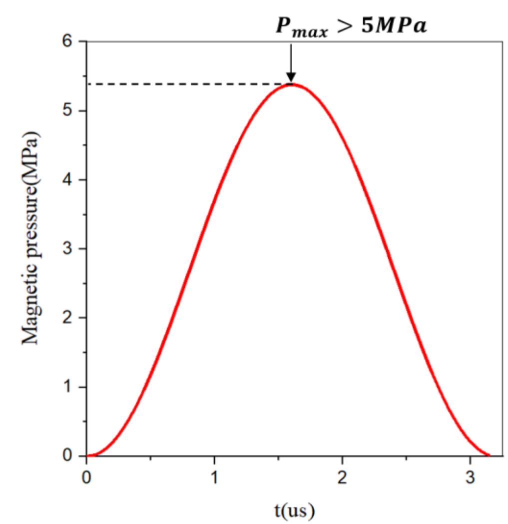

Sandia’s Z machine is the world's most powerful and efficient laboratory radiation source

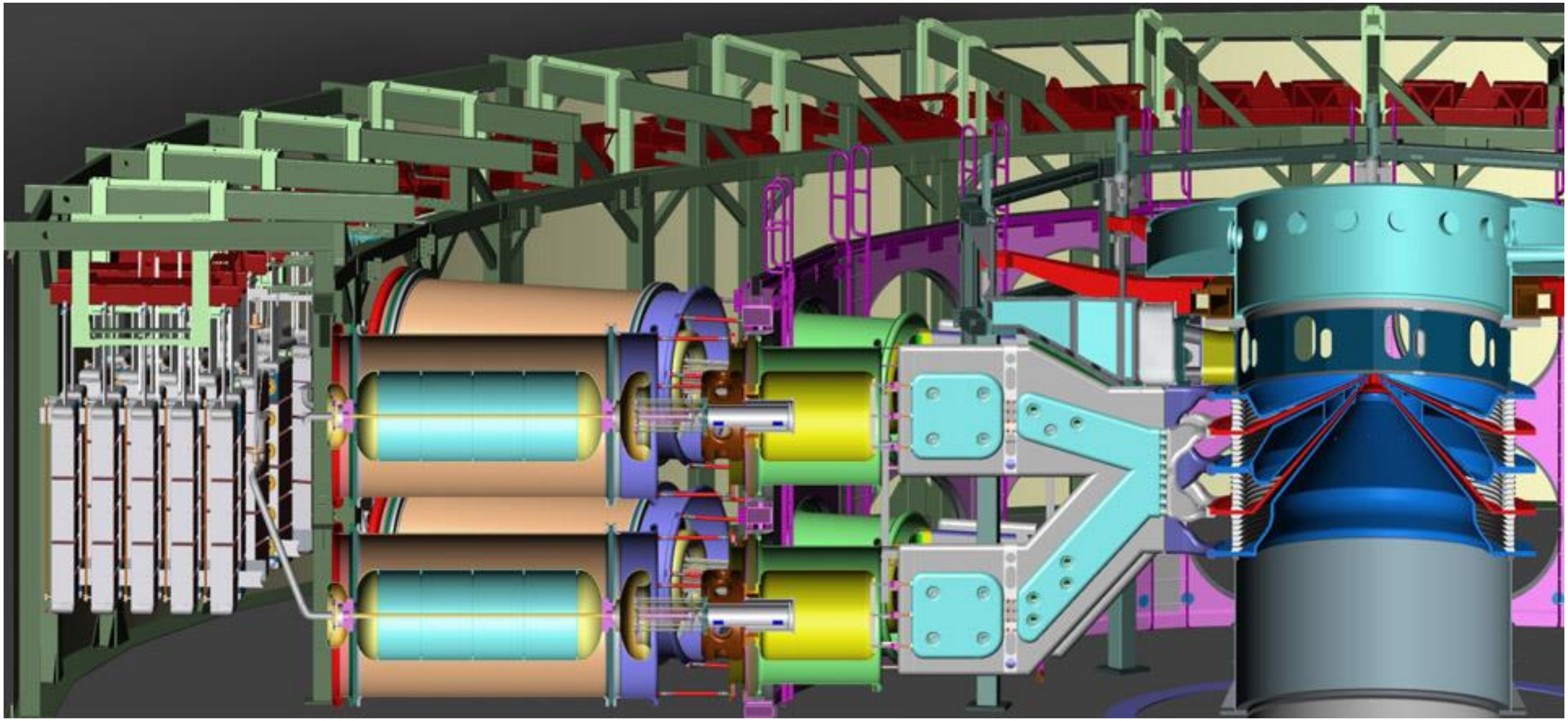

- Stored energy: 20 MJ
- Marx charge voltage: 85 kV
- Peak electrical power: 85 TW

- Peak current: 26 MA
- Rise time: 100 ns
- Peak X-ray emissions: 350 TW
- Peak X-ray output: 2.7 MJ

Z machine discharge

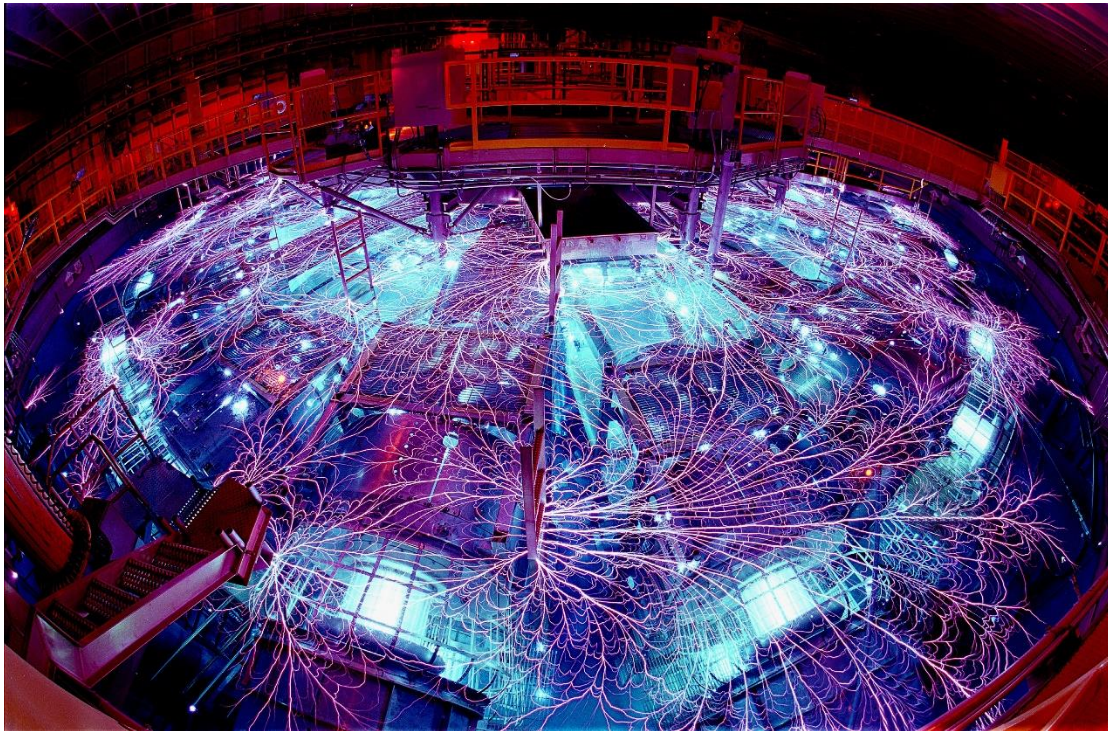

Z machine

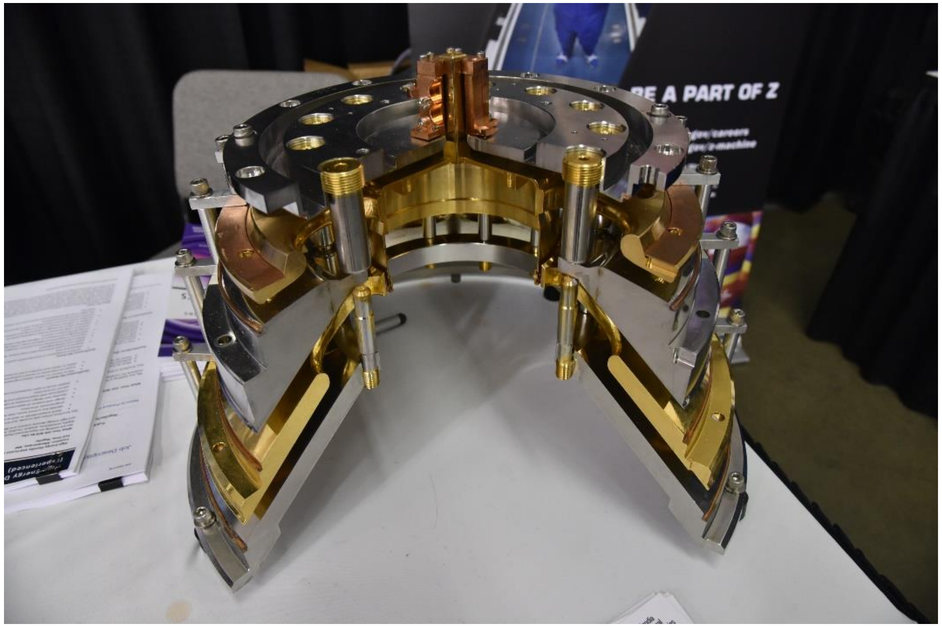

The flyer plate used in the Z machine

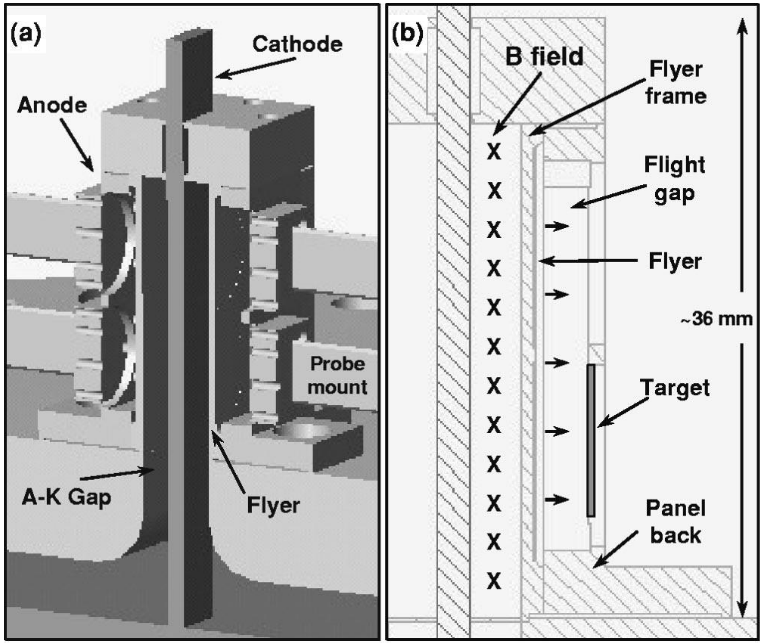

M. D. Knudson, etc., J. Applied Physics 94, 4420 (2003)
https://newsreleases.sandia.gov/releases/2005/nuclear-power/z-saturn.html
Pulsed Power Driven Experiments in the Institute of Shock Physics, by Simon Bland

Before and after shots

- **Before shots**

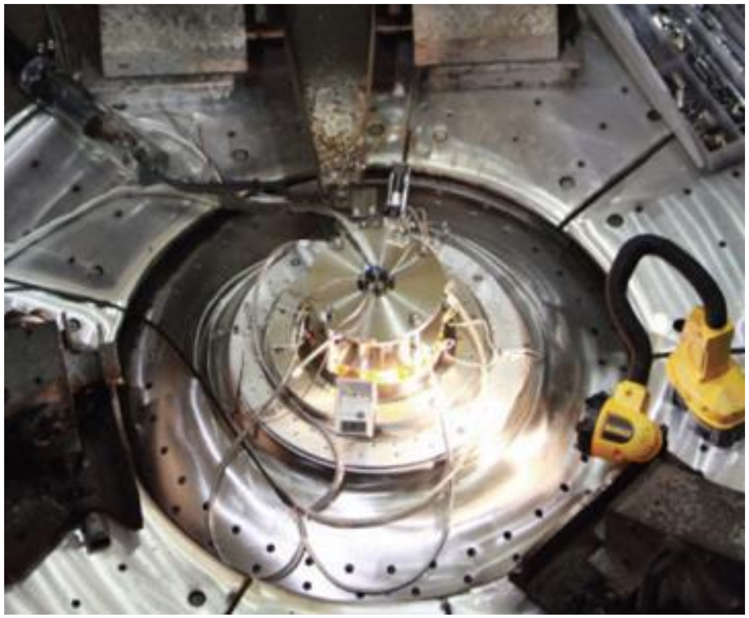

- **After shots**

SAND2017-0900PE_The sandia z machine - an overview of the world's most powerful pulsed power facility.pdf

Imperial College MAGPIE facility

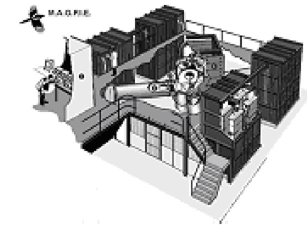

At Imperial the 1.5MA 240 ns MAGPIE generator drives HEDP experiments on a daily basis

Mega
Ampere
Generator for
Plasma
Implosion
Experiments

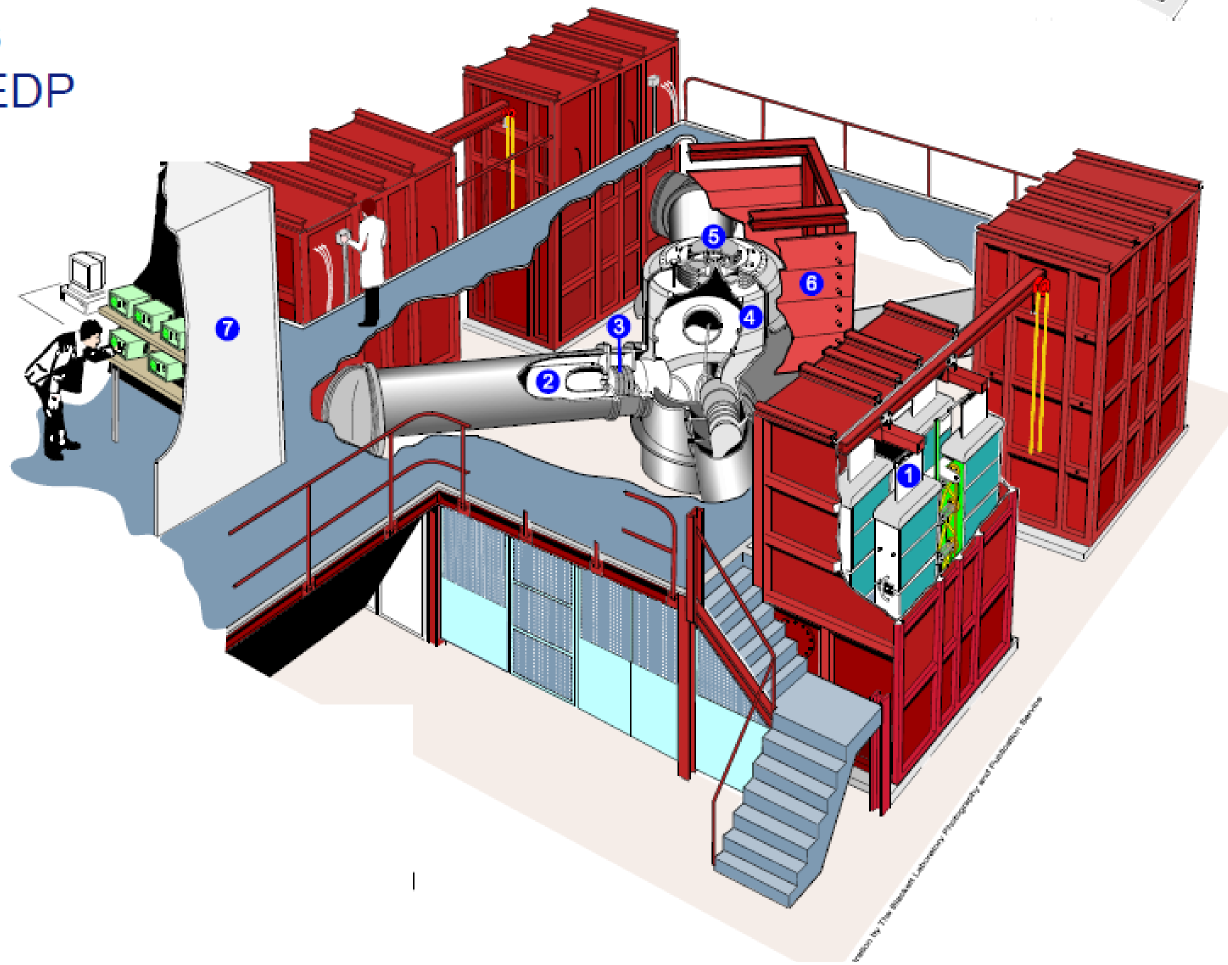

Get experience in magnetically driven isentropic compression experiments

Can also look at shocks in plasmas - e.g. astro relevant radiative shock waves

And using plasma explore new methods of applying high pressures to targets

Imperial College London

Prelude to experiments: new power feed and vacuum chamber

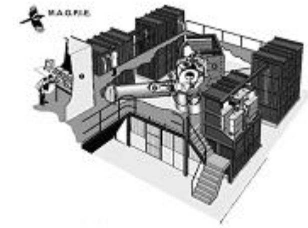

Original vacuum chamber was only ~30cm diameter x 15cm tall

Anode and cathode move by 6mm during vacuum

Water ingress meant vacuum time was 3hrs

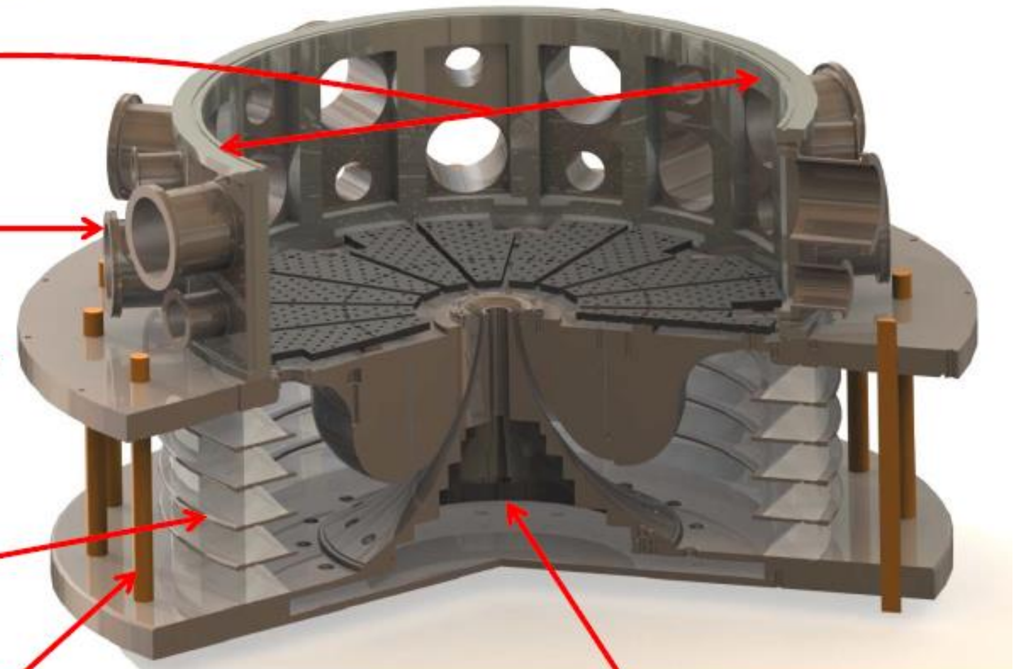

~70cm internal diameter

Chamber surrounded by 16 port plates with ISO100 and ISO 63

Reinforced steel plates to reduce flex

Rexolite diode rings increase strength reduce water absorption

New Torlon bolts don't stretch

Vacuum section below MITL removes force on cathode

Anode and cathode now move ~25um

Vacuum time <1hr

Imperial College
London

Initial experiments: Feb 2010

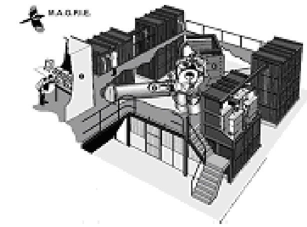

Design and manufacturing issues:

- Will the gap breakdown?
- How uniform is the drive?

EM simulations difficult due to large scale of electrodes c.f. gap in stripline...

=> electrodes designed from simple assumptions and results will serve as test for code

1 – 2 mm gap in stripline

voltages ~200kV

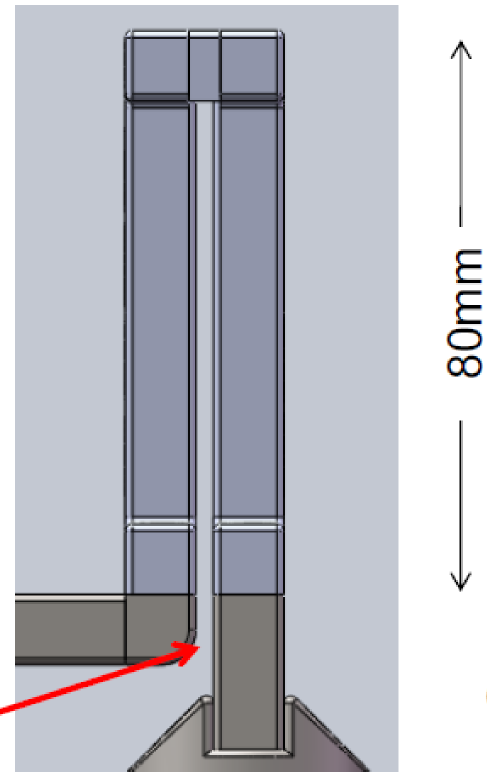

Side view of stripline

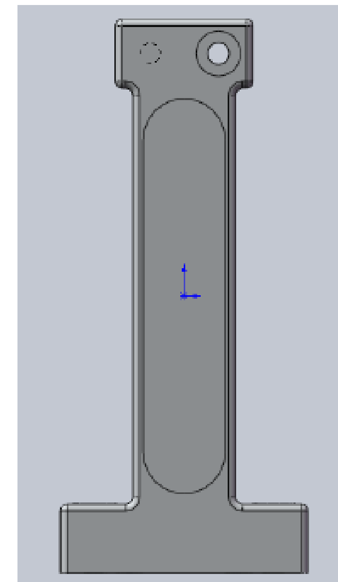

Front view of one electrode with target area outlined

- Need to use a soft material and needs to be easily machined - Copper
- Target thicknesses 1-7mm - shocks expected after ~5mm thickness
- How to support over large areas, polish etc

Imperial College
London

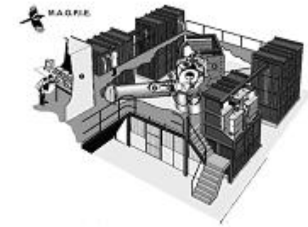

Initial experiments: Feb 2010

Typically for shock experiments:

flatness ~5um, roughness <um via. diamond machining

Overkill for initial experiments (and very expensive)

Tour de Force by Imperial College Instrumentation workshop

2 part ‘glued electrode’ electrode - target area and support

4 axis CNC mill allows fast production of blanks

Precision ground then hand polished – mirror finish ~5um

Return electrode

Gap (2mm)

Target area
(60x17mm)

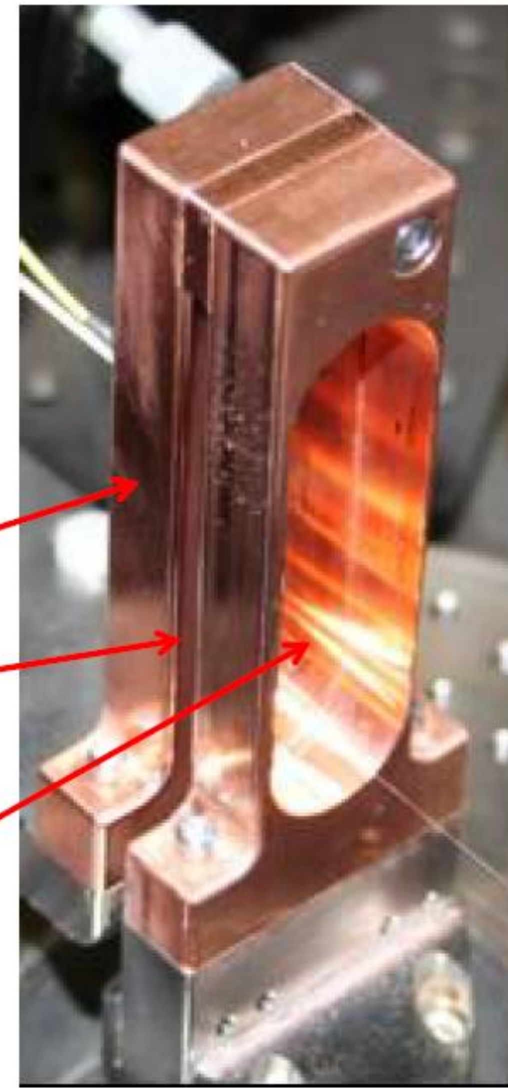

Close up of 20mm wide copper strip line in MAGPIE

Imperial College London

Initial experiments: Feb 2010

Holder for Het-V probes

Stripline mounted on break away system to prevent damage to MAGPIE

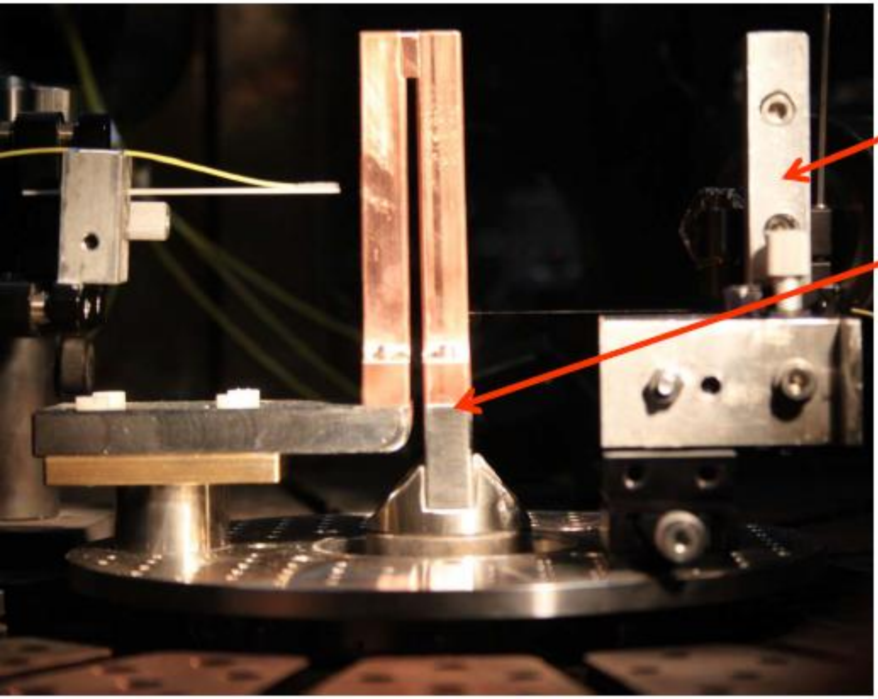

Side view of strip line

Top down view

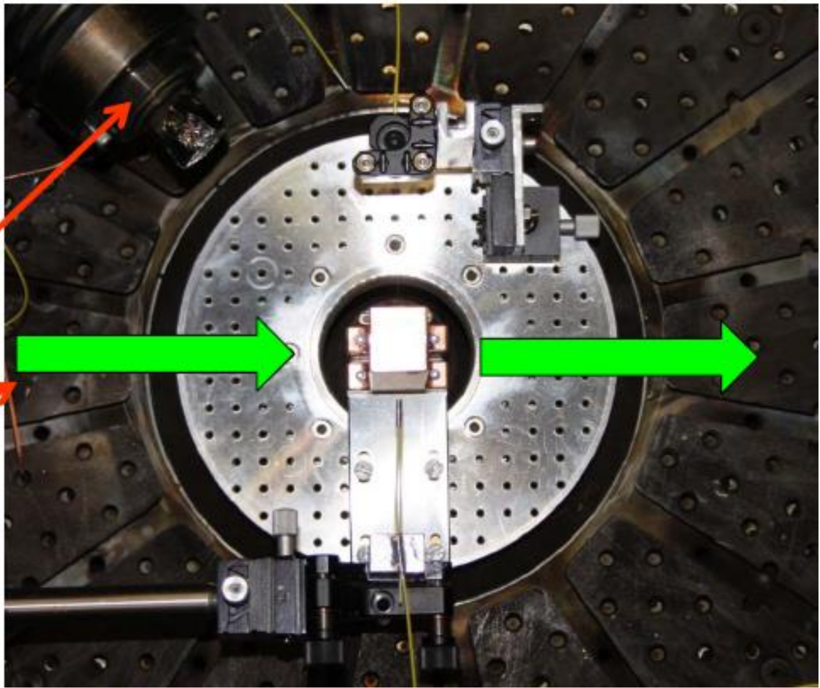

Resistive voltage probe

Path of probing laser

½ inch armoured plate top and bottom to 'catch' stripline (not shown)

Pulsed Power Driven Experiments in the Institute of Shock Physics, by Simon Bland

The design of our flyer-plate launcher

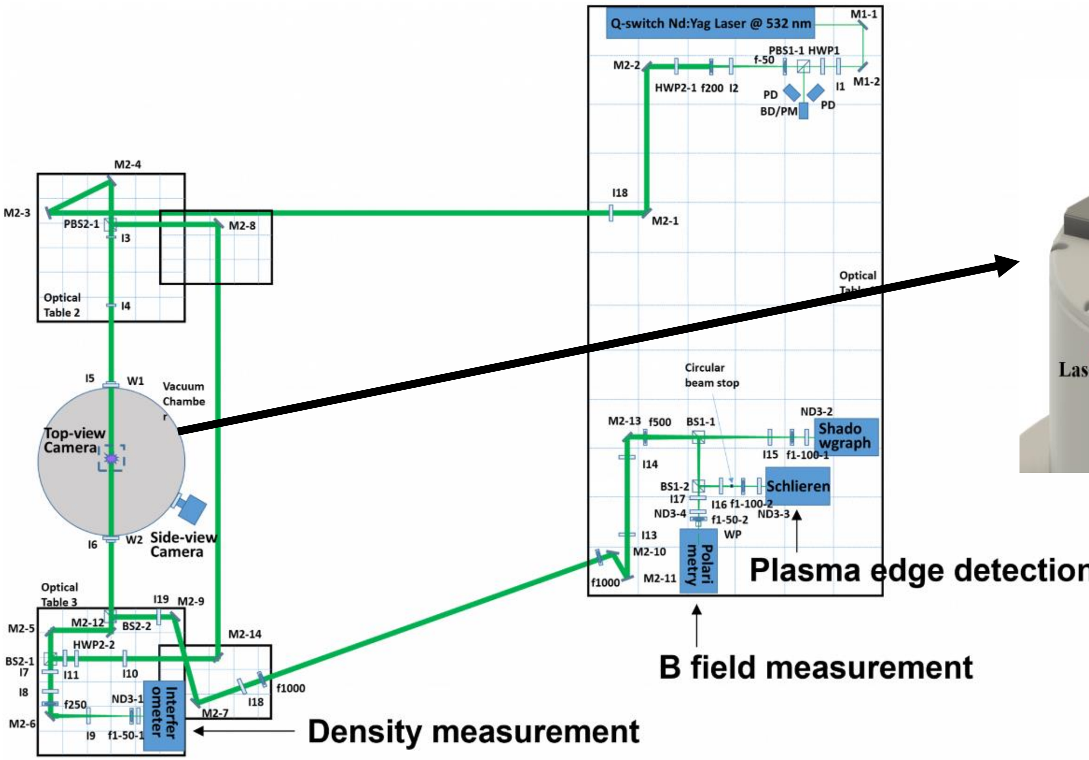

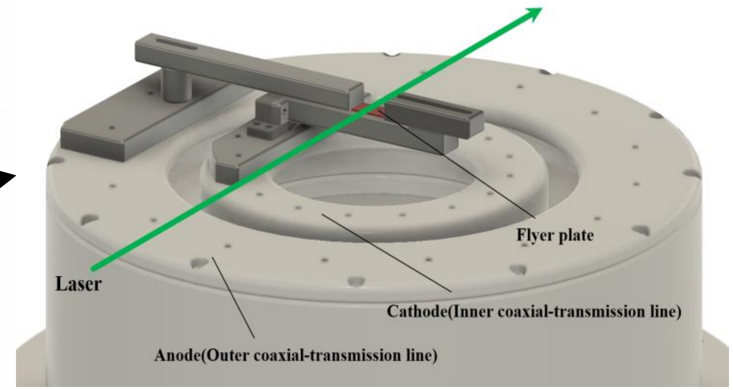

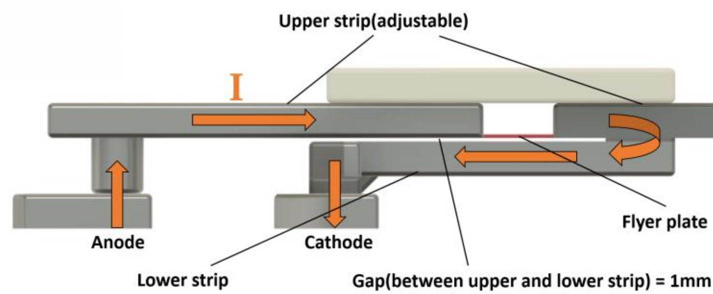

Y.-Z. Pan, Science day, College of Science, NCKU 2023
Y.-Z. Pan, Progress report, Pulsed-Plasma Laboratory 2023

Photos of our flyer-plate launcher

- **Assembly with target**

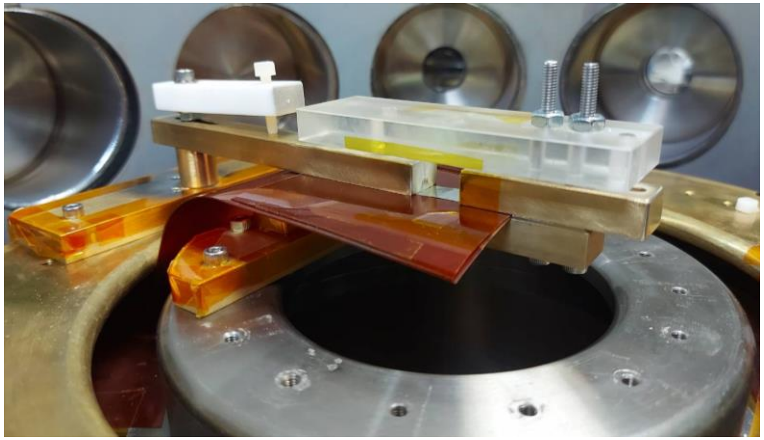

- **Assembly w/o target**

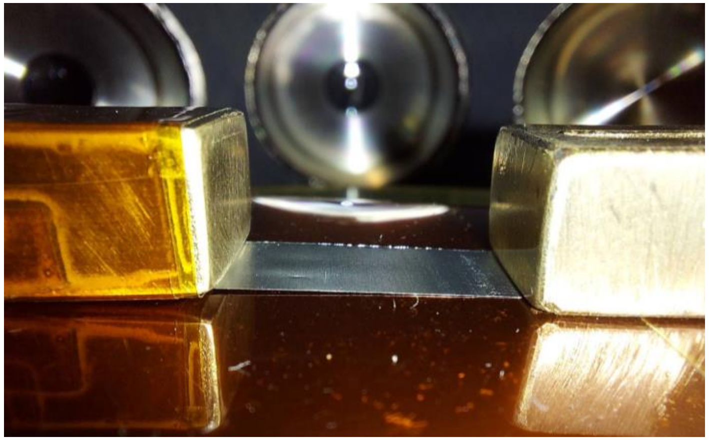

- **Self emission w/o a target**

- **Self emission w/ a target**

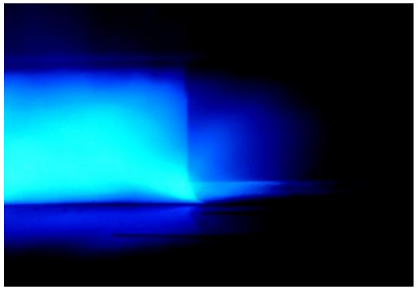

- **After shot**

Y.-Z. Pan, Science day, College of Science, NCKU 2023
Y.-Z. Pan, Progress report, Pulsed-Plasma Laboratory 2023

Velocities of the flyer plate were different when experiments were conducted in 1 atm and in vacuum

- @ ~1 atm

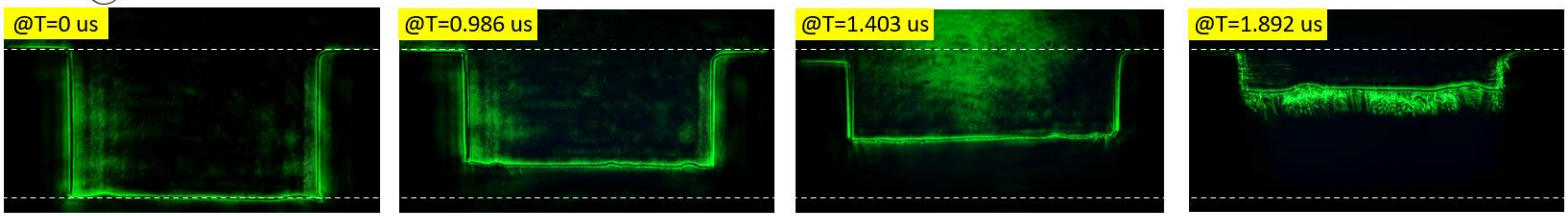

- @ ~10^{-5} torr

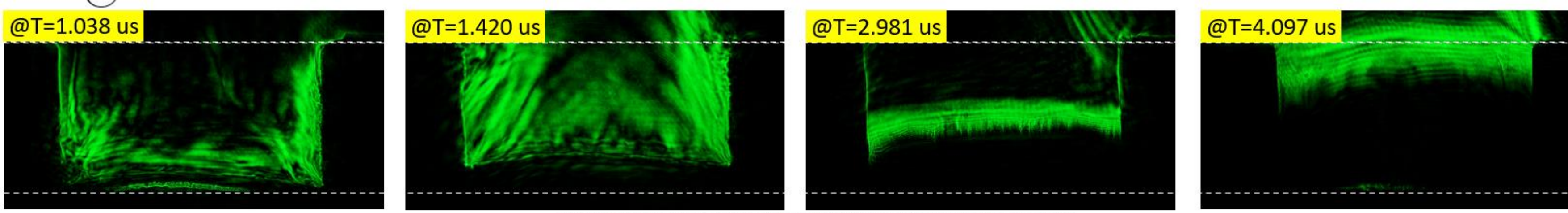

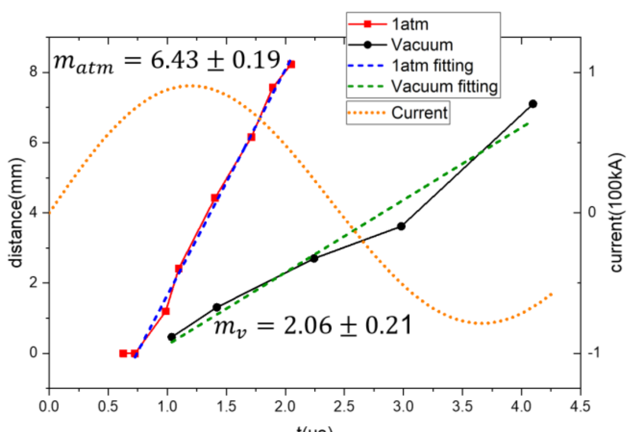

- @ 1 atm

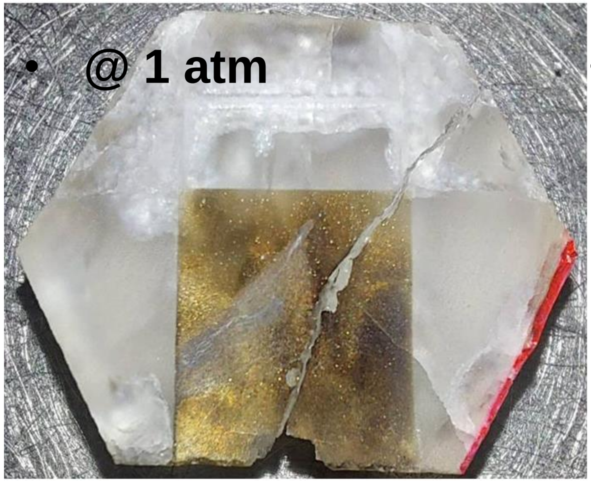

- @ ~10^{-5} torr

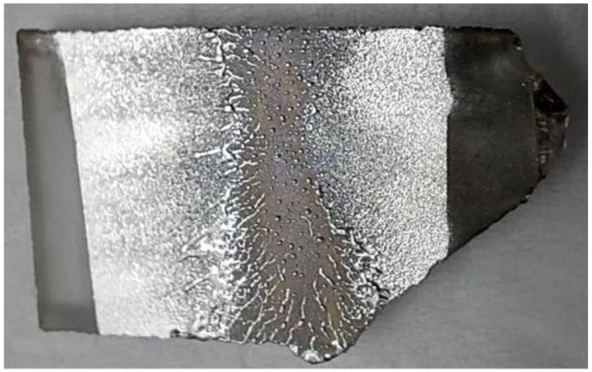

Y.-Z. Pan, Science day, College of Science, NCKU 2023

Raman shift of the SiO2 sample behaved differently after being shocked

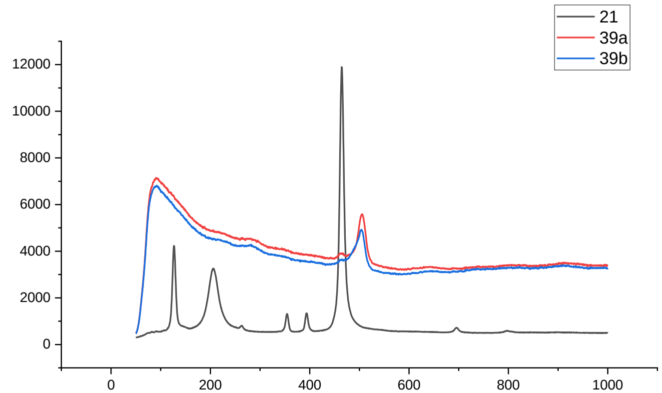

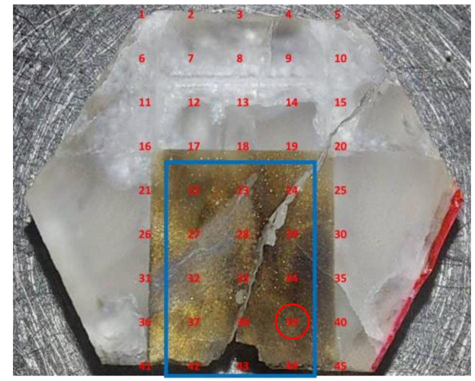

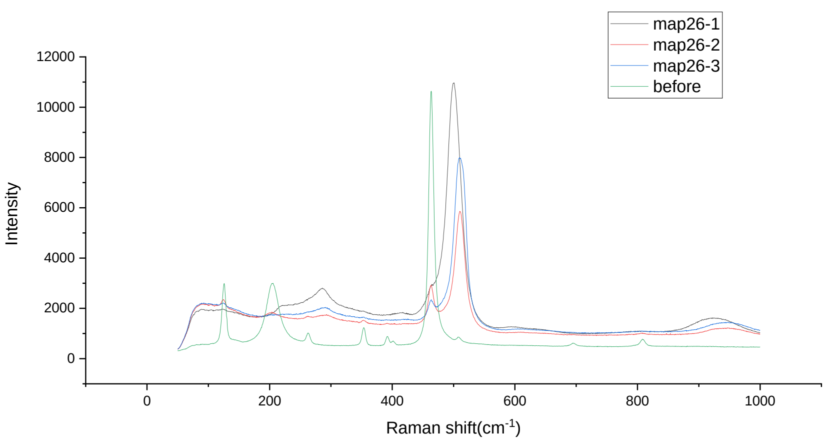

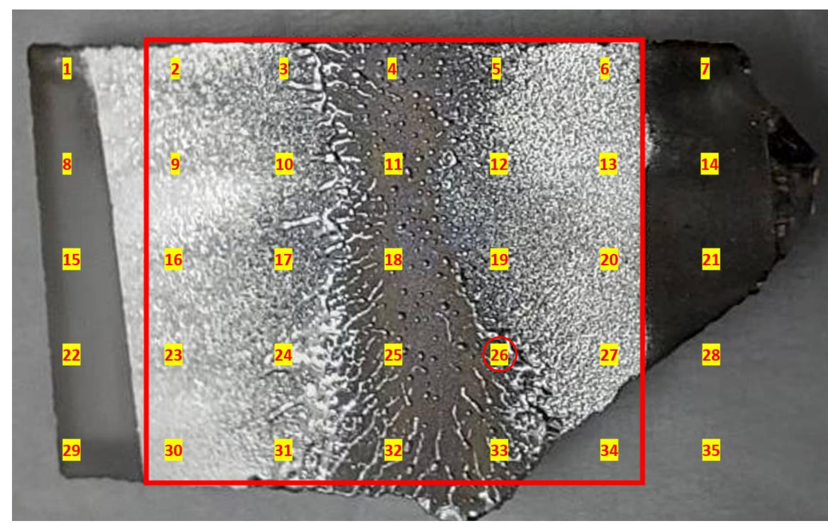

Raman shift of 520 cm-1 was observed suggesting that Coesite was formed

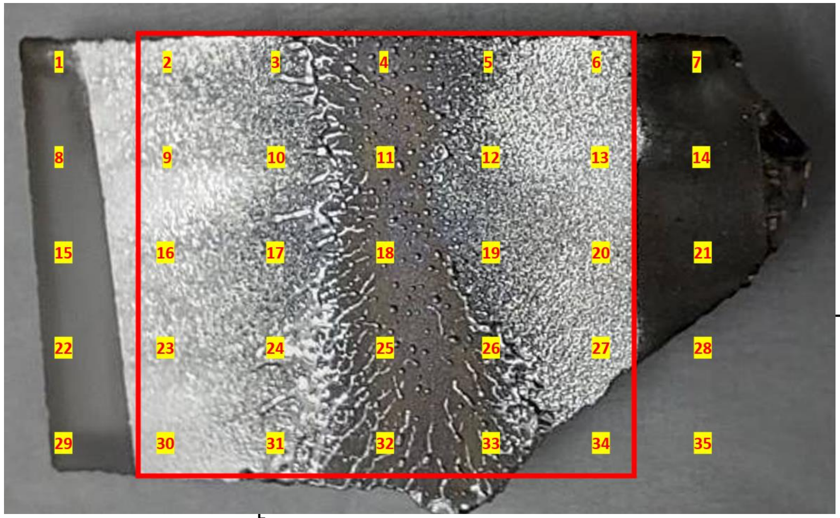

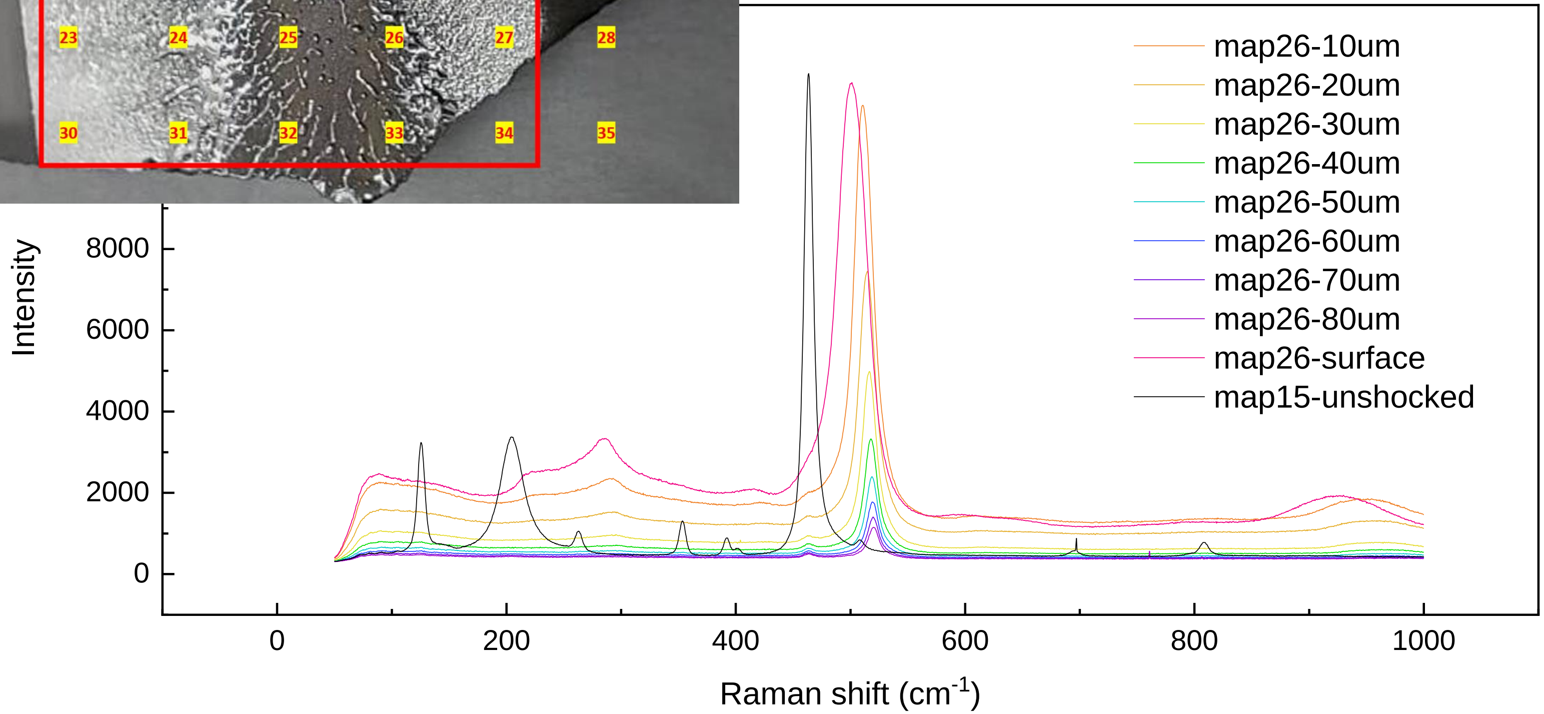

The raman shift indicated that a pressure more than 2 Gpa was generated

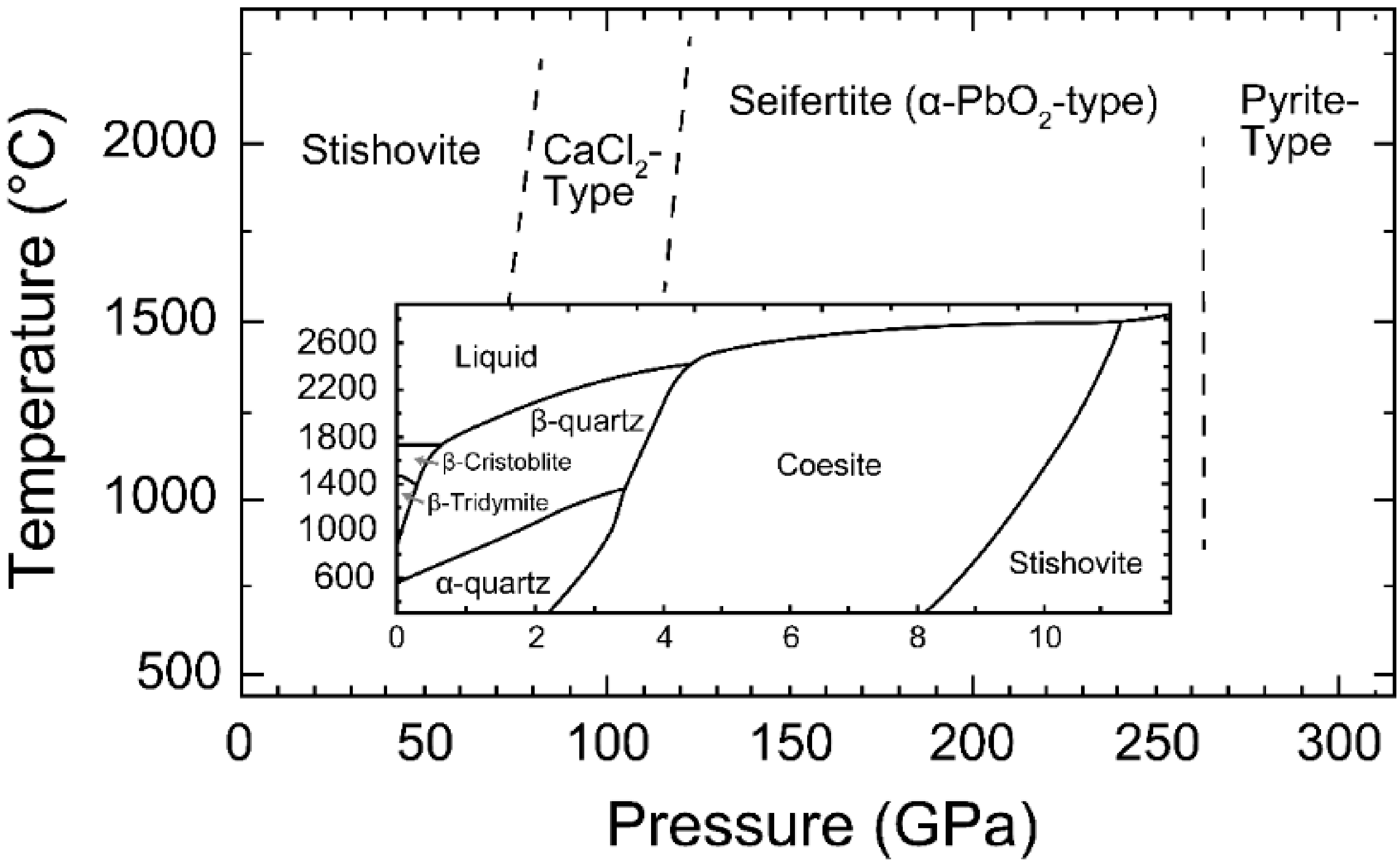

M. Kayama, etc., Minerals 8, 267 (2018)